

**Substitution-dependent  
Photophysical Properties of  
Organic Fluorophores**

Inaugural-Dissertation

to obtain the academic degree

Doctor rerum naturalium (Dr. rer. nat.)

submitted to the Department of Biology, Chemistry, Pharmacy  
of Freie Universität Berlin

by

**Philipp Rietsch**

September 2020

The work presented here was carried out between 12/2016 and 09/2020 at *Freie Universität Berlin* (14195 Berlin, Germany) in the Department of Biology, Chemistry and Pharmacy under the supervision of Prof. Dr. Siegfried Eigler.

1.) Referee: Prof. Dr. Siegfried Eigler (Freie Universität Berlin)

2.) Referee: Prof. Dr. Stefan Hecht (DWI - Leibniz-Institut für Interaktive Materialien Aachen)

Disputation at: 20.11.2020

*meiner Familie*

## Table of Contents

1	Summary.....	1
1.1	Overview of Presented Topics.....	1
1.2	Overview of Collaborations.....	1
1.3	Summary of Results.....	1
1.4	Zusammenfassung der Ergebnisse.....	4
2	Introduction.....	8
2.1	Prologue: History of the Emission of Light.....	8
2.2	Photophysical Fundamentals of Light Absorption and Emission.....	9
2.2.1	Perrin-Jablonski diagram.....	9
2.2.2	Stokes shift.....	11
2.2.3	Fluorescence quantum yield and fluorescence lifetime.....	11
2.2.4	Solvatochromism.....	11
2.2.5	The electric dipole moment in molecules.....	14
2.2.6	Dimer formation in molecules with high dipole moments.....	15
2.3	General Relations Between Molecular Structure and Emissive Properties.....	16
2.3.1	The $\pi$ -system: red shift of absorption and emission.....	16
2.3.2	The effect of heteroatoms on the emissive properties of $\pi$ -systems.....	17
2.4	Fluorescence Quenching.....	18
2.4.1	Fluorescence quenching by internal rotations.....	18
2.4.2	Intersystem crossing (ISC).....	19
2.4.3	Fluorescence quenching caused by aggregation.....	21
2.5	Classes of Fluorophores: Classic Examples and Recent Approaches.....	22
2.5.1	Coumarins and Rhodamines – established fluorophores.....	22
2.5.2	Polycyclic Aromatic Hydrocarbons (PAHs) as fluorophores.....	23
2.5.3	Small organic fluorophores with one benzene unit.....	25
3	Synopsis of Results.....	30
3.1	Diaminodicyanoquinones.....	30
3.1.1	A novel class of fluorescent dyes.....	30
3.1.2	Aggregation behaviour of Diaminodicyanoquinones.....	32

3.2	Highly Fluorescent Benzothiadiazoles as Redox Switches .....	34
3.3	Polycyclic Aromatic Hydrocarbons as Fluorophores .....	38
3.3.1	Fluorescence of a chiral pentaphene derivative derived from the hexabenzocoronene motif .....	38
3.3.2	Substitution-pattern controlled tuning of the fluorescence lifetime of fluoranthene dyes .....	39
4	Publications - Major Contributions .....	42
4.1	Diaminodicyanoquinones: Fluorescent Dyes with High Dipole Moments and Electron-Acceptor Properties .....	42
4.2	Fluorescence of a Chiral Pentaphene Derivative Derived from the Hexabenzocoronene Motif .....	84
4.3	Identification of the Irreversible Redox Behaviour of Highly Fluorescent Benzothiadiazoles .....	111
4.4	Substitution-Pattern Controlled Tuning of the Fluorescence Lifetime of Fluoranthene Dyes .....	136
5	Publications - Minor Contributions .....	180
5.1	Unravelling Diaminodicyanoquinone Aggregation Behavior in Solution: Complex Photophysical Properties Induced by Metastable Dimers .....	180
5.2	Between Aromatic and Quinoid Structure: A Symmetric UV to Vis/NIR Benzothiadiazole Redox-Switch .....	245
	List of Abbreviations .....	276
	List of Publications .....	279
	References .....	280
	Acknowledgments .....	286
	Statement of the Author .....	287

# 1 Summary

## 1.1 Overview of Presented Topics

In this cumulative dissertation the following topics are presented:

1. Diaminodicyanoquinones (DADQs)
  - a. A novel class of fluorescent dyes
  - b. The aggregation behaviour of DADQs
2. Highly fluorescent Benzothiadiazoles (BTDs) as redox switches
3. Polycyclic aromatic hydrocarbons as fluorophores:
  - a. Fluorescence of a chiral Pentaphene derivative derived from the Hexabenzocoronene motif
  - b. Substitution-pattern controlled tuning of the fluorescence lifetime of Fluoranthene dyes

## 1.2 Overview of Collaborations

The research was conducted in collaboration with the groups of:

- Dr. Ute Resch-Genger from the Federal Institute for Materials Research and Testing (German: Bundesanstalt für Materialforschung und -prüfung = BAM),
- Prof. Dr. Beate Paulus from the Institute of Chemistry and Biochemistry at Freie Universität Berlin,
- Prof. Dr. Biprajit Sarkar from the Institute of Inorganic Chemistry at the University of Stuttgart (formerly at Freie Universität Berlin),
- Prof. Dr. Dieter Lentz from the Institute of Chemistry and Biochemistry at Freie Universität Berlin,
- Dr. Alexey Popov from the Leibniz Institute for Solid State and Materials Research in Dresden.

The detailed results and experimental information are included in form of the attached publications in section 4 and section 5.

## 1.3 Summary of Results

### 1.3.1 Diaminodicyanoquinones

- a) A novel class of fluorescent dyes

Diaminodicyanoquinones (DADQs) have been widely researched due to their high dipole moment of roughly 10-30 Debye.<sup>[1]</sup> However, fluorescence quantum yields ( $\Phi$ ) in solution were reported to be below 0.01.<sup>[2]</sup>

In this work, a series of new DADQ derivatives was synthesized. The photophysical investigation revealed that benzene functionalized derivatives have fluorescence quantum yields ( $\Phi$ ) in solution exceeding 0.9. Through an experimental-theoretical approach (collaboration with Dr. Ute Resch-Genger and Prof. Dr. Beate Paulus), we successively investigated the fluorescence quenching processes of DADQs. Due to their bipolar structure, the

bonds between the diamino moiety and the benzene ring, as well as the dicyano moiety and the benzene ring, are susceptible to rotations. It was shown that the rotation around the dicyano-benzene bond is the main reason for fluorescence quenching in non-benzene functionalized derivatives. Due to low energetic barriers of rotation in the excited state  $S_1$ , non-radiative relaxation through internal conversion (IC) and intersystem crossing (ISC) is possible. Crucial for this revelation was the comparison of differently substituted derivatives and their photophysical analysis in solvents of different polarity, proticity and viscosity, as well as at different temperatures.

With the discovery of those properties, DADQs may now be considered as fluorescent dyes. Furthermore, the theoretical approach can be used to predict the emissive properties of novel derivatives.

#### b) The aggregation behaviour of Diaminodicyanoquinones

DADQs show two concentration dependent absorption bands in the UV/Vis spectrum. Beside the monomer band, a bathochromically (red-) shifted aggregate band is observed at high concentrations. In the well-established framework of H- and J-aggregates, bathochromically shifted bands are typically highly emissive (J-aggregates), and hypsochromically (blue-) shifted bands are non-emissive (H-aggregates). However, the red shifted aggregate band of the investigated DADQs is non-emissive. Through a combined approach of experiment and theory (collaboration with Prof. Dr. Beate Paulus), we unravelled the untypical aggregation behaviour of DADQs and propose metastable dimeric J-aggregates as the reason. Thus, DADQs are a rare case of J-aggregates with non-fluorescent properties.

Crucial for this discovery was the synthesis of two differently substituted series of DADQ compounds and the analysis of their absorption and emission spectra at different concentrations, in solvents of different polarity and proticity, with (polar) additives and at increasing temperatures. Those investigations revealed that hydrogen bonding is of major importance in the aggregation. The Paulus group took the coulomb term of the Kasha Model into account, and supplemented it by the consideration of charge transfer terms. Furthermore, the intensity of the electronic transition along a line of displacement was considered.

### 1.3.2 Highly fluorescent Benzothiadiazoles as redox switches

Changing the absorption or the emission properties of a material by redox processes is used in smart windows and rear-view mirrors,<sup>[3]</sup> and potentially applicable in light harvesting, sensors, and biomedicine. However, most of the known organic redox switches possess complex molecular structures.<sup>[4]</sup>

A series of unsymmetrical push-pull benzothiadiazole (BTD) derivatives and a symmetric diphenylmethoxy BTD, which were proven suitable for absorption switching between ultraviolet (UV), visible (Vis) and near-infrared (NIR) by redox processes, were synthesized. Through the measurement of cyclic voltammetry (CV), coupled with UV/Vis/NIR-spectroscopy (collaboration with Prof. Dr. Biprajit Sarkar), we reveal that the processes, which are seemingly reversible in the CV, are partly irreversible. The alkyne motif, which the unsymmetrical compounds incorporate, is the likely cause for the complete irreversibility of the oxidative processes, as well as for the partial irreversibility of the reductive processes. Therefore, such alkyne functionalized compounds would have limited

use as switches. The symmetric BTD compound, however, features two reversible oxidations which can be used for absorption switching between UV (neutral form), Vis ( $2^+$ ) and NIR ( $1^+$ ). Coupling of CV with electron paramagnetic resonance (EPR) spectroscopy revealed a strong delocalization of the radical over the whole  $\pi$ -system after first oxidation. Our calculations indicate an increasing quinoidal distortion upon oxidation that matches with the delocalization of the radical and the measured absorption spectra. Furthermore, measurements in collaboration with Dr. Alexey Popov revealed that the strong fluorescence in the neutral state is quenched upon oxidation. Therefore, fluorescence, instead of absorption could be used as the output signal for the redox switching process.

In addition, the different effects of viscosity and polarity on the emissive properties of the BTD derivatives were separated. Whereas a polarity-induced reduction of fluorescence quantum yield in solution ( $\Phi_{Sol}$ ) and fluorescence lifetime ( $\tau$ ) was observed, the emissive properties are independent of the solvent viscosity. The first finding can be rationalized by intramolecular charge transfer (ICT) states, which are exclusively formed in polar, protic solvents. The latter finding suggests that a molecular motion, like a rotation in the excited state, is not involved in non-radiative deactivation of the excited states of the BTD dyes. The solid state emission is not drastically reduced by non-radiative relaxation, such as  $\pi$ - $\pi$  stacking. The BTD dyes possess solid state fluorescence quantum yields ( $\Phi_{SS}$ ) of 0.30-0.70 (collaboration with Dr. Ute Resch-Genger). These emissive properties could be used for polarity probes, dye lasers or in more sophisticated redox switches. For the latter, alkyne moieties should be avoided, and the quinoid motif, which is induced upon oxidation and enabled through the methoxy groups, should be utilized to yield reversible switching processes between the UV and the Vis/NIR region.

### 1.3.3 Polycyclic aromatic hydrocarbons as fluorophores

#### a) Fluorescence of a Chiral Pentaphene Derivative Derived from the Hexabenzocoronene Motif

Pentaphenes, a sub-class of polycyclic aromatic hydrocarbons (PAHs), were investigated for their photophysical properties in the 1990s.<sup>[5]</sup> However, no fluorescence quantum yields, fluorescence lifetimes or solid state emissive properties were reported.

In this work, an unprecedented Scholl oxidation reaction was used as the last step to synthesize an enantiomeric pentaphene derivative which bears a 4[helicene] motif and, compared to hexabenzocoronene (HBC), lacks one C-atom in its basal plane. The reproducibility of the ring closing reaction under Scholl oxidation conditions was confirmed by a test reaction on a phenanthrene derivative. The photophysical properties of the pentaphene were compared to a structurally closely related HBC derivative. In solution and the solid state, the pentaphene is about five times more fluorescent than the HBC derivative. The single crystal X-Ray diffraction (XRD) data revealed that  $\pi$ - $\pi$  stacking with an interplanar distance of about 3.5 Å is the likely cause of fluorescence quenching for the HBC-derivative in the solid state. The pentaphene, however, has more than 9 Å interplanar distance, which makes non-radiative relaxation through  $\pi$ - $\pi$  stacking unlikely. Density functional theory (DFT) calculations revealed a racemization barrier of about 10 kcal/mol for the 4[helicene] motif in the pentaphene, thus showing that the enantiomers are inseparable in solution at room temperature. To elucidate the role of the



higher flexibility of the pentaphene derivative, fluorescence lifetimes and emission spectra at elevated (50 °C) and lowered (-100 °C) temperatures were measured. The emissive properties of both, the pentaphene and the compared HBC, reveal the same percentage change. This finding suggests that the flexibility of the [4]helicene motif in the pentaphene does not lead to non-radiative relaxation in solution.

#### b) Substitution-Pattern Controlled Tuning of the Fluorescence Lifetime of Fluoranthene Dyes

For the application of fluorescent dyes in lifetime multiplexing, substitution and solvent independent absorption and emission wavelength, as well as a large relative difference (100-1000 %) of the fluorescence lifetime ( $\tau$ ) of the used dyes is crucial. Compared to small organic molecules, PAHs are typically less susceptible to solvatochromic effects. Even so, organic dyes are rarely considered for their applications in lifetime multiplexing.

A series of fluoranthene derivatives (collaboration with Prof. Dr. Dieter Lentz) with substitution-pattern controlled lifetimes between 6 and 34 ns and substitution, as well as polarity independent absorption and emission wavelengths, were investigated. By measuring two component dye mixtures of different mixing ratios, the general suitability for lifetime multiplexing was proven (collaboration with Dr. Ute Resch-Genger). The solid state emissive properties, fluorescence quantum yields, emission spectra and emission-wavelength dependent fluorescence lifetimes were examined and the structure related differences were explained. Through the analysis of the single crystal XRD structures, it was revealed that the aggregation induced quenching through  $\pi$ - $\pi$  stacking occurs exclusively in derivatives which feature a pyracene unit. Nevertheless, the dyes can be embedded in polystyrene particles (PSP) without loss of emissive properties due to aggregation. With these characteristics, fluoranthene compounds are promising candidates for their use in lifetime multiplexing, for barcoding or in flow setups.

## 1.4 Zusammenfassung der Ergebnisse

### 1.4.1 Diaminodicyanochinone

#### a) Eine neue Klasse der Fluoreszenzfarbstoffe

Diaminodicyanochinone (DADQs) wurden aufgrund ihres hohen Dipolmoments umfassend erforscht.<sup>[1]</sup> Die Fluoreszenzquantenausbeuten ( $\Phi$ ) in Lösung lagen jedoch unter 0.01.<sup>[2]</sup>

In dieser Arbeit wurden Untersuchungen an einer Reihe von DADQ-Derivaten durchgeführt, die zeigten, dass Benzol-funktionalisierte Derivate in Lösung eine Fluoreszenzquantenausbeute ( $\Phi$ ) von über 0.9 haben. Durch einen experimentell-theoretischen Ansatz (Zusammenarbeit mit Dr. Ute Resch-Genger und Prof. Dr. Beate Paulus) untersuchten wir sukzessive die Fluoreszenzlöschungprozesse von DADQs. Aufgrund ihrer bipolaren Struktur können die Bindungen zwischen dem Diaminorest und dem Benzolring, sowie dem Dicyanorest und dem Benzolring rotieren. Es konnte gezeigt werden, dass die Rotation um die Dicyano-Benzol-Bindung der Hauptgrund für die Fluoreszenzlöschung in nicht-benzol-funktionalisierten Derivaten ist. Aufgrund der energetisch niedrigen Rotationsbarrieren im angeregten Zustand  $S_1$  ist eine strahlungsfreie Relaxation durch interne Konversion (IC) und Intersystem-Crossing (ISC) möglich. Ausschlaggebend für diese Erkenntnis war der

Vergleich unterschiedlich substituierter Derivate und die photophysikalischen Messungen in Lösungsmitteln unterschiedlicher Polarität, Protizität und Viskosität sowie Untersuchungen bei unterschiedlichen Temperaturen.

Mit der Entdeckung dieser Eigenschaften können DADQs nun als Fluoreszenzfarbstoffe betrachtet werden. Darüber hinaus kann der theoretische Ansatz zur Vorhersage der Emissionseigenschaften von neuartigen Derivaten verwendet werden.

#### b) Das Aggregationsverhalten von Diaminodicyanochinonen

DADQs zeigen zwei konzentrationsabhängige Absorptionsbanden im UV/Vis-Spektrum. Neben der Monomerbande wird bei höheren Konzentrationen eine bathochrom (rot-) verschobene Aggregatbande beobachtet. Im Rahmen der etablierten Modelle von H- und J-Aggregaten sind bathochrom verschobene Banden typischerweise stark emittierend (J-Aggregate), während hypsochrom (blau-) verschobene Banden nicht emittieren (H-Aggregate). Die rotverschobene Aggregatbande von DADQs ist jedoch nicht emittierend. Durch einen kombinierten Ansatz aus Experiment und Theorie (Zusammenarbeit mit Prof. Dr. Beate Paulus) haben wir das untypische Aggregationsverhalten von DADQs untersucht und vermuten metastabile dimere J-Aggregate als Ursache. Somit sind DADQs ein seltener Fall von J-Aggregaten mit nicht-fluoreszierenden Eigenschaften.

Ausschlaggebend für diese Entdeckung war die Synthese und Analyse von zwei unterschiedlich substituierten Reihen von DADQ-Verbindungen in unterschiedlichen Konzentrationen, in Lösungsmitteln unterschiedlicher Polarität und Protizität, mit (polaren) Additiven und bei steigenden Temperaturen. Diese Untersuchungen ergaben, dass Wasserstoffbrückenbindungen bei der Aggregation eine wichtige Rolle spielen. Die Paulus-Gruppe berücksichtigte den Coulomb-Term des Kasha-Modells und ergänzte ihn durch die Berücksichtigung von Ladungstransfertermen. Weiterhin wurde die Intensität des elektronischen Übergangs entlang einer Verschiebungslinie berücksichtigt.

#### 1.4.2 Stark emittierende Benzothiadiazole als Redoxschalter

Die Veränderung der Absorptions- oder Emissionseigenschaften eines Materials durch Redoxprozesse wird in *Smart Windows* und Rückspiegeln verwendet.<sup>[3]</sup> Zudem sind solche Materialien von potenziellem Interesse für den Einsatz in Solarzellen, Sensoren und in der Biomedizin. Die meisten der bekannten organischen Redoxschalter sind jedoch komplexe molekulare Strukturen.<sup>[4]</sup>

Es wurde eine Reihe von unsymmetrischen Push-Pull-Benzothiadiazol (BTD)-Derivaten sowie ein symmetrisches Diphenylmethoxy-BTD synthetisiert, die als Absorptionsschalter zwischen ultraviolettem (UV), sichtbarem (Vis) und nah-Infrarotem (NIR) Bereich durch Redox-Prozesse geeignet sind. Durch die Messung der zyklischen Voltammetrie (CV), gekoppelt mit UV/Vis/NIR-Spektroskopie (Zusammenarbeit mit Prof. Dr. Biprajit Sarkar), zeigen wir, dass die im CV scheinbar reversiblen Prozesse teilweise irreversibel sind. Die Alkin-Einheit der unsymmetrischen Verbindungen ist die wahrscheinlichste Ursache für die vollständige Irreversibilität der oxidativen Prozesse und die unvollständige Reversibilität der reduktiven Prozesse. Daher wären solche Alkin-funktionalisierten Verbindungen als Schalter nur begrenzt einsetzbar. Die symmetrische BTD-Verbindung weist

jedoch zwei reversible Oxidationen auf, die für den Prozess der schaltbaren Lichtabsorption zwischen UV (neutrale Form), Vis ( $2^+$ ) und NIR ( $1^+$ ) verwendbar sind. Die Kopplung von CV mit der Elektronenspinresonanz Spektroskopie (engl. EPR) zeigte eine starke Delokalisierung des Radikals über das gesamte  $\pi$ -System nach der ersten Oxidation. DFT-Berechnungen deuten auf eine zunehmende chinodiale Verzerrung nach der Oxidation hin, die mit der Delokalisierung des Radikals und den gemessenen Absorptionsspektren übereinstimmt. Darüber hinaus zeigten Messungen in Zusammenarbeit mit Dr. Alexey Popov, dass die starke Fluoreszenz des Moleküls im neutralen Zustand nach der Oxidation nicht mehr zu beobachten ist. Somit könnte anstelle des Absorptionssignals auch das Fluoreszenzsignal für den Redox-Schaltprozess verwendet werden.

Außerdem wurde der Einfluss von Viskosität und Polarität auf die Emissionseigenschaften von BTDs untersucht. Darüber hinaus konnte die polaritätsinduzierte Reduktion von  $\Phi_{Sol}$  und  $\tau$  sowie die Unabhängigkeit der Emissionseigenschaften von der Lösungsmittelviskosität gezeigt werden. Der erste Befund lässt sich durch intramolekulare Ladungstransferzustände (ICT) erklären, die bevorzugt in polaren, protischen Lösungsmitteln gebildet werden. Der zweite Befund legt nahe, dass eine molekulare Bewegung, zum Beispiel eine Rotation im angeregten Zustand, nicht an der strahlungslosen Deaktivierung der angeregten Zustände der BTDFarbstoffe beteiligt ist. Im Festkörper wurden Fluoreszenzquantenausbeuten ( $\Phi_{SS}$ ) von 0.30-0.70 gemessen (Zusammenarbeit mit Dr. Ute Resch-Genger). Dies lässt die Schlussfolgerung zu, dass es zu keiner drastischen Reduktion der Emission durch strahlungslose Relaxation, z.B. durch  $\pi$ - $\pi$  Wechselwirkungen, kommt.

Die genannten Emissionseigenschaften der BTDs können für Polaritätssonden, Farbstofflaser oder in anspruchsvolleren Redox-Schaltern genutzt werden. Bei Letzteren sollten Alkine vermieden, und das bei der Oxidation induzierte und zumindest teilweise durch die Methoxygruppen aktivierte Chinoid-Motiv genutzt werden, um reversible Schaltprozesse zwischen dem UV- und dem Vis/NIR-Bereich zu erhalten.

#### 1.4.3. Polyzyklische aromatische Kohlenwasserstoffe als Fluoreszenzfarbstoffe

##### a) Fluoreszenz eines vom Hexabenzocoronon-Motiv abgeleiteten chiralen Pentaphenderivats

Pentaphene, eine Unterklasse der polyzyklischen aromatischen Kohlenwasserstoffe (PAKs), wurden in den 1990er Jahren photophysikalisch untersucht.<sup>[5]</sup> Es wurde jedoch nicht über Fluoreszenzquantenausbeuten, Fluoreszenzlebensdauern oder vorhandene Festkörperemission berichtet.

In dieser Arbeit konnte über eine nicht publizierte Scholl-Oxidationsreaktion als letzten Schritt ein enantiomeres Pentaphenderivat mit einem 4[Helicen]-Motiv synthetisiert werden, dem im Vergleich zu Hexabenzocoronon (HBC) ein C-Atom in seiner Basalebene fehlt. Die Reproduzierbarkeit der Ringschlussreaktion unter Scholl-Oxidationsbedingungen wurde durch eine Testreaktion an einem Phenanthren-Derivat nachgewiesen. Die photophysikalischen Eigenschaften des Pentaphens wurden mit einem strukturell eng verwandten HBC-Derivat verglichen. In Lösung und im festen Zustand ist das Pentaphen etwa fünfmal stärker fluoreszierend als das HBC-Derivat. Die Einkristall-Röntgenbeugungsdaten (XRD) ergaben, dass  $\pi$ - $\pi$  Wechselwirkungen (interplanare Distanz 3.5 Å) die wahrscheinliche Ursache der Fluoreszenzlöschung für das HBC-derivat im festen Zustand sind. Das Pentaphen hat jedoch einen interplanaren Abstand von mehr als 9 Å, was eine strahlungsfreie Relaxation durch  $\pi$ - $\pi$ -Wechselwirkung weniger wahrscheinlich macht. Dichtefunktionaltheorie (DFT)-Berechnungen

ergaben für das 4[Helicen]-Motiv im Pentaphen eine Razemisierungsbarriere von etwa 10 kcal/mol. Dies zeigt, dass die Enantiomere in Lösung bei Raumtemperatur nicht separierbar sind. Um den Einfluss der höheren Flexibilität des Pentaphenderivats zu untersuchen, wurden Fluoreszenzlebensdauermessungen und Emissionsspektren bei erhöhten (50 °C) und erniedrigten (-100 °C) Temperaturen gemessen. Die Emissionseigenschaften des Pentaphens, als auch des HBC-derivats, zeigen die gleiche prozentuale Veränderung. Dieses Ergebnis legt nahe, dass die Flexibilität des [4]Helicen-Motivs im Pentaphen nicht zu einer strahlungsfreien Relaxation in Lösung beiträgt.

#### b) Substitutionsmuster kontrollierte Einstellung der Fluoreszenzlebenszeit in Fluoranthenfarbstoffen

Für die Anwendung von Fluoreszenzfarbstoffen im Lebensdauer-Multiplexing ist die Substitutions- und Lösungsmittel unabhängige Absorptions- und Emissionswellenlänge, sowie ein großer relativer Unterschied (100-1000 %) der Fluoreszenzlebensdauer ( $\tau$ ) der verwendeten Farbstoffe entscheidend. Im Vergleich zu kleinen organischen Molekülen sind PAK typischerweise weniger anfällig für solvatochrome Effekte. Trotzdem werden organische Farbstoffe selten für ihre Anwendungen im Lebensdauermultiplexing in Betracht gezogen.

Eine Reihe von Fluoranthen-Derivaten (Zusammenarbeit mit Prof. Dr. Dieter Lentz) mit Substitutionsmusterkontrollierten Lebensdauern zwischen 6 und 34 ns und Substitutions- sowie Polaritäts-unabhängigen Absorptions- und Emissionswellenlängen wurden untersucht. Durch Messung von Zweikomponenten-Farbstoffmischungen mit unterschiedlichen Mischungsverhältnissen wurde die generelle Eignung für Anwendungen im Lebensdauer-Multiplexing nachgewiesen (Zusammenarbeit mit Dr. Ute Resch-Genger). Die Festkörper-Emissionseigenschaften, Fluoreszenzquantenausbeuten, Emissionsspektren und Emissionswellenlängen-abhängigen Fluoreszenzlebensdauern wurden untersucht und durch die strukturellen Unterschiede der verschiedenen Derivate erklärt. Durch die Analyse der XRD-Strukturen konnte gezeigt werden, dass das Löschen der Fluoreszenz im Festkörper durch  $\pi$ - $\pi$  Wechselwirkungen ausschließlich in Derivaten auftritt, die eine Pyraceneinheit aufweisen. Dennoch können die Farbstoffe in Polystyrolpartikel (PSP) eingebettet werden, ohne dass die Emissionseigenschaften durch Aggregation verloren gehen. Mit diesen Eigenschaften sind Fluoranthene eine vielversprechende Farbstoffklasse für den Einsatz im Lebensdauer-Multiplexing, im Bereich der Kodierung oder für die Durchflusszytometrie.

## 2 Introduction

### 2.1 Prologue: History of the Emission of Light

In 1565, Spanish physician Nicolas Monardes observed the blue emission of an infusion of Lignum Nephriticum, a traditional diuretic made from two species of wood. Today, we know an oxidized flavonoid was responsible



Figure 1: Tonic water, containing fluorescent quinine sulfate, under daylight (left) and under UV light (right).<sup>[7]</sup>

for that emission.<sup>[6]</sup> Throughout the years, numerous bright people, among them Isaac Newton, investigated that phenomena but could not make sense of it. In the early 19<sup>th</sup> century, the emission of light from naturally occurring compounds was investigated further. Several scientists described the phenomenon of light emission, for example from chlorophyll and quinine (Figure 1<sup>[7]</sup>), as well as inorganic materials.<sup>[8]</sup> It was Sir George Gabriel Stokes who, in 1852, derived the word “fluorescence” from the mineral fluor-spar (Figure 2<sup>[9]</sup>), i.e. fluorite (calcium difluoride), which was found to emit blue light.<sup>[10]</sup>

Even though a deeper understanding of the phenomenon and the underlying chemical structures was still to be found, first synthetic emissive organic compounds and first applications of fluorescence arose. In 1877, the geologist Adolf Knop proved the, controversially debated, connection between the Danube and the Rhine by pouring 10 kg of sodium fluorescein, first synthesized by Adolf von Baeyer in 1871, in the “Danube sinkhole” around Tuttlingen. 60 hours later, the green emission of light of fluorescein in the Aachtopf spring, which belongs to the Rhine river system, closed the debate.<sup>[11]</sup>

In the 20<sup>th</sup> century and especially during World War II, the interest in antimalaria drugs, including quinine, increased and consequently led to the development of the first spectrofluorometers in the 1950s. Simultaneously, synthetic and analytical methods improved drastically, so that increasing numbers of fluorescent organic compounds could be synthesized.

Today, the advances in technology have enabled fluorescence to be used even at the level of single-molecule detection, for example in cellular and molecular imaging.<sup>[12]</sup> This high resolution, together with the sensitivity to the microenvironment and the possibility to read spatial as well as temporal information has led to numerous applications of fluorescence. That includes lasers,<sup>[13]</sup> Organic Light-Emitting Diodes (OLEDs)<sup>[14]</sup>, biomedical imaging,<sup>[15]</sup> data storage<sup>[16]</sup>, anticounterfeiting<sup>[17]</sup> and DNA sequencing.<sup>[18]</sup>

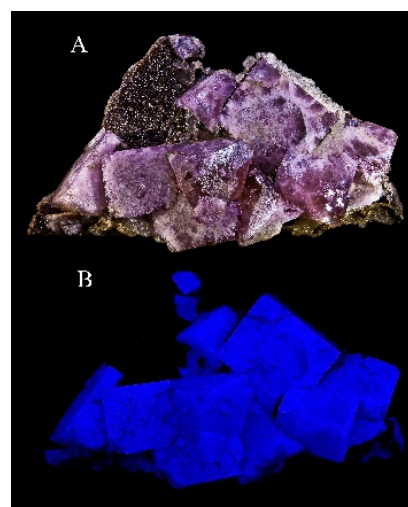


Figure 2: A crystalline probe of fluorite (calcium difluoride) under daylight (A) and under UV light (B).<sup>[9]</sup>

## 2.2 Photophysical Fundamentals of Light Absorption and Emission

Fluorescence is the emission of light from a substance, induced by the relaxation of an electronically excited singlet state. Thus, it is the pairing of an excited electron with a second, spin opposite, electron in the ground-state and typically happens on the nanosecond time scale. The phenomenon of fluorescence, its concomitant features and competing processes are best described in the so-called Perrin-Jablonski diagram (Figure 3), named after the two physicists Aleksander Jablonski (1898-1980) and French Nobel prize winner Jean-Baptiste Perrin (1870-1942), who first used such a diagram in 1929 and received the Nobel prizes for physics in 1926 for his work on the sedimentation equilibrium.<sup>[19]</sup>

### 2.2.1 Perrin-Jablonski diagram

The absorption of light normally happens from the singlet ground state,  $S_0$ , into higher electronic singlet states  $S_1$ ,  $S_2$ , ...,  $S_n$ . In photophysical aspects, the terms HOMO (highest occupied molecular orbital) and LUMO (lowest unoccupied molecular orbital) are commonly used. In each of the electronic states, vibrational energy levels exist (Figure 3, grey lines). Light absorption occurs on the femtosecond timescale, around  $10^{-15}$  s, and is therefore faster than the relocation of nuclei according to the Born-Oppenheimer approximation. The fact that excitation leads to an initially unchanged state (geometry) of all nuclei of the fluorophore and the surrounding molecules, is part of the Frank-Condon principle. This state is sometimes therefore referred to as the Frank-Condon state.

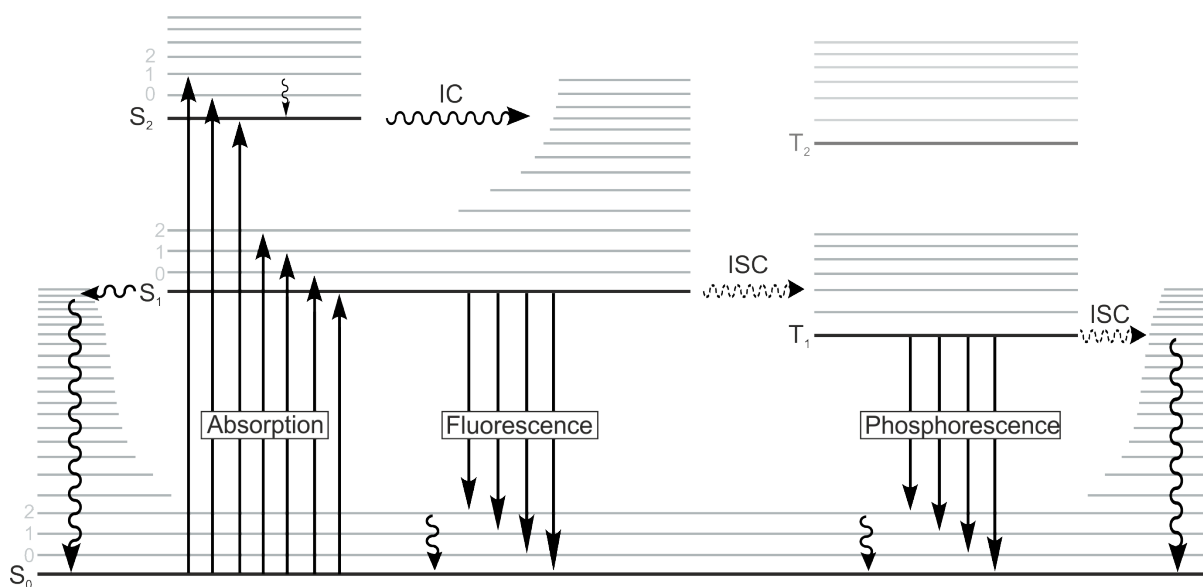


Figure 3: Perrin-Jablonski diagram showing the process of light absorption and the multiple ways of relaxation. IC = internal conversion, horizontal solid curved arrow; ISC = intersystem crossing, dotted horizontal curved arrow. Vertical solid curved arrows are vibrational relaxations. The straight vertical arrows are absorption or emission (fluorescence or phosphorescence) processes.

One direct consequence of the Frank-Condon principle is that absorption spectra can provide only limited information, as they describe a compound in its ground state exclusively. After excitation in the higher electronic states, mostly  $S_1$  and/or  $S_2$ , and their higher vibrational states, vibrational relaxation, a rapid non-radiative relaxation to the lowest vibrational level of the respective electronic state, typically occurs on the picosecond timescale, in about  $10^{-12}$  s (Table 1). From the vibrational ground state of an electronic state,

internal conversion (IC), a non-radiative conversion between two electronic states (Figure 3, horizontal solid curved arrows), can take place in around  $10^{-10}$  s. Internal conversion between the  $S_1$  and a high vibrational level of  $S_0$ , and subsequent vibrational relaxation to the vibrational ground state of  $S_0$  is one possible non-radiative relaxation pathway. One shiny alternative is fluorescence, which typically occurs from the vibrational ground state of the  $S_1$  state to different vibrational levels of the  $S_0$ , according to the Kasha-Vavilov rule.<sup>[20]</sup> Typical fluorescence lifetimes are about  $10^{-8}$  s. Even though the process of spontaneous emission is as fast as the process of absorption, around  $10^{-15}$  s, fluorophores tend to stay in the excited state for time ranges between picoseconds and hundreds of nanoseconds. Therefore, the excited state is accessible to dynamic phenomena, e.g. solvent interactions, and nuclei relaxations, and in general to competing (non-radiative) relaxation processes.

Table 1: Characteristic time ranges of the absorption, emission and competing processes taken from Reference.<sup>[19b]</sup>

Absorption	$10^{-15}$ s
Vibrational relaxation	$10^{-12}$ s
Intersystem crossing (ISC)	$10^{-10}$ - $10^{-8}$ s
Internal Conversion (IC)	$10^{-11}$ - $10^{-9}$ s
Lifetime of the excited singlet state $S_1$	$10^{-10}$ - $10^{-7}$ s
Lifetime of the excited singlet state $T_1$	$10^{-6}$ - 1 s

Another alternative is intersystem crossing (ISC) from the singlet state  $S_1$  to an isoenergetic vibrational level of a triplet state (e.g.  $T_1$ ). That involves an electron spin flip and is therefore a transition between states of different multiplicity. As such, it is a forbidden process with low transition probabilities (Figure 3, dashed horizontal curved arrow). From that triplet state  $T_1$ , which has relatively long lifetimes of  $10^{-6}$  to 1 s, the system might phosphoresce. As this process incorporates again a transition between states of different multiplicity, the emission rates are typically very low.

Due to the long lifetime of the excited triplet state, phosphorescence is often quenched by competing faster, non-radiative processes, such as oxygen quenching. Nevertheless, the probability of phosphorescence can be increased through different effects, e.g. spin-orbit coupling. Thus, it can act as a pathway for fluorescence quenching. Fluorescence quenching mechanisms will be described in more detail in section 2.4. From the fundamental standpoint, fluorescence occurs if no (faster) alternative pathways for energetic relaxation are feasible, which every excited state “seeks for”.

The energetic levels between vibrational levels in the  $S_1$  and  $S_0$  state are very similar.<sup>[20a]</sup> This, and the Kasha-Vavilov rule, are the reasons why the absorption and emission spectra typically mirror each other. Furthermore, fluorescence is preceded by vibrational relaxation and is therefore red shifted (lower in energy) compared to absorption. That shift, the Stokes shift will be described in the next section. The same is true for phosphorescence in comparison to fluorescence, the  $T_1$  vibrational ground level is typically lower in energy than the  $S_1$  vibrational ground level.

### 2.2.2 Stokes shift

Besides coining the term fluorescence, Sir Professor Stokes (1819-1903) made a very fundamental observation concerning the nature of fluorescence. He used a blue glass filter, which selectively transmitted light below 400 nm, UV light, to excite quinine sulfate in an aqueous solution. Using a yellow glass filter as an emission filter, allegedly a yellow-glass of wine, which transmitted light above 400 nm, he realized, that the emission occurs at lower energies (higher wavelength) compared to the excitation. Even though Sir William Herschel as well as Edmond Becquerel, father of Henri Becquerel, made similar observations before, it was Stokes who formulated the thesis that emission is always red shifted in comparison to the absorption. Today, we call that shift the Stokes shift and measure it from the maximum of the  $S_0$ - $S_1$  absorption band to the maximum of the  $S_1$ - $S_0$  emission band. The Stokes shift can be rationalized with the Perrin-Jablonski diagram (Figure 3). However, other effects, such as excited state reactions, solvent interactions or aggregation can drastically affect the Stokes shift.

### 2.2.3 Fluorescence quantum yield and fluorescence lifetime

The fluorescence quantum yield  $\Phi$  and fluorescence lifetime  $\tau$  are the most important characteristics of a fluorophore.  $\Phi$  is the percentage of emitted photons relative to the absorbed photons. It is described through Equation 1, where the radiative rate  $k_r$  is divided through the sum of the radiative rate  $k_r$  and the non-radiative rate  $k_{nr}$ . The equation shows that fluorescence intensity is a direct competition of radiative and non-radiative rates, both depopulating the excited state. Fundamentally, control over  $\Phi$  can be attained by affecting one or both rates.

$$\Phi = \frac{k_r}{k_r + k_{nr}}$$

Equation 1: The relation of fluorescence quantum yield ( $\Phi$ ), radiative rate  $k_r$  and non-radiative rate  $k_{nr}$ .

The fluorescence wavelength and the fluorescence quantum yield are for most compounds independent of the excitation wavelength, as fluorescence is typically the transition from vibrational ground-state of  $S_1$  to  $S_0$  (Kasha-Vavilov rule).

The fluorescence lifetime is the mean time a fluorophore remains in the excited state before the emission of light. During that time, dynamic phenomena like interactions with the microenvironment and structural relaxation occur. Therefore, the lifetime of the excited state is valuable to understand the fundamental properties of an emissive compound. In addition, fundamental processes, e.g. singlet fission, can be unravelled with the help of the lifetimes of different states.<sup>[21]</sup> Many applications, for instance the performance of organic solar cells,<sup>[22]</sup> are highly dependent on the evaluation and design of molecules with appropriate lifetimes. Besides, the fluorescence lifetime is used in multiplexed assays,<sup>[23]</sup> bioimaging<sup>[15]</sup>, and DNA sequencing.<sup>[18]</sup> Therein, spectral multiplexing, with all its disadvantages (spectral cross talk, concentration dependence, intensity variations caused by fluorophore leaking and bleaching) was typically employed. However, the pioneering groups of Niessner<sup>[24]</sup>, Wolfrum,<sup>[25]</sup> McGown,<sup>[26]</sup> and Soper<sup>[27]</sup> suggested the use of the fluorescence lifetime as observable, which was taken on by many groups and advanced, as one example, for the use in vivo molecular imaging.<sup>[28]</sup>



Fluorescence is one type of spontaneous emission. Thus, after the excitation of a fluorophore with a short pulse of light, the number of molecules in the excited state will decrease exponentially. Since the fluorescence lifetime is a measure for the population duration of molecules in the excited state, the relaxation process can be described by Equation 2. In the equation,  $n(t)$  is the number of excited molecules at time  $t$ ,  $n(0)$  the number of molecules excited right after the light pulse at time 0,  $k_r$  is the radiative rate and  $k_{nr}$  the non-radiative rate.

$$\frac{dn(t)}{dt} = -(k_r + k_{nr}) \cdot n(t)$$

Equation 2: Formula describing the relation between the number of excited molecules  $n$  at a time  $t$  in relation to the radiative rate  $k_r$  and the non-radiative rate  $k_{nr}$ .

$$\tau = \frac{1}{k_r + k_{nr}}$$

Equation 3: The relation between mean fluorescence lifetime, the radiative rate  $k_r$  and the non-radiative rate  $k_{nr}$ .

$$I(t) = I_0 \cdot e^{-t/\tau}$$

Equation 4: Formula describing the relation between the fluorescence intensity  $I$  at a time  $t$ , the initial intensity at  $t = 0$  and the fluorescence lifetime  $\tau$ .

Making use of Equation 3 and the fact that the fluorescence intensity  $I$  is directly proportional to the number of excited molecules leads to Equation 4. That equation determines the average fluorescence lifetime through exponential approximation. The relation between quantum yield and fluorescence lifetime, expressed in Equation 5 and Equation 6, facilitate the calculation of the radiative and non-radiative rates if both values were measured under the same conditions.

$$k_r = \frac{\Phi}{\tau}$$

Equation 5: Relationship between radiative rate, quantum yield  $\Phi$  and fluorescence lifetime  $\tau$ .

$$k_{nr} = \frac{1}{\tau} - k_r$$

Equation 6: Relationship between fluorescence lifetime  $\tau$ , radiative rate  $k_r$  and non-radiative rate  $k_{nr}$ .

Dependent on the type of relaxation pathways which compete, a proportionality between  $\Phi$  and  $\tau$  might exist. In the case of dynamic quenching, e.g. variation of temperature, both values are proportional, in case of static quenching, e.g. ground-state complex formation, the lifetime remains stable but the quantum yield is reduced. Typical fluorescence lifetimes of organic fluorophores are between 1 and 10 ns. Non-radiative rates are about  $10^9 \text{ s}^{-1}$ .<sup>[20a]</sup> When interpreting fluorescence quantum yields and lifetimes, one should be aware of the many factors, such as temperature, solvent polarity, pH, viscosity, non-covalent interaction as well as a combination of those factors, which can influence both values.

## 2.2.4 Solvatochromism

Solvatochromism is the effect of solvent polarity on the absorption and emission maxima of a solute. There are two forms of solvatochromism, negative and positive. It is rationalized by the change of charge distribution induced by the electronic excitation. That leads either to a reduced, or an increased dipole moment (see section 2.2.5) of a molecule upon excitation. As absorption is faster ( $1 \times 10^{-15}$  s) than solvent relaxation ( $10\text{-}100 \times 10^{-12}$  s), the ground and the Frank-Condon state are exposed to the same solvent environment. Therefore, the absorption spectrum is normally little affected by solvent polarity. As fluorescence lifetimes (1-10 ns) are long compared to the time required for solvent relaxation, the effect on the emission spectra can be immense, especially if the change of charge distribution is large. That is the case for many donor-acceptor dyes. If the charge distribution and therefore the dipole moment increases upon excitation, a positive solvatochromism is observed, whereas a decrease of charge distribution and therefore dipole moment upon excitation is called negative solvatochromism.<sup>[29]</sup> For dyes with negative solvatochromism, a hypsochromic shift (blue shift) is observed with increasing solvent polarity. A molecular example for negative solvatochromism are merocyanines.<sup>[30]</sup> Positive solvatochromism incorporates a bathochromic (red shift) and is observed for benzothiadiazoles (BTD) and coumarins.<sup>[31]</sup>

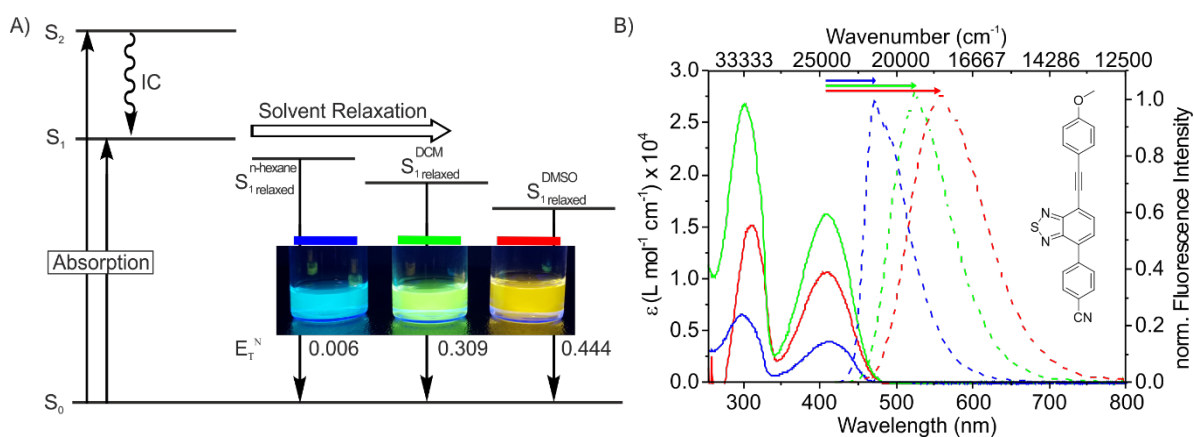


Figure 4: Depiction of the positive solvatochromism of a benzothiadiazole (BTD) derivative. A) Schematic Perrin-Jablonski diagram showing the absorption from  $S_0$  into the  $S_2$  and  $S_1$  state, internal conversion (IC) from  $S_2$  to  $S_1$  and the subsequent solvent relaxation leading to solvent relaxed  $S_1$  states. Here, three exemplary states in *n*-hexane, dichloromethane (DCM) and dimethylsulfoxide (DMSO) are shown. For the sake of clarity, the three are put in one diagram. The inset shows solutions of the BTD in solvents of the same proticity (aprotic) but different polarity (left to right: hexane, DCM, DMSO) under illumination with 366 nm. Values for the normalized Dimroth-Reichardt Parameter  $E_T^N$  were taken from reference.<sup>[29]</sup> B) Absorption spectra (solid) and normalized fluorescence emission spectra (dashed, excitation at 410 nm) of the BTD shown in the inset. Hexane = blue, DCM = green, DMSO = red. Arrows indicate the respective Stokes shift. The dye concentrations used for these measurements were  $10^{-5}$  M.

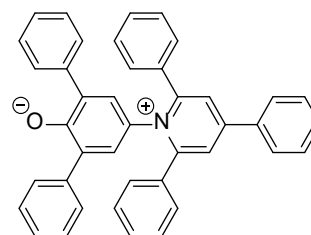
In Figure 4, the positive solvatochromism of a BTD derivative is shown. In that case, the solvents of higher polarity, e.g. dimethylsulfoxide (DMSO), lead to an energetic lowering of the  $S_1$  state, and thus to a decreased  $S_1$ - $S_0$  gap. The emission is therefore red shifted in comparison to apolar *n*-hexane and less polar dichloromethane. The depiction of the three solutions under illumination with 366 nm exemplify the Stokes shift. In Figure 4B, the absorption and emission spectra are shown in the respective color code. For BTDs, the wavelengths of the absorption maxima are unaffected by the solvent. However, for other compounds, e.g. zinc porphyrins, the interaction with the solvent, for instance non-covalent interaction, can lead to a shift of the

absorption bands.<sup>[32]</sup> One possibility to describe solvatochromism in more detail, and extract information from the measurements in different solvents is the Lippert-Mataga model.<sup>[20a, 33]</sup> It uses the Stokes shift and two solvent parameters, the dielectric constant of the solvent and the refractive index, to calculate the change of dipole moment upon excitation. However, it should be noted that a dipole moment is not a necessity for the observation of solvatochromism. There are examples of symmetric compounds featuring strong solvatochromism due to the change of quadrupole moment and/or intramolecular charge transfer upon excitation (Figure 16, structure 5).<sup>[34]</sup>

An experimental parameter for the description of the polarity of the solvent is the Reichardt parameter  $E_T^N$ . It was introduced by Christian Reichardt in 1963, using 2,6-Diphenyl-4-(2,4,6-triphenyl-1-pyridinio)phenolate (Table 2, right side), today also called the Reichardt dye.<sup>[29, 35]</sup> Dependent on the solvent, its absorbance can be varied over the whole visible spectrum and was thus used by Reichardt to postulate a scale for solvent polarity, where tetramethylsilane has a value of 0 and water a value of 1. The  $E_T^N$  values for some common organic dyes are given in Table 2. Nevertheless, effects like hydrogen bonding, highly viscous solvents or solvents at very low temperature can have an extreme effect on solvatochromism and are known to even lead to completely inverted solvatochromism.<sup>[29]</sup>

Table 2: Values of the Reichardt parameter  $E_T^N$  of some common solvents and structure of 2,6-Diphenyl-4-(2,4,6-triphenyl-1-pyridinio)phenolate, the Reichardt dye. Values were taken from reference.<sup>[29]</sup>

Solvent	$E_T^N$
Tetramethylsilane	0.000
<i>n</i> -Hexane	0.006
DCM	0.309
DMSO	0.444
EtOH	0.654
H <sub>2</sub> O	1.000



### 2.2.5 The electric dipole moment in molecules

Separated electric charges of positive and negative sign induce an electric dipole moment in a molecule, which is also referred to as the polarity of the compound. The dipole moment is typically denoted in the unit Debye (D), which is defined as  $3.33563 \times 10^{-30}$  Coulomb-meters (Cm). The unit exemplifies that the amount of the two charges and the spatial separation of the two opposing charges determine the size of the dipole moment. For instance, the dipole moment of inorganic salts like KBr or LiBr are between 8 D and 11 D.<sup>[36]</sup> For organic compounds, ground state dipole moments range from 0 D up to 15 D, with some exceptions, e.g. merocyanines, which were found to have ground state dipole moments around 20 D.<sup>[37]</sup> As described above, electronic excitation typically leads to a displacement of charges. Fundamentally, absorption is the interaction of light, an oscillating electromagnetic field, with electrons in the respective molecule. The change of dipole moment that occurs upon excitation (transient dipole) is referred to as the transition moment.<sup>[19b]</sup> The excitation is most efficient if the electric vector of the incidental light is parallel to the transition moment of the molecule. The

dipole moment before light absorption, induced or permanent, and the transition moment, can help to explain absorption and emission characteristics. Examples are induced charge transfer states, electrostatic interactions or energy transfers such as the Förster resonance energy transfer.<sup>[20a, 37c, 38]</sup> The dipole moment, or at least the change of dipole moment upon excitation, can be experimentally determined. Besides the Lippert-Mataga concept (section 2.2.4), electro-optical absorption (EOA) spectroscopy, which is based on the Stark effect, can be employed to derive the ground state dipole moment, as well as the change of dipole moment upon excitation, of a molecule.<sup>[39]</sup> In general, large dipole moments can be beneficial for applications in non-linear optics,<sup>[2a]</sup> sensing applications<sup>[40]</sup> or used for controlled aggregation.<sup>[41]</sup>

## 2.2.6 Dimer formation in molecules with high dipole moments

In the 1930s, E.E. Jelley and G. Scheibe discovered independently that the dye pseudoisocyanine chloride (Figure 5A), which shows two absorption bands in ethanol, features a third, very sharp and, with regard to the other two bands, bathochromically shifted absorption band when it is dissolved in water.<sup>[42]</sup> Furthermore, the excitation of that sharp, red shifted band, leads to a strong emission with a small Stokes shift. Today, we refer to these aggregates as J-aggregates (J denotes Jelley). Aggregates which feature a hypsochromically shifted band (again with regard to the monomer band) and exhibit very low or no emission were later termed H-aggregates (H denotes hypsochromic).

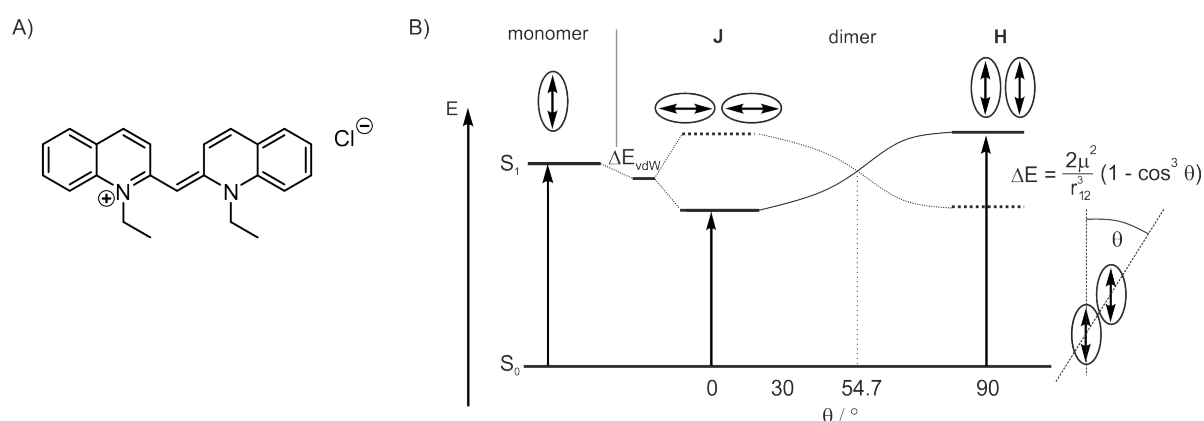


Figure 5: A) Molecular structure of pseudoisocyanine chloride (1,1'-diethyl-2,2'-cyanine chloride), the first compound investigated for its formation of J-aggregates.<sup>[42]</sup> B) Depiction of a schematic energy diagram for the aggregation of two monomers (left side) to dimers with co-planar aligned transition dipoles. Allowed states are depicted in bold lines, forbidden states are depicted in dotted lines. The geometry of the monomers to each other, with the slip angle  $\theta$  is depicted on the right side together with the formula postulated by Kasha *et al.*<sup>[43]</sup>  $\mu$  denotes the transition dipole moment of each monomer,  $r_{12}$  the distance of the centres of the monomers and  $\theta$  the angle of the monomers to each other as depicted below the formula. For geometries where  $\theta < 54.7^\circ$ , the transition to the lower energy state is allowed (bathochromically shifted absorption band, J-aggregates), for geometries with  $\theta > 54.7^\circ$ , the transition to the higher energy state is allowed (hypsochromically shifted absorption band, H-aggregates).  $\Delta E_{vdW}$  = difference in van der Waals interaction energies between ground and excited states. Figure redrawn based on reference.<sup>[43]</sup>

Later, Kasha used the molecular exciton coupling theory, i.e. the coupling of the transition moments of two dye molecules, to rationalize these experimental findings (Figure 5B).<sup>[43]</sup> He differentiated between parallel aligned transition dipoles, in-line transition dipoles, co-planar transition dipoles, oblique transition dipoles and non-planar transition dipoles. In these categories, J-aggregates would correspond to the in-line case, whereas H-aggregates would correspond to the parallel case. Both can be categorized as co-planar transition dipoles and are therefore interconnected by the slip angle  $\theta$  according to the formula and the depiction given on the right

side of Figure 5B. Due to the exciton coupling interaction of two monomers, the energy level of the excited state is separated in two energetically states. One higher, and the other one lower in energy, compared to the energy level of the excited monomer. For geometries where  $\theta < 54.7^\circ$ , the transition to the lower energy state is allowed (bathochromically shifted absorption band, J-aggregates), for geometries with  $\theta > 54.7^\circ$ , the transition to the higher energy state is allowed (hypsochromically shifted absorption band, H-aggregates).

However, fluorescence typically progresses from the lowest excited state according to the Kasha-Vavilov rule (see section 2.2.1). Therefore, the energetic state, which is higher in energy and exclusively populated in H-aggregates, often relaxes non-radiatively through intersystem-crossing. That is why H-aggregates are usually non-emissive. The opposite case (excitation to the lower energetic dimer level) rationalizes the observed strong emission of J-aggregates. Numerous examples which fit into the H and J model are known.<sup>[44]</sup> Still, the model does not account for the vibronic fine structure present in many aggregates, and only considers “through space” coulomb interactions, thereby neglecting short-range wave function overlap and intermolecular charge transfer.<sup>[45]</sup> Therefore, it is not surprising that there are several publications of non-Kasha aggregates, e.g. fluorescent H-aggregates.<sup>[46]</sup> Refining Kasha’s theory by the consideration of both, long-range coulomb interaction and short-range wave function overlap, can rationalize these experimental findings.<sup>[45, 47]</sup>

## 2.3 General Relations Between Molecular Structure and Emissive Properties

### 2.3.1 The $\pi$ -system: red shift of absorption and emission

Applications of fluorophores, e.g. in OLEDs, sensors and in biomedicine, induce a steadily growing demand for new fluorophores in general, and red-emissive fluorophores particularly. Most of the common organic fluorophores possess a  $\pi$ -system. In orbital terms, absorption in the UV/Vis region is typically a  $\pi - \pi^*$  transition or a  $n - \pi^*$  transition. Therefore, one general strategy to induce a red shift of the absorption and emission bands is the extension of the  $\pi$ -system of a compound. This reduces the energetic difference of the  $\pi$  and  $\pi^*$  orbital, and thereby the HOMO-LUMO gap.

A high absorbance and a high fluorescence quantum yield are prerequisites for the application of fluorophores. Thus, it is beneficial that the molar absorption coefficient as well as the fluorescence quantum yield are typically increasing with the size of the  $\pi$ -system. One great example for that behaviour are  $\alpha$ -oligothiophenes. Irrespective of the solvent, comparing the series of one to seven thiophene units, the absorption red shifts from about 230 nm to 441 nm, the extinction coefficient  $\epsilon$  rises from around  $8,000 \text{ M}^{-1} \text{ cm}^{-1}$  to  $50,000 \text{ M}^{-1} \text{ cm}^{-1}$ ,  $\Phi$  is increasing from 0 to about 0.32, and  $\tau$  increases from  $<0.1 \text{ ns}$  to about  $0.9 \text{ ns}$ .<sup>[48]</sup> Another example for that fundamental observation are linear aromatic hydrocarbons (Figure 6). Whereas benzene, naphthalene and anthracene absorb in the UV region, tetracene and pentacene absorb in the visible region. The fluorescence quantum yield increases from 0.05 for benzene to 0.27 for anthracene.<sup>[49]</sup> In 2009, the fluorescence quantum yield of a triisopropylsilylethynyl substituted pentacene molecule was measured to be 0.75.<sup>[50]</sup> The fact that triisopropylsilylethynyl substitution is necessary, exemplifies one of the major drawbacks of the extension of  $\pi$ -systems to induce a red shift of absorption and emission. The large planar  $\pi$ -system leads to low solubility and

those compounds are susceptible for  $\pi$ - $\pi$  stacking, an efficient fluorescence quenching process (see section 2.4.3). Furthermore, these bulky structures can modify the affinity for targets or interfere with metabolite traffic in cells due to their size, which makes them inapplicable in biomedicine.<sup>[51]</sup>

Of course, some of these problems can be circumvented by bulky substituents as shown for the pentacene derivative, hexacenes<sup>[52]</sup> or for perylenes.<sup>[53]</sup> However, the introduction of bulky substituents makes the sometimes complex synthesis and purification of those compounds even more tedious. That is a major drawback when it comes to the idea of quickly synthesizing a row of derivatives for the deeper understanding of their (photophysical) properties.

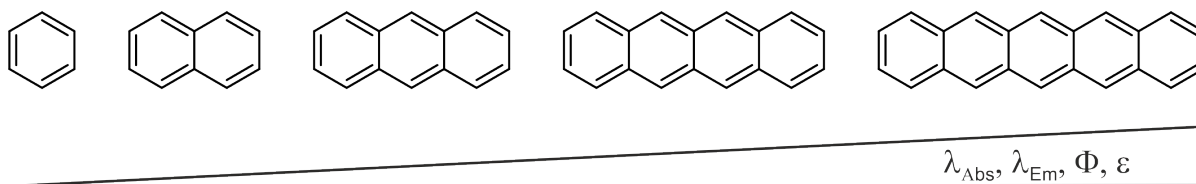


Figure 6: With increasing size of the  $\pi$ -system, the absorption wavelength ( $\lambda_{\text{Abs}}$ ), emission wavelength ( $\lambda_{\text{Em}}$ ), fluorescence quantum yield ( $\Phi$ ) and the molar absorption coefficient ( $\epsilon$ ) of linear hydrocarbons increase. From left to right: benzene, naphthalene, anthracene, tetracene and pentacene.

Therefore, small organic fluorophores with a few steps, simple synthesis and absorption and emission in the Vis region are in high demand. Instead of using the extension of the  $\pi$ -system for the red shift of the absorption and emission bands, donor-acceptor frameworks on small aromatic units can be employed. In recent years, numerous highly emissive fluorophores with a single benzene skeleton have been introduced.<sup>[54]</sup> The emissive properties of such compounds are due to their charge distributions responsive to the change of the microenvironment, e.g. solvent polarity, and are thus interesting for sensory applications.

### 2.3.2 The effect of heteroatoms on the emissive properties of $\pi$ -systems

When one carbon atom in the aromatic system is replaced by a heteroatom, a  $n - \pi^*$  transition might replace the  $\pi - \pi^*$  transition as the lowest lying transition. That reduces the molar absorption coefficient and enlarges the natural fluorescent lifetime drastically. Therefore, competing non-radiative relaxation will reduce the emission.<sup>[19b]</sup>

This effect can also be observed for heteroatom substituents on the aromatic system. In these cases, it depends if and how the lone pair of the heteroatom interacts with the aromatic system. If the substituents are heavy atoms, e.g. bromine or iodine, the fluorescence is reduced due to intersystem crossing (see section 2.4.2). It should be denoted that in general and especially with heteroatoms, even a minor change in polarity and/or

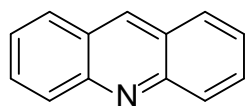


Figure 7: Molecular structure of acridine.

hydrogen bonding capacity of the solvent is able to shift energy levels of the orbitals so that quenching might occur. One example for this effect are acridines (Figure 7). Acridines dissolved in methanol have a ten-fold higher fluorescence quantum yield compared to solutions of acridines in *n*-hexane.<sup>[55]</sup> However, the introduction of heteroatoms in and on an aromatic system can be used to alter the electronic structure

in the ground and the excited state, and thus influence the fluorescence properties immensely. Numerous classes of fluorophores with one, two or more heteroatoms showcase that (see section 2.5). Nevertheless, some

functional groups, e.g.  $-\text{NO}_2$ , are generally known to alleviate intersystem crossing and thus enable phosphorescence instead of fluorescence.<sup>[19b]</sup> However, general statements which functional groups lead to increased or decreased fluorescence should be handled with caution.

## 2.4 Fluorescence Quenching

To design fluorescent compounds, one has to be aware of possible fluorescence quenching mechanisms. The absence of those will lead to strong fluorescence. When fluorescence quenching is discussed, a first separation between intermolecular and intramolecular quenching must be made. Intermolecular quenching can be a collision with other species, the formation of excited dimers (excimer) or an excited complex (exciplex). Furthermore, electron, proton, or energy transfer are intermolecular quenching mechanisms. Proton transfer will only work with a respective acid or base in close vicinity to the excited compound. Energy and electron transfer typically need an acceptor of the respective format of energy. These processes are concentration dependent and categorized furthermore into dynamic quenching, if the process is diffusion controlled, or static quenching. Therefore, fluorescence quenching is regularly used as the underlying principle of sensor applications with fluorophores. Furthermore, differentiation between types of quenching can yield information about the molecular system, for instance, the distance between compounds or molecular motifs. Regarding intermolecular quenching, the focus in this thesis will be on self-quenching of fluorophores described in 2.4.3.

Intramolecular quenching typically progresses through a combination of internal rotations, internal conversion (IC) and intersystem crossing (ISC). Internal conversion is one fundamental way of fluorescence quenching. However, it is very inefficient for the  $S_1$ - $S_0$  transition, due to the large  $S_1$ - $S_0$  energy gap, at least compared to the  $S_2$ - $S_1$  transition.

### 2.4.1 Fluorescence quenching by internal rotations

Internal rotations are efficient non-radiative relaxation pathways, as the comparison of rhodamine B and rhodamine 101 shows (Figure 8). Fixing both amine moieties through julolidyl rings increases the quantum yield in ethanol from 0.65 for rhodamine B to 0.95 for rhodamine 101.<sup>[56]</sup> If the emissive unit is unaffected by the rotation, as it is for the benzoic acid group in rhodamines and fluoresceins, the fluorescence can be strong despite of internal rotations.

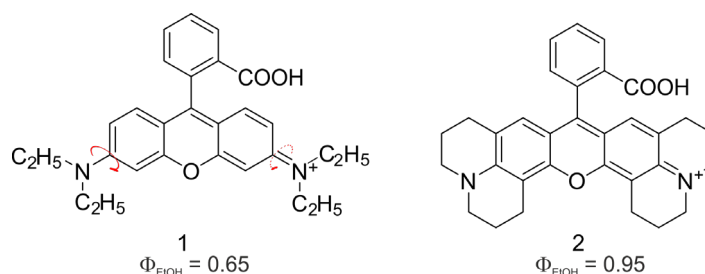


Figure 8: Structures of rhodamine B (1) and rhodamine 101 (2). Blocking the rotations around the C-N bond (red arrows) by the fixation of both amine moieties in rhodamine 101 increases the fluorescence quantum yield in ethanol from 0.65 for rhodamine B to 0.95 for rhodamine 101.<sup>[56]</sup>

However, internal rotations can affect the emissive properties of fluorophores drastically and even lead to polarity dependent second emission bands. In Figure 9, examples for that phenomena are depicted. 4-*N,N*-dimethylaminobenzonitrile (DMABN) was intensively studied as it shows two emission bands in polar solvents and has a simple structure.<sup>[37c, 57]</sup> In its ground state, DMABN is planar. Upon excitation, the dipole moment of DMABN is drastically increased due to its push-pull character. Therefore, the Frank-Condon state, sometimes referred to as the locally excited (LE) state, is not in equilibrium with the surrounding solvent molecules. As described in section 2.2.4, if the fluorescence lifetime of the excited state is sufficiently long, the solvent molecules will reorientate and stabilize another, energetically relaxed state, the so-called intramolecular charge transfer (ICT) state. This leads to a polarity dependent shift of emission, which can be used for polarity probes. If rotations are possible in that ICT state, as for DMABN, another state, the twisted intramolecular charge transfer (TICT) state can be reached and induce a second, red shifted emission band or shoulder to the LE band. That is proven by the absence of the TICT band in compound 2 (Figure 9), where the rotation of the amine is hindered, as was done in rhodamine 101 by a julolidyl moiety.

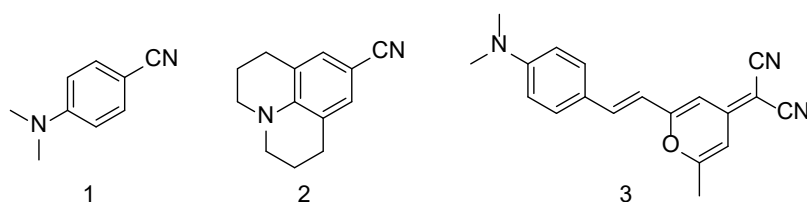


Figure 9: Structures of 4-*N,N*-dimethylaminobenzonitrile (1, DMABN) which shows two emissions bands in polar solvents. In molecule 2, which is closely related to DMABN, the rotation of the amine group is hindered by the julolidyl ring. The compound shows only one emission band. Structure 3 is the merocyanine 4-dicyanomethylene-2-methyl-6-(*p*-dimethylamino-styryl)-4-pyran, where photoisomerization influences the emission properties.

Due to the structural simplicity of DMABN, the interplay of LE and TICT state, is relatively easy to understand. In other commonly used dyes, for example the class of merocyanines, the influence of the TICT state is much harder to elucidate, as rotations around multiple bonds are possible. Furthermore, other effects, in the case of 4-dicyanomethylene-2-methyl-6-(*p*-dimethylamino-styryl)-4-pyran (Figure 9, structure 3) photoisomerization, influences the emission properties.<sup>[19b]</sup>

#### 2.4.2 Intersystem crossing (ISC)

If a vibronically relaxed, but electronically excited fluorophore in its  $S_1$  state undergoes a non-radiative transition to an isoenergetic vibrational level of a triplet state (T), that is called intersystem crossing. In principle, transitions between states of different multiplicity are spin-forbidden. Nevertheless, with times of about  $10^{-8}$  s, ISC is fast enough to effectively depopulate the  $S_1$  state and thus quench fluorescence. Vibrational relaxation will then lead to the lowest vibrational level of  $T_1$ . From there, the fluorophore will either phosphoresce or relax in a non-radiative fashion.

Typically, this non-radiative relaxation pathway is the interaction with the ubiquitous diradical dioxygen. That is the main reason why organic molecules in solution and at room temperature rarely phosphoresce. Degassed, oxygen free solutions of some fluorophores are known to show phosphorescence. Examples are the



phosphorescence of fluoranthenes at 77 K,<sup>[58]</sup> or thiocarbonyl heterocycles. The latter were found to be phosphorescent even at room temperature.<sup>[59]</sup>

The efficiency of ISC is increased if any of the following conditions are fulfilled:

- Spin-orbit coupling (coupling between the orbital magnetic moment and the spin magnetic moment).
- The involved singlet and triplet states belong to different electronic configurations, e.g.  $^1(n, \pi^*) \rightarrow ^3(\pi, \pi^*)$ , known as El-Sayed rule.<sup>[60]</sup>
- The energy between the involved electronic states is low, sometimes referred to as the energy gap law.<sup>[19b]</sup>

Spin orbit coupling is mostly observed in the presence of heavy atoms, e.g. Br or Pb. As an example, the fluorescence quantum yield of naphthalene in a rigid matrix is 0.55, the phosphorescence quantum yield is 0.051. For 1-bromonaphthalene in the same matrix, the fluorescence quantum yield is 0.0026, basically absent, but the phosphorescence quantum yield is 0.27.<sup>[61]</sup>

Besides spin-orbit coupling, especially through the heavy atom effect, benzophenone, as one extensively studied example of low temperature (77 K) phosphorescence, exemplifies the other two conditions and helps to understand fluorescence quenching. As visible from its Perrin-Jablonski diagram (Figure 10), the energy gap  $S_1-T_2$  is relatively small. Furthermore, it is an  $^1(n, \pi^*) \rightarrow ^3(\pi, \pi^*)$  transition which is allowed according to the El-Sayed rule. The fact that benzophenone encounters an internal conversion from  $T_2$  to  $T_1$ , the latter being a  $(n, \pi^*)$  state is the reason why benzophenone has both, a high phosphorescence quantum yield (= 0.90), and long lifetime ( $6 \times 10^{-3}$  s) of its excited state.<sup>[61]</sup>

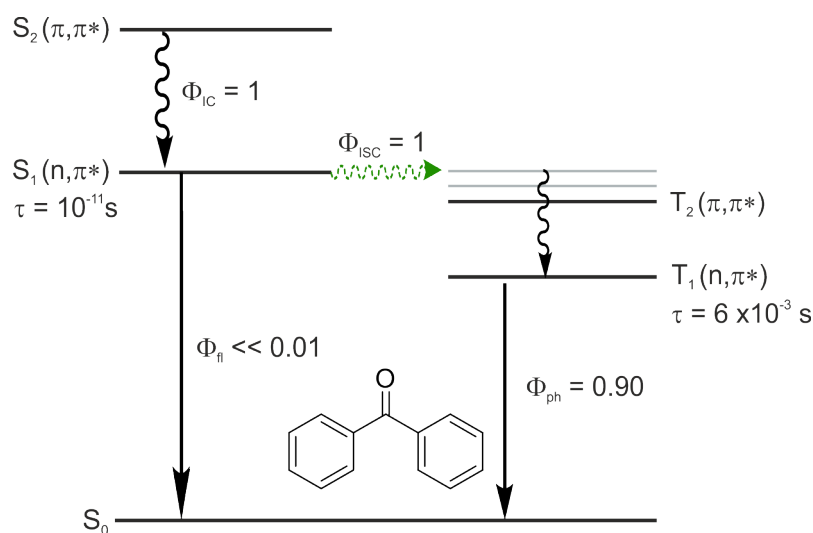


Figure 10: Schematic Perrin-Jablonski diagram for benzophenone in a rigid matrix at 77 K. The solid straight lines show emissive processes, fluorescence (fl) or phosphorescence (ph). The, according to the El-Sayed rule allowed transition, an ISC with a quantum yield of 1, is marked green. IC = internal conversion, ISC = intersystem crossing. n and  $\pi$  denote the respective orbitals. All values were taken from reference.<sup>[61]</sup>

Just as for benzophenone, the phosphorescence of other organic compounds, e.g. fluorescein<sup>[62]</sup> or fluoranthene,<sup>[58]</sup> in cooled solvents, reaching a rigid glassy state, has been shown. The cooling is shifting energy orbital levels to a favourable state for ISC. As bright phosphorescence with a long lifetime or dual emission

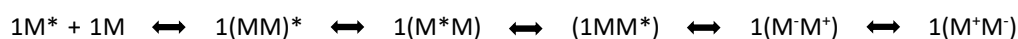
(fluorescence and phosphorescence) are desired for applications like OLEDs, numerous other ways have been found to fulfil the above-mentioned conditions. Examples are crystallization<sup>[63]</sup>, polymer matrices containing donor-acceptor compounds<sup>[64]</sup>, aggregation<sup>[65]</sup> and of course the heavy atom effect, for instance in tungsten complexes.<sup>[66]</sup>

At the same time, these investigations shed light on the relationship between molecular structure and undesired fluorescence quenching via ISC. Therefore, intersection of singlet and triplet states, their orbital states and relative energies must be considered when strong (or weak) fluorescence is desired or rationalized.

### 2.4.3 Fluorescence quenching caused by aggregation

In 1955, Förster and Kasper, investigated the concentration dependence of the absorption and emission spectra of pyrene and coined the term “excimer” for excited state dimer.<sup>[67]</sup> By the variation of the pyrene concentration between  $10^{-4}$  mol/L and  $10^{-2}$  mol/L, they observed that: a) the absorbance is concentration independent, b) the intensity of emission at about 380 nm is decreasing with increasing concentration and c) a new emission band at 470 nm arises with increasing concentration.<sup>[20a]</sup> Through measurements in solvents of different viscosity, they clarified that the formation of the excimer is a dynamic process. For instance, the half value concentration (concentration where  $\Phi_{\text{Monomer}} = \Phi_{\text{Excimer}}$ ) is increasing from  $0.3 \times 10^{-3}$  mol/L in non-viscous pentane (0.23 cP) to  $1.2 \times 10^{-2}$  mol/L in viscous paraffin oil (12.8 cP). The excimer formation in pyrene leads to a new emissive band, as such an early example of aggregation induced emission (AIE). Today, excimer formation (of pyrene) found its way into numerous applications.<sup>[68]</sup> However, it remains as a persistent and efficient pathway of fluorescence quenching in molecular compounds with a large planar system, e.g. poly aromatic hydrocarbons (PAH), as well as polymers.<sup>[19b, 69]</sup>

The principle of excimer formation can be formulated in the following way:



In short, an excited molecule  $1M^*$  forms a complex with an unexcited molecule  $1M$  which leads to an excited dimer  $1(MM)^*$ . That excited dimer can be expressed in different forms due to electron resonance. Just as multiple mesomeric structures are an indication for high molecular stability, the excimer is stabilized through that resonance. Stabilization of an excited state is, as outlined before, often disadvantageous for the emissive properties. The reason are non-radiative processes which lead to non-radiative relaxation. For an excimer, three non-radiative pathways are imaginable:



It requires extensive experimental and/or theoretical work to figure out which of the three pathways are the main cause of fluorescence quenching. Nevertheless, a real photodimer could probably be spotted as a new species through mass spectrometry or even NMR spectroscopy. ISC, leading to a triplet state ( $3D^*$ ) would be more likely with heavy atoms, like bromine or iodine as substituents and could be spotted by delayed

fluorescence or phosphorescence bands. As one example of such procedure, Dempster and Chandross investigated the excimer formation of naphthalene compounds extensively.<sup>[70]</sup> They were able to isolate a real photodimer and used temperature dependent measurements to calculate the activation barrier for the quenching of the different naphthalene dimers. As excimer formation requires contact of two molecules in form of their electronic structure, it is a short range interaction. Typical distance are 3 Å to maximal 6-7 Å.<sup>[20a, 69b-d]</sup> However, at such distances and parallel molecular orientation, repulsion (Pauli exchange repulsion) of the filled  $\pi$ -orbitals should be strong. Theoretical studies using experimental data showed by the comparison of saturated and unsaturated hydrocarbons of the same size, that the strength of the dispersion forces become significant at 10-15 carbon atoms.<sup>[71]</sup> Furthermore, the attractive forces will overcome the repulsive ones, only in a stacked arrangement with a parallel displacement, to minimize unfavourable electrostatic effects. Today, fluorescence quenching through excimer formation, sometimes also referred to as  $\pi$ - $\pi$  quenching, is overcome synthetically by bulky substituents or in some cases even used to induce another emissive band, which stems from emissive aggregates.<sup>[53, 72]</sup>

## 2.5 Classes of Fluorophores: Classic Examples and Recent Approaches

As outlined in the introduction, the targeted synthesis of fluorescent organic compounds has started in the 19<sup>th</sup> century. Since then, numerous classes of compounds were found to be fluorescent and to possess interesting photophysical properties of which some recent examples will be presented in the following section. Those are separated in poly aromatic hydrocarbon (PAH) based compounds and small organic compounds, with mainly a single substituted benzene ring in the fluorescent motif. Beside those organic fluorophores, inorganic compounds, organometallic complexes, stained glasses, quantum dots and many more fluorescent materials exist.

### 2.5.1 Coumarins and Rhodamines – established fluorophores

Coumarin (Figure 11, structure 1) was first isolated in 1820 from the tonka bean and synthesized by William Henry Perkin in 1868.<sup>[73]</sup> Today, coumarins are, together with rhodamines, the most commonly used dyes in dye lasers.<sup>[74]</sup> Coumarin itself is poorly fluorescent, but introducing a hydroxy group yields Umbelliferone (Figure 11, structure 2), which has, compared to coumarin, a drastically increased quantum yield and is pH-sensitive.<sup>[75]</sup> Replacing the hydroxy group by an amine group yields coumarins which can undergo a photoinduced charge-transfer (Figure 11, structures 3 - 3') due to their conjugation between an electron donating (amine) and an electron withdrawing group (carbonyl). These compounds are even more sensitive to changes in the microenvironment, e.g. solvent polarity, due to their push-pull system.<sup>[76]</sup>

Two common classes of fluorophores with long-standing history and numerous applications, rhodamines and fluoresceins, are both derivatives of oxa-anthracene, also called xanthene (Figure 11, structure 4). Rhodamines are cationic compounds with two amines on the xanthene core and typically emit between 500 and 700 nm. Rhodamine 6G (Figure 11, structure 5) for example has a high photostability and high fluorescence quantum yield of 0.95 and is thus used in numerous applications.<sup>[56b]</sup> Fluorescein (Figure 11, structure 6), first synthesized

by Adolf von Baeyer in 1871,<sup>[77]</sup> and its derivatives, e.g. the regularly used Eosin Y (Figure 11, structure 7), show a pH-dependent emission.<sup>[78]</sup> The highly emissive state of fluorescein is generally reached after twofold deprotonation of the carboxylic acid and the hydroxyl group respectively.

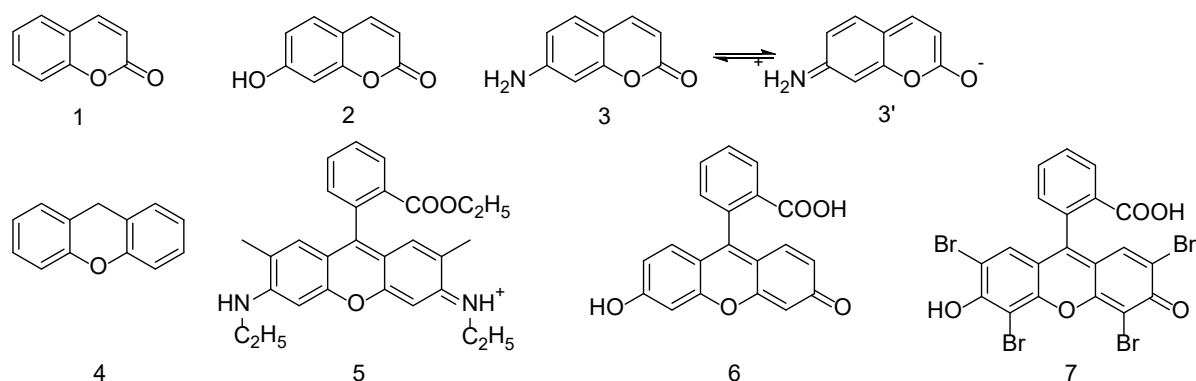


Figure 11: Chemical structures of coumarin (1), coumarin derivative umbelliferone (2), the mesomeric structures of an amine-substituted coumarin (3), xanthene (4), rhodamine 6G (5), fluorescein (6) and eosin Y (7).

### 2.5.2 Polycyclic Aromatic Hydrocarbons (PAHs) as fluorophores

PAHs are co-products of all kind of natural and men-made thermal decompositions, wildfires, fuel engines, and burning cigarettes, but they are also found in natural resources like coal and oil.<sup>[79]</sup> As they are relatively toxic and highly carcinogenic<sup>[80]</sup> they are labelled as waste products, environmental pollutants and health threats. In research, the perception of these versatile compounds is quite the opposite. PAH and their properties, which result from their large aromatic system, are investigated for their use in optical and electronic applications,<sup>[81]</sup> self-assembly,<sup>[81b, 82]</sup> surface functionalisation,<sup>[83]</sup> the bottom-up synthesis of graphene,<sup>[84]</sup> polymer electrolyte membrane fuel cells (PEMFC),<sup>[85]</sup> as active components in OLEDs<sup>[14a, 14b, 86]</sup> and as chemosensors.<sup>[87]</sup> Some of the manifold subclasses of PAHs are presented in Figure 12.

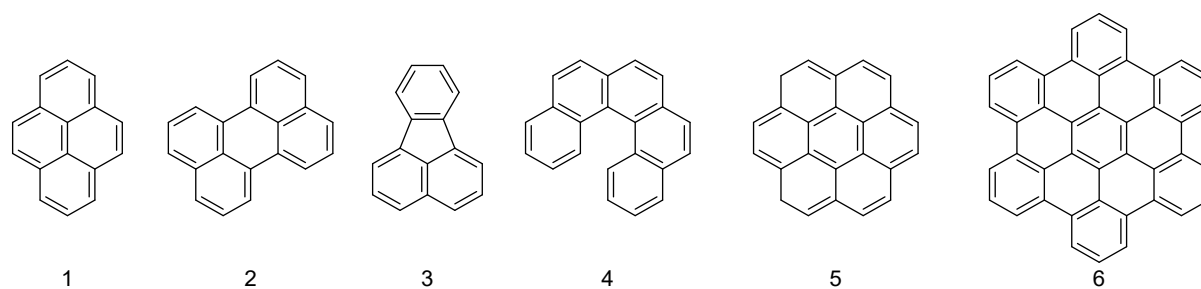


Figure 12: Subclasses of polycyclic hydrocarbons. Pyrene (1), perylene (2), fluoranthene (3), helicene (4), coronene (5) and hexabenzocoronene (6).

It is difficult to summarize the synthesis of these subclasses briefly, as most of the synthetic routes use a plethora of C-C bond forming reactions, e.g. metal catalysed coupling reactions like the Suzuki- or Sonogashira-coupling, Diels-Alder reaction, oxidations/dehydrogenations under harsh conditions or cycloadditions. The synthesis of a hexabenzocoronene (HBC) derivative, depicted in Figure 13, illustrates that fact.

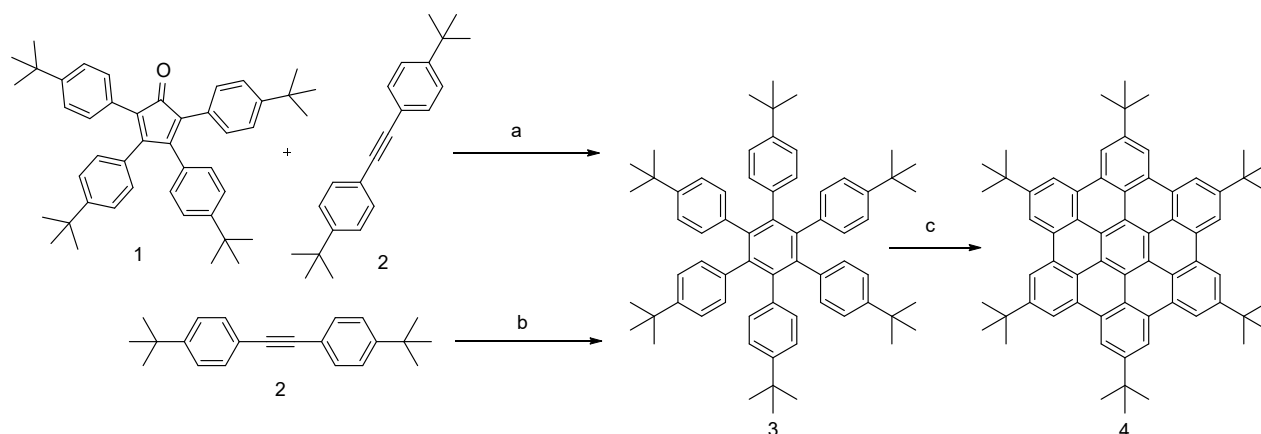


Figure 13: Different synthetic routes to a hexabenzocoronene derivative. a) Diels-Alder reaction of a cyclopentadienone 1 and a diphenyl alkyne 2 in diphenylether, yield = 50 % b) Cyclotrimerization of diphenylalkyne 2 with  $\text{Co}_2(\text{CO})_8$  as catalyst in dioxane, yield = 90 %.<sup>[88]</sup> c) Scholl oxidation of hexaphenylbenzene derivative 3 with  $\text{FeCl}_3$  in dichloromethane and nitromethane to yield hexabenzocoronene 4, yield = 75 %.<sup>[89]</sup>

The typical final step towards HBCs is a Scholl oxidation which leads to the formation of six C-C bonds. In that case, treatment of hexaphenylbenzene (HPB) 3 with ferric chloride in dichloromethane and nitromethane yielded the well soluble HBC derivative 4 (Figure 13) in a yield of 75 %.<sup>[89]</sup> HPB 3 can be synthesized in different ways. Route "a" in Figure 13 is a Diels-Alder reaction between cyclopentadienone 1 and diphenyl alkyne 2 with a yield of 50 %. Diphenyl alkyne 2 can also be used in a cyclotrimerization reaction to obtain 3 with a yield of 90 %, using  $\text{Co}_2(\text{CO})_8$  as catalyst.<sup>[88]</sup> Whereas the cyclotrimerization reaction is the efficient way to symmetrically substituted HBCs, route "a" gives the possibility to synthesize unsymmetrically substituted HPBs and HBCs.<sup>[90]</sup> Metal-catalyzed C-C couplings are employed to yield complex, unsymmetrical HPB and HBC compounds.<sup>[91]</sup>

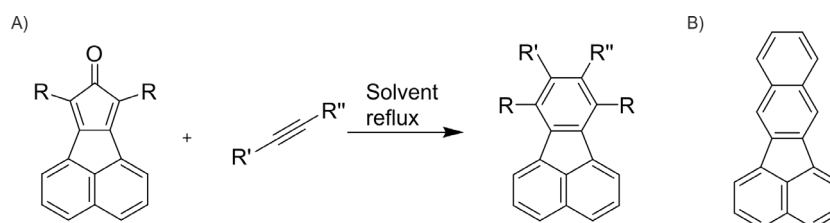


Figure 14: A) Diels-Alder reaction of a disubstituted cyclopentadienone with an unsymmetrical alkyne to substituted fluoranthene-derivative. B) Structure of benzo(k)fluoranthene which has a fluorescence quantum yield reaching unity in *n*-heptane.<sup>[92]</sup>

One synthetic route to the fluoranthene motif employs the Diels-Alder reaction as the key step (Figure 14A). By the use of unsymmetrical cyclopentadienones and unsymmetrical alkynes, the substitution pattern on the fluoranthene can be varied. The class of fluoranthene hosts one example of a highly fluorescent, unsubstituted PAH: Benzo(k)fluoranthene (Figure 14B), which is reported with a fluorescence quantum yield reaching unity in *n*-heptane.<sup>[92]</sup> However, most unsubstituted PAHs, especially bigger ones, face solubility and aggregation issues, which often lead to fluorescence quenching.

Therefore, tedious, synthetic strategies have been employed over the past decades to yield highly fluorescent PAHs.<sup>[53, 93]</sup> It should be noted that many of these compounds are in a strict sense no longer PAHs, as they

incorporate heteroatoms. Nevertheless, the PAH core unit is most of the time preserved. Two recent exemplary PAHs with impressive photophysical properties are depicted in Figure 15.

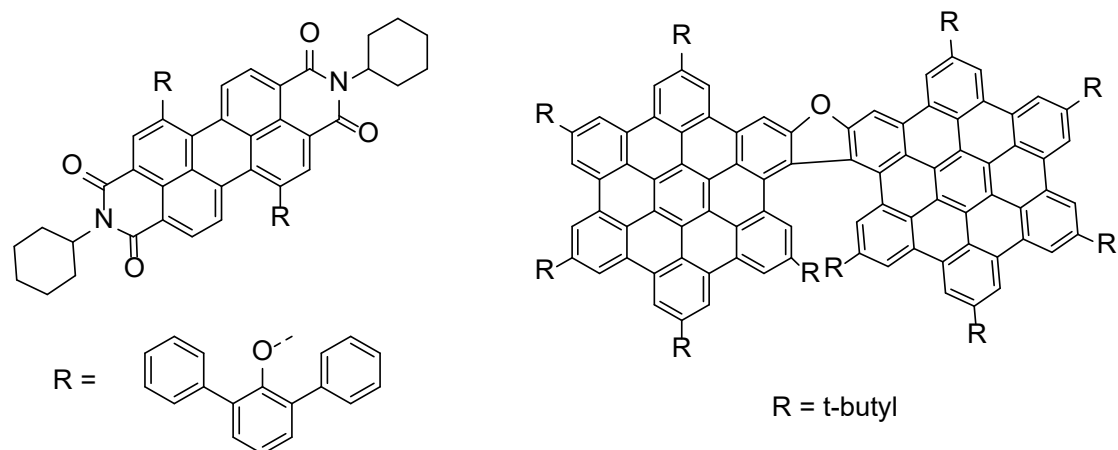


Figure 15: Two highly fluorescent PAH derivatives. Left side: Substituted perylene derivative with a fluorescence quantum yield of 0.99 in the solid state.<sup>[53]</sup> Right side: “Super-helicene” connecting two hexabenzocoronene (HBC) moieties with a [7]oxahelicene. The fluorescence quantum yield exceeds 0.80.<sup>[93a]</sup>

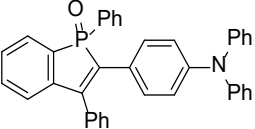
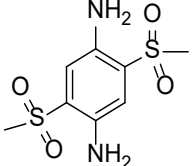
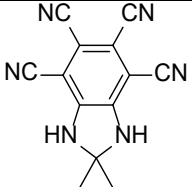
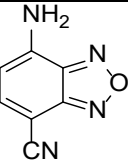
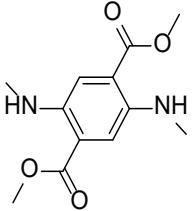
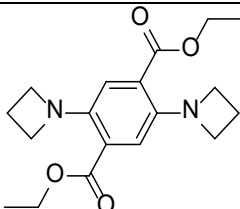
The perylene derivative on the left side (Figure 15), published by Würthner *et al.* in 2012,<sup>[53]</sup> was equipped with bulky triphenyl groups on the perylene core to prevent  $\pi$ - $\pi$  stacking in the solid state. The impressive fluorescence quantum yield of 0.99 in the solid state shows how efficient perylenes fluoresce, once the main relaxation pathway is blocked. On the right side, a “super-helicene”, published by Jux *et al.* in 2018, is depicted.<sup>[93a]</sup> Two flat HBC moieties are substituted with *tert*-butyl groups and connected via a [7]oxahelicene. In that way,  $\pi$ - $\pi$  stacking is prevented by increased solubility through the *tert*-butyl groups and immense space requirement of the rigid structure. The compound absorbs light from 300 nm to 540 nm and shows an emission band with two maxima between 490 and 670 nm. The fluorescence quantum yield exceeds 0.80.

In conclusion, strong fluorescence of PAHs can be achieved by different strategies. Preventing  $\pi$ - $\pi$  stacking by bulky substituents or non-planarity, or the introduction of heteroatoms, such as oxygen, nitrogen, phosphorus or sulfur, are some examples.<sup>[53, 93a, 94]</sup> However, these measures are often synthetically demanding, and it is furthermore hard to predict photophysical properties of the compounds before synthesis by theoretical means.<sup>[95]</sup> That is why the demand for synthetically, easy accessible fluorophores is constantly rising. Some recent examples for such compounds will be presented in the next section.

### 2.5.3 Small organic fluorophores with one benzene unit

Organic donor-acceptor compounds have been researched for their use in nonlinear optics,<sup>[2a, 96]</sup> solar cells,<sup>[97]</sup> light switches,<sup>[98]</sup> sensors,<sup>[54b, 99]</sup> and bioimaging.<sup>[54a]</sup> Some recent examples and their photophysical properties are summarized in Table 3. One striking similarity in all of these publications is that all of them synthesized a row of similar molecules, with only minor changes in substitution, to gain a deeper understanding of the fluorescence phenomena. That is possible due to the mostly short synthesis and simple purification procedure of those compounds. Thus, familiar compounds can easily be designed and fit to applications.

Table 3: Overview of recently published small organic donor-acceptor fluorophores and their photophysical data. The absorption, emission, fluorescence quantum yield  $\Phi$  and fluorescence lifetime  $\tau$  are given in ranges because all compounds, except entry 3, where investigated in different solvents and exhibit solvatochromism. The table was adapted from reference [34] and extended.

Entry	Structure	$\lambda_{\text{Abs}}^{\text{Range}}$ [nm]	$\lambda_{\text{Em}}^{\text{Range}}$ [nm]	$\Phi$	$\tau$ [ns]	Reference
1		403-420	528-601	0.58-0.94	5.2-7.3	<i>Angew. Chem. Int. Ed.</i> , 2015, <b>54</b> , 4539-4543.
2		377-394	490(477) <sup>a</sup> - 517	0.47-0.70	n.a.	<i>Angew. Chem. Int. Ed.</i> , 2015, <b>54</b> , 7332-7335.
3		380	445	0.41	n.a.	<i>Angew. Chem. Int. Ed.</i> , 2016, <b>55</b> , 3220-3223.
4		397-430	522-612	0.00-0.33	n.a.	<i>J. Org. Chem.</i> , 2017, <b>82</b> , 8842-8847
5		479-488	585-601 (620) <sup>a</sup>	0.25-0.33	7.6-8.2	<i>Angew. Chem. Int. Ed.</i> , 2017, <b>56</b> , 12543-12547.
6		398-412	542-610	0.21-0.95	5.01- 17.72	<i>Chem. Eur. J.</i> , 2019, <b>25</b> , 16732-16739.

For instance, the benzophosphole oxide derivative in entry 1<sup>[54a]</sup> of Table 3 was prepared in a two-step process and compared to four closely related derivatives with varied donor-acceptor moieties. The depicted benzophosphole oxide has high quantum yields of 0.58 in polar ethanol to 0.94 in apolar toluene. In addition, the benzophosphole shows positive solvatochromism following the Lippert-Mataga model. Varying the donor and acceptor moieties, and in combination with time dependent-density functional theory (TD-DFT) calculations,

the authors unravel why the other synthesized derivatives are less fluorescent or show weaker solvatochromism. For instance, the  $S_0$ - $S_1$  transition in the depicted compound has ICT character, whereas the  $S_0$ - $S_1$  transition in a related compound (-OMe instead of -NPh<sub>2</sub> as electron donor) features a  $\pi$ - $\pi$  transition with a drastically reduced ( $1.87 \times 10^{-4} \text{ M}^{-1}\text{cm}^{-1}$  vs.  $1.03 \times 10^{-4} \text{ M}^{-1}\text{cm}^{-1}$ ) molar extinction coefficient. The benzophosphole, with its advantageous characteristics, was then tested for its application in cell imaging.

Just as the benzophosphole, the emission of the sulfonylaniline-based compound<sup>[54b]</sup> (Table 3, entry 2) is environment/polarity sensitive and furthermore, as it is, well soluble in water, pH-sensitive. It was synthesized in four steps with an overall yield of 62 % and no column chromatography was required for the purification of any intermediate or the product. Besides its water-solubility, it is also soluble in polar organic solvents, with THF being the least polar. Featuring a positive solvatochromism, it has a maximal Stokes shift of 140 nm in water. It has high (0.51-0.70) fluorescence quantum yields in solution and a fluorescence quantum yield of 0.69 in the solid state, owing to intra- and intermolecular hydrogen bonding, which prevent  $\pi$ - $\pi$  stacking.

The tetracyanated dihydrobenzimidazoles (Table 3, entry 3) published by the group of Klaus Müllen in 2016,<sup>[37b]</sup> has an dipole moment of over 10 D and a fluorescence quantum yield of 0.41. Even though the focus was on the measurement and calculation of the dipole moment, it is very likely that the compound would show solvatochromism as well as other solvent dependent effects.

Benzo(heteroatom)diazoles are a class of known fluorophores, with benzothiadiazoles and benzooxadiazoles being sub-classes. In entry 4, a small push-pull benzooxadiazole is depicted.<sup>[40]</sup> It exhibits solvent dependent fluorescence quantum yields of basically 0 in water and over 0.30 in apolar hexane. Moreover, the compound shows positive solvatochromism, with a large Stokes shift of 182 nm in water. Thus, at least two measures, the fluorescence quantum yield and the emission wavelength, can be valuable in a potential polarity probe using that compound. The quenching of fluorescence of benzo(heteroatom)diazoles in polar solvents is attributed to the formation of a non-emissive ICT state in polar solvents. In apolar solvents, the emission stems from a locally excited (LE) state.<sup>[20a, 31a, 100]</sup>

The 2,5-bis(alkylamino)terephthalate (entry 5) is prepared from commercially available 1,4-cyclohexandione-2,5-dicarboxylate.<sup>[101]</sup> A condensation with methylamine and subsequent oxidation with Br<sub>2</sub> afforded the target compound in an overall yield of 48 % and without use of any column chromatography. It shows almost no sensitivity of fluorescence quantum yield (0.33 in toluene, 0.25 in DMSO) or fluorescence lifetime to solvent polarity and a very small positive solvatochromic effect with large Stokes shifts (Abs/Em in toluene: 488 nm/585 nm, Abs/Em in DMSO: 486 nm/601 nm). It must be mentioned that no protic solvents, which could form hydrogen bonds, were tested. The fact that absorption and emission are both in the visible region is remarkable for a compound with such a small  $\pi$ -system. In the solid state, the emission is red shifted, with a maximum at 620 nm, and the fluorescence quantum yield of 0.40. The fluorescence lifetime in the solid state is 12.3 ns. From the calculation of the radiative and non-radiative rates, the authors conclude that the suppression of the non-radiative rate is responsible for the increased values in the solid state, compared to the ones in solution. Again, a combined experimental-theoretical approach was used to understand these advantageous characteristics. The di-methylated compound, unable to form hydrogen bonds, was synthesized and crystallized.



Both in solution and the solid state, its emission is blue shifted compared to the non-methylated compound. The comparison of the crystal structures of these two compounds reveal improved planarization and negligible  $\pi$ - $\pi$  interaction, due to the strong intramolecular bonds, in the depicted compound. TD-DFT calculations revealed that the intramolecular hydrogen bonds lead to a higher HOMO level and thus a smaller band gap in the hydrogen bond forming compound. With this understanding and analysis, the authors were able to test the compounds' suitability for amplified spontaneous emission, a prerequisite for its use in organic lasers.

Last but not least, a structurally related compound to entry 5 is shown in entry 6. It is a symmetric single benzene based compound with two azetidinium and two ethoxycarbonyl moieties as electron donating and electron accepting groups.<sup>[34]</sup> Both, the high fluorescence quantum yield as well as the fluorescence lifetime are solvent dependent but show no proportionality to solvent polarity. The values are maximal in DMSO, with a fluorescence quantum yield of 0.95 and 17.72 ns fluorescence lifetime, which is relatively long for small organic fluorophores. The compound has large Stokes shift, between 132 nm (*n*-hexane) to 207 nm (water), and exhibits a positive solvatochromism.

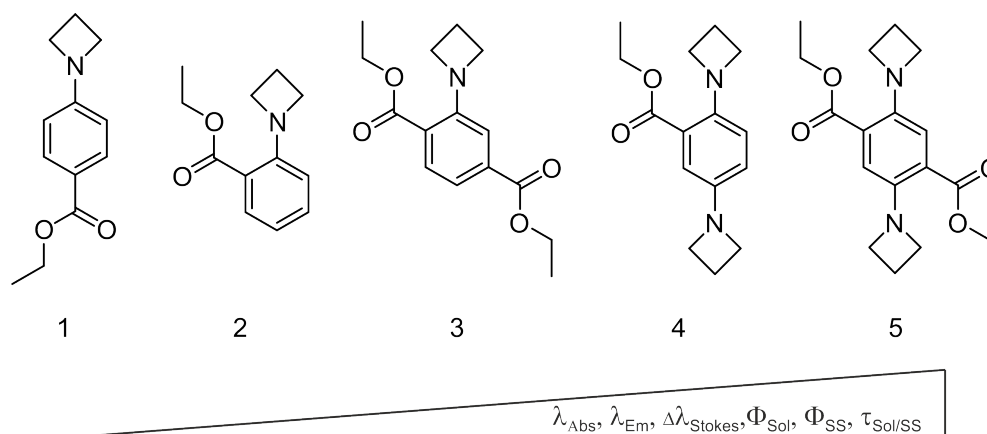


Figure 16: The five push-pull derivatives with varying substitution pattern of both electron-donating and accepting groups investigated by Ding *et al.*<sup>[34]</sup> The absorption wavelength ( $\lambda_{Abs}$ ), the emission wavelength ( $\lambda_{Em}$ ), the stokes shift ( $\Delta\lambda_{Stokes}$ ), the quantum yield in solution ( $\Phi_{Sol}$ ) and solid state ( $\Phi_{SS}$ ) as well as the fluorescence lifetime in solution and solid state ( $\tau_{Sol/SS}$ ) are increasing with increasing numbers of substituents on the benzene ring.

However, the major finding is the correlation of the photophysical properties with the substitution pattern of both, electron-donating and -accepting groups. Ding *et al.* compared the five compounds depicted in Figure 16. From compound 1, featuring a linear push-pull system, to compound 5, the absorption shifts from the UV at 305 nm to the visible region at 406 nm. The emission shifts from 350 nm (compound 1) to 566 nm (compound 5). That clearly illustrates a decreasing HOMO-LUMO gap with the increase of electron donor and accepting moieties on the benzene core unit. With TD-DFT calculations the authors show, that the change of dipole moment for compound 5 upon excitation is zero (for compound 1 it is 2.26 D). Therefore, they assessed the quadrupole moment. That can be expressed as two opposite dipoles separated by a distance  $d$ . For compound 5, the value of the change of quadrupole moment upon excitation was calculated to be 32 D Å. The change of dipole moment on one push-pull branch of the compound was estimated to be 5.0 D. Therefore, the strong solvent dependency is explained by the induced ICT state between each donor-acceptor pair. Besides, the solid state fluorescence quantum yield was found to reach unity for compound 5, indicating that non-radiative

relaxation pathways are completely blocked in the crystal material. This finding is explained by the ordered crystal structure, directed by O-H interactions between the aromatic hydrogens and the ethoxy group, as well as the  $\pi$ - $\pi$  distance of 5.35 Å.

That comparison of those recently published small fluorophores exemplifies how donor-acceptor substitution is used to yield compounds with desired photophysical characteristics. Polarity probes, cell imaging, amplified spontaneous emission, OLED materials or non-linear optics are applications where such molecules are needed. The combined experimental-theoretical approaches, which complement each other and thus lead to a deeper understanding, are possible because the size of such compounds makes theoretical calculations, and synthesis of slightly different substituted molecules feasible.

## 3 Synopsis of Results

### 3.1 Diaminodicyanoquinones

#### 3.1.1 A novel class of fluorescent dyes

P. Rietsch, F. Witte, S. Sobottka, G. Germer, A. Becker, A. Guttler, B. Sarkar, B. Paulus, U. Resch-Genger, and S. Eigler; Diaminodicyanoquinones: Fluorescent Dyes with High Dipole Moments and Electron-Acceptor Properties. <i>Angew. Chem. Int. Ed.</i> <b>2019</b> , <i>58</i> , 8235-8239.	4.1
--	-----

Compounds with high dipole moments are of general interest and can be applied in non-linear optics or controlled aggregation.<sup>[2a, 37b, 41b, 102]</sup> The class of diaminodicyanoquinones (DADQ), which possesses a strong electron push-pull system and therefore a high dipole moment, was first mentioned in 1962 by Acker *et al.*<sup>[1]</sup> Throughout the years, those compounds were investigated for their large dipole moment, as well as their photophysical properties.<sup>[2, 102-103]</sup> However, most derivatives have fluorescence quantum yield in solution ( $\Phi_{Sol}$ ) below 0.01, due to non-radiative relaxations of the excited state,<sup>[2b]</sup> and are only fluorescent in the solid state, with  $\Phi_{SS}$  of about 0.45.<sup>[2c]</sup>

A series of DADQ derivatives (Figure 17) was synthesized and revealed that benzene functionalized DADQs have high  $\Phi_{Sol}$  exceeding 0.90 (collaboration with Dr. Ute Resch-Genger). Through a combined experimental-theoretical approach (collaboration with Prof. Dr. Beate Paulus), we explain the strong fluorescence of benzene functionalized DADQs and investigate the processes which lead to fluorescence quenching in the non-fluorescent compounds. Internal conversion (IC) and intersystem crossing (ISC) are inhibited by relatively high rotational barriers in benzene-functionalized derivatives. Of particular importance to unravel the difference in fluorescence was the comparison of the highly fluorescent benzene functionalized compound **4** with: the ethylene-functionalized compound **1**, the cyclohexane functionalized compound **3** and the dimethylated benzene functionalized compound **7**, which all show only weak fluorescence.

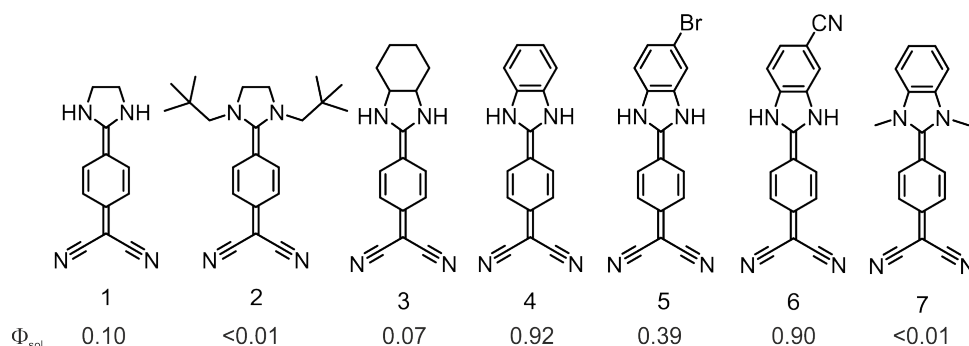


Figure 17: Structures of the investigated diaminodicyanoquinone (DADQ) derivatives **1-7** and their respective fluorescence quantum yields in dimethylsulfoxide.

The compounds were synthesized in a three-step procedure, starting by the activation of 7,7,8,8-tetracyanoquinodimethane with pyrrolidine to yield 7-pyrrolidino-7,8,8-tricyanoquinomethane (PTCNQ), a deep purple crystalline solid with no detectable fluorescence. The reaction of PTCNQ with the respective diamine yields compounds **1-7** in yields of 40-80 %. The photophysical properties were investigated in seven solvents of varying polarity, THF being the least polar and MeOH the most polar. Due to their high dipole ground state moment of about 30 D, the compounds are highly polar and thus face solubility issues. To circumvent aggregation effects, all measurements were done in concentrations of about  $5 \times 10^{-6}$  M or even less. The position of the  $S_0$ - $S_1$  absorption band depends on substitution and solvent and is located between 300 and 400 nm with molar extinction coefficients between  $20,000 \text{ M}^{-1} \text{ cm}^{-1}$  and  $60,000 \text{ M}^{-1} \text{ cm}^{-1}$ . The emission band is shifted by 40-90 nm, so that a blue emission can be seen by the naked eye. The solvatochromism (see section 2.2.4) of those compounds is interfered by non-covalent interactions, namely hydrogen bonding. In contrast to the benzothiadiazole derivatives described in section 3.2, which show a neat bathochromic shift, only of the emission spectra upon increasing solvent polarity, the absorption and the emission spectra of DADQ compounds show a hypsochromic shift upon increasing solvent polarity. As both, absorption and emission are blue shifting, the stokes shift has no clear trend. However, the blue shift indicates that the DADQs exhibit negative solvatochromism and our theoretical investigations confirm that the dipole moment decreases from about 30 D to about 22 D upon excitation. The  $\Phi_{Sol}$  are highly solvent dependent, with maximum values in DMSO of 0.92 for compound **4**. The fluorescence lifetimes of the emissive derivatives are maximal about 6 ns (**4** in acetonitrile) with most values around 2-3 ns. The radiative ( $k_r$ ) and non-radiative ( $k_{nr}$ ) rates of **4**, derived from the measured  $\Phi_{Sol}$  and  $\tau$  values (see section 2.2.3), shed light on the differences in emission, e.g. in MeOH ( $\Phi_{Sol} = 0.35$ ) vs. DMSO ( $\Phi_{Sol} = 0.92$ ). In MeOH,  $k_r$  is  $9.18 \text{ s}^{-1}$  and  $k_{nr}$  is  $17.1 \text{ s}^{-1}$ , giving a  $k_r/k_{nr}$  ratio of 0.54, whereas the ratio is 12 ( $k_r = 5.16 \text{ s}^{-1}$  and  $k_{nr} = 0.43 \text{ s}^{-1}$ ) in DMSO (all values  $\times 10^8$ ).

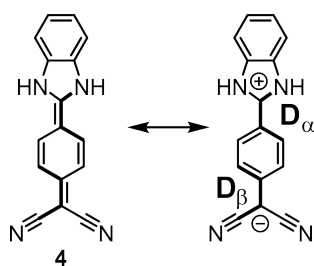


Figure 18: Mesomeric forms of benzene functionalized diaminodicyanoquinone derivative **4** and the definition of the dihedral angles  $D_\alpha$  and  $D_\beta$ .

The role of rotations was investigated experimentally by fluorescence measurements in solvent mixtures of varying viscosity (EtOH-PEG). The benzene functionalized compound **4** shows no increase of  $\Phi_{Sol}$  and  $\tau$  upon increasing viscosity.  $\Phi_{Sol}$  of the non-benzene functionalized compounds **1-3**, however, increases by a factor of three to seven, and  $\tau$  increases as well by a factor of 2 (compound **3**) to 6 (compound **2**), upon increasing viscosity. The same trend was observed for cooling between  $0^\circ \text{C}$  to  $-100^\circ \text{C}$ . The  $\Phi_{Sol}$  of **1-3** increases by about 20 times, whereas  $\Phi_{Sol}$  of **4** increases about seven times. The fluorescence lifetimes are generally following the trend of  $\Phi_{Sol}$ . Elevated temperature,  $40^\circ \text{C}$  to  $110^\circ \text{C}$ , leads to decreased emission in all compounds. These results

indicate that rotations around the two dihedral angles  $D_\alpha$  and  $D_\beta$  (Figure 18) play a major role to control the  $\Phi$  in DADQs.

The Paulus group used TD-DFT calculations at the CAM-B3LYP level with implicit and explicit solvent molecules.<sup>[104]</sup> Multireference states were accounted for by the DFT/MRCI (multi-reference configuration interaction) method with the orbital basis generated at the CPCM/BHLYP/def2-TZVP level.<sup>[105]</sup> The two dihedral angles  $D_\alpha$  and  $D_\beta$  were treated separately, as first calculations revealed their independence. Rotations are hindered in the ground state  $S_0$ , with rotational barriers about 60 kJ/mol. However, in the excited state  $S_1$ , rotational barriers around  $D_\beta$  of 12 kJ/mol for **1-3** to 25 kJ/mol for **4** and **7** were found. Vice versa, the opposite was found for  $D_\alpha$ . The orbital overlaps in the respective state,  $S_0$  and  $S_1$ , explain the difference in rotational barrier around  $D_\alpha$  and  $D_\beta$ . For instance, the orbital overlap of the  $\pi$ -orbitals of the phenyl ring and those at the nitrile groups in the HOMO induce the large rotational barrier around  $D_\beta$  in the ground state. One likely non-radiative relaxation pathway is through the low rotational barrier around  $D_\beta$  in the excited state and subsequent IC or ISC events. However, the rotational barrier of **4** is only about twice the size (25 kJ/mol) compared to the one of **1-3**. Using the Arrhenius equation to define the reciprocal rate constant for the rotation around  $D_\beta$ , **4** is about 480 more likely to fluoresce than **1**, giving a more appropriate relation. The other non-radiative relaxation pathway most likely occurs through ISC events. ISC around  $D_\alpha$  is the likely cause of quenching in dimethylated benzene functionalized derivative **7** but of only minor importance for **1-4**. However, at a dihedral angle  $D_\beta$  of 90°,  $S_1$  and  $T_0$  states are very close. Thus, quenching through ISC is directly linked to the rotational barrier around  $D_\beta$ , which is much larger in benzene functionalized compounds.

Furthermore, a complex redox behaviour of DADQ derivatives **1-4** with partly reversible oxidations and irreversible reductions was revealed (collaboration with Prof. Dr. Biprajit Sarkar). The latter is most likely induced by the proton of the secondary amines and might be a hint for an electrochemical follow-up reaction. Compared to TCNQ, which features two reversible reductions at -0.16 V and -0.77 V, the compounds are more electron rich and the reduction processes are shifted to about -2.3 V and -3.0 V.

### 3.1.2 Aggregation behaviour of Diaminodicyanoquinones

F. Witte, P. Rietsch, S. Sinha, A. Krappe, J. O. Joswig, J. P. Götze, N. Nirmalanathan-Budau, U. Resch-Genger, S. Eigler and B. Paulus; Unraveling diaminodicyanoquinone aggregation behavior in solution: Complex photophysical properties induced by metastable dimers. submitted	5.1
---	-----

Our investigations about DADQs described in section 3.1.1 revealed that those compounds possess a dipole moment of about 30 D in their ground state. Together with intermolecular hydrogen bonding, this leads to anomalous photophysical effects, such as the described negative solvatochromism with shifts of the emission and the absorption spectra. In addition, UV/Vis and fluorescence dilution studies revealed substitution dependent aggregation behaviour. However, our observations do not fit into the model of J- and H-aggregates, as our red shifted aggregate band (J-aggregate) is non-emissive (H-aggregate). Through a combination of

experiment and theory (collaboration with Prof. Dr. Beate Paulus), we investigated this complex aggregation behaviour. Figure 19 illustrates the investigated six DADQ derivatives. Those can be separated in two series, one with an ethane bridge (**1**, **1Me**, **1Me<sub>2</sub>**) and the other one with benzene functionality (**2**, **2Me**, **2Me<sub>2</sub>**). In each series, the compounds differ in the methylation of the secondary amine moieties. Non-methylated, on one side methylated and both sides methylated compounds were compared. Below each structure, a dilution row (absorbance/concentration) of its UV/Vis absorption spectra in ACN is depicted, with concentrations between  $1 \times 10^{-4}$  M and  $5 \times 10^{-7}$  M.

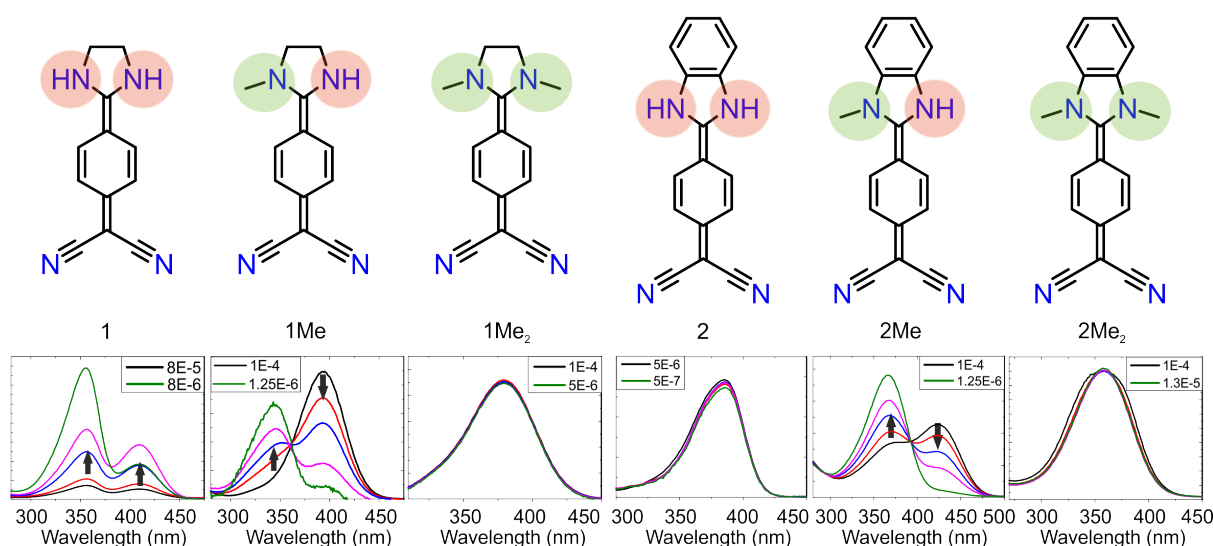


Figure 19: Molecular structures of diaminodicynoquinone derivatives **1-2Me<sub>2</sub>** and their concentration dependent UV/Vis absorption spectra in acetonitrile. The different amine substitution patterns are highlighted. Depicted below each compound is the absorbance divided by the concentration of each respective curve. Arrows point in the direction of decreasing concentration.

**1Me<sub>2</sub>** and **2Me<sub>2</sub>**, both with two tertiary amines and thus unable to form hydrogen bonds, show only one concentration independent absorption maximum. **1Me** and **2Me**, both with one tertiary amine, show isosbestic points and a red shifted absorption band, which is decreasing upon decreasing concentration. **1** shows no isosbestic point but two absorption bands, whereas **2** shows just one absorption in ACN. Its solubility in ACN and the sensitivity of the apparatus are too low to investigate its aggregation behaviour. However, dilution series in DMSO and MeOH revealed that the aggregation of **2** is comparable to the one of compound **1**. Increasing the temperature from 25 °C to 75 °C reduced the intensity of the red shifted absorption peak, which is most likely induced by dimer formation. The addition of polar additives (H<sub>2</sub>O, DMSO, PEG) to the high concentrated ACN solutions have a comparable effect, a decrease of the red shifted absorption band. In accordance with the study described in section 3.1.1, the  $\Phi_{Sol}$  of the benzene functionalized compounds are generally higher than for the ethane bridged compounds. Just as **2Me<sub>2</sub>**, **1Me<sub>2</sub>** has  $\Phi_{Sol}$  smaller than 0.01. The methylated compound **1Me** is also non-emissive, with one exception of  $\Phi_{Sol} = 0.04$  in dimethylformamide (DMF). However, **2Me** has solvent dependent high  $\Phi_{Sol}$  of 0.90 in DMF and 0.79 in ACN. According to Kasha's fundamental work (see section 2.2.6) about molecular aggregates, red shifted absorption bands (with respect to the monomer band) are a strong indication for the formation of J-aggregates, which are typically highly emissive.<sup>[43]</sup> However, very low emission upon excitation of that red shifted dimer band was observed. Non-emissive dimer bands are typically

categorized as H-aggregates. However, the dimer band of H-aggregates is typically blue shifted with regard to the monomer band.

Therefore, Felix Witte from the Paulus group investigated this unusual behaviour by dispersion-corrected DFT based methods, DFT/MRCI and Spano's extended HJ-aggregate theory.<sup>[45, 105a, 105b]</sup> Due to their high dipole moment, the DADQs compounds tend to stabilize themselves by the formation of anti-dimers. That cancels out the dipole moments and is responsible for about 50 to 75 % of the stabilization between the monomers. Through relaxed potential energy surface (PES) scans along the displacement coordinate of the monomers, the evaluation of charge transfer influence beside the coulomb coupling, and the evaluation of Laporte's rule (electronic transitions are only allowed between states of different inversion symmetry), it was possible to rationalize the red shifted absorption band by antiparallel displaced, transient dimers. The quenched emission of the red shifted band is explained by an excited state optimisation of a  $\pi$ -stacked dimer. The excited dimer relaxes along the displacement coordinate in a non-emissive state, where the oscillator strength is neglectable due to symmetry reasons.

In conclusion, the contradictory experimental findings of a red shifted, but non-emissive absorption band was explained by the formation of displaced, metastable dimers, which could be described as a rare case of non-emissive J-aggregates.

### 3.2 Highly Fluorescent Benzothiadiazoles as Redox Switches

P. Rietsch, S. Sobottka, K. Hoffmann, P. Hildebrandt, B. Sarkar, U. Resch-Genger, and S. Eigler; Identification of the Irreversible Redox Behaviour of Highly Fluorescent Benzothiadiazoles <i>ChemPhotoChem.</i> <b>2020</b> , <i>4</i> , 1-7.	4.3
P. Rietsch, S. Sobottka, K. Hoffmann, P. Hildebrandt, B. Sarkar, U. Resch-Genger, and S. Eigler; Between Aromatic and Quinoid Structure: A symmetric UV to Vis/NIR Benzothiadiazole Redox-Switch submitted to <i>Chem. Eur. J.</i> , under minor Revision	5.2

Changing the absorption or the emission properties of a material by redox processes is used in smart windows and rear-view mirrors<sup>[3]</sup> and potentially applicable in light harvesting, sensors, and biomedicine. However, beside viologens, most of the known organic redox switches are complex molecular structures which employ tetrathiafulvalene or quinone motifs as redox active systems.<sup>[4]</sup> The benzothiadiazole (BTD) core is an apolar, aromatic fluorophore, accessible from *o*-phenylenediamines and synthetically versatile using coupling reactions, such as the Sonogashira or the Suzuki coupling.<sup>[106]</sup> BTD derivatives have been applied in OLED materials,<sup>[107]</sup> polymers with defined electronic and optical properties,<sup>[108]</sup> in sensory metal-organic frameworks,<sup>[109]</sup> solar cells<sup>[110]</sup> or in field-effect transistors (FET).<sup>[111]</sup> Recently, strong electrochemiluminescence of symmetric dithienyl BTDs and triphenylamine BTDs, in solution and solid films, has been demonstrated, and even used as a sensor for dopamine.<sup>[112]</sup> However, BTDs have not been considered as absorption switches through redox processes.

Starting from *o*-phenylenediamine, a series of unsymmetrical push-pull BTD derivatives, bearing an alkyne-phenylmethoxy moiety as electron donor, and a variation of electron acceptors, namely -H (**1**), -Br (**2**), a phenyl group (**3**), and a *para*-cyanophenyl group (**4**, Figure 20), were synthesized. Building on these results, the symmetric diphenylmethoxy BTD was synthesized, which will here be numbered compound **5**. The analysis of the photophysical properties of **1-5** was done in solvents of varying polarity and proticity (*n*-hexane, DCM, DMSO, EtOH). BTDs typically feature two absorption bands, one  $\pi$ - $\pi^*$  transition at 280 nm to 320 nm and the HOMO-LUMO transition at about 400 nm.<sup>[100, 113]</sup> The molar extinction coefficient of asymmetric **1-4** is maximal at about 300 nm with values up to 35,000 M<sup>-1</sup> cm<sup>-1</sup> and 10,000 M<sup>-1</sup> cm<sup>-1</sup> at about 400 nm. Compared to that, the symmetric derivative **5** has blue shifted absorption maxima, at 280 nm and 350 nm, with lower extinction coefficients (20,000 and 8500 M<sup>-1</sup> cm<sup>-1</sup>). An excitation emission matrix (EEM) of **3** in hexane revealed that excitation at both absorption maxima induce an emission at 473 nm. Further investigations were thus focused on the HOMO-LUMO absorption band at higher wavelength (lower energy), as it is more likely to be the S<sub>0</sub>-S<sub>1</sub> transition.

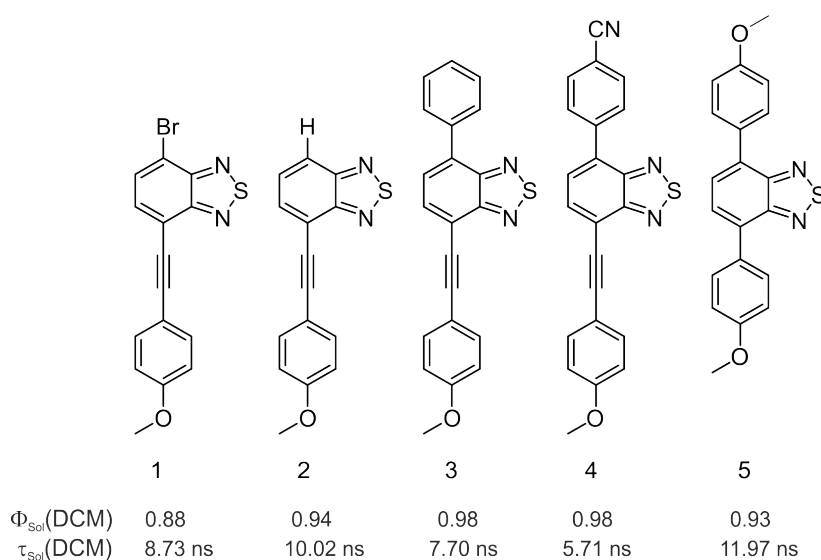


Figure 20: Structures of benzothiadiazole derivatives investigated for their photophysical, electrochemical and absorption switching properties in the publications found in section 4.3 (**1-4**) and section 5.2 (**5**). Below each structure, the fluorescence quantum yield ( $\Phi$ ) and the fluorescence lifetime ( $\tau$ ) in DCM are given.

Whereas the absorption bands are independent of the solvent polarity, all compounds feature a strong fluorosolvatochromism (see section 2.2.4). The fluorescence maxima are bathochromically shifted by 70-80 nm, from around 470 nm in *n*-hexane, to about 550 nm in DMSO. The fluorescence quantum yields are maximal in DCM for all compounds, almost reaching unity, 0.98, for **3** and **4**. The symmetric BTD **5** has a maximum  $\Phi$  of 0.93 in DCM and, compared to **1-4**, long fluorescent lifetimes of about 10 ns in all solvents.  $\tau$  of **1-4** vary around 4-7 ns for **3** and **4**, and between 2.42 ns (**2** in EtOH) up to 10.02 ns (**2** in DCM), showing a strong solvent effect. Overall, a strong solvent effect on the Stokes shift (positive solvatochromism),  $\Phi$  and  $\tau$  is observed.  $\Phi$  and  $\tau$  are particularly reduced in polar, protic EtOH. All five compounds are fluorescent in the crystalline solid state, with solid state fluorescence quantum yields ( $\Phi_{\text{ss}}$ ) of 0.33 (**1**) to 0.72 (**3**). The solid state emission spectra of **1-4** are shifted bathochromically compared to the spectra in *n*-hexane, with maxima at around their DCM emission



spectra (500-520 nm). For **5**, the solid state emission spectrum resembles the one in *n*-hexane. The change of dipole moment upon excitation was investigated through the Lippert-Mataga model.<sup>[33]</sup> The dipole change upon excitation is lowest for **1** and **5** (12.26 and 12.38 D) and highest for **4** (18 D).

To separate the effect of proticity, polarity and viscosity, the fluorosolvatochromism of **4** and **5** in primary alcohols of different chain length, from EtOH to 1-decanol (1-dec), and in mixtures of EtOH and PEG containing increasing percentages of PEG400, was compared. In the EtOH-PEG mixtures, there is almost no difference of the Dimroth-Reichardt polarity parameter  $E_T^N$  (PEG400 = 0.66; EtOH = 0.65), but a strong increase of viscosity upon increasing amount of PEG.<sup>[29, 114]</sup> In the primary alcohols, the viscosity is increasing with increasing chain length (1-dec is about 12 times more viscous than EtOH) while the polarity is decreasing with increasing chain length, from EtOH ( $E_T^N = 0.654$ ) to 1-dec ( $E_T^N = 0.525$ ).

For the EtOH-PEG mixtures, no shift in the absorption maximum and a small bathochromic shift of approximately 4 nm for the fluorescence maximum with increasing viscosity of the dye microenvironment was observed. Furthermore,  $\Phi$  and  $\tau$  are increasing only slightly from the 100/0 EtOH-PEG mixture to the 25/75 EtOH-PEG mixture (changes in % for **4**:  $\Phi = 7.8\%$ ,  $\tau = 1.2\%$ ; for **5**:  $\Phi = 12.6\%$  and  $\tau = 12.3\%$ ). Increases of  $\Phi$  and  $\tau$  with increasing viscosity are well known phenomena.<sup>[115]</sup> However, for the primary alcohols,  $\Phi$  and  $\tau$  of the push-pull derivative **4** are increasing from EtOH to 1-dec by 47 % and 12.5 %, respectively. In contrast,  $\Phi$  and  $\tau$  of the symmetric compound **5** are only increasing by 9.4 % and 1.5 %. The Lippert-Mataga plot of **5** derived from the three aprotic solvents, *n*-hexane, DCM and DMSO yields a change of dipole moment upon excitation of 18 D. In the series of primary alcohols, the change of dipole moment derived from the Lippert-Mataga plot is 19 D.

In conclusion, the polarity and the proticity, not the viscosity, of the primary alcohols seem to be responsible for the observed difference in the Lippert-Mataga plot and the decreased  $\Phi$  and  $\tau$  values. The latter finding can be rationalized by the difference in the ground state and excited state dipole moments of symmetrical **5** and the unsymmetrical push-pull BTD **4**. That is directly linked to the accessibility and separation of the ICT and LE state (see section 2.4.1). The commonly less emissive ICT state is more accessible in structures which enable strong charge separation, e.g. push-pull systems, and in polar protic, solvents.<sup>[20a, 31a, 37c]</sup>

The cyclic voltammograms (CV) of **1-4** feature one irreversible oxidation and one, seemingly reversible reduction around -1.75 V (collaboration with Prof. Dr. Biprajit Sarkar). Compounds **2** and **4** feature a second reduction around -2.15 V. The irreversible oxidation processes around +1 V most likely induce a chemical reaction involving the alkyne moiety. This chemical reaction might be a ring-closure with the nitrogen atoms, as this seems to be a common feature in electrochemical reactions of similar compounds.<sup>[116]</sup> Using optically transparent thin layer electrochemical cells (OTTLE),<sup>[117]</sup> we measured UV/Vis/NIR-spectroelectrochemistry of **3** and **4** (the CVs of **1** and **2** already indicated irreversible processes). The absorption bands of the radical anions **3<sup>-</sup>** and **4<sup>-</sup>** formed upon reduction of **3** and **4** cover the whole visible spectrum and extend to the NIR. The respective maxima are located at 503 nm and 544 nm for **3<sup>-</sup>** and **4<sup>-</sup>** and have molar extinction coefficients of 12,000 and 14,000 M<sup>-1</sup> cm<sup>-1</sup>, respectively. Both radical anions feature two absorption maxima on the red edge of the Vis region, **3<sup>-</sup>** at about 800 nm ( $\epsilon = 3,000 \text{ M}^{-1} \text{ cm}^{-1}$ ), **4<sup>-</sup>** red shifted at around 900 nm ( $\epsilon = 3,000 \text{ M}^{-1} \text{ cm}^{-1}$ ). After re-oxidation of **3<sup>-</sup>** and **4<sup>-</sup>**, the absorption spectra are reduced in intensity, relative to the initial spectrum of the neutral compounds, by

about 25 % and 35 % for **3** and **4**, respectively. Furthermore, polymerization seems to reduce the reversibility of the process for **4**. Exemplarily, the oxidation of **3** was investigated, which leads to a decreased and slightly shifted absorption in the UV region at 307 nm with a molar extinction coefficient of about  $18,000 \text{ M}^{-1} \text{ cm}^{-1}$  and a broad absorption covering the complete Vis region extending up to 1,000 nm with molar extinction coefficients around  $4,000 \text{ M}^{-1} \text{ cm}^{-1}$  and a weak maximum at 566 nm. Re-reduction does not regain the initial spectrum of **3**, thus proving the irreversibility, which was for the oxidative process already suspected from the CV. However, switching the absorbance from UV to Vis/NIR through redox processes, seems to be generally feasible with BTDC compounds.

The electrochemical properties of symmetric BTDCs were investigated before, showing two reversible oxidation and one reversible reduction process in the CV.<sup>[112a, 112b]</sup> However, the UV/Vis/NIR-spectroelectrochemical properties were not investigated. The symmetric compound **5** was synthesized, which lacks the alkyne moiety **1-4** feature. In the CV, the compound shows one reversible reduction process at -1.96 V and two electrochemically reversible one-electron oxidation processes at +0.87 V and +1.09 V. This proves the hypothesis, that the alkyne moiety in **1-4** leads to the irreversibility of the oxidation process. Oxidation of **5** to **5<sup>+</sup>** shifts the absorption from the UV in the Vis/NIR-region, with four distinct bands at 531, 666, 832 and 1124 nm and high extinction coefficients ( $10,000\text{-}20,000 \text{ M}^{-1} \text{ cm}^{-1}$ ).

Similar spectra have been observed for related semiquinone anion radicals, which are isolobal to diamino radical cations and our BTDC derivatives.<sup>[118]</sup> In accordance, our structure optimization (D3-BP86/def2-TZVP) for **5**, **5<sup>+</sup>** and **5<sup>2+</sup>** predict an increasing quinoidal distortion of the aromatic system upon oxidation. The second oxidation to **5<sup>2+</sup>** leads to a strong absorption band at 654 nm with  $\epsilon = 50,000 \text{ M}^{-1} \text{ cm}^{-1}$ . Whereas the initial absorption bands of **5** are attributed to a  $\pi\text{-}\pi^*$  transition from the  $\pi$ -systems of the electron-rich methoxy-phenylene moieties to the central electron-poor BTDC  $\pi$ -system, the transition of **5<sup>2+</sup>** most likely involves a charge transfer from the BTDC  $\pi$ -system to the adjacent methoxy-phenyl rings, which are very electron-deficient after double oxidation. The reduction of **5** yields an absorption spectrum with very broad bands in the Vis and NIR region. However, the initial spectrum of **5** is not regained after re-oxidation, which might be due to electro-polymerization occurring on the electrode. The investigation of the radical cation **5<sup>+</sup>** by CV, coupled with electron paramagnetic resonance (EPR), showed an isotropic signal at room temperature and a rich hyperfine structure, which suggests strong delocalization of the radical over the whole  $\pi$ -system. The EPR spectrum could be simulated by coupling to two nitrogen nuclei ( $I = 1$ ) and 10 hydrogen nuclei ( $I = \frac{1}{2}$ ).

We furthermore measured the fluorescence intensity during the oxidation processes (collaboration with Dr. Alexey Popov). The strong emission of the neutral compound (excitation at 405 nm) is reduced upon oxidation and restored upon re-reduction. The excitation at the absorption maximum of **5<sup>2+</sup>** (638 nm) yields no fluorescence signal at all. The compound could thus be used as a fluorescence ON/OFF switch with an excitation wavelength of 405 nm.

In conclusion, it was shown that the reversibility of redox processes in the cyclic voltammogram can be deceptive. More sophisticated methods, such as spectroelectrochemistry, are necessary to evaluate the (ir-)reversibility of the seemingly reversible processes in the CV. Furthermore, BTDCs were revealed as possible

absorption switches, both in the oxidative and the reductive direction. However, up to now only the oxidative direction was found to be close to reversible. For the oxidative side, it was shown that fluorescence ON/OFF switching is possible. Structurally, alkyne moieties should be avoided, and the quinoid motif, which is induced upon oxidation and at least partly enabled through the methoxy groups, should be utilized to yield reversible switching processes between UV and the Vis/NIR region.

### 3.3 Polycyclic Aromatic Hydrocarbons as Fluorophores

#### 3.3.1 Fluorescence of a chiral pentaphene derivative derived from the hexabenzocoronene motif

<p>P. Rietsch, J. Soyka, S. Brülls, J. Er, K. Hoffmann, J. Beerhues, B. Sarkar, U. Resch-Genger, and S. Eigler; Fluorescence of a Chiral Pentaphene Derivative Derived from the Hexabenzocoronene Motif. <i>Chem. Commun.</i> <b>2019</b>, 55, 10515-10518.</p>	<p>4.2</p>
---	------------

Polyaromatic hydrocarbons (PAH) are known to be fluorescent if aggregation, i.e. low solubility and thus  $\pi$ - $\pi$  stacking (their main non-radiative relaxation pathway), is hindered. Among them, hexabenzocoronenes (HBCs), helicenes and hybrids of both were found to be highly emissive.<sup>[93a, 93f, 119]</sup> Pentaphene, another sub-class of PAHs, was also investigated for its photophysical properties in the 1990s by Fetzer *et al.*<sup>[5]</sup> However, no fluorescence quantum yields, fluorescence lifetimes or solid state emissive properties were reported.

We synthesized a chiral, enantiomeric pentaphene derivative (Figure 21) by an unprecedented Scholl oxidation

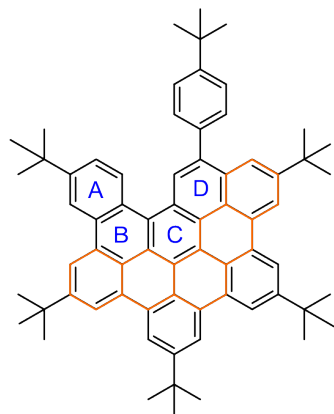


Figure 21: Chemical structure of the Pentaphene derivative with the pentaphene core marked in orange and the benzene rings forming the [4]helicene unit labelled A-D.

of a hexaphenylbenzene (HPB) with one alkyne moiety. The HPB was synthesized by a Diels-Alder reaction between a buta-1,3-diyne derivative and a cyclopenta-2,4-dien-1-one derivative, the latter being a standard intermediate in the synthesis of HBCs.<sup>[89]</sup> The ring-closing reaction between the alkyne moiety and the benzene ring proceeds in analogy to the synthesis of, e.g. corannulenes, HBCs or naphthalenes.<sup>[120]</sup> The reproducibility of the ring-closure through a Scholl oxidation was proven on a phenanthrene derivative, a smaller PAH system.

Due to the close similarity of the pentaphene to the HBC motif, it lacks only one carbon atom in its basal plane, its photophysical properties were compared with a hexa-*tert*-butyl substituted HBC. The absorption spectra of both compounds feature two absorption maxima, one at about 220 nm and the other around 350 nm. The broad maximum of the pentaphene around 350 nm has multiple local maxima and shoulders, owing to its asymmetry. The emission maximum of both compounds is located around 500 nm. Again, the pentaphene features shoulders on the blue as well as the red edge, which are in accordance with the literature on pentaphenes.<sup>[5]</sup> The compounds exhibit no solvent dependent effects.

However, the fluorescence quantum yield, in solution and the solid state, is about 5 times higher for the pentaphene derivative ( $\Phi_{Sol} = 0.16$  vs. 0.03,  $\Phi_{SS} = 0.11$  vs. 0.02). The solid state emission band of the pentaphene is bathochromically shifted by 35 nm with regard to the emission in DCM and slightly broadened. The HBC solid state emission band on the other hand is barely shifted (4 nm) but drastically broadened by about 100 nm. Inhomogeneous broadening and the packing motifs, which will be discussed later, might be the reason for that difference. The fluorescence lifetimes of both compounds are maximal in DCM, with 21.4 ns for the pentaphene and 14.2 ns for the HBC analogue. As the pentaphene derivative features a [4]helicene motif (Figure 21), it has a higher flexibility than the HBC. By density functional theory (DFT) at the B3LYP/6-31G(d) level of theory the racemisation barrier of the pentaphene was calculated.<sup>[121]</sup> The racemisation barrier is about 10 kcal/mol, which explains why the enantiomers of the pentaphene cannot be separated at room temperature. An increase in fluorescence lifetime upon cooling has been observed for many dye classes (see section 3.1)<sup>[115a, 122]</sup> and typically suggests that at least one non-radiative decay channel involves a rotation that is slowed down or even completely hindered at low temperatures.<sup>[19b]</sup> Therefore, the fluorescence decay kinetics upon cooling from 50 °C to -100 °C were investigated. Surprisingly, the mean fluorescence lifetime increases for both compounds by about a factor of 3.5. This finding suggests that the flexibility of the [4]helicene motif in the pentaphene does not interfere with its photophysical properties in solution. In contrast, the difference of  $\Phi_{SS}$  of both compounds can be indirectly linked to the helicene motif. Single crystal XRD data reveal a herringbone structure with a interplanar  $\pi$ - $\pi$  distance of 3.52 Å for the HBC. That most likely leads to an aggregation induced quenching of the fluorescence. The pentaphene however, shows a separation of its graphitic planes of 9.24 Å, a distance too large for excimer formation (see section 2.4.3). That is induced by a twist of 32.46° from phenyl ring A to phenyl ring D in the helicene motif.

In conclusion, an unprecedented Scholl oxidation was discovered that yielded a novel pentaphene derivative which exhibits strong fluorescence in solution and solid state compared to a closely related HBC derivative. It circumvents fluorescence quenching through  $\pi$ - $\pi$  stacking by the twist induced by its [4]helicene motif, which also leads to enantiomeric pairs found in the single crystal XRD structure. Increasing that twist and/or the racemisation barrier might increase fluorescence quantum yields and yield separable enantiomers.

### 3.3.2 Substitution-pattern controlled tuning of the fluorescence lifetime of fluoranthene dyes

P. Rietsch, M. Zeyat, K. Hoffmann, M. Kutter, A. Paskin, J. Uhlig, D. Lentz, U. Resch-Genger, and S. Eigler; Substitution-pattern Controlled Tuning of the Fluorescence Lifetime of Fluoranthene Dyes submitted	4.4
--	-----

Spectral multiplexing or encoding utilizes sets of fluorophores that are commonly excited at the same wavelength but emit light at distinguishable wavelength. However, spectral multiplexing is limited due to spectral cross talk, i.e. the overlap of absorption and emission bands of the dyes, and changes in intensity caused by fluorophore leaking and bleaching. Therefore, the discrimination of fluorophores by their, concentration

independent, fluorescence lifetime was investigated in the 1990s. [24-27, 123] However, these approaches were mostly a combination of separation methods (high-performance liquid chromatography, electrophoresis) and fluorescence detection in the low nanosecond range. In recent years, lifetime multiplexing has been demonstrated using quantum dots together with fluorophores, or copper complexes. [15a, 124] However, the use of organic dyes for lifetime multiplexing remains a challenge, as the relative difference of the fluorescence lifetimes needs to be 100-1000 % and the dyes have to absorb and emit at a common wavelength.

A series of fluoranthene derivatives (Figure 22) with substitution-pattern controlled lifetimes between 6 and 34 ns, and substitution, as well as polarity independent absorption and emission wavelengths was investigated (collaboration with Prof. Dr. Dieter Lentz and Dr. Ute Resch-Genger). Furthermore, their suitability for lifetime multiplexing by measuring dye mixtures was proven and it was shown that these dyes can be embedded in polystyrene particles (PSP), a way to circumvent toxicity and to yield selective accumulation at specific sites in bioimaging. [125] The synthesis of the fluoranthene dyes was accomplished by a Diels-Alder cycloaddition between an acetylene derivative and cyclopentadienone as the final step (see section 2.5.2). A Sonogashira coupling or a Knoevenagel condensation were used to synthesize the respective educts.

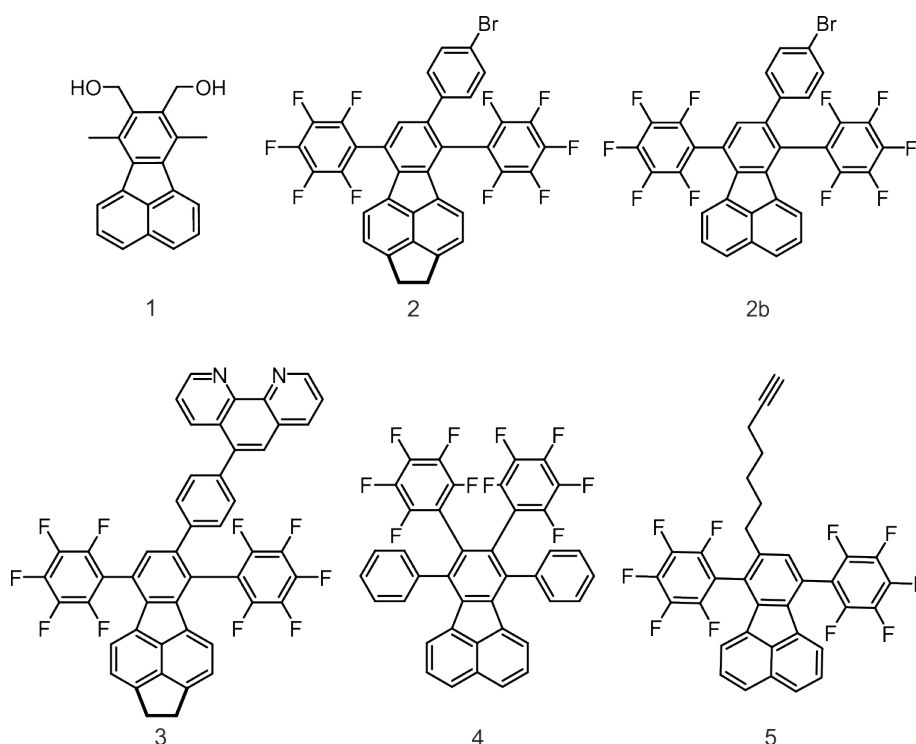


Figure 22: Molecular structures of the fluoranthene dyes investigated for their use in lifetime multiplexing. The ethane bridge forming the pyracene subunit in **2** and **3** are marked in bold bonds.

All dyes feature three absorption maxima between 200 nm to 410 nm, with maximal molar extinction coefficients around 240 nm ( $\epsilon = 30,000\text{-}50,000 \text{ M}^{-1} \text{ cm}^{-1}$ ) and about  $10,000 \text{ M}^{-1} \text{ cm}^{-1}$  around 375 nm, the wavelength which was commonly used for excitation. However, irrespective of the excitation wavelength, a slightly structured emission from about 390-600 nm is observed for all dyes. The photophysical properties were investigated in four solvents of different polarity and proticity, cyclohexane (CH), tetrahydrofuran (THF), DCM and methanol (MeOH), as well as in PSP and solid state by means of absorption, emission and excitation spectra,

excitation-emission matrices (EEM), time-correlated single photon counting (TCSPC) and confocal laser scanning microscopy (CLSM). In contrast to DADQs (section 3.1) and BTDs (section 3.2), and just like the pentaphene derivative (section 3.3.1), both the absorption and emission are barely affected by substitution pattern, solvent polarity or dye microenvironment. The insensitivity to the excitation wavelength, the polarity and the microenvironment can be rationalized by the complete lack of charge transfer character, leading to a  $S_1-S_0$  transition from a locally excited singlet state.<sup>[58]</sup> The fluorescence quantum yield in solution ( $\Phi_{Sol}$ ), PSP ( $\Phi_{PSP}$ ) and solid state ( $\Phi_{SS}$ ) are between 12 % and 55 %, with two exceptions.  $\Phi_{SS}$  of two derivatives, **2** and **3**, which both feature a pyracene unit (Figure 22, bold bonds), is drastically reduced to 5 % and 2 %, respectively. Furthermore, the biexponential lifetime decays in the solid state reveal fluorescence lifetimes for both compounds that are strongly emission wavelength dependent, with a relative increase of  $\tau$  from the blue edge to the red edge of the emission band of about 60 % (**2**) and 500 % (**3**). To investigate the structure-emission relationship, we synthesized compound **2b**, which lacks the ethane bridge at the bottom of the fluoranthene core that completes the pyracene subunit. Compound **2b** has emission wavelength independent monoexponential lifetime decays and  $\Phi_{SS}$  of 10 %.

The single crystal XRD structures suggest that the pyracene unit influences the crystallization motif so that  $\pi$ - $\pi$  stacking is possible. The interplanar distances are less than 4 Å, and thus, as observed for the HBC derivative in section 3.3.1, the likely cause for fluorescence quenching is  $\pi$ - $\pi$  stacking (see section 2.4.3). The emission wavelength dependence can be rationalized by the formation of different, weakly emissive species through the  $\pi$ - $\pi$  interaction. The single crystal XRD structures of **1**, **2b**, **4** and **5** show that their  $\pi$ -systems are shifted or twisted, relative to neighbouring molecules.

To test their suitability for lifetime multiplexing, THF solutions of the two derivatives **2** ( $\tau = 6.52$  ns) and **4** ( $\tau = 31.07$  ns) were mixed in different,  $\Phi_{Sol}$  weighted ratios, and the fluorescence lifetime decays were measured. From the respective biexponential fit, the fluorescence lifetime of each single dye could be reproduced, and the mean fluorescence lifetime could be adjusted through the mixing ratios. For instance, a **2/4** ratio of 0.7/0.3 yielded a relative short mean  $\tau$  of 12.94 ns, whereas a 0.2/0.8 ratio yielded a relative long lifetime of 24.95 ns.

The dyes were embedded in PSP using a standard protocol.<sup>[126]</sup> The excitation spectra of these PSP in water resemble the absorption spectra of the dyes in THF, and the emission spectra of the PSP are comparable to the ones in all other solvents. Compared to the solid state,  $\Phi_{PSP}$  of all compounds remain reasonably high (> 10 %). The fluorescence lifetimes are slightly shortened for **2** and **3** (about 15 %), elongated for **1** (25 %) and **5** (14 %) and constant for **4**.

In conclusion, the possibility to use differently substituted fluoranthene dyes for lifetime multiplexing or encoding applications was demonstrated. Furthermore, the fundamental effect of the pyracene sub-unit on the solid state emissive properties was rationalized. The embedded dyes can furthermore be used for follow-up experiments in flow cytometers.

## 4 Publications - Major Contributions

### 4.1 Diaminodicyanoquinones: Fluorescent Dyes with High Dipole Moments and Electron-Acceptor Properties

---

<b>Authors</b>	<b>Philipp Rietsch, Felix Witte, Sebastian Sobottka, Gregor Germer, Alexander Becker, Arne Guttler, Biprajit Sarkar, Beate Paulus, Ute Resch-Genger, and Siegfried Eigler</b>
<b>Journal</b>	Angew. Chem. Int. Ed. 2019, 58, 8235-8239
<b>DOI</b>	10.1002/anie.201903204
<b>Links</b>	<a href="https://doi.org/10.1002/anie.201903204">https://doi.org/10.1002/anie.201903204</a>
<b>Detailed scientific contribution</b>	<p>The concept of this manuscript was elaborated by P. Rietsch, F. Witte, Prof. Dr. S. Eigler.</p> <p>The theoretical work was done by F. Witte. G. Germer synthesized compound 5 and 6 and did the photophysical characterization of them. A. Becker synthesized compound 7 and carried out the photophysical characterization of it. The rest of the synthesis and photophysical measurements were done by P. Rietsch, in case of the cooling experiments with the help of A. Guttler. S. Sobottka did the complete electrochemical characterization and analysis. Dr. U. Resch-Genger, Prof. Dr. B. Sarkar, Prof. Dr. B. Paulus and Prof. Dr. S. Eigler supervised the theoretical and experimental work.</p> <p>The manuscript was mainly written by P. Rietsch, F. Witte and Prof. Dr. S. Eigler.</p>
<b>Estimated own contribution</b>	~40 %

---

## Fluorescent Dyes

International Edition: DOI: 10.1002/anie.201903204  
German Edition: DOI: 10.1002/ange.201903204

## Diaminodicyanoquinones: Fluorescent Dyes with High Dipole Moments and Electron-Acceptor Properties

Philipp Rietsch<sup>+</sup>, Felix Witte<sup>+</sup>, Sebastian Sobottka, Gregor Germer, Alexander Becker, Arne Güttler, Biprajit Sarkar, Beate Paulus,\* Ute Resch-Genger,\* and Siegfried Eigler\*

Dedicated to Professor Hans-Ulrich Reißig on the occasion of his 70th birthday

**Abstract:** Fluorescent dyes are applied in various fields of research, including solar cells and light-emitting devices, and as reporters for assays and bioimaging studies. Fluorescent dyes with an added high dipole moment pave the way to nonlinear optics and polarity sensitivity. Redox activity makes it possible to switch the molecule's photophysical properties. Diaminodicyanoquinone derivatives possess high dipole moments, yet only low fluorescence quantum yields, and have therefore been neglected as fluorescent dyes. Here we investigate the fluorescence properties of diaminodicyanoquinones using a combined theoretical and experimental approach and derive molecules with a fluorescence quantum yield exceeding 90%. The diaminodicyanoquinone core moiety provides chemical versatility and can be integrated into novel molecular architectures with unique photophysical features.

Applications of fluorescent dyes range from light harvesting in solar cells,<sup>[1]</sup> in light-emitting devices,<sup>[2]</sup> as reporters for the life sciences,<sup>[3]</sup> as molecular switches,<sup>[4]</sup> and in nonlinear optics.<sup>[4–5]</sup> 7,7,8,8-Tetracyanoquinodimethane (TCNQ) is a strong electron acceptor used in conductive donor–acceptor systems like TCNQ–tetrathiafulvalene compounds.<sup>[6]</sup> An interesting subclass are diamino-substituted TCNQ derivatives, namely diaminodicyanoquinones (DADQs), which possess electron-donating and -accepting moieties linked by a  $\pi$ -system, resulting in high dipole moments of 10–20 Debye.<sup>[7]</sup> DADQ derivatives have been discussed as

novel materials, for example, for applications in nonlinear optics.<sup>[7a]</sup> However, their fluorescence quantum yields (QYs) in solution are generally below 0.5% due to nonradiative relaxations of the excited state on the ps timescale.<sup>[8]</sup> Only in the solid state are DADQs moderately emissive with QYs of up to 45%.<sup>[9]</sup> Consequently, DADQ derivatives are not considered as fluorescent dyes. Conformational relaxations can have a high impact on fluorescence,<sup>[10]</sup> as exploited, for example, for aggregation-induced emission,<sup>[11]</sup> where blocking these pathways is used to generate a signal amplification or used as sensing principle for viscosity<sup>[12]</sup> and temperature-responsive molecules.<sup>[10b,13]</sup>

Here we demonstrate that QYs in DADQs can be finetuned by adjusting the substitution pattern, such that QYs exceeding 90% is possible (see Figure 1). Theoretical calculations reveal that benzene-functionalized DADQs show high QYs as their molecular structures remain close to the ground state conformation after photoexcitation and are not submitted to internal conversion (IC) or intersystem crossing (ISC). Accordingly, DADQ derivatives may now be considered as fluorescent dyes and thus applications, such as optical switches or nonlinear optics, are within reach.

First TCNQ was reacted with pyrrolidine to activate the substitution of the geminal cyano groups of TCNQ in the 7,7 position.<sup>[14]</sup> This 7-pyrrolidino-7,8,8-tricyanoquinomethane (PTCNQ) reacts with the respective amine to give compounds **1–4** (Figure 1A) in 40–80% yields. The compounds were characterized by <sup>1</sup>H and <sup>13</sup>C NMR spectroscopy, FTIR spectroscopy, elemental analysis (EA), and mass spectrometry (MS). In addition, the absorption and fluorescence properties were investigated in selected solvents.

The molar absorption coefficients are solvent dependent and reach values of up to 58000 L mol<sup>-1</sup> cm<sup>-1</sup> in acetonitrile (ACN) as depicted in Figure 2 for **4**. While the unstructured absorption band lies between 300 and 400 nm, the fluorescence is shifted bathochromically by 40–90 nm ( $25 \times 10^4$ – $11.1 \times 10^4$  cm<sup>-1</sup>).

The difference densities between the ground state and the excited state (inset Figure 2) illustrate the shift in electron density from the dicyanomethane group to the amine groups upon photoexcitation. This transition leads to a notable reduction of the dipole moment in the excited state from approximately 30 D to 22 D (Table S9). This transition is well known for DADQs, and is the reason for the observed negative solvatochromism (Figure S2 and Table S2).<sup>[15]</sup> In addition, the S<sub>0</sub>–S<sub>1</sub> transition in **4** is extended across the

[\*] M. Sc. P. Rietsch<sup>[+]</sup>, M. Sc. F. Witte<sup>[+]</sup>, M. Sc. G. Germer, B. Sc. A. Becker, Prof. Dr. B. Paulus, Prof. Dr. S. Eigler  
Institute of Chemistry and Biochemistry, Freie Universität Berlin  
Takustraße 3, 14195 Berlin (Germany)  
E-mail: b.paulus@fu-berlin.de  
siegfried.eigler@fu-berlin.de

Dipl.-Ing. A. Güttler, Dr. U. Resch-Genger  
Bundesanstalt für Materialforschung und -prüfung (BAM)  
Department 1, Division Biophotonics  
Richard Willstätter Straße 11, 12489 Berlin (Germany)  
E-mail: ute.resch@bam.de

M. Sc. S. Sobottka, Prof. Dr. B. Sarkar  
Institute of Chemistry and Biochemistry, Freie Universität Berlin  
Fabeckstraße 34–36, 14195 Berlin (Germany)

[+] These authors contributed equally to this work.

[++] Co-first authors

Supporting information and the ORCID identification number(s) for the author(s) of this article can be found under:  
<https://doi.org/10.1002/anie.201903204>



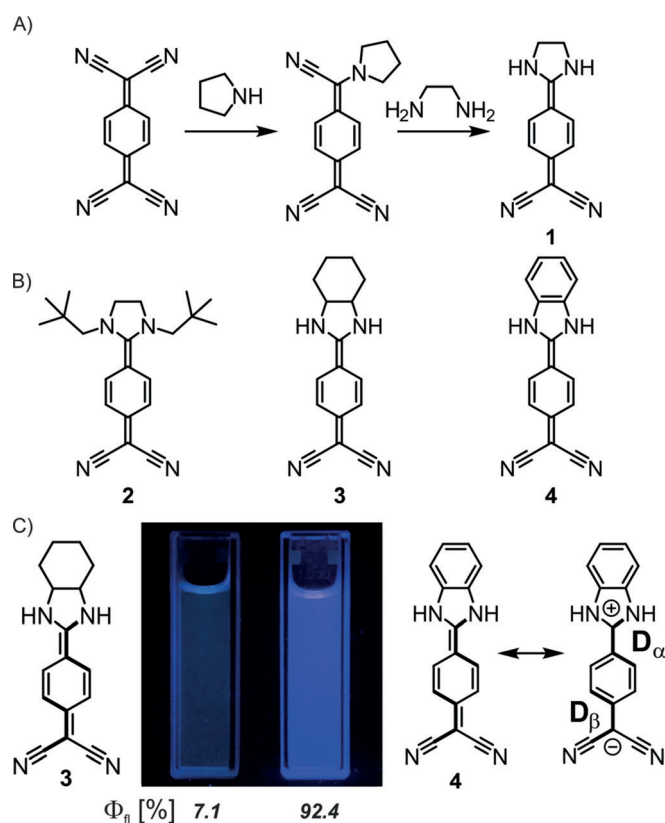


**Figure 1.** A) Synthetic route starting with the activation of TCNQ by reaction with pyrrolidine and subsequent reaction with the respective diamine (ethylene diamine is shown) to yield compounds 1–7. B) Chemical structures of 1–4. C) Photographs of 3 (left) and 4 (right) under illumination with 366 nm light with the respective fluorescence quantum yields in DMSO. Right side: Mesomeric forms of 4 and the definition of the dihedral angles  $D_\alpha$  and  $D_\beta$ .

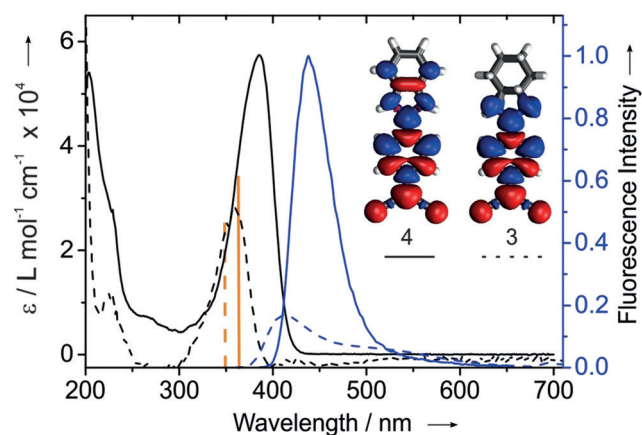


**Figure 2.** Absorption (black) and fluorescence spectra (blue) of 3 (dashed) and 4 (solid) in acetonitrile (normalized with respect to the fluorescence of 4). The vertical orange bars represent transitions of compound 3 (349 nm, oscillator strength: 1.02 a.u.) and 4 (363 nm, oscillator strength: 1.30 a.u.) calculated using TD-DFT at the CAM-B3LYP level. Insets: Difference densities between ground state and excited state of 4 (left) and 3 (right) to visualize the electron flow during the electronic excitation. Blue and red areas correspond to areas of electron enhancement and depletion, respectively. Isovalue = 0.005  $\text{\AA}^{-3}$ .

enlarged  $\pi$ -system, including the phenyl ring. The absolute QY values are summarized in Table 1. Compound 4 shows very high QYs in all solvents, with values of 92% in dimethyl sulfoxide (Figure 1C), around 70% in tetrahydrofuran, dimethylformamide, and acetonitrile, and 56% and 35% in ethanol and methanol, respectively. In contrast, 1 and 3 show

**Table 1:** Fluorescence quantum yields of compounds 1–7 in solvents of different polarity. Values for the normalized Dimroth–Reichardt parameter  $E_T^N$  were taken from Ref. [16].

$E_T^N$	Solvent	1 $\Phi$ [%]	2 $\Phi$ [%]	3 $\Phi$ [%]	4 $\Phi$ [%]	5 $\Phi$ [%]	6 $\Phi$ [%]	7 $\Phi$ [%]
0.207	THF	7	<1	7	73	34	69	<1
0.386	DMF	7	<1	10	72	62	81	3
0.444	DMSO	10	<1	7	92	39	90	<1
0.460	ACN	7	<1	12	71	18	53	<1
0.654	EtOH	<1	<1	<1	56	63	70	<1
0.762	MeOH	<1	<1	<1	35	20	30	<1

QYs in the range of 0–12% and 2 QYs of <1%. The fluorescence lifetimes of 1–4 and the calculated radiative and nonradiative rate constants (Tables S3 and S4) do not show a straightforward correlation with the QY data. QY measurements in solvents of varying viscosity confirm the assumption that rotations around the dihedral angles  $D_\alpha$  and  $D_\beta$  play a significant role for the nonradiative excited-state deactivation of 1–3. By increasing the fraction of polyethylene glycol (PEG) in ethanol (PEG–EtOH) from 0% to 75%, we observe a 3–7-fold increase in fluorescence intensity for 1–3 (Figure 3 and Figure S7), resulting in an increase of QY of 2 from 0.4% to 2.9%. In contrast, the fluorescence of 4 is barely affected by an increase in solvent viscosity (Figure S7D).

For compounds 1–4 the fluorescence intensity decreases by more than 30% with increasing temperature in the temperature range of 40°C to 110°C (Figure S9). Upon decreasing the temperature (273–173 K), the fluorescence

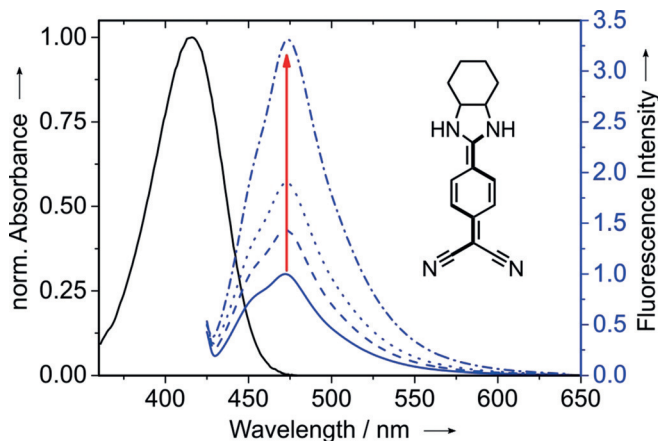


**Figure 3.** Absorption spectrum and emission spectra of 3 in EtOH–PEG mixtures ranging from 0 to 75% PEG in steps of 25%, depicted by the red arrow. Solid line 0%, dashed line 25%, dotted line 50%, dashed–dotted line 75%. With an increasing ratio of PEG and hence increasing viscosity, the fluorescence intensity increases by a factor of 3.3.

intensity increases qualitatively for **1–4** (Figure S11). A closer look at the shape of the fluorescence signals indicates that various fluorescent states are populated (Figure S12). As we did not thoroughly study the viscosity effects and aggregation upon these temperature changes, the observed trends are qualitative.

The experimental results indicate that rotations play a major role in controlling the QY. In particular, the N-substituted derivatives **2** and **7** (Figures 1 and 4), twisted in their ground-state structure at  $D_\alpha$  (Figure S17C), are non-fluorescent. In analogy to **4**, compounds **5** (Br derivative) and **6** (CN derivative), both with a benzene unit, are highly fluorescent (Figure 4 and Table 1).

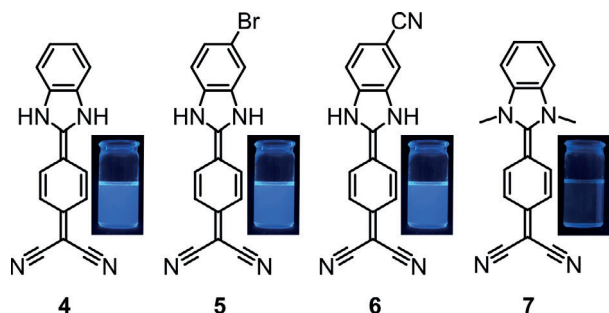


**Figure 4.** Chemical structures of compounds **4–7** with photographs showing their fluorescence (excitation wavelength 366 nm).

To gain more insight into the optical properties of our DADQ derivatives and to elucidate the remarkable QY of **4**, we performed time-dependent density functional theory (TD-DFT) calculations at the CAM-B3LYP<sup>[17]</sup> level for **1–4** and **7** using ACN as the solvent with CPCM ( $\epsilon = 37.5$ ).<sup>[18]</sup> A prerequisite for a high QY is a close similarity between the relaxed structures of the excited state and the ground state without IC or ISC events influencing the photoexcitation process.

The fluorescence deactivation of the DADQ species may be controlled by two photoinduced intramolecular torsions at dihedral angles  $D_\alpha$  and  $D_\beta$  (Figure 5). To our surprise, the ground ( $S_0$ ) and excited state ( $S_1$ ) structures of all compounds hardly differ (Figure S16) and the oscillator strengths remain rather constant (Table S8). As this would imply all compounds show similar QYs, a more detailed look at the potential energy surfaces (PES) of the intramolecular rotations is needed. To account for the influence of multireference states we opted for the DFT/MRCI method originally proposed by Grimme and Waletzke<sup>[19]</sup> and revised by Marian et al.<sup>[20]</sup> with a Kohn–Sham orbital basis generated at the CPCM/BHLYP/def2-TZVP<sup>[21]</sup> level to obtain accurate energies. Test calculations showed that the rotational barriers at  $D_\alpha$  and  $D_\beta$  do not critically influence each other (Figure S17A, B), which is why we will treat  $D_\alpha$  and  $D_\beta$  separately. In the ground state  $S_0$ , rotation around  $D_\beta$  at the Franck–Condon point is hindered by large barriers of around  $60 \text{ kJ mol}^{-1}$  for all compounds, but a rotation around  $D_\alpha$  is possible except for **2** and **7** where the N substituents block the way (Figures S17C and S18A). In contrast, in the excited

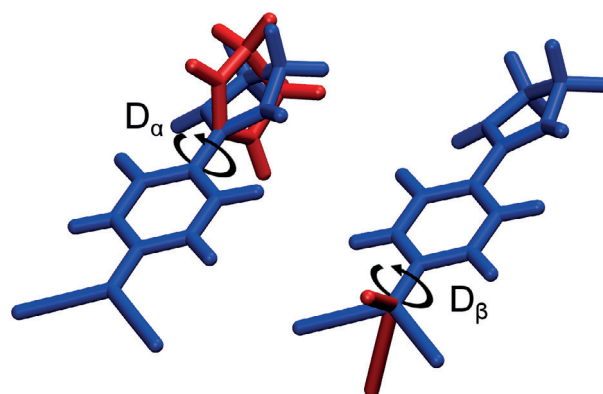


**Figure 5.** Two kinds of torsion angles (shown for **1**) that affect the fluorescence deactivation mechanism in DADQs:  $D_\alpha$  (left) and  $D_\beta$  (right).

state  $S_1$ , rotation around  $D_\alpha$  is prevented with barriers of  $60\text{--}100 \text{ kJ mol}^{-1}$ , but rotation around  $D_\beta$  shows barriers of around  $12 \text{ kJ mol}^{-1}$  (**1–3**) to  $25 \text{ kJ mol}^{-1}$  (**4**, **7**) (Figures S17D and S18B). Large barriers arise as a rotation around  $D_\beta$  diminishes the basis function overlap between the  $\pi$ -orbitals centered at the phenyl ring and those at the nitrile groups in the HOMO, while a rotation around  $D_\alpha$  decreases the overlap between the phenyl ring's  $\pi$ -orbitals and the p-orbitals of the amino groups in the LUMO. Low barriers are explained by nodes present in the HOMO at  $D_\alpha$  and in the LUMO at  $D_\beta$ , where an intramolecular torsion would not impede any orbital overlap (Figure 6).

The PES at  $D_\alpha$  is less important for **2**, **3**, and **4**, where an electronic excitation starting from  $S_0$  on the  $S_1$  PES will just recover the  $S_0$  minimum structure. However, this torsion may account for fluorescence quenching by IC or ISC in **7** and slightly in **1**. For **1–4**, QY loss is expected to mainly occur due to the relatively small rotational barrier in the  $S_1$  at  $D_\beta$  (Figure 7). As expected, the respective rotational barrier is highest for **4** and lowest for **1**. This can be attributed to the stabilization of the ground state geometry of **4** through the extended  $\pi$ -system. Using the Arrhenius' equation at  $T =$

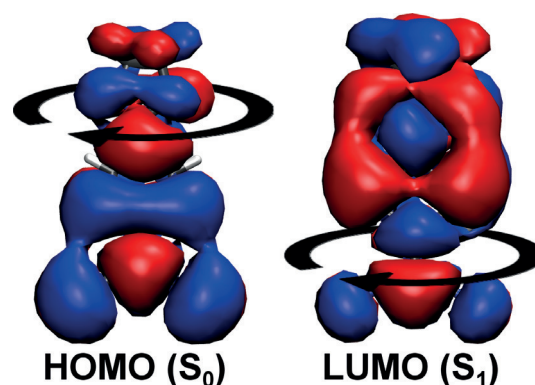


**Figure 6.** HOMO (left) and LUMO (right) obtained at the BHLYP/def2-TZVP level. Rotations (indicated by arrows) are favored due to nodal planes in the orbitals, while orbital overlap keeps the structures rigid at  $D_\beta$  in the HOMO (left) and at  $D_\alpha$  in the LUMO (right), isovalue =  $0.003 \text{ \AA}^{-3}$ .

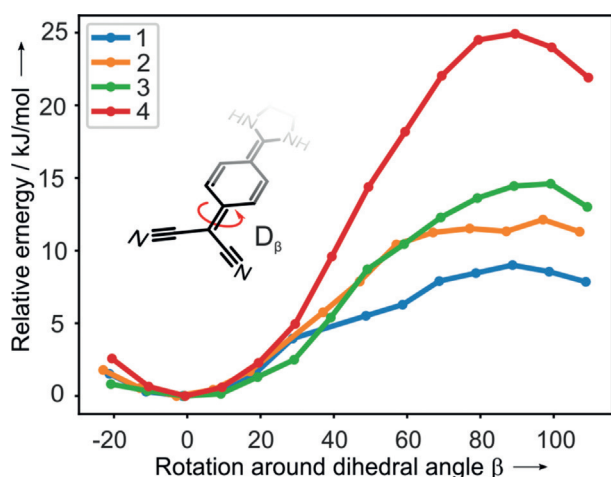


**Figure 7.** PES scan of the  $S_1$  state around dihedral angle  $D_\beta$  for **1–4** computed at the CPCM/BHLYP/def2-TZVP/MRCI level. **7** is omitted as its fluorescence deactivation mechanism is different.

300 K, we define  $k_{\text{rot}}^{-1}$  (the reciprocal rate constant for the rotation around  $D_\beta$ ; see Equation S5) as a relative measure to compare rotational barriers. Relating  $k_{\text{rot}}^{-1}$  for **1–4** illustrates that **4** is up to 480 times more likely than **1–3** to fluoresce after photoexcitation into the  $S_1$ .

$$k_{\text{rot}}^{-1}(\mathbf{1}) : k_{\text{rot}}^{-1}(\mathbf{2}) : k_{\text{rot}}^{-1}(\mathbf{3}) : k_{\text{rot}}^{-1}(\mathbf{4}) = 1 : 3 : 12 : 481$$

ISC events between singlet and triplet surfaces contribute to fluorescence quenching in all compounds. For **7** the most likely deactivation mechanism is via an ISC of the  $S_1$  with  $T_1$  and  $T_2$  along  $D_\alpha$  (Figure S19A). This mechanism may play a role for **1** as well; however, it is assumed to have a smaller impact (Figure S19B). At  $D_\beta$  all compounds show a singlet/triplet separation energy of around 0.7 eV at the Franck–Condon point, which should be just large enough to prevent ISC events. However, as the  $S_1$  and the  $T_0$  eventually come very close at an angle of around  $90^\circ$  (Figure S20) in all molecules, the rotational barrier presented by  $k_{\text{rot}}^{-1}$  and the nonradiative relaxation through ISC events are directly linked. Since **1–3** are much more likely to overcome the rotational barrier at  $D_\beta$  than **4**, their QYs are significantly lower.

While this qualitatively accounts for the drastic differences in QY, it does not fully explain the large QY of **4** by itself. As solvent effects have only been included in an implicit way, an explicit solvent environment of ACN was set up (Figure S21A) and the rotational barrier at  $D_\beta$  was recalculated for **1** and **4** with the smaller def2-SVP basis set and fixed solvent molecules to save computational resources (Figure S21B). While the total barrier hardly changed for **1**, the barrier height for **4** increased by roughly 30%. Thus, the solvent shell may play a significant role at least in the case of **4**, where it likely contributes to its large QY.

To further characterize **1–4**, we performed cyclic voltammetry (CV) experiments in a 0.1 M  $\text{Bu}_4\text{NPF}_6$  solution of DMF (Figure S14). The molecules show a complex redox behavior, with mostly reversible oxidations (for **4**) and irreversible

reductions (quasi reversible for **2**), which likely involve the proton of the secondary amine and provide a hint for an electron transfer followed by a chemical reaction (EC mechanism).<sup>[22]</sup> As expected, the replacement of the cyano moieties with secondary and tertiary amines favors oxidation processes, which are not observed for TCNQ (Figure S15). This also renders the molecules more electron-rich and causes a cathodic shift of the reduction potentials. (see Table S7 for more details). The HOMO–LUMO gaps were calculated at the CPCM/BHLYP/MRCI level. The trends between experiment and theory show overall agreement (Table 2). The electrochemically measured gaps differ slightly in absolute values, as the solvent model neglects bulk effects at the electrode.<sup>[23]</sup>

**Table 2:** Electrochemical, theoretical, and optical data of compounds **1–4** with the resulting orbital energies and HOMO–LUMO gaps ( $E_g$ ) [eV].

	CV data <sup>[a]</sup>		Optical data <sup>[b]</sup>		Theory <sup>[c]</sup>
	$E_{\text{HOMO}}$ [eV]	$E_{\text{LUMO}}$ [eV]	$E_g^{\text{el}}$ [eV]	$E_g^{\text{opt}}$ [eV]	$E_g^{\text{theo}}$ [eV]
<b>1</b>	−2.37	0.16	2.53	3.31	3.24
<b>2</b>	−2.42	0.12	2.54	2.87	3.49
<b>3</b>	−2.27	−0.14	2.13	3.16	3.17
<b>4</b>	−2.22	−0.21	2.01	2.94	2.98

[a] Orbital energies calculated from the first reduction or oxidation half-wave potentials referenced to  $\text{FcH}/\text{FcH}^+$  (−4.80 eV):  $\epsilon = -(E_{1/2} - 4.80)$  eV [b] The optical HOMO–LUMO gap was determined from the onset at the red edge of the absorption band [c] CPCM/BHLYP/def2-TZVP/MRCI.

In conclusion, we synthesized highly fluorescent diamino-dicyanoquinones showing quantum yields of over 90% when benzene-substituted. We attribute the high fluorescence quantum yields mainly to restricted internal rotations, while quenching occurs through the intersection of singlet and triplet states. However, other effects, such as molecular aggregation, may contribute as well. The electrochemical characterization of these molecules reveals complex redox activity. In summary, we could show that diamino-dicyanoquinone derivatives are a novel class of fluorescent dyes customizable for photophysical applications, the potential of which needs to be studied in more detail.

## Acknowledgements

B.P. and F.W. acknowledge the Deutsche Forschungsgemeinschaft (DFG) for financial support within the collaborative research area “Multivalenz als chemisches Organisations- und Wirkprinzip: Neue Architekturen, Funktionen und Anwendungen” SFB 765 and the High-Performance Computing resources of the Zentraleinrichtung für Datenverarbeitung (ZEDAT) of Freie Universität Berlin; B.S. and S.S. are grateful to the DFG Priority Program SPP 2102, “Light-controlled reactivity of metal complexes” (SA 1840/7-1) for financial support. U.R.G. gratefully acknowledges financial support by DFG (RE1203/23-1).

**Conflict of interest**

The authors declare no conflict of interest.

**Keywords:** dipole moment · fluorescence · quantum yield · quinones

**How to cite:** *Angew. Chem. Int. Ed.* **2019**, *58*, 8235–8239  
*Angew. Chem.* **2019**, *131*, 8320–8325

- [1] a) C. Climent, L. Cabau, D. Casanova, P. Wang, E. Palomares, *Org. Electron.* **2014**, *15*, 3162; b) P. Gratia, A. Magomedov, T. Malinauskas, M. Daskeviciene, A. Abate, S. Ahmad, M. Gratzel, V. Getautis, M. K. Nazeeruddin, *Angew. Chem. Int. Ed.* **2015**, *54*, 11409; *Angew. Chem.* **2015**, *127*, 11571; c) R. Grisorio, B. Roose, S. Colella, A. Listorti, G. P. Suranna, A. Abate, *ACS Energy Lett.* **2017**, *2*, 1029; d) U. Würfel, M. Seßler, M. Unmüßig, N. Hofmann, M. List, E. Mankel, T. Mayer, G. Reiter, J.-L. Bubendorff, L. Simon, M. Kohlstädt, *Adv. Energy Mater.* **2016**, *6*, 1600594; e) A. Hagfeldt, G. Boschloo, L. Sun, L. Kloo, H. Pettersson, *Chem. Rev.* **2010**, *110*, 6595.
- [2] K. T. Kamtekar, A. P. Monkman, M. R. Bryce, *Adv. Mater.* **2010**, *22*, 572.
- [3] A. L. Antaris, H. Chen, S. Diao, Z. Ma, Z. Zhang, S. Zhu, J. Wang, A. X. Lozano, Q. Fan, L. Chew, M. Zhu, K. Cheng, X. Hong, H. Dai, Z. Cheng, *Nat. Commun.* **2017**, *8*, 15269.
- [4] F. Castet, V. Rodriguez, J. L. Pozzo, L. Ducasse, A. Plaquet, B. Champagne, *Acc. Chem. Res.* **2013**, *46*, 2656.
- [5] a) M. Albota, *Science* **1998**, *281*, 1653; b) G. J. Ashwell, E. J. C. Dawney, A. P. Kuczynski, M. Szablewski, I. M. Sandy, M. R. Bryce, A. M. Grainger, M. Hasan, *J. Chem. Soc. Faraday Trans.* **1990**, *86*, 1117; c) J. L. Bredas, C. Adant, P. Tackx, A. Persoons, B. M. Pierce, *Chem. Rev.* **1994**, *94*, 243; d) I. Paci, J. C. Johnson, X. Chen, G. Rana, D. Popovic, D. E. David, A. J. Nozik, M. A. Ratner, J. Michl, *J. Am. Chem. Soc.* **2006**, *128*, 16546; e) J. M. Hales, J. Matichak, S. Barlow, S. Ohira, K. Yesudas, J. L. Bredas, J. W. Perry, S. R. Marder, *Science* **2010**, *327*, 1485; f) B. J. Walker, A. J. Musser, D. Beljonne, R. H. Friend, *Nat. Chem.* **2013**, *5*, 1019.
- [6] a) D. S. Acker, W. R. Hertler, *J. Am. Chem. Soc.* **1962**, *84*, 3370; b) L. R. Melby, R. J. Harder, W. R. Hertler, W. Mahler, R. E. Benson, W. E. Mochel, *J. Am. Chem. Soc.* **1962**, *84*, 3374; c) D. S. Acker, R. J. Harder, W. R. Hertler, W. Mahler, L. R. Melby, R. E. Benson, W. E. Mochel, *J. Am. Chem. Soc.* **1960**, *82*, 6408; d) H. Akiyoshi, H. Goto, E. Uesugi, R. Eguchi, Y. Yoshida, G. Saito, Y. Kubozono, *Adv. Electron. Mater.* **2015**, *1*, 1500073; e) J. Ferraris, D. O. Cowan, V. Walatka, J. H. Perlstein, *J. Am. Chem. Soc.* **1973**, *95*, 948.
- [7] a) M. Szablewski, P. R. Thomas, A. Thornton, D. Bloor, G. H. Cross, J. M. Cole, J. A. K. Howard, M. Malagoli, F. Meyers, J.-L. Brédas, W. Wenseleers, E. Goovaerts, *J. Am. Chem. Soc.* **1997**, *119*, 3144; b) M. Ravi, D. N. Rao, S. Cohen, I. Agranat, T. P. Radhakrishnan, *J. Mater. Chem.* **1996**, *6*, 1853.
- [8] M. Szablewski, M. A. Fox, F. B. Dias, H. Namih, E. W. Snedden, S. M. King, D. Dai, L. O. Pålsson, *J. Phys. Chem. B* **2014**, *118*, 6815.
- [9] a) P. Srujana, T. Gera, T. P. Radhakrishnan, *J. Mater. Chem. C* **2016**, *4*, 6510; b) D. Bloor, Y. Kagawa, M. Szablewski, M. Ravi, S. J. Clark, G. H. Cross, L.-O. Pålsson, A. Beeby, C. Parmer, G. Rumbles, *J. Mater. Chem.* **2001**, *11*, 3053.
- [10] a) K. H. Drexhage, *J. Res. Natl. Bur. Stand. Sect. A* **1976**, *80*, 421; b) S. Upadhyayula, V. Nunez, E. M. Espinoza, J. M. Larsen, D. Bao, D. Shi, J. T. Mac, B. Anvari, V. I. Vullev, *Chem. Sci.* **2015**, *6*, 2237.
- [11] a) J. Mei, Y. Hong, J. W. Lam, A. Qin, Y. Tang, B. Z. Tang, *Adv. Mater.* **2014**, *26*, 5429; b) J. Mei, N. L. Leung, R. T. Kwok, J. W. Lam, B. Z. Tang, *Chem. Rev.* **2015**, *115*, 11718.
- [12] a) R. M. Yusop, A. Unciti-Broceta, M. Bradley, *Bioorg. Med. Chem. Lett.* **2012**, *22*, 5780; b) N. Vo, N. L. Haworth, A. M. Bond, L. L. Martin, *ChemElectroChem* **2018**, *5*, 1173.
- [13] a) F. K. Zhou, J. Y. Shao, Y. B. Yang, J. Z. Zhao, H. M. Guo, X. L. Li, S. M. Ji, Z. Y. Zhang, *Eur. J. Org. Chem.* **2011**, 4773; b) S. Jayanty, T. P. Radhakrishnan, *Chem. Eur. J.* **2004**, *10*, 791; c) N. Scholz, A. Jadhav, M. Shreykar, T. Behnke, N. Nirmalanathan, U. Resch-Genger, N. Sekar, *J. Fluoresc.* **2017**, *27*, 1949; d) M. Vogel, W. Rettig, R. Sens, K. H. Drexhage, *Chem. Phys. Phys. Lett.* **1988**, *147*, 452; e) K. G. Casey, E. L. Quitevis, *J. Chem. Phys.* **1988**, *92*, 6590.
- [14] W. R. Hertler, H. D. Hartzler, D. S. Acker, R. E. Benson, *J. Am. Chem. Soc.* **1962**, *84*, 3387.
- [15] a) M. R. Bryce, E. Chinarro, A. Green, N. Martín, A. J. Moore, L. Sánchez, C. Seoane, *Synth. Met.* **1997**, *86*, 1857; b) Valeur, *Molecular Fluorescence: Principles and Applications*, Wiley-VCH, Weinheim, **2002**.
- [16] C. Reichardt, *Chem. Rev.* **1994**, *94*, 2319.
- [17] T. Yanai, D. P. Tew, N. C. Handy, *Chem. Phys. Lett.* **2004**, *393*, 51.
- [18] a) V. Barone, M. Cossi, *J. Phys. Chem. A* **1998**, *102*, 1995; b) I. M. Smallwood, *Handbook of Organic Solvent Properties*, Elsevier, Amsterdam, **1996**.
- [19] S. Grimme, M. Waletzke, *J. Chem. Phys.* **1999**, *111*, 5645.
- [20] I. Lyskov, M. Kleinschmidt, C. M. Marian, *J. Chem. Phys.* **2016**, *144*, 034104.
- [21] a) A. D. Becke, *J. Chem. Phys.* **1993**, *98*, 1372; b) F. Weigend, R. Ahlrichs, *Phys. Chem. Chem. Phys.* **2005**, *7*, 3297.
- [22] O. A. Levitskiy, D. A. Dulov, O. M. Nikitin, A. V. Bogdanov, D. B. Eremin, K. A. Paseshnikchenko, T. V. Magdesieva, *ChemElectroChem* **2018**, *5*, 3391.
- [23] S. Sinnecker, A. Rajendran, A. Klamt, M. Diedenhofen, F. Neese, *J. Phys. Chem. A* **2006**, *110*, 2235.

Manuscript received: March 14, 2019

Version of record online: May 7, 2019

Supporting Information

**Diaminodicyanoquinones: Fluorescent Dyes with High Dipole Moments and Electron-Acceptor Properties**

*Philipp Rietsch<sup>†</sup>, Felix Witte<sup>†</sup>, Sebastian Sobottka, Gregor Germer, Alexander Becker, Arne Güttler, Biprajit Sarkar, Beate Paulus,\* Ute Resch-Genger,\* and Siegfried Eigler\**

anie\_201903204\_sm\_miscellaneous\_information.pdf

### 1. General Information

All reagents were purchased from commercial sources and used without further purification. Dry solvents were purchased from Acros Organics. ALUGRAM Xtra SIL G/UV<sub>254</sub> plates by Macherey-Nagel were used for thin-layer chromatography. Isolation of products by chromatography was performed with silica from Macherey-Nagel Silica 60 M (0.04-0.063 mm).

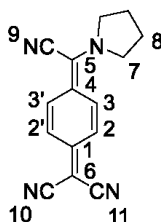
NMR spectra were recorded on a JOEL ECX 400 (<sup>1</sup>H 400 MHz, <sup>13</sup>C 101 MHz), JEOL Eclipse+ 500 (<sup>1</sup>H 500 MHz, <sup>13</sup>C 126 MHz) and BRUKER AVANCE 700 (<sup>1</sup>H 700 MHz, <sup>13</sup>C 176 MHz) spectrometer at 25 °C. The chemical shifts  $\delta$  are calibrated on the respective solvent peak as internal standard. All shifts are reported in ppm and NMR multiplicities are abbreviated as s (singlet), d (duplet), t (triplet), m (multiplet). Coupling constants J are reported in Hz. UV/Vis spectra were recorded on a Cary 50 Bio photo spectrometer (Varian). Fluorescence spectra were recorded on a LS 50 B luminescence spectrometer from PerkinElmer. UV/Vis and Fluorescence spectra were measured in quartz glass cuvettes with 1 cm path length. IR Spectra were recorded on a FT/IR 4100 spectrometer from JASCO. Elemental analysis was performed on an VARIO EL from Elementar.

## SUPPORTING INFORMATION

## 2. Synthetic Procedures

The synthetic procedure was employed from Ref. [1] and used with only minor modifications.

## 2-(4-(cyano(pyrrolidin-1-yl)methylene)cyclohexa-2,5-dien-1-ylidene)malononitrile (8)



To a stirred warm solution of TCNQ (250.0 mg, 1.22 mmol, 1 eq.) in acetonitrile (20 mL), pyrrolidine (69.7 mg, 0.98 mmol, 0.8 eq.) was added in one shot. The solution turned green and then purple. After stirring for 4 hours at 70 °C the solution was cooled to room temperature and then stored in the fridge for 3 days. The precipitate was filtered and washed with cooled acetonitrile (3x 5 mL) to yield the product as fine purple crystal needles (232.4 mg, 0.93 mmol, 76.5%).

<sup>1</sup>H NMR (400 MHz, DMSO-d<sub>6</sub>, RT): δ (ppm) = 7.73 (dt, <sup>4</sup>J = 0.7Hz, <sup>3</sup>J = 7Hz, 2H, 3), 7.81 (dt, <sup>4</sup>J = 0.7Hz, <sup>3</sup>J = 7Hz, 2H, 2), 4.11 (bs, 4H, 7), 2.08 (m, 4H, 8)

<sup>13</sup>C NMR (100 MHz, DMSO-d<sub>6</sub>, RT): δ (ppm) = 153.95 (1C, 6), 137.76 (1C, 4), 134.32 (2C, 2), 120.11 (2C, 3), 118.92 (1C, 10), 116.78 (1C, 11), 113.09 (1C, 9), 57.40 (1C, 6), 50.92 (2C, 7), 25.60 (2C, 8)

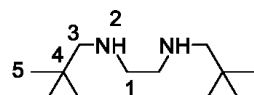
FT-IR (ATR)  $\tilde{\nu}$  (cm<sup>-1</sup>): 2190 (m), 2164 (s), 1611 (s), 1536 (m), 1474 (w), 1381 (s), 1341 (m), 1207, (s), 861 (s), 823 (s), 727 (m), 650 (s)

UV/Vis (ACN)  $\lambda_{\text{max}}$  nm ( $\epsilon$  [Lmol<sup>-1</sup> cm<sup>-1</sup>]): 275 (6300), 480 (13000)

MS (EI): m/z = 249.1 (20); 248.0 (100)[MH]<sup>+</sup>; 221.1 (15); 179.1 (17); 154.1 (20)

EA: C<sub>15</sub>H<sub>12</sub>N<sub>4</sub>; calc.: C, 72.56; N, 22.57, H, 4.87; meas.: C, 72.74; N, 21.57; H, 4.89

## N1,N2-dineopentylethane-1,2-diamine (9)



Ethylenediamine (180.0 mg, 3.0 mmol, 1.0 eq.) and Pivalaldehyde (593.3 mg, 6.9 mmol, 2.3 eq.) were stirred in dry MeOH (20 mL) under argon atmosphere for 12 hours. NaBH<sub>4</sub> (453.2 mg, 12.0 mmol, 4 eq.) was added stepwise and the reaction mixture was refluxed for 2 hours. The reaction was quenched with water (10 mL), and the aqueous phase was extracted with hexane (3x 15 mL). The combined organic phases were dried over MgSO<sub>4</sub> filtrated and evaporated under reduced pressure. The crude product was purified by column chromatography (Ethyl acetate / MeOH 90 / 10 with 1%v/v 7M NH<sub>3</sub> in MeOH) to yield a white solid (520 mg, 2.6 mmol, 86.7%, RF = 0.2).

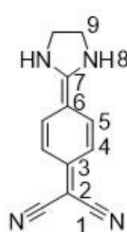
<sup>1</sup>H NMR (400 MHz, DMSO-d<sub>6</sub>, RT): δ (ppm) = 2.68 (s, 4H, 1), 2.30 (s, 4H, 3), 0.90 (s, 18H, 5)

<sup>13</sup>C NMR (100 MHz, DMSO-d<sub>6</sub>, RT): δ (ppm) = 62.32 (2C, 1), 49.91 (2C, 3), 31.58 (2C, 4), 27.77 (6C, 5)

FT-IR (ATR)  $\tilde{\nu}$  (cm<sup>-1</sup>): 2962 (s), 2866 (w), 2811 (w), 1541 (m), 1478 (s), 1456 (s), 1364 (m), 910 (s), 760 (m), 733 (s)

## SUPPORTING INFORMATION

## 2-(4-(imidazolidin-2-ylidene)cyclohexa-2,5-dien-1-ylidene)malononitrile (1)



Ethylenediamine (26.6 mg, 0.44 mmol, 1 eq.) was added to a 40 °C warm solution of **8** (110 mg, 0.44 mmol, 1 eq.) in acetonitrile (10 mL). The solution turned deep green immediately and to yellow in the next minutes. The solution was stirred at 70 °C for 4 hours and then cooled to room temperature. The precipitate was filtered off and washed with cooled acetonitrile (3x 5 mL) to yield the product as a yellow fine-grain powder (73.4 mg, 0.35 mmol, 78.8%).

<sup>1</sup>H NMR (500 MHz, DMSO-d<sub>6</sub>, RT): δ (ppm) = 9.76 (s, 2H, 8), 7.57 (d, <sup>3</sup>J = 5.0 Hz, 2H, 4), 6.82 (d, <sup>3</sup>J = 5.0 Hz, 2H, 5), 3.87 (bs, 4H, 9)

<sup>13</sup>C NMR (125 MHz, DMSO-d<sub>6</sub>, RT): δ (ppm) = 164.73 (1C, 7), 150.53 (2C, 1), 129.48 (1C, 3), 124.40 (2C, 4), 117.90 (2C, 5), 108.73 (2C, 6), 44.36 (2C, 9), 35.42 (2C, 2)

FT-IR (ATR)  $\tilde{\nu}$  (cm<sup>-1</sup>): 3084 (w), 3022 (vw), 3009 (vw), 2183 (s), 2144 (vs), 1594 (s), 1580 (s), 1507 (s), 1332 (s), 1282 (s), 1236 (w), 1199 (m), 952 (w), 873 (s), 747 (m)

UV/Vis (DMSO)  $\lambda_{\text{max}}$  nm ( $\epsilon$  [Lmol<sup>-1</sup> cm<sup>-1</sup>]): 405 (22800)

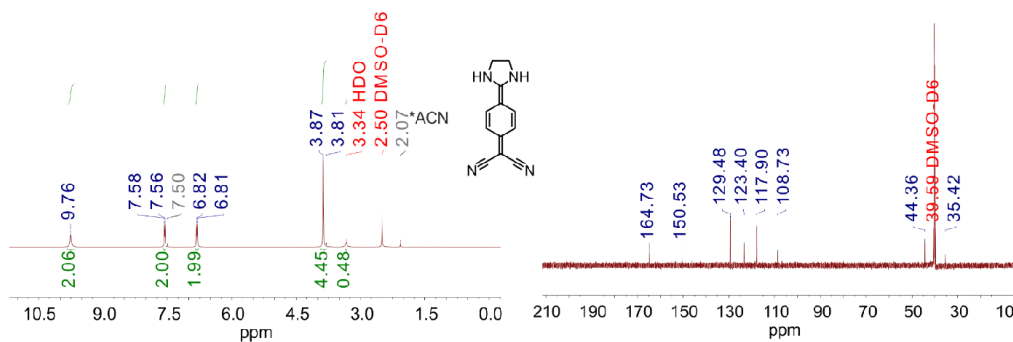
UV/Vis (ACN)  $\lambda_{\text{max}}$  nm ( $\epsilon$  [Lmol<sup>-1</sup> cm<sup>-1</sup>]): 357 (4000), 409 (4000)

UV/Vis (DMF)  $\lambda_{\text{max}}$  nm ( $\epsilon$  [Lmol<sup>-1</sup> cm<sup>-1</sup>]): 363 (13000), 410 (18000)

UV/Vis (Methanol)  $\lambda_{\text{max}}$  nm ( $\epsilon$  [Lmol<sup>-1</sup> cm<sup>-1</sup>]): 395 (36875)

MS (EI): m/z = 210.1 (100)[MH]<sup>+</sup>; 209.1 (50); 182.1 (40); 181.1 (100); 155.1 (15); 141.0 (15); 114 (15)

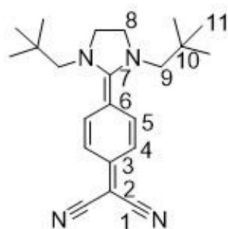
EA: C<sub>15</sub>H<sub>12</sub>N<sub>4</sub>; calc.: C, 68.56; N, 26.65; H, 4.79 meas.: C, 68.22; N, 25.76; H, 5.03





## SUPPORTING INFORMATION

## 2-(4-(1,3-dineopentylimidazolidin-2-ylidene)cyclohexa-2,5-dien-1-ylidene)malononitrile (2)



Compound **9** (95 mg, 0.47 mmol, 1 eq.), dissolved in acetonitrile (5 mL), was added to a 40 °C warm solution of compound **8** (117.7 mg, 0.47 mmol, 1 eq.) in acetonitrile (7 mL). After 4 hours at 75 °C the solution was deep yellow and allowed to cool to room temperature over night. The precipitate, a yellow powder, was filtered off, washed with cooled acetonitrile (3x 3 mL) and recrystallized in acetonitrile to form neat orange crystals (113.9 mg, 0.32 mmol, 65.4%).

$^1\text{H NMR}$  (500 MHz,  $\text{DMSO-d}_6$ , RT):  $\delta$  (ppm) = 7.11 (d, 2H,  $^3J = 10.0$  Hz, 4), 6.86 (d, 2H,  $^3J = 10.0$  Hz, 5), 4.03 (s, 4H, 7), 3.11 (s, 4H, 8), 0.78 (s, 18H, 10)

$^{13}\text{C NMR}$  (125 MHz,  $\text{DMSO-d}_6$ , RT):  $\delta$  (ppm) = 168.87 (1C, 7), 146.96 (2C, 1), 129.73 (1C, 3), 124.57 (2C, 4), 118.08 (2C, 5), 109.05 (2C, 6), 58.77 (2C, 8), 50.86 (2C, 9), 39.58 (1C, 2), 33.10 (1C, 2), 31.86 (2C, 10), 28.33 (6C, 11)

FT-IR (ATR)  $\tilde{\nu}$  ( $\text{cm}^{-1}$ ): 2975 (s), 2891 (m), 1648 (m), 1455 (w), 1418 (m), 1378 (m), 1318 (vw), 1085 (vs), 1045 (s), 879 (s)

UV/Vis (Ethanol)  $\lambda_{\text{max}}$  nm ( $\epsilon$  [ $\text{Lmol}^{-1} \text{cm}^{-1}$ ]): 363 (16218)

UV/Vis (Methanol)  $\lambda_{\text{max}}$  nm ( $\epsilon$  [ $\text{Lmol}^{-1} \text{cm}^{-1}$ ]): 354 (16800)

UV/Vis (THF)  $\lambda_{\text{max}}$  nm ( $\epsilon$  [ $\text{Lmol}^{-1} \text{cm}^{-1}$ ]): 334 (6250), 410 (22750)

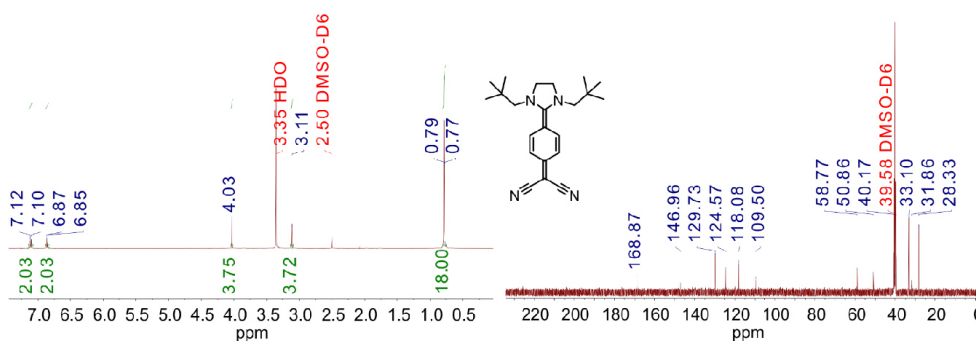
UV/Vis (ACN)  $\lambda_{\text{max}}$  nm ( $\epsilon$  [ $\text{Lmol}^{-1} \text{cm}^{-1}$ ]): 362 (11500)

UV/Vis (DMSO)  $\lambda_{\text{max}}$  nm ( $\epsilon$  [ $\text{Lmol}^{-1} \text{cm}^{-1}$ ]): 363 (19000)

UV/Vis (DMF)  $\lambda_{\text{max}}$  nm ( $\epsilon$  [ $\text{Lmol}^{-1} \text{cm}^{-1}$ ]): 366 (12000)

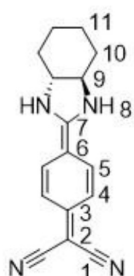
MS (ESI):  $m/z$  = 389.21 (10) [ $\text{M-K}^+$ ], 373.24 (25) [ $\text{M-Na}^+$ ], 351.25 (100) [ $\text{M}^+$ ], 281.18 (8), 211.10 (5)

EA:  $\text{C}_{22}\text{H}_{30}\text{N}_4$ ; calc.: C, 75.39; N, 15.98; H, 8.63 meas.: C, 75.39; N, 16.04; H, 8.77



## SUPPORTING INFORMATION

## 2-(4-(octahydro-2H-benzo[d]imidazol-2-ylidene)cyclohexa-2,5-dien-1-ylidene)malononitrile (3)



Under argon atmosphere (1*R*,2*R*)-(-)-1,2-Diaminocyclohexane (32.2 mg, 0.28 mmol, 1 eq.), dissolved in acetonitrile (8 mL), was added to a 40 °C warm solution of 8 (70 mg, 0.28 mmol, 1 eq.) in acetonitrile (12 mL). The solution turned yellow after 2 hours at 70 °C. After cooling to room temperature, the solution stood for 2 days in the fridge. Filtration then yielded a fine grain greenish powder which was washed with cooled acetonitrile (3x 3 mL). The product was recrystallized from acetonitrile to yield fine yellow crystals (50.1 mg, 0.19 mmol, 67.2%).

<sup>1</sup>H NMR (700 MHz, DMSO-*d*<sub>6</sub>, RT): δ (ppm) = 10.01 (bs, 2H, 8), 7.61 (d, <sup>3</sup>*J* = 7.0 Hz, 2H, 4), 6.83 (d, <sup>3</sup>*J* = 7.0 Hz, 2H, 5), 3.43 (m, 2H, 9), 2.16 (d, 2H, 10a), 1.81 (d, 2H, 10b), 1.56 (quint., 2H, 11a), 1.36 (quint., 2H, 11b),

<sup>13</sup>C NMR (176 MHz, DMSO-*d*<sub>6</sub>, RT): δ (ppm) = 166.43 (1C, 7), 151.04 (1C, 1), 129.44 (1C, 3), 123.01 (2C, 4), 117.90 (2C, 5), 108.73 (2C, 6), 64.19 (2C, 9), 36.27 (1C, 2), 28.24 (2C, 10), 23.85 (2C, 11)

FT-IR (ATR)  $\tilde{\nu}$  (cm<sup>-1</sup>): 3182 (w), 2939 (vw), 2182 (w), 2139 (s), 1588 (vs), 1496 (vs), 1456 (m), 1331 (s), 1299 (vs), 1196 (vs), 1141 (m), 1106 (m), 832 (vs), 734 (s), 718 (m)

All Coefficients calculated from 1E-5 M Solutions

UV/Vis (Acetone)  $\lambda_{\text{max}}$  nm ( $\epsilon$  [Lmol<sup>-1</sup> cm<sup>-1</sup>]): 366 (22600), 432 (17900)

UV/Vis (DMF)  $\lambda_{\text{max}}$  nm ( $\epsilon$  [Lmol<sup>-1</sup> cm<sup>-1</sup>]): 367 (15800), 419 (31700)

UV/Vis (Ethanol)  $\lambda_{\text{max}}$  nm ( $\epsilon$  [Lmol<sup>-1</sup> cm<sup>-1</sup>]): 416 (54100)

UV/Vis (Methanol)  $\lambda_{\text{max}}$  nm ( $\epsilon$  [Lmol<sup>-1</sup> cm<sup>-1</sup>]): 407 (44000)

UV/Vis (Benzonitrile)  $\lambda_{\text{max}}$  nm ( $\epsilon$  [Lmol<sup>-1</sup> cm<sup>-1</sup>]): 438 (41500)

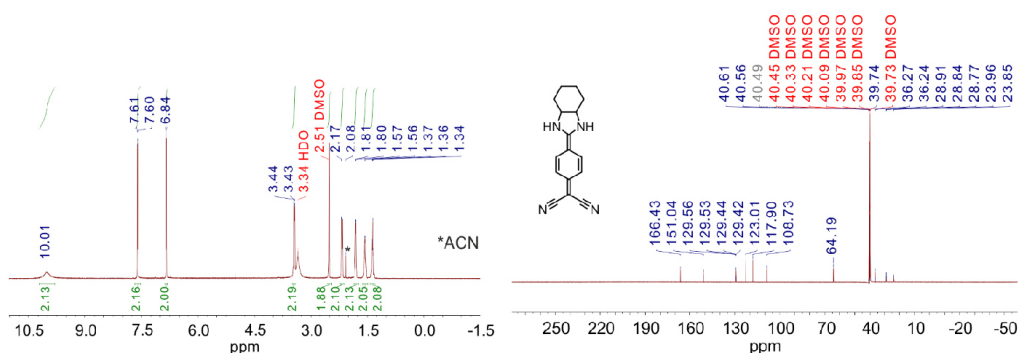
UV/Vis (THF)  $\lambda_{\text{max}}$  nm ( $\epsilon$  [Lmol<sup>-1</sup> cm<sup>-1</sup>]): 451 (46600)

UV/Vis (DMSO)  $\lambda_{\text{max}}$  nm ( $\epsilon$  [Lmol<sup>-1</sup> cm<sup>-1</sup>]): 418 (45500)

UV/Vis (Acetonitrile)  $\lambda_{\text{max}}$  nm ( $\epsilon$  [Lmol<sup>-1</sup> cm<sup>-1</sup>]): 361 (13900), 424 (14900)

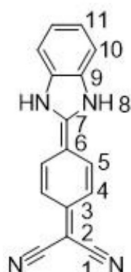
MS (EI): *m/z* = 264 [MH]<sup>+</sup> (35), 235 (20), 221 (100), 222 (25), 209 (22), 168 (15), 68 (32)

EA: C<sub>16</sub>H<sub>16</sub>N<sub>4</sub>; calc.: C, 72.70; N, 21.20; H, 6.10; meas.: C, 72.91; N, 21.11; H, 6.12



## SUPPORTING INFORMATION

## 2-(4-(1,3-dihydro-2H-benzof[d]imidazol-2-ylidene)cyclohexa-2,5-dien-1-ylidene)malononitrile (4)



Under argon atmosphere, ortho-Phenyldiamine (70.0 mg, 0.64 mmol, 1 eq.), dissolved in acetonitrile (15 mL), was added to a 40 °C warm solution of compound 8 (160.0 mg, 0.64 mmol, 1 eq.) in acetonitrile (20 mL). The solution turned red after 20 hours at 70 °C. After cooling to room temperature, the solution stood for 4 days in the fridge. Filtration then yielded a fine grain greenish powder which was washed with cooled acetonitrile (3x 5 mL). The product was recrystallized from acetonitrile to yield fine yellow crystals (70.2 mg, 0.27 mmol, 42.5%).

$^1\text{H NMR}$  (700 MHz,  $\text{DMSO-d}_6$ , RT):  $\delta$  (ppm) = 14.35 (bs, 2H, 8), 7.86 (d,  $^3J = 8.7$  Hz, 2H, 4), 7.69 (q,  $^3J = 8.7$  Hz, 2H, 11), 7.47 (q,  $^3J = 8.6$  Hz, 2H, 10), 6.95 (d,  $^3J = 8.7$  Hz, 2H, 5)

$^{13}\text{C NMR}$  (176 MHz,  $\text{DMSO-d}_6$ , RT):  $\delta$  (ppm) = 150.27 (1C, 1), 149.31 (1C, 7), 132.26 (1C, 3), 128.54 (1C, 4), 125.48 (2C, 10), 123.51 (2C, 9), 118.49 (2C, 5), 113.47 (2C, 11), 79.63 (1C, 6), 35.11 (1C, 2)

FT-IR (ATR)  $\tilde{\nu}$  ( $\text{cm}^{-1}$ ): 2952 (w), 2877 (w), 2849 (w), 2761 (w), 2190 (s), 2140 (s), 1637 (w), 1612 (m), 1503 (m), 1459 (m), 1387 (m), 1336 (m), 1230 (m), 1201 (m), 819 (s), 742 (s)

UV/Vis (DMF)  $\lambda_{\text{max}}$  nm ( $\epsilon$  [ $\text{Lmol}^{-1} \text{cm}^{-1}$ ]): 391 (56500)

UV/Vis (ACN)  $\lambda_{\text{max}}$  nm ( $\epsilon$  [ $\text{Lmol}^{-1} \text{cm}^{-1}$ ]): 385 (86800)

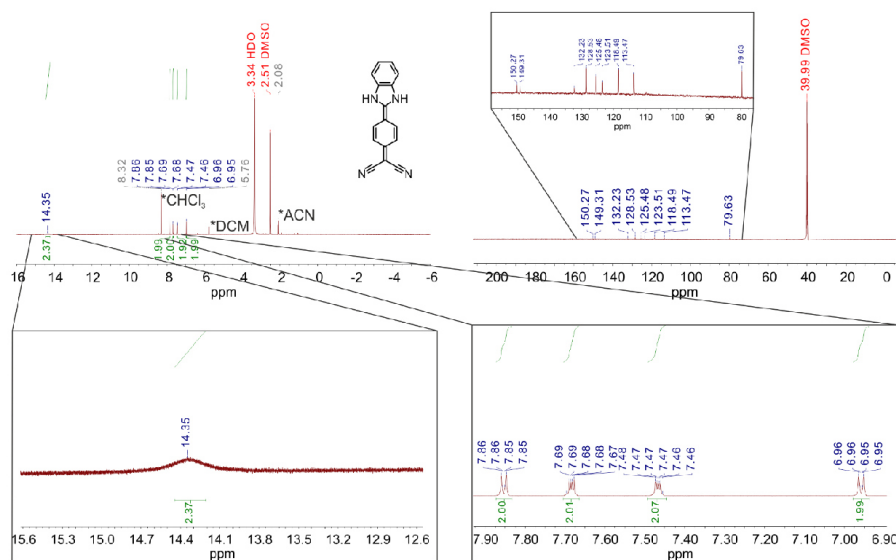
UV/Vis (DMSO)  $\lambda_{\text{max}}$  nm ( $\epsilon$  [ $\text{Lmol}^{-1} \text{cm}^{-1}$ ]): 392 (42200)

UV/Vis (THF)  $\lambda_{\text{max}}$  nm ( $\epsilon$  [ $\text{Lmol}^{-1} \text{cm}^{-1}$ ]): 388 (7000)

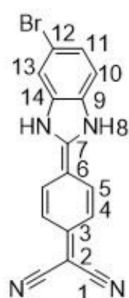
UV/Vis (MeOH)  $\lambda_{\text{max}}$  nm ( $\epsilon$  [ $\text{Lmol}^{-1} \text{cm}^{-1}$ ]): 424 (20000)

MS (EI):  $m/z = 259.10$  (15), 258.09 [ $\text{MH}]^+$  (100), 257.10 (5), 232 (5)

EA:  $\text{C}_{16}\text{H}_{16}\text{N}_4$ ; calc.: C, 74.40; N, 21.69; H, 3.90; meas.: C, 74.31; N, 21.78; H, 4.07;



## SUPPORTING INFORMATION

**2-(4-(5-bromo-1,3-dihydro-2H-benzo[d]imidazol-2-ylidene)cyclohexa-2,5-dien-1-ylidene)malononitrile (5)**

Under argon atmosphere 1,2-Diamino-4-Bromobenzene (494.0 mg, 2.640 mmol, 1 eq.) was added to a solution of compound 8 (637.0 mg, 2.570 mmol, 1 eq.) in ethanol (30 mL). After 12 hours under reflux conditions the solution turned red and a yellow powder precipitated. It was filtrated and washed with cooled ethanol (3x 5 mL) to yield a yellow powder (298.7 mg, 0.885 mmol, 34.0%).

**<sup>1</sup>H NMR** (700 MHz, DMSO-d<sub>6</sub>, RT): δ (ppm) = 14.32 (bs, 2H, 8), 7.83 (d, 1H, <sup>3</sup>J = 14.0 Hz, 4), 7.81 (s, 1H, 13), 7.58 (multiplet, 2H, <sup>3</sup>J = 14.0 Hz, 10+11), 6.93 (d, 2H, <sup>3</sup>J = 7.0 Hz, 5)

**<sup>13</sup>C NMR** (176 MHz, DMSO-d<sub>6</sub>, RT): δ (ppm) = 151.29 (2C, 1), 149.48 (1C, 7), 134.03 (1C, 3), 131.88 (2C, 4), 128.67 (1C, 13), 128.14 (1C, 10), 123.80 (1C, 14), 118.48 (1C, 9), 117.23 (2C, 5), 116.05 (1C, 11), 115.21 (1C, 6), 109.53 (1C, 12), 35.56 (1C, 2)

**FT-IR** (ATR)  $\tilde{\nu}$  (cm<sup>-1</sup>): 819.63 (s), 856.28 (w), 1051.07 (m), 1504.28 (s), 1575.63 (w), 1604.56 (s), 2138.78 & 2192.78 (s), 2235.20 (w)

**UV/Vis** (DMF)  $\lambda_{\text{max}}$  nm ( $\epsilon$  [Lmol<sup>-1</sup> cm<sup>-1</sup>]): 398 (34470)

**UV/Vis** (ACN)  $\lambda_{\text{max}}$  nm ( $\epsilon$  [Lmol<sup>-1</sup> cm<sup>-1</sup>]): 392 (46170) (2.5E-6 mol/L Solution)

**UV/Vis** (DMSO)  $\lambda_{\text{max}}$  nm ( $\epsilon$  [Lmol<sup>-1</sup> cm<sup>-1</sup>]): 398 (108600)

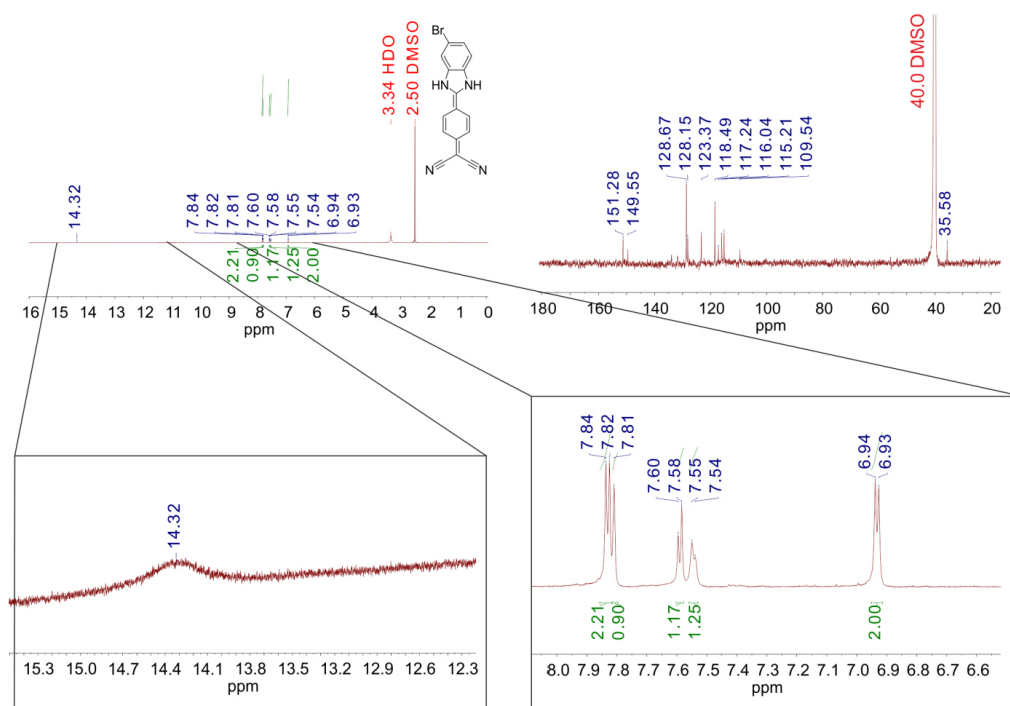
**UV/Vis** (THF)  $\lambda_{\text{max}}$  nm ( $\epsilon$  [Lmol<sup>-1</sup> cm<sup>-1</sup>]): 398 (53670)

**UV/Vis** (MeOH)  $\lambda_{\text{max}}$  nm ( $\epsilon$  [Lmol<sup>-1</sup> cm<sup>-1</sup>]): 317 (87490)

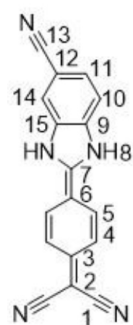
**MS** (ESI<sup>+</sup>):  $m/z$  = 334.99, 335.97, 336.99, 337.99 [MH]<sup>+</sup>: 334.99, 335.99, 336.99, 337.995

**EA**: C<sub>16</sub>H<sub>9</sub>BrN<sub>4</sub>; calc.: C, 57.00; N, 16.62; H, 2.69; Br, 23.70; meas.: C, 57.05; N, 16.64; H, 3.61; other, 23.15;

## SUPPORTING INFORMATION



**2-(4-(5-cyano-1,3-dihydro-2H-benzo[d]imidazol-2-ylidene)cyclohexa-2,5-dien-1-ylidene)malononitrile (6)**



Under argon atmosphere 3,4-Diaminobenzonitrile (39.8 mg, 0.30 mmol, 1 eq.) was added to a solution of **8** (75.0 mg, 0.30 mmol, 1 eq.) in ethanol (8 mL). After 3 days at 65 °C the solution turned red and yellow powder precipitated. It was filtrated and washed with cooled ethanol (3x 5 mL) to yield a yellow powder (16.0 mg, 0.056 mmol, 18.0%).

<sup>1</sup>H NMR (700 MHz, DMSO-d<sub>6</sub>, RT): δ (ppm) = 16.00 (bs, 2H, 8), 8.18 (s, 1H, 14), 7.88 (d, <sup>3</sup>J = 7.0 Hz, 2H, 4), 7.83 (d, 1H, <sup>3</sup>J = 7.0 Hz, 11), 7.80 (d, 1H, <sup>3</sup>J = 7.0 Hz, 10), 6.95 (d, <sup>3</sup>J = 7.0 Hz, 2H, 5)

<sup>13</sup>C NMR (176 MHz, DMSO-d<sub>6</sub>, RT): δ (ppm) = 153.02 (2C, 1), 149.92 (1C, 13), 136.17 (1C, 7), 133.00 (1C, 3), 128.93 (2C, 4), 128.92 (2C, 10), 123.26 (1C, 15), 119.37 (1C, 9), 118.53 (2C, 5), 118.05 (1C, 14), 114.61 (1C, 11), 109.59 (1C, 6), 106.96 (1C, 12), 36.03 (1C, 2)

## SUPPORTING INFORMATION

**FT-IR (ATR)**  $\tilde{\nu}$  (cm<sup>-1</sup>): 817.67 (s), 949.77 (m), 1204.33 (m), 1340.28 (m), 1604.48 (s), 2146.38 (vs), 2196.52 (m), 2229.31 (w), 2852.2 (w)

**UV/Vis (DMF)**  $\lambda_{\text{max}}$  nm ( $\epsilon$  [Lmol<sup>-1</sup> cm<sup>-1</sup>]): 318 (32460)

**UV/Vis (ACN)**  $\lambda_{\text{max}}$  nm ( $\epsilon$  [Lmol<sup>-1</sup> cm<sup>-1</sup>]): 335 (19600)

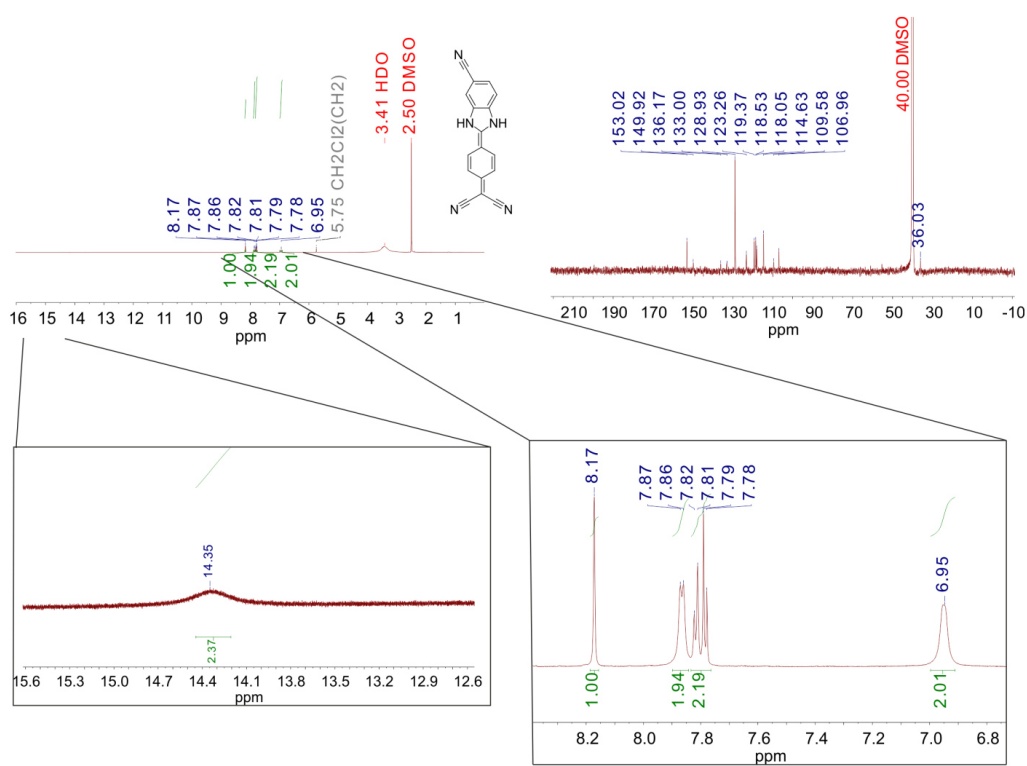
**UV/Vis (DMSO)**  $\lambda_{\text{max}}$  nm ( $\epsilon$  [Lmol<sup>-1</sup> cm<sup>-1</sup>]): 360 (24750)

**UV/Vis (THF)**  $\lambda_{\text{max}}$  nm ( $\epsilon$  [Lmol<sup>-1</sup> cm<sup>-1</sup>]): 319 (40710)

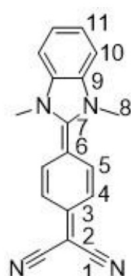
**UV/Vis (MeOH)**  $\lambda_{\text{max}}$  nm ( $\epsilon$  [Lmol<sup>-1</sup> cm<sup>-1</sup>]): 316 (30310)

**MS (ESI)**:  $m/z$  = 282.07, 283.07, 284.07, 284.09 [M]<sup>+</sup> 282.079, 283.076, 283.082, 284.085

**EA**: C<sub>20</sub>H<sub>12</sub>N<sub>4</sub>; calc.: C, 72.08; N, 24.72; H, 3.20; meas.: C, 67.34; N, 21.11; H, 3.23;



## SUPPORTING INFORMATION

**2-(4-(1,3-Dimethyl-1,3-dihydro-2H-benzo[d]imidazol-2-ylidene)cyclohexa-2,5-dien-1-ylidene)malononitrile (7)**

43.5  $\mu\text{L}$  *N,N'*-Dimethyl-1,2-phenylenediamin (0.054 g, 0.4 mmol) was added to a warm solution of **8** (0.1 g, 0.4 mmol) in acetonitrile (13 mL). The solution was stirred for 20 hours at 70 °C. After cooling to room temperature filtration yielded a fine grain yellow powder which was washed with cooled acetonitrile (3x 5 mL). Yield: 28.3 mg, 0.1 mmol, 25%.

**<sup>1</sup>H NMR** (700 MHz, DMSO-*d*<sub>6</sub>, RT):  $\delta$  (ppm) = 8.01 (dd,  $J$  = 6.0, 3.0 Hz, 2H, 11), 7.67 (dd,  $J$  = 6.0, 2.9 Hz, 2H, 10), 7.49 (d,  $J$  = 8.5 Hz, 2H, 4), 6.98 (d,  $J$  = 8.2 Hz, 2H, 5), 3.92 (s, 6H, 8)

**<sup>13</sup>C NMR** (176 MHz, DMSO-*d*<sub>6</sub>, RT):  $\delta$  (ppm) = 151.89 (1C, 1), 148.15 (1C, 7), 132.18 (1C, 3), 131.36 (2C, 5), 126.40 (2C, 9), 123.82 (2C, 11), 118.04 (2C, 4), 113.26 (1C, 10), 109.87 (2C, 8), 106.88 (2C, 6), 32.92 (2C, 2)

**FT-IR** (ATR)  $\tilde{\nu}$  (cm<sup>-1</sup>): 151.54 (1C, 1), 147.79 (1C, 7), 131.82 (1C, 3), 131.00 (2C, 5), 126.04 (2C, 9), 123.46 (2C, 11), 117.68 (2C, 4), 112.90 (1C, 10), 109.51 (2C, 8), 106.52 (2C, 6), 32.92 (2C, 2)

**UV/Vis** (DMF)  $\lambda_{\text{max}}$  nm ( $\epsilon$  [Lmol<sup>-1</sup> cm<sup>-1</sup>]): 415 (24100)

**UV/Vis** (ACN)  $\lambda_{\text{max}}$  nm ( $\epsilon$  [Lmol<sup>-1</sup> cm<sup>-1</sup>]): 409 (22200)

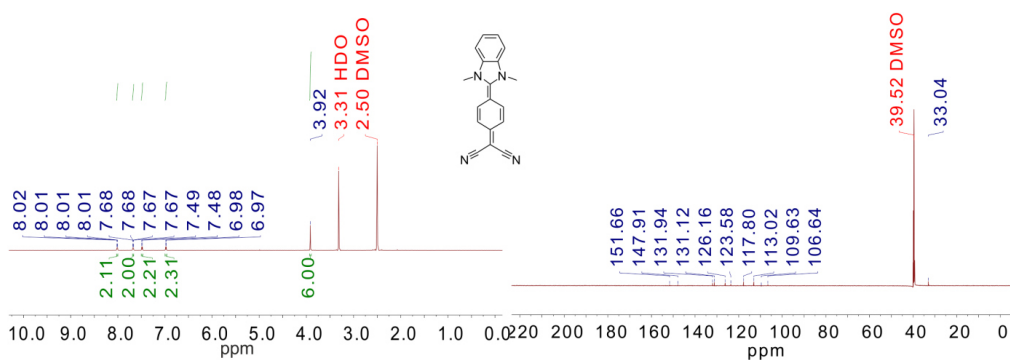
**UV/Vis** (DMSO)  $\lambda_{\text{max}}$  nm ( $\epsilon$  [Lmol<sup>-1</sup> cm<sup>-1</sup>]): 410 (20950)

**UV/Vis** (THF)  $\lambda_{\text{max}}$  nm ( $\epsilon$  [Lmol<sup>-1</sup> cm<sup>-1</sup>]): 454 (11600)

**UV/Vis** (MeOH)  $\lambda_{\text{max}}$  nm ( $\epsilon$  [Lmol<sup>-1</sup> cm<sup>-1</sup>]): 396 (16500)

**MS** (EI):  $m/z$  = 881.34 (23) [3 M-Na]<sup>+</sup>, 611.20 (26) [2 M-K]<sup>+</sup>, 595.22 (55) [2 M-Na]<sup>+</sup>, 325.08 (90) [M-K]<sup>+</sup>, 309.10 (100) [M-Na]<sup>+</sup>, 287.12 (55) [MH]<sup>+</sup>

**EA**: C<sub>18</sub>H<sub>14</sub>N<sub>4</sub>; calc.: C, 75.50; N, 19.57; H, 4.93; meas.: C, 71.13; N, 17.76; H, 5.11;



## SUPPORTING INFORMATION

## 3. Crystal Structures

Table S1: Crystallographic data and structure refinement details of 1-3. <sup>a)</sup> Data taken from [1]

	1 <sup>a</sup>	2	3
Empirical formula	C15 H17 N5 O	C22 H30 N4	C16 H16 N4
Weight	284.34	350.50	264.33
Temperature of measurement	100 K	100 K	101 K
Crystal System	N/A	monoclinic	monoclinic
Space Group	P-1	P 21/c	P2 <sub>1</sub>
Unit Cell Dimensions and volume	a = 5.6328(5) b = 11.2617(10) c = 11.2686(10) $\alpha$ = 86.4430(10) $\beta$ = 77.4390 (10) $\gamma$ = 85.4860(10)	a = 9.3411(2) b = 19.6042(3) c = 11.8719(2) $\alpha$ = 90 $\beta$ = 109.8547(7) $\gamma$ = 90	a = 9.4240(2) b = 11.9409(2) c = 12.0647(2) $\alpha$ = 90 $\beta$ = 91.446(2) $\gamma$ = 90
Volume[Å <sup>3</sup> ]	694.81 (11)	2044.81(6)	1357.22(4)
No. of units in unit cell (Z)	2	4	4
$\rho_{\text{calc}}$ [g/cm <sup>3</sup> ]	1.354	1.139	1.294
$\mu$ [mm <sup>-1</sup> ]	0.090	0.068	0.605
F(000)	300.0	760.0	560.0
Crystal size [mm <sup>3</sup> ]	0.5 x 0.34 x 0.1	0.560 x 0.480 x 0.180	0.370 x 0.060 x 0.020
Radiation and wavelength	MoK $\alpha$ ( $\lambda$ = 0.71073)	MoK $\alpha$ ( $\lambda$ = 0.71073)	MoK $\alpha$ ( $\lambda$ = 1.54178)
2 $\theta$ range for data collection [°]	3.7 to 52.76	4.636 to 51.464	7.33 to 133.602
Index ranges	-7 $\leq$ h $\leq$ 7, -14 $\leq$ k $\leq$ 14, -14 $\leq$ l $\leq$ 14	-11 $\leq$ h $\leq$ 11, -23 $\leq$ k $\leq$ 23, -14 $\leq$ l $\leq$ 14	-11 $\leq$ h $\leq$ 11, -12 $\leq$ k $\leq$ 14, -14 $\leq$ l $\leq$ 14
No. of Refl	7425	19722	11121
Independent Refl.	2813 [R <sub>int</sub> = 0.0360, R <sub>sigma</sub> = N/A]	3889 [R <sub>int</sub> = 0.0310, R <sub>sigma</sub> = 0.0228]	4200 [R <sub>int</sub> = 0.1331, R <sub>sigma</sub> = 0.1230]
Data/restraints/parameters	2813/0/258	3889/0/242	4200/1/356
Goodness-of-fit on F <sup>2</sup>	1.047	1.037	1.032
Final R indexes [ $ I  \geq 2\sigma(I)$ ]	R <sub>1</sub> = 0.0360, wR <sub>2</sub> = 0.1000	R <sub>1</sub> = 0.0384, wR <sub>2</sub> = 0.0918	R <sub>1</sub> = 0.0704, wR <sub>2</sub> = 0.1415
Final R indexes [all data]	R <sub>1</sub> = 0.0375, wR <sub>2</sub> = 0.1016	R <sub>1</sub> = 0.0444, wR <sub>2</sub> = 0.0954	R <sub>1</sub> = 0.1221, wR <sub>2</sub> = 0.1636
Largest diff. peak/hole [e Å <sup>-3</sup> ]	0.24/-0.23	0.30/-0.21	0.34/-0.27

Despite multiple efforts to crystalize compound **4** from different solvents and solvents mixtures it was not possible to get a measurable single crystal of the molecule.



## SUPPORTING INFORMATION

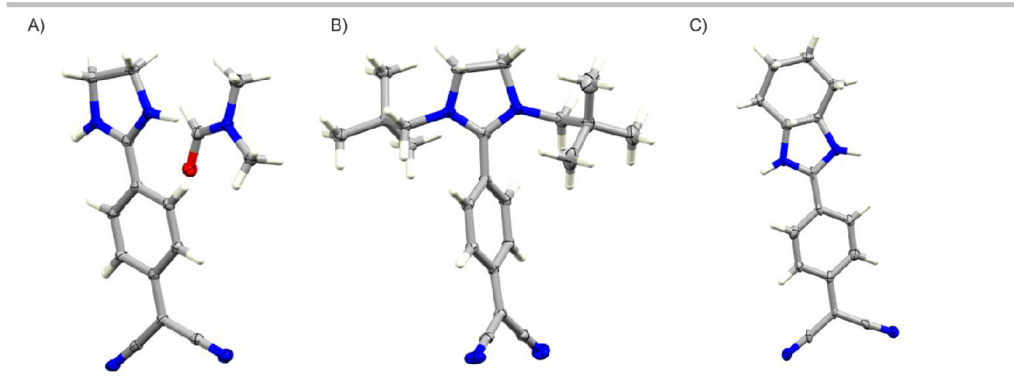


Figure S1: Crystal structures of compound 1 (A), taken from [1] crystallized with one molecule of dimethylformamide per unit cell, compound 2 (B) and compound 3 (C).

## SUPPORTING INFORMATION

## 4. UV/Vis and Fluorescence measurements

The absorption and fluorescence spectra are recorded at concentrations of  $10^{-6}$  M to avoid association phenomena.

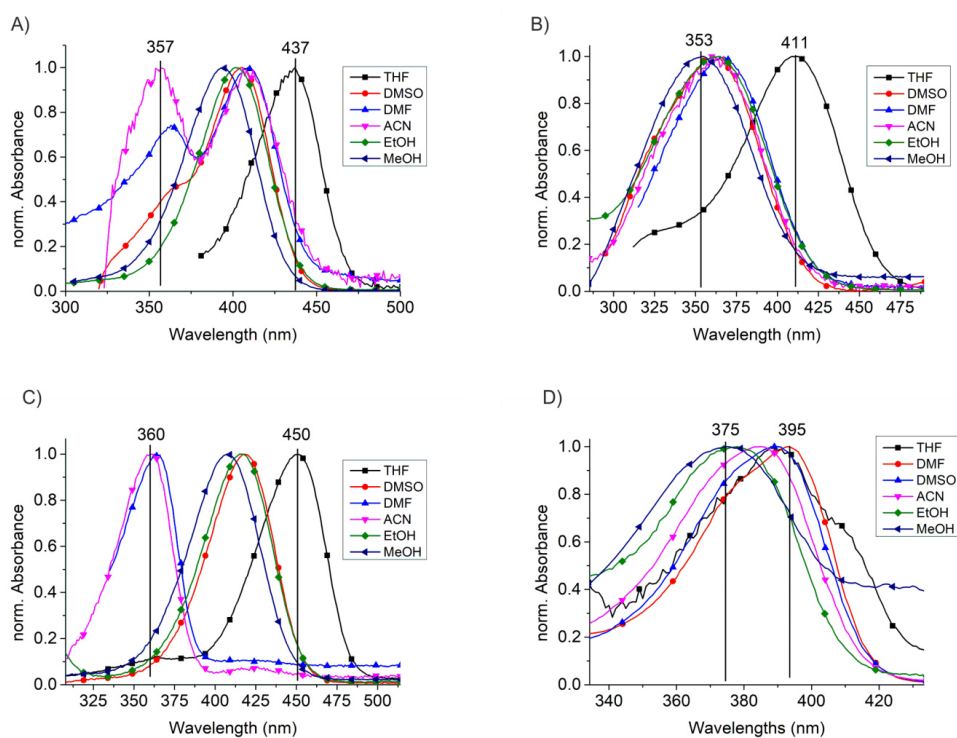


Figure S2: Normalized absorption spectra of compounds A) ethyl-bridged (1) B) Neopentyl-ethyl-bridged (2) C) cyclohexyl-bridged (3) D) benzene-bridged (4) in six solvents of increasing polarity: tetrahydrofuran, dimethylformamide, dimethyl sulfoxide, acetonitrile, ethanol, methanol.

Table S2: Absorption- and fluorescence-maxima with calculated Stokes shift for compound 1-4

$E_T^N$	Solvent	1			2			3			4		
		Abs <sub>max</sub> [nm]	Em <sub>max</sub> [nm]	Stokes Shift [nm]	Abs <sub>max</sub> [nm]	Em <sub>max</sub> [nm]	Stokes Shift [nm]	Abs <sub>max</sub> [nm]	Em <sub>max</sub> [nm]	Stokes Shift [nm]	Abs <sub>max</sub> [nm]	Em <sub>max</sub> [nm]	Stokes Shift [nm]
0.207	tetrahydrofuran	436	478	42	410	489	79	450	490	40	389	431	42
0.386	dimethylformamide	363	405	42	366	490	124	364	408	44	393	430	37
0.444	dimethyl sulfoxide	359	435	76	362	441	79	418	465	47	389	436	47
0.460	acetonitrile	355	417	62	361	500	139	360	413	53	385	439	54
0.654	ethanol	402	456	54	362	450	88	417	462	45	314	404	90
0.762	methanol	394	450	56	354	486	132	408	461	53	425	486	61

## SUPPORTING INFORMATION

## 5. Quantum Yield and Fluorescence Lifetimes measurements

Photoluminescence quantum yields ( $\Phi$ ) were determined absolutely with an integrating sphere setup from Hamamatsu (Quantaurus-QY C11347-11). All  $\Phi$  measurements were performed at 25 °C using special 10 mm x 10 mm long neck quartz cuvettes from Hamamatsu. Values below 1% quantum yield are not reliable in the measurement setup and are therefore given as < 1%. The uncertainty of  $\Phi$  measurements over 10% absolute value is about 5%.<sup>[2]</sup>

The fluorescence lifetime ( $t$ ), the average time in which the fluorophore is in an excited state before it relaxes to the ground state, was recorded on a fluorometer FLS 920 (Edinburgh Instruments) equipped with a Hamamatsu R3809U-50 (range 200–850 nm, response width <25 ps), Multi-Channel Plate (MCP) detector, Czerny-Turner double monochromators and either a supercontinuum laser (Fianium SC400-2-PP) or a Edinburgh Instrument EPLED-375 (picosecond pulsed light emitting diode) for excitation at 375 nm, or a Edinburgh Instrument EPL-330 (picosecond pulsed diode laser) for excitation at 330 nm. All the measurements were performed at T = 298 K using 10 mm x 10 mm quartz cuvettes from Hellma GmbH always filled with 2 mL of solvent or dye solution. Before each measurement, the instrument response function (IRF) was measured, which is important for the correct fit of the then measured data. The lifetime measurements were analysed with Edinburgh Instruments FAST Software and fitted with a reconvolution fit. All the lifetimes could be evaluated mono, bi- or tri-exponentially with a reduced  $\chi^2$  between 0.8 and 3.0. An exemplary formular for a multi exponential decay is given in Equations S1. From the multi-exponential decays, the intensity-weighted average lifetimes were calculated using Equation S2 and the fit parameter given by the FAST Software (see Figure S6 and Figure S8 / Figure S9)

$$I(t) = I_0 \times \sum B_i e^{-\frac{t}{\tau_i}}$$

*Equation S1: Formula for a multi-exponential decay.  $B_i$  is the pre-exponential factor.  $B_1$  is the amplitude of the first exponential term,  $B_2$  that of the second one and so on.  $\tau_i$  is the fluorescence lifetime.*

$$\tau = \frac{\sum B_i \tau_i^2}{\sum B_i \tau_i}$$

*Equation S2: Equation used for the evaluation of the fit parameters  $B_i$  and  $\tau_i$  given by the reconvolution fit of the multi-exponential decays to the measured fluorescence decays (see Figure S8).*

## SUPPORTING INFORMATION

❖ Exponential Components Analysis (Reconvolution)						
Fitting range	[679; 2000] channels					
$\chi^2$	1.067					
	$B_i$	$\Delta B_i$	$f_i$ (%)	$\Delta f_i$ (%)	$\tau_i$ (ns)	$\Delta \tau_i$ (ns)
1	0.0211	0.0014	2.616	2.67	0.271	0.259
2	0.1213	0.0008	97.384	0.668	1.756	0.0007
Shift	0.012 ( $\pm$ 0.926 ns)					
Decay Bac	2.655 ( $\pm$ 0.198 )					
IRF backgr	0					

Figure S3: Exemplary fit parameters given by the reconvolution fit of the multi-exponential decays using the Edinburgh Instruments FAST Software. The fit parameters  $B_i$  and  $\tau_i$  are used according to equation S2 to calculate the average lifetime of the excited state.  $B_i$  is the pre-exponential factor.  $\Delta B_i$  is the standard deviation of the associated  $B$  value.  $f_i$  is the "fraction of fluorescence intensity" in %. It is calculated from  $B_i$  and  $\tau_i$ .  $f_i$  characterises the brightness of the fluorescence component (which scales with the pre-exponential factor and the lifetime).  $\Delta f_i$  is the associated error of  $f_i$ .  $\Delta \tau_i$  standard deviation of the calculated lifetime. A shift parameter is fitted alongside the lifetime parameters. This shift characterises the delay of the decay process in respect to the IRF measurement. The fluorescence decay might be superimposed by a constant background. This background often originates from dark count rates of the detector, but might also be caused by light leaks to ambient light. IRF Background is the analogue to the decay background. Both should be close to zero. A constant background of hundreds or even thousands of counts in average is not unusual.

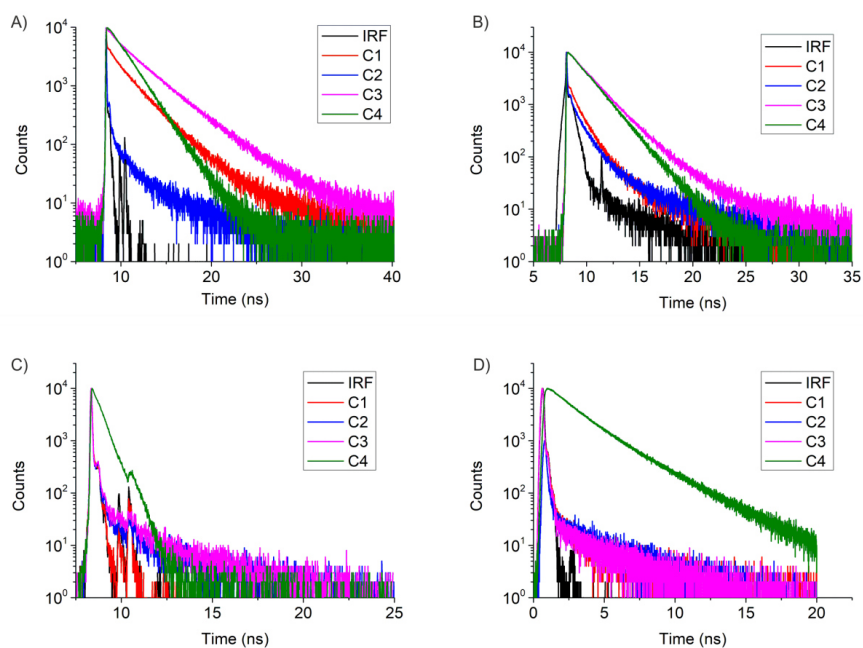


Figure S4: Fluorescence lifetime decays of compound 1-4 (1 red, 2 blue, 3 pink, 4 green) in dimethylformamide (A), DMSO (B), methanol (C) and tetrahydrofuran (D).

## SUPPORTING INFORMATION

A)

v Exponential Components Analysis (Reconvolution)						
Fitting range		[695; 2000] channels				
$\chi^2$		1.122				
	$B_i$	$DB_i$	$f_i$ (%)	$Df_i$ (%)	$t_i$ (ns)	$Dt_i$ (ns)
1	0.1315	0.0005	99.486	0.535	1.815	0.002
2	0.0001	0.0003	0.514	1.252	9.323	0.378
Shift	-0.046 ( $\pm$ )		0.576 ns)			
Decay Background	0.707 ( $\pm$ )		7.69 )			
IRF background	0.2					

B)

v Exponential Components Analysis (Reconvolution)						
Fitting range		[679; 2000] channels				
$\chi^2$		1.067				
	$B_i$	$DB_i$	$f_i$ (%)	$Df_i$ (%)	$t_i$ (ns)	$Dt_i$ (ns)
1	0.0211	0.0014	2.616	2.67	0.271	0.259
2	0.1213	0.0008	97.384	0.668	1.756	0.0007
Shift	0.012 ( $\pm$ )		0.926 ns)			
Decay Background	2.655 ( $\pm$ )		0.198 )			
IRF background	0					

C)

v Exponential Components Analysis (Reconvolution)						
Fitting range		[689; 2000] channels				
$\chi^2$		0.922				
	$B_i$	$DB_i$	$f_i$ (%)	$Df_i$ (%)	$t_i$ (ns)	$Dt_i$ (ns)
1	0.3521	0.1596	8.321	9414.047	0.015	17.19
2	0.0786	0.2477	51.033	690.807	0.417	4.335
3	0.0625	0.2477	40.646	693.117	0.418	5.474
Shift	0.017 ( $\pm$ )		0.3 ns)			
Decay Background	0.987 ( $\pm$ )		0.073 )			
IRF background	0.2					

Figure S5: Exemplary Fit parameters given by the reconvolution fit of the multi-exponential decays using the Edinburgh Instruments FAST Software for compound 4 in A) DMF, B) DMSO and C) MeOH. The decays in DMF and DMSO were fitted with a two-exponential function, the decay in MeOH with a three-exponential function. D denotes  $\Delta$  (see Figure S3 for details on all given values).

## SUPPORTING INFORMATION

A) $\nu$ Exponential Components Analysis (Reconvolution)						
Fitting range	[261; 4000] channels					
$\chi^2$	1.313					
	$B_i$	$DB_i$	$f_i$ (%)	$Df_i$ (%)	$t_i$ (ns)	$Dt_i$ (ns)
1	0.0112	9.10E-06	100	0.099	1.82	0.0003
Shift	0.001 ( $\pm$ 0.024 ns)					
Decay Background	1.247 ( $\pm$ 0.114 )					
IRF background	920					
B) $\nu$ Exponential Components Analysis (Reconvolution)						
Fitting range	[200; 2500] channels					
$\chi^2$	1.109					
	$B_i$	$DB_i$	$f_i$ (%)	$Df_i$ (%)	$t_i$ (ns)	$Dt_i$ (ns)
1	0.0152	0.0008	59.857	3.552	1.67	0.014
2	0.0049	0.0008	40.143	6.539	3.494	0.018
Shift	-0.084 ( $\pm$ 1.168 ns)					
Decay Background	-11.561 ( $\pm$ 8.734 )					
IRF background	5.9					
C) $\nu$ Exponential Components Analysis (Reconvolution)						
Fitting range	[609; 4000] channels					
$\chi^2$	1.078					
	$B_i$	$DB_i$	$f_i$ (%)	$Df_i$ (%)	$t_i$ (ns)	$Dt_i$ (ns)
1	0.0856	0.0016	5.295	3.882	0.176	0.125
2	0.0595	0.0003	38.47	0.241	1.838	0.003
3	0.016	0.0001	56.236	0.376	9.992	0.0005
Shift	-0.024 ( $\pm$ 0.432 ns)					
Decay Background	15.33 ( $\pm$ 0.69 )					
IRF background	0.2					

Figure S6: Fit parameters given by the reconvolution fit of the multi-exponential decays using the Edinburgh Instruments FAST Software for compound **4** in A) EtOH B) THF and C) CAN. The decays in DMF and DMSO were fitted with a two-exponential function, the decay in MeOH with a three-exponential function. D denotes  $\Delta$  (see Figure S3 for details on all given values).

## SUPPORTING INFORMATION

Table S3: Fluorescence Quantum Yields, Fluorescence lifetimes and calculated radiative / non-radiative rates of Compounds 1-4 in Solvents of different Polarity. Values for the normalized Dimroth-Reichardt parameter  $E_T^N$  were taken from ref.<sup>[3]</sup>

$E_T^N$	Solvent	1		2		3		4	
		$\Phi$ [%]	$\tau$ [ns]	$\Phi$ [%]	$\tau$ [ns]	$\Phi$ [%]	$\tau$ [ns]	$\Phi$ [%]	$\tau$ [ns]
0.207	THF	7.0	< 0.2	< 1	0.42	7.1	< 0.2	73.0	2.40
0.386	DMF	6.8	2.14	< 1	< 0.2	9.8	3.06	71.9	1.84
0.444	DMSO	10.1	0.75	< 1	0.43	7.1	2.79	92.4	1.79
0.460	ACN	7.3	< 0.2	< 1	2.40	12.2	6.74	71.3	6.33
0.654	EtOH	< 1	< 0.2	< 1	< 0.2	< 1	< 0.2	55.7	1.82
0.762	MeOH	< 1	< 0.2	< 1	3.18	< 1	< 0.2	34.9	0.38

Values below 0.2 ns are not reliable in this measurement setup and are therefore given as "< 0.2" ns.

Radiative and non-radiative rates were calculated using the following formula<sup>[4]</sup>:

$$k_r = \frac{\Phi}{\tau} \quad k_{nr} = \frac{1}{\tau} - k_r$$

Equation S3: Relationship between radiative rate, quantum yield  $\Phi$  and fluorescence lifetime  $\tau$  (left side).

Equation S4: Relationship between fluorescence lifetime  $\tau$ , radiative rate  $k_r$  and non-radiative rate  $k_{nr}$ .

Table S4: Radiative and non-radiative decay rates calculated from measured quantum yields and fluorescence lifetimes of compound 1-4. Values were determined from the equations given in reference [5] a) ( $10^8 \text{ s}^{-1}$ ). Values are omitted where the measurement of either quantum yield or fluorescence lifetime were below the measurement limit.

$E_T^N$	Solvent	1		2		3		4	
		$k_r$ ( $10^8 \text{ s}^{-1}$ )	$k_{nr}$ ( $10^8 \text{ s}^{-1}$ )	$k_r$ ( $10^8 \text{ s}^{-1}$ )	$k_{nr}$ ( $10^8 \text{ s}^{-1}$ )	$k_r$ ( $10^8 \text{ s}^{-1}$ )	$k_{nr}$ ( $10^8 \text{ s}^{-1}$ )	$k_r$ ( $10^8 \text{ s}^{-1}$ )	$k_{nr}$ ( $10^8 \text{ s}^{-1}$ )
0.207	THF	--	--	--	--	--	--	3.04	1.13
0.386	DMF	0.32	4.36	--	--	0.32	2.95	3.19	1.53
0.444	DMSO	1.35	0.12	0.05	23.21	0.25	3.33	5.16	0.43
0.460	ACN	--	--	--	--	0.18	1.30	1.13	0.45
0.654	EtOH	--	--	--	--	--	--	3.06	2.43
0.762	MeOH	--	--	--	--	--	--	9.18	17.1

## SUPPORTING INFORMATION

**6. Fluorescence measurement in solvent mixtures of differing viscosity and polarity**

To study the fluorescence behaviour in solvents of different viscosity ethanol-poly ethylene glycol mixtures of the same concentration were prepared and measured at constant parameters, i.e. slit width, excitation wavelengths etc., for each molecule respectively. From the absolute determined quantum yield in pure ethanol, we have then calculated the relative quantum yields in the EtOH-PEG mixtures by literature known procedures.<sup>[5]</sup> Solvent viscosities for all solvents used are listed in table S5. Since the difference in solvent viscosity is small and dimethylformamide, as one example, shows relatively high quantum yields for all molecules, but has a lower viscosity than dimethyl sulfoxide and methanol, the fluctuation of solvent viscosity without addition of an extremely viscous solvent like PEG can be neglected. With addition of 50% PEG to ethanol, the viscosity increases to 8.3 mPa s, in a mixture of 80% PEG the viscosity is 34.1 mPa s.

Table S5: Viscosity of the used solvents, ordered in increasing polarity. <sup>a)</sup> Values taken from reference <sup>[6]</sup>

$E_T^N$	Solvent	Viscosity [25 °C, mPa s] <sup>a)</sup>
0.207	tetrahydrofuran	0.55
0.386	dimethylformamide	0.82
0.444	dimethyl sulfoxide	2.00
0.460	acetonitrile	0.37
0.654	ethanol	1.08
0.762	methanol	0.60
--	PEG400/EtOH (80/20)	34.1



## SUPPORTING INFORMATION

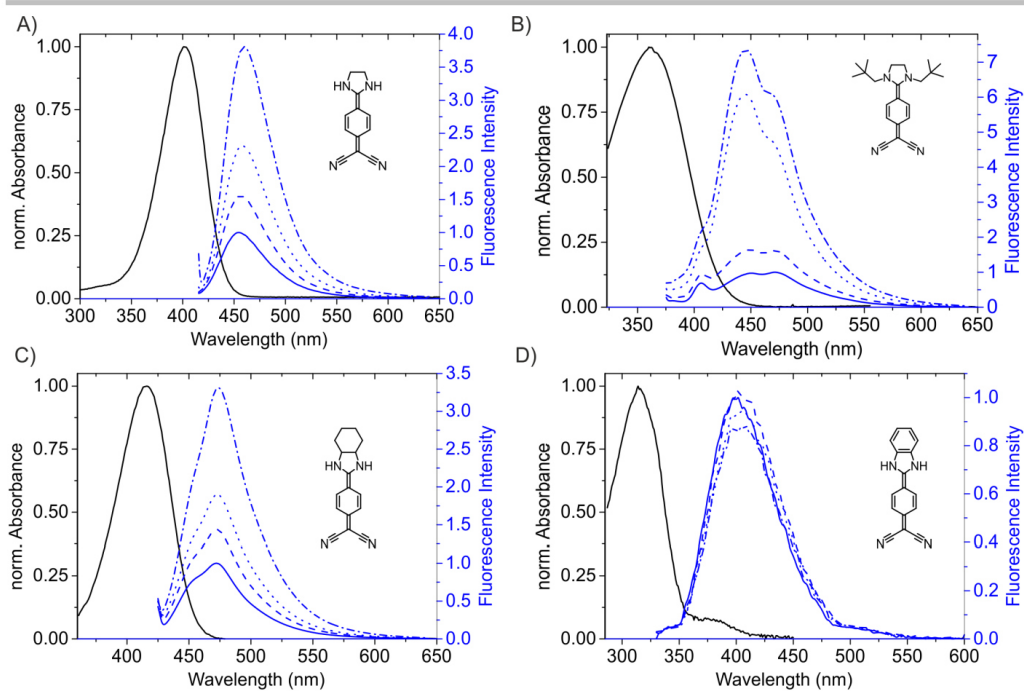


Figure S7: Normalized absorption spectrum and four emission spectra, respectively, of EtOH-PEG mixtures ranging from 0 to 75% PEG. A) Compound 1 Exc. Wavelength: 400 nm; Slit width 5 nm, Fluorescence Increase from 0% to 75% PEG by factor 3.8 B) Compound 2, Exc. Wavelength: 360 nm; Slit width 10 nm, Fluorescence Increase from 0% to 75% PEG by factor 7.6 C) Compound 3, Exc. Wavelength: 415 nm; Slit width 5 nm, Fluorescence Increase from 0% to 75% PEG by factor 3.3 D) Compound 4, Exc. Wavelength: 315 nm; Slit width 3 nm, Fluorescence Increase from 0% to 25% PEG by factor 1.03, decrease from 25% to 75% PEG.

## SUPPORTING INFORMATION

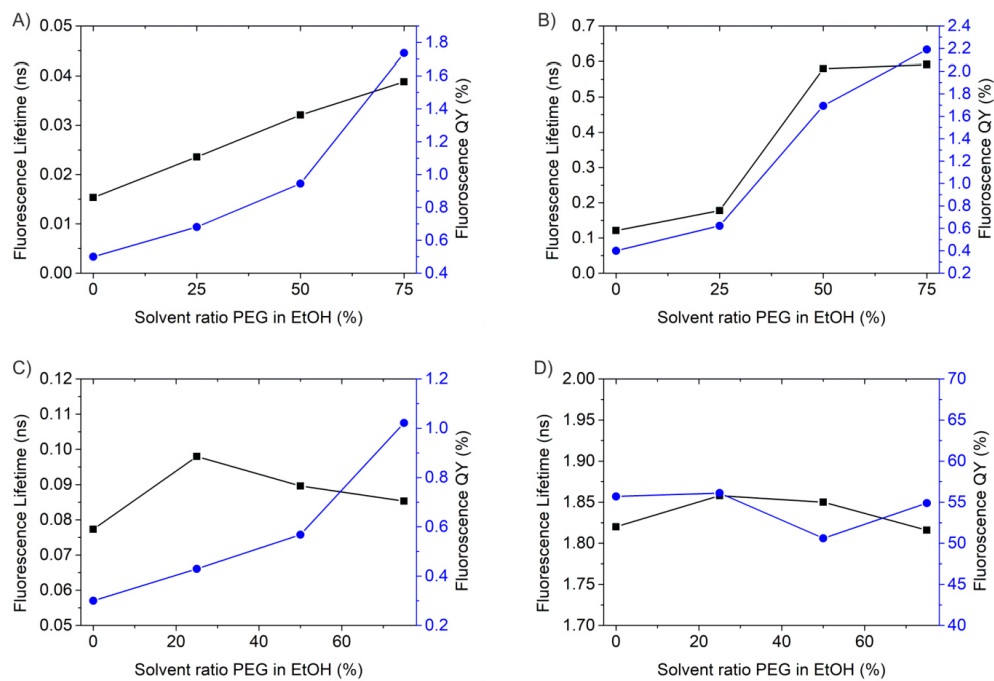


Figure S8: Fluorescence Lifetime (square) and Fluorescence Quantum Yield (circle) of EtOH-PEG mixtures ranging from 0 to 75% PEG for compound 1-4 (A-D).

## SUPPORTING INFORMATION

## 7. Fluorescence Measurements at elevated and reduced Temperatures

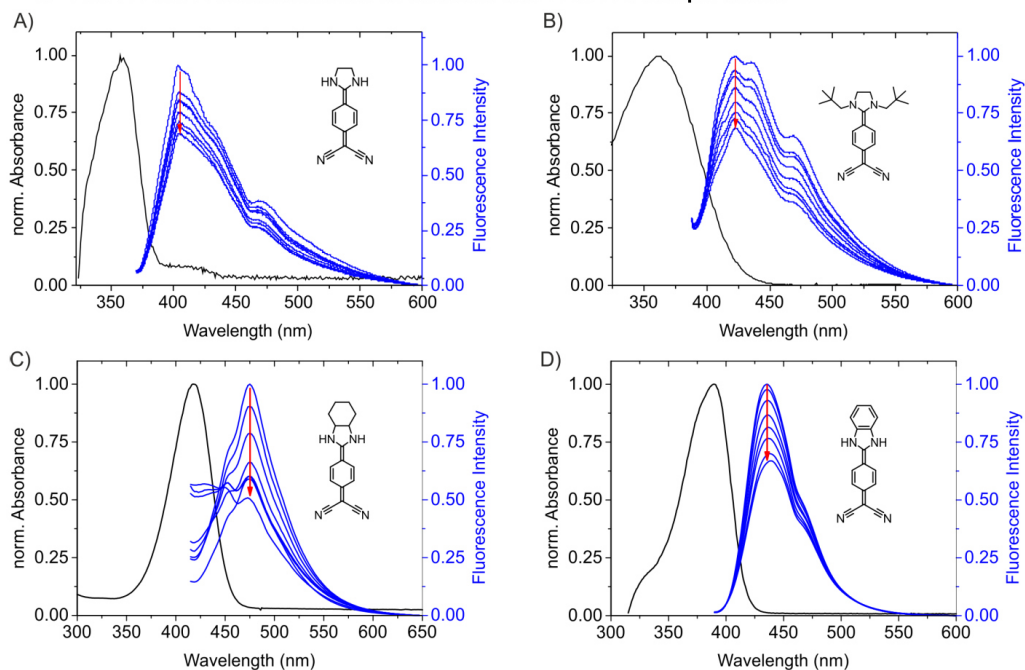


Figure S9: normalized Absorption spectrum (black) and fluorescence spectra (blue) at increasing temperature (red arrow, 40 to 110 °C in 10 °C steps) of **1-4** (A-D) in DMSO. The fluorescence decreases from 40 °C to 110 °C by 31% per for compound **1**, 32% per for compound **2**, 47% per for compound **3** and 33% for compound **4**.

## SUPPORTING INFORMATION

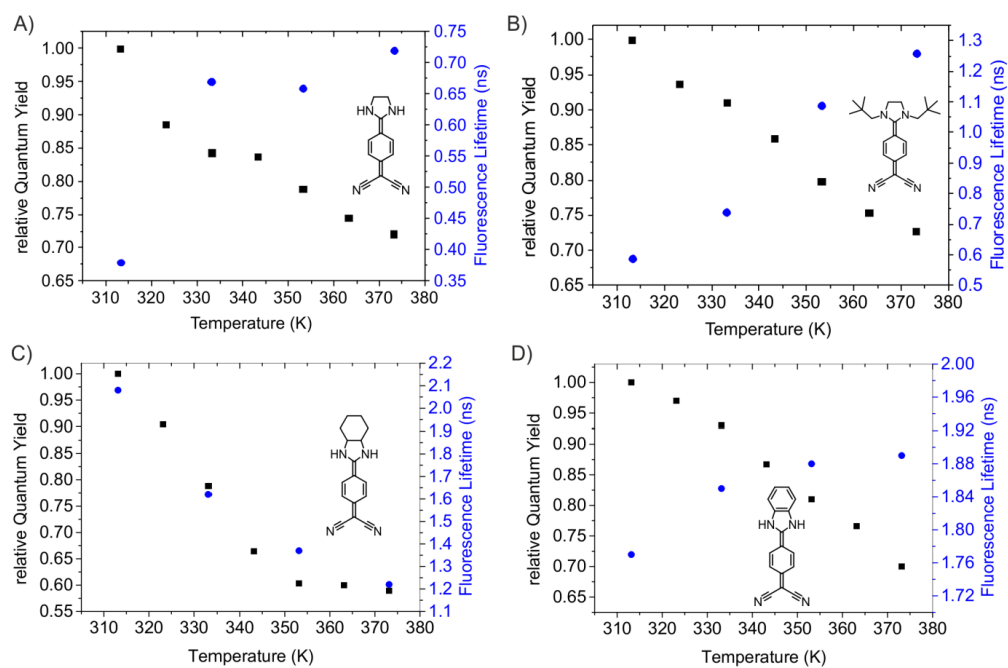


Figure S10: Relative Quantum Yields (normalized to the spectra at 40 °C) and Fluorescence lifetimes of Compound 1-4 (A-D) upon heating in DMSO in 10 °C (QY) and 20 °C (Fluorescence lifetime) steps. Whereas the QY decreases for all compounds, the lifetime increases for 1-2 and 4 but decreases for 3. The change of fluorescence lifetime is relatively small for compound 4 (1.77 ns (40 °C) to 1.89 ns (100 °C)) compared to 1-3. For example, compound 2 changes from 0.59 ns (40 °C) to 1.26 (100 °C), more than 100% change.

## SUPPORTING INFORMATION

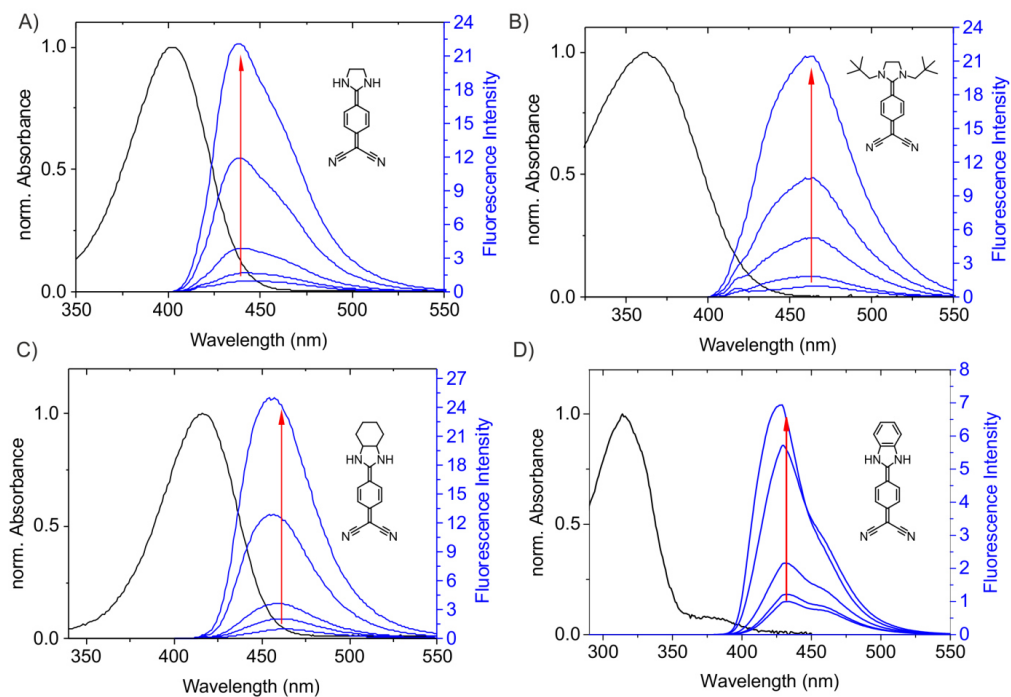


Figure S11: normalized Absorption spectra (black) and fluorescence spectra at decreasing temperature (red arrow, from 0 °C to -100 °C in 25 °C steps) of compound 1-4 (A-D) in EtOH. The fluorescence was normalized to the value at 0 °C respectively. The Fluorescence increases from 0 °C to -100 °C about 7 times for compound 4 (D), and over 20 times for compound 1-3 (25 for compound 3)

## SUPPORTING INFORMATION

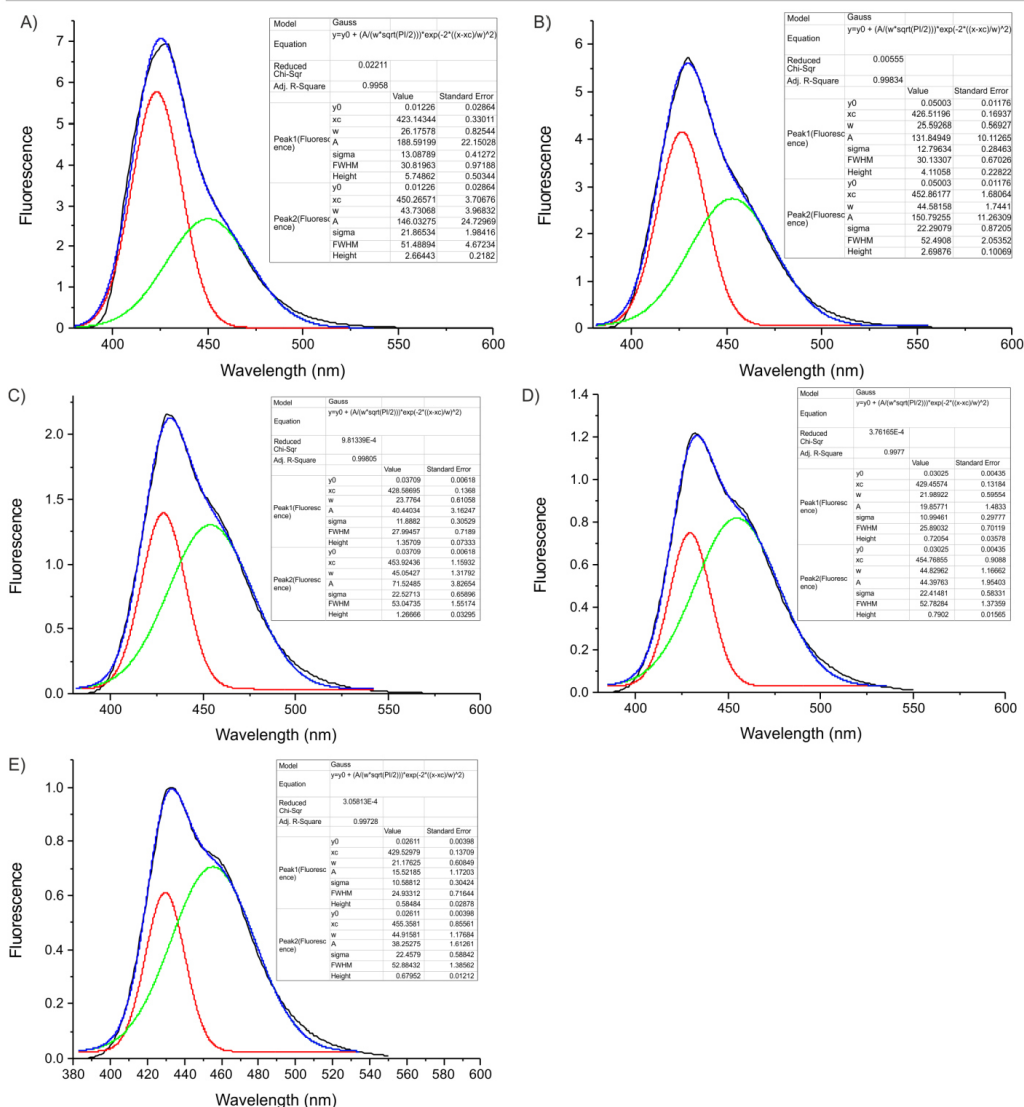


Figure S12: Fluorescence spectra (black) and fitted spectra (blue) of compound **4** upon cooling in EtOH (depicted in Figure S11D) A) 173 K B) 198 K C) 223 K D) 248 K E) 273 K. Red and green are the two peaks fitted inside the main peak, indicating that two species might be responsible for the emission. The ratio of the peaks change with temperature.

## SUPPORTING INFORMATION

## 8. Comparison of benzene functionalized derivatives

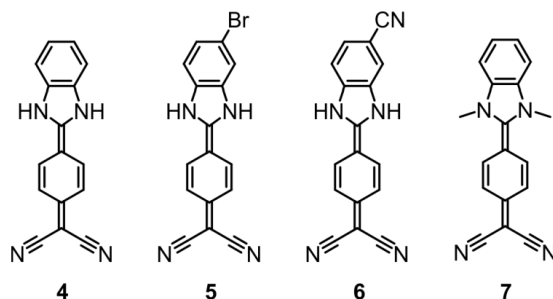


Figure S13: Molecular structures of compound 4-7

Table S6: Fluorescence Quantum Yields and Fluorescence lifetimes of Compounds 4-7 in Solvents of different Polarity. Values for the normalized Dimroth-Reichardt parameter  $E_T^N$  were taken from ref. [3]

$E_T^N$	Solvent	4		5		6		7	
		$\Phi$ [%]	$\tau$ [ns]	$\Phi$ [%]	$\tau$ [ns]	$\Phi$ [%]	$\tau$ [ns]	$\Phi$ [%]	$\tau$ [ns]
0.207	THF	73.0	2.4	33.9	0.5	68.5	1.4	< 1	--
0.386	DMF	71.9	1.8	61.6	1.8	81.3	2.0	3.3	0.5
0.444	DMSO	92.4	1.8	38.5	1.4	90.1	2.1	< 1	0.5
0.460	ACN	71.3	6.3	17.9	2.0	53.1	2.1	< 1	1.1
0.654	EtOH	55.7	1.8	62.8	1.4	70.3	1.8	< 1	--
0.762	MeOH	34.9	0.4	19.8	0.5	30.5	1.4	< 1	< 0.2

## 9. Cyclic voltammetry measurements

Cyclic voltammetry was carried out in dry and degassed dimethylformamide (DMF) solutions with tetrabutylammonium hexafluorophosphate (0.1 M) using a three-electrode configuration (glassy carbon, Pt counter electrode, Ag wire as pseudoreference) and a PAR VersaSTAT 4 (Princeton Applied Research) potentiostat. The S3 decamethylferrocene/decamethylferrocenium ([FeCp2\*]<sup>+/0</sup>) was used as the internal reference and referred to the ferrocene/ferrocenium (FcH<sup>+/0</sup>) couple.<sup>[7]</sup> The second and third cycle are always depicted and were taken for all evaluation of the data.

## SUPPORTING INFORMATION

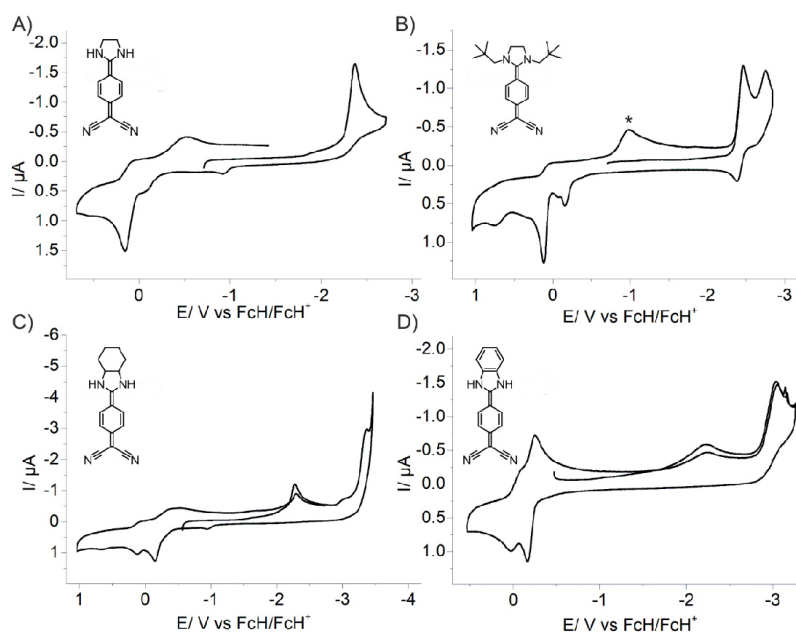


Figure S14: Voltammograms of compound 1-4 (A-D) measured in dimethylformamide solutions with tetrabutylammonium hexafluorophosphate (0.1M). Decamethylferrocene/decamethylferrocenium ([FcCp2\*]<sup>+/0</sup>) was used as the internal reference and referred to the ferrocene/ferrocenium (FcH<sup>+/0</sup>) couple. The molecular concentrations were  $\sim 10^{-2}$ . \* second scan wave.

Compounds 2-4 show two distinct reduction processes between -2 and -3.5 V (All values vs. FcH/FcH<sup>+</sup>). Compound 1 shows only one irreversible reduction process at -2.37 V. There might be another reduction at lower potentials undetected because of the limited solvent window. Compounds 3 and 4 show two oxidations in close proximity, e.g. 4 at -0.21 and -0.07 V. Compounds 1 and 2 show only one oxidation process. Whereas the oxidations seem to be at least partly reversible for all molecules, the reduction processes differ. Compounds 3 and 4 show two irreversible processes indicating follow-up reactions (EC mechanism).<sup>[6]</sup> Compound 2 shows a reversible reduction process at -2.42 V and an irreversible one at -2.75. The single reduction of 1 seems to be irreversible and lies at -2.37 V. The differences between 1 and 2 are probably induced by the substitution at the N atoms (2) and the size of the N-bridging moieties (3, 4).



## SUPPORTING INFORMATION

Table S7: Redox potentials  $E$  vs  $FcH/FcH^+$  measured in DMF / 0.1 NBu<sub>4</sub>PF<sub>6</sub> at 100 mVs<sup>-1</sup> at room temperature.

	$E_1$ (1 <sup>st</sup> Red) / V	$E_2$ (2 <sup>nd</sup> Red) / V	$E_3$ (1 <sup>st</sup> Ox) / V	$E_4$ (2 <sup>nd</sup> Ox) / V
<b>1</b>	-2.37	---	0.16	---
<b>2<sup>[d]</sup></b>	-2.42	-2.75 <sup>[a]</sup>	0.12 <sup>[c]</sup>	---
<b>3</b>	-2.27 <sup>[a]</sup>	-3.36 <sup>[a]</sup>	-0.14 <sup>[a,e]</sup>	0.12 <sup>[a,e]</sup>
<b>4</b>	-2.22 <sup>[a]</sup>	-3.03	-0.21	-0.07 <sup>[b]</sup>
<b>TCNQ</b>	-0.16	-0.77	---	---

All values given were measured with GCWE at 100 mVs<sup>-1</sup> given in Volts.  
 [a] Peak current [b] Due to overlap with 1<sup>st</sup> oxidation, potential was determined by DPV  
 [c] Rereduction at -0.93 V [d] Reoxidation at -0.16 V from 1<sup>st</sup> Red. and at -0.04 V and 0.74 V from 2<sup>nd</sup> Red. [e] Rereduction peaks poorly defined

## Comparison to TCNQ

TCNQ shows two reversible reduction potentials around -0.06 V and -0.6 V in acetonitrile against a  $Ag/Ag^+$  electrode.<sup>[9]</sup> Since a comparison to our measurements would lack 100% identical measurement conditions (electrode and solvent) we have measured TCNQ in DMF under the same conditions as compound 1-4. The voltammogram shows two reversible reduction processes with potentials at -0.16 V and -0.77 V.

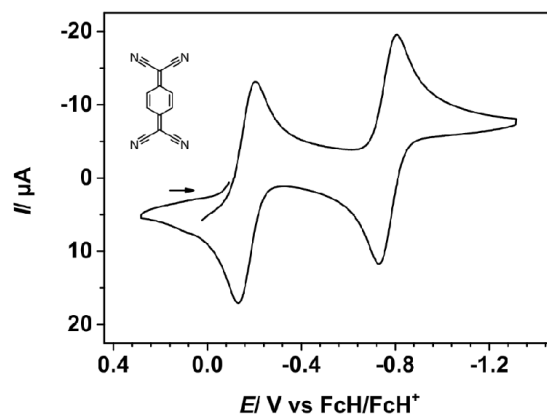


Figure S15: Voltammogram of TCNQ, measured in dimethylformamide solution with tetrabutylammonium hexafluorophosphate (0.1 M). Decamethylferrocene/decamethylferrocenium ( $[FcCp_2^+]$  +/0) was used as the internal reference and referred to the ferrocene/ferrocenium ( $FcH^+/0$ ) couple. The molecular concentration was 1.37 mmol/L.

## SUPPORTING INFORMATION

## 10. Computational Details

Quantum chemical calculations have been conducted to study the cause of the drastic fluorescence enhancement in **4** as compared to the other investigated substances. Geometry optimizations and potential energy surface (PES) scans were performed using the program package ORCA (4.0.0)<sup>[10]</sup> and the stand-alone program DFT/MRCI,<sup>[11]</sup> respectively. Ground state geometry optimizations were carried out at the RIJCOSX-CAM-B3LYP-D3(BJ)/def2-TZVP<sup>[12]</sup> level of density functional theory (DFT). Since hydrogen bonding-induced fluorescence quenching in protic solvents (MeOH, EtOH) and fluorescence enhancement by solvents with a high viscosity (DMSO) are well known phenomena for charge transfer-operated dyes and for molecules where the nonradiative excited state involves intramolecular rotations of functional moieties.<sup>[13]</sup> We opted for acetonitrile ( $\epsilon = 37.5$  at 20 °C)<sup>[6]</sup> as the solvent which was incorporated in the calculations with the implicit solvent model CPCM.<sup>[14]</sup> ORCA's default thresholds (e.g., 5  $\mu$ Hartree for energy change) were used for the calculations.

CAM-B3LYP was used as it has been shown to perform accurately for excited states and species displaying a strong charge-transfer character.<sup>[15]</sup> The structures were confirmed to be genuine minima on the PES by showing no negative (imaginary) frequencies. Excited state geometry optimizations were performed using time-dependent DFT (TD-DFT)<sup>[16]</sup> at the same level. Note that the implicit solvation cavity here is the one obtained for the ground state electronic structure. No separation of slow and fast term contributions was performed.<sup>[17]</sup> While the reduced dipole moment of the excited state (Table S8) may introduce some error for the optimization of the excited state geometry, the inclusion of state-specific solvent effects would have required the use of a different program which was not deemed necessary for our purposes.

Table S8: Oscillator strengths (length representation) for the  $S_0 \rightarrow S_1$  excitation and dipole moments (given in Debye) of  $S_0$  and  $S_1$  for all compounds optimized in their respective electronic state at the CPCM/CAM-B3LYP-D3(BJ)/def2-TZVP level.

	Structure optimized for	1	2	3	4	7
$f_{\text{osc}}(S_0 \rightarrow S_1)$	$S_0$	1.06	0.74	1.18	1.57	1.33
	$S_1$	0.99	0.84	1.04	1.50	1.30
$D$	$S_0$	30.82	31.01	30.91	29.34	29.85
	$S_1$	25.08	24.40	24.61	23.74	22.57

## SUPPORTING INFORMATION

## Ground state vs excited state structures

The differences between excited state and ground state geometries are almost negligible and are only expressed in the fact that the dihedral angle  $D_\alpha$  opens up a little (Figure S16). Test calculations showed that the inclusion of explicit solvent molecules may cause more significant changes in the structures (structures not shown). However, this is only the case if the implicit solvent model is excluded.

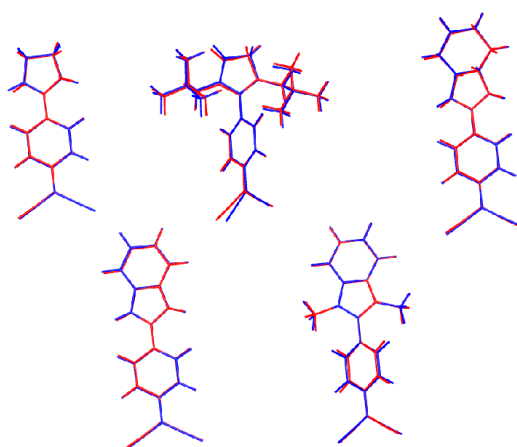


Figure S16: Comparison of the ground state (blue) and excited state (red) structures calculated at the CPCM/CAM-B3LYP-D3(BJ) level of DFT and TD-DFT, respectively.

## PES scan

Obviously, the slight structural changes upon excitation do not account for the drastic differences in fluorescence QY. Therefore, we took a closer look at the PES of the intramolecular rotations around dihedral angles  $D_\alpha$  and  $D_\beta$  (main text) that are likely responsible for the fluorescence deactivation. The DFT/MRCI scheme was utilized with orbitals generated at the CPCM/BHLYP/def2-TZVP<sup>[19]</sup> level as the basis to construct the configuration space. Table S9 shows the recalculated oscillator strengths (in length representation) and dipole moments of the  $S_0$  and  $S_1$  state evaluated at the Franck-Condon point.

Table S9: Oscillator strengths (length representation) for the  $S_0 \rightarrow S_1$  coupling and dipole moments (given in Debye) of  $S_0$  and  $S_1$  for all compounds at the Franck-Condon point computed at the CPCM/BHLYP/def2-TZVP/MRCI level.

		1	2	3	4	7
	$f_{osc}(S_0 \rightarrow S_1)$	0.95	0.74	0.96	1.26	1.20
$D$	$S_0$	31.85	35.00	33.52	32.78	33.59
	$S_1$	22.88	23.91	23.72	22.15	21.76

## SUPPORTING INFORMATION

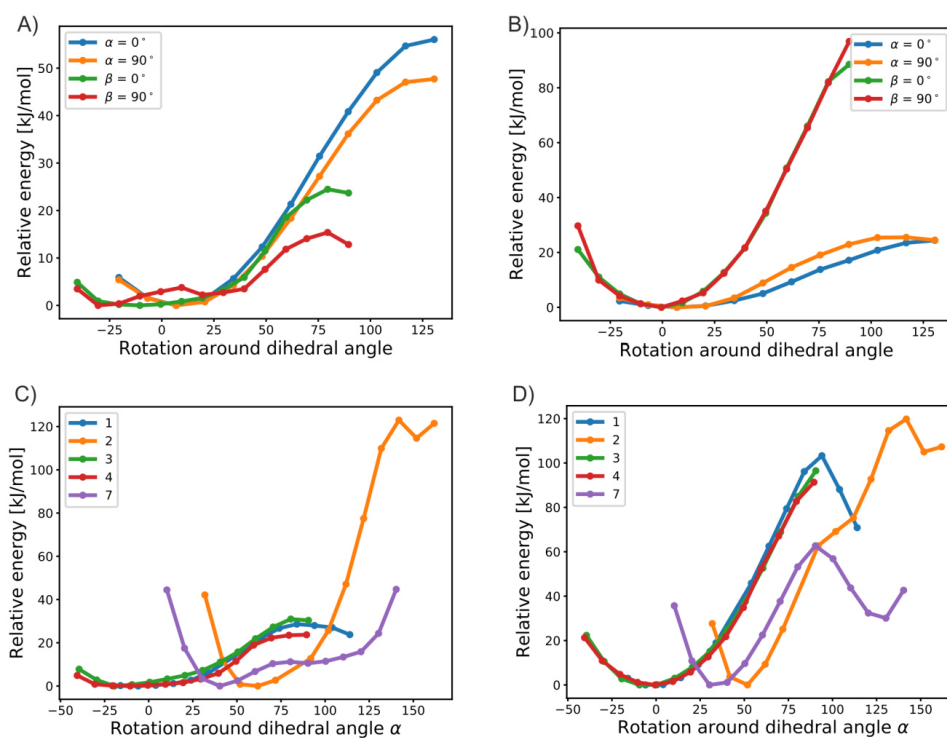


Figure S17: A) PES scan for the S0 state around dihedral angle  $D\alpha$  and  $D\beta$  while the respective other angle is fixed at a certain angle (see legend) for 4 computed at the CPCM/BHLYP/def2-TZVP/MRCI level. B) PES scan for the S1 state around dihedral angle  $D\alpha$  and  $D\beta$  while the respective other angle is fixed at a certain angle (see legend) for 4 computed at the CPCM/BHLYP/def2-TZVP/MRCI level. C) PES scan for the S0 state around dihedral angle  $D\alpha$  for all compounds computed at the CPCM/BHLYP/def2-TZVP/MRCI level. D) PES scan for the S1 state around dihedral angle  $D\alpha$  for all compounds computed at the CPCM/BHLYP/def2-TZVP/MRCI level.

Initial test calculations showed that both angles can be assumed to be decoupled (Figure S17A and B). If one angle is changed, e.g., from 0° to 90°, this has a small effect on the shape of the PES of the other rotation but does almost not change the rotational barrier at all.

## SUPPORTING INFORMATION

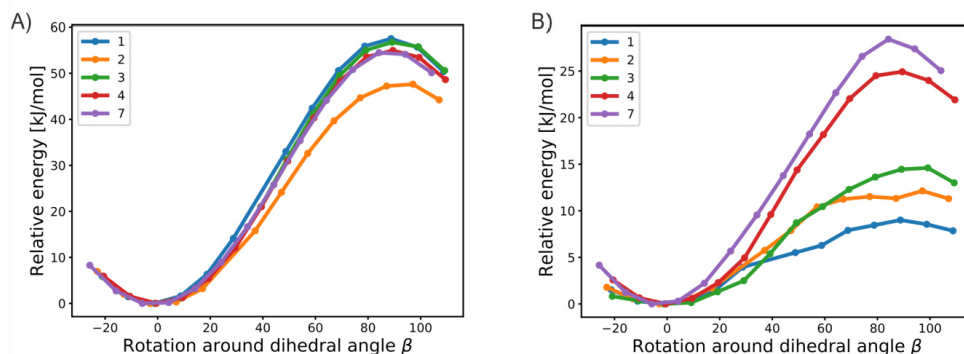


Figure S18: A) PES scan for the  $S_0$  state around dihedral angle  $D_\beta$  for all compounds computed at the CPCM/BHLYP/def2-TZVP/MRCI level. Note that for 1 and 2 values at  $40^\circ$  and  $30^\circ$ , respectively, were masked as these calculations had trouble with the configuration space and converged toward an unreasonable energy. B) PES scan for the  $S_1$  state around dihedral angle  $D_\beta$  for all compounds computed at the CPCM/BHLYP/def2-TZVP/MRCI level. Note that for 1 and 2 values at  $40^\circ$  and  $30^\circ$ , respectively, were masked as these calculations had trouble with the configuration space and converged toward an unreasonable energy.

### Fluorescence deactivation through rotation around $D_\alpha$ in 1 and 7

QY loss by rotation around  $D_\alpha$  in the  $S_1$  can be achieved in 1 by ISC to the  $T_1$  at an angle of  $60^\circ$  by ISC and IC events at an angle of  $90^\circ$  with the  $S_2$ ,  $T_2$  and  $T_3$  (Figure S19 B). As it is quite unlikely for 1 to reach these displacements along  $D_\alpha$ , this mechanism will contribute only to a small extent to the overall QY loss. However, for 7 this rotation is the most likely deactivation mechanism since it can access another local minimum on the  $S_0$  PES of  $D_\alpha$  at ca.  $80^\circ$  (Figure S17 C). At this point the substance may be directly photoexcited into an ISC of the  $S_1$  with the  $T_1$  and  $T_2$  (Figure S19 A) drastically diminishing its chance to fluoresce.

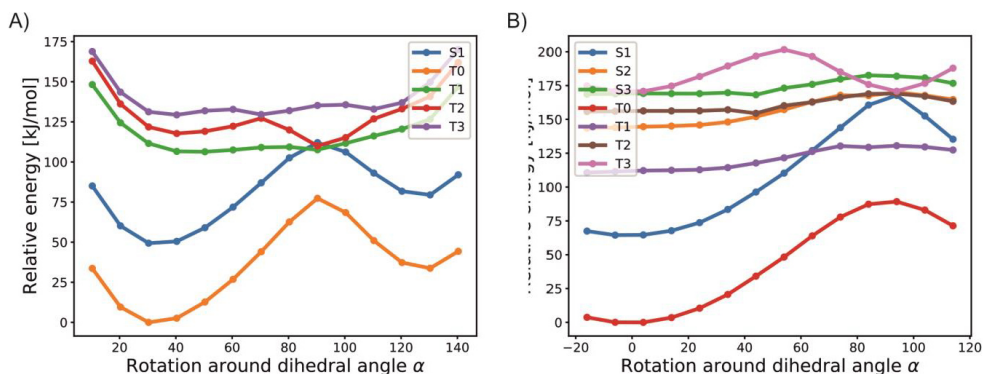


Figure S19: A) PES scan along dihedral angle  $D_\alpha$  for 7 computed at the CPCM/BHLYP/def2-TZVP/MRCI level to estimate fluorescence quenching through IC and ISC events. B) PES scan along dihedral angle  $D_\alpha$  for 1 computed at the CPCM/BHLYP/def2-TZVP/MRCI level to estimate fluorescence quenching through IC and ISC events.

## SUPPORTING INFORMATION

Fluorescence deactivation through rotation around  $D_\beta$  in 1, 2, 3, and 4

To relate the probabilities of the substances to overcome a rotational barrier, we introduce the reciprocal rate constant, (Equation S5):

$$k_{\text{rot}}^{-1} = A^{-1} e^{\frac{E_{\text{rot}}}{RT}} \quad (\text{Equation S5})$$

where  $R$  is the ideal gas constant, and  $T$  is the temperature (here constant at 300 K).  $E_{\text{rot}}$  is the rotational barrier height.  $A$  is the frequency factor which is approximated by the zero-point vibrational energy  $E_0$ , (Equation S6), of the harmonic potential fitted to the rotational energy profile  $E(\varphi)$  with  $\varphi$  being the angle of rotation, (Equation S7).

$$A \sim E_0 = \frac{1}{2} \hbar \omega_0 \quad (\text{Equation S6})$$

$$E(\varphi) \approx a\varphi^2 + b \quad (\text{Equation S7})$$

The potential's second derivative gives its curvature, (Equation S8), which is related to the force constant of the potential, (Equation S9).

$$\frac{\partial^2 E}{\partial \varphi^2} = 2a = k \quad (\text{Equation S8})$$

$$\omega_0 \sim \sqrt{k} \quad (\text{Equation S9})$$

It follows that the frequency factor is proportional to the square root of the curvature at the minimum of the rotational potential (Equation S10),

$$A \sim E_0 \sim \sqrt{a} \quad (\text{Equation S10})$$

The reader is referred to standard quantum chemistry and physical chemistry textbooks for a more profound derivation of the underlying mathematical principles.

## SUPPORTING INFORMATION

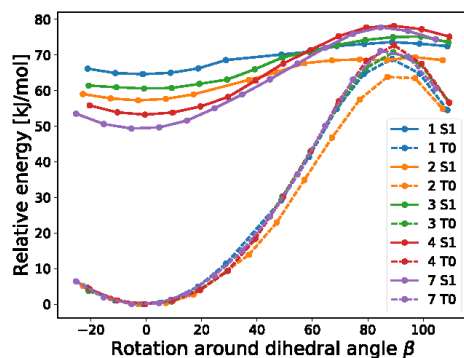


Figure S20: PES scan for the  $S_1$  and  $T_0$  states around dihedral angle  $D_\beta$  for all compounds computed at the CPCM/BHLYP/def2-TZVP/MRCI level to assess possible ISC events.

### Incorporating explicit solvent effects

While the PES scans may account for the differences in QY, they do not fully explain the large QY of **4** by itself. As solvent effects have only been included in an implicit way by the continuum model CPCM, an explicit solvent cavity consisting of six ACN molecules (two near  $D_\alpha$  and four near  $D_\beta$ , respectively) was set-up and the rotational barrier at  $D_\beta$  was recalculated for **1** and **4** with the smaller def2-SVP basis set and fixed solvent molecules to save computational resources (Figure S21A and B). The explicit solvent cavity was prepared by manually placing the solvent molecules at the desired positions and optimizing the solvent molecules with a distance constraint to the solute so that the dicyano moiety can still rotate rather freely at the CAM-B3LYP/def2-SVP level with ORCA's "loose" geometry optimization criteria. While in both cases the smooth shape of the PES naturally deteriorated, surprisingly, for **1** the total barrier hardly changed at all by less than 1 kJ/mol. **4** on the other hand shows a slight increase in barrier height by ca. 5 kJ/mol, which amounts to roughly a third of the barrier from the calculation using only an implicit solvent cavity. While these numbers are more prone to errors due to the smaller basis set, it can be deduced that the solvent shell around the molecules may play a significant role at least in the case of **4**, where it likely contributes to its large QY.

## SUPPORTING INFORMATION

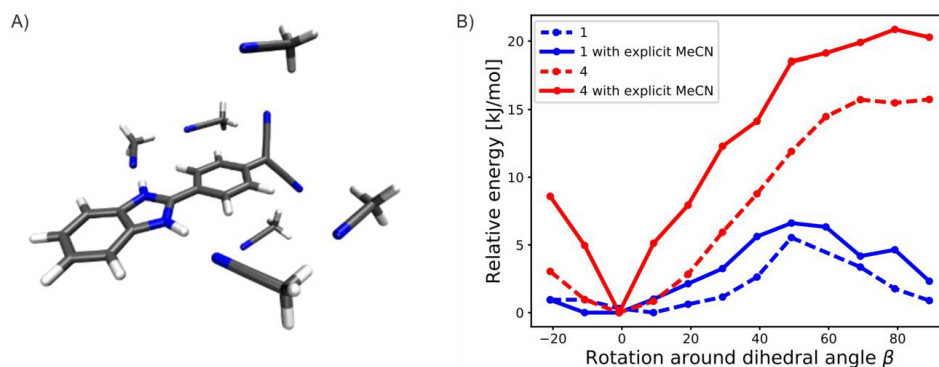


Figure S21: A) Explicit solvent molecules placed in the vicinity of the solute to estimate solvent effects for the rotational potential at  $D_{\beta}$ . B) PES scan for the  $S_1$  state around dihedral angle  $D_{\beta}$  for **1** and **4** with (solid) and without (dashed) six explicit ACN molecules computed at the CPCM/BHLYP/def2-SVP/MRCI level to assess the influence of solvent effects on the potential barrier.

- [1] P. Srujana, T. Gera, T. P. Radhakrishnan, *J. Mater. Chem. C* **2016**, *4*, 6510.
- [2] a) C. Würth, M. Grabolle, J. Pauli, M. Spieles, U. Resch-Genger, *Anal. Chem.* **2011**, *83*, 3431; b) C. Würth, J. Pauli, C. Lochmann, M. Spieles, U. Resch-Genger, *Anal. Chem.* **2012**, *84*, 1345.
- [3] C. Reichardt, *Chem. Rev.* **1994**, *94*, 2319.
- [4] K. G. Casey, E. L. Quitevis, *J. Chem. Phys.* **1988**, *92*, 6590.
- [5] C. Wuerth, M. Grabolle, J. Pauli, M. Spieles, U. Resch-Genger, *Nat. Protoc.* **2013**, *8*, 1535.
- [6] I. M. Smallwood, *Handbook of Organic Solvent Properties*, Elsevier Ltd., **1996**.
- [7] J. R. Aranzaes, M.-C. Daniel, D. Astruc, *Can. J. Chem.* **2006**, *84*, 288.
- [8] a) O. A. Levitskiy, D. A. Dulov, O. M. Nikitin, A. V. Bogdanov, D. B. Eremin, K. A. Paseshnichenko, T. V. Magdesieva, *ChemElectroChem* **2018**, *5*, 3391; b) O. H. B. Speiser, *Organic Electrochemistry*, CRC Press, Boca Raton, FL, USA, **2016**; c) B. R. Rosen, E. W. Werner, A. G. O'Brien, P. S. Baran, *J. Am. Chem. Soc.* **2014**, *136*, 5571.
- [9] a) T. H. Le, A. Nafady, X. Qu, L. L. Martin, A. M. Bond, *Anal. Chem.* **2011**, *83*, 6731; b) T. H. Le, A. Nafady, X. Qu, A. M. Bond, L. L. Martin, *Anal. Chem.* **2012**, *84*, 2343; c) N. Vo, N. L. Haworth, A. M. Bond, L. L. Martin, *ChemElectroChem* **2018**, *5*, 1173.
- [10] F. Neese, *Wiley Interdiscip. Rev.: Comput. Mol. Sci.* **2018**, *8*.
- [11] a) S. Grimme, M. Waletzke, *J. Chem. Phys.* **1999**, *111*, 5645; b) I. Lyskov, M. Kleinschmidt, C. M. Marian, *J. Chem. Phys.* **2016**, *144*, 034104.
- [12] a) F. Neese, F. Wennmohs, A. Hansen, U. Becker, *Chem. Phys.* **2009**, *356*, 98; b) T. Yanai, D. P. Tew, N. C. Handy, *Chem. Phys. Lett.* **2004**, *393*, 51; c) S. Grimme, J. Antony, S. Ehrlich, H. Krieg, *J. Chem. Phys.* **2010**, *132*, 154104; d) S. Grimme, S. Ehrlich, L. Goerigk, *J. Comput. Chem.* **2011**, *32*, 1456; e) F. Weigend, R. Ahlrichs, *Phys. Chem. Chem. Phys.* **2005**, *7*, 3297.
- [13] N. Scholz, A. Jadhav, M. Shreykar, T. Behnke, N. Nirmalanathan, U. Resch-Genger, N. Sekar, *J. Fluoresc.* **2017**, *27*, 1949.
- [14] V. Barone, M. Cossi, *J. Phys. Chem.* **1998**, *102*, 1995.
- [15] B. Karasulu, J. P. Gotze, W. Thiel, *J. Chem. Theory Comput.* **2014**, *10*, 5549.
- [16] E. Runge, E. K. U. Gross, *Phys. Rev. Lett.* **1984**, *52*, 997.
- [17] M. Cossi, V. Barone, *J. Phys. Chem.* **2000**, *104*, 10614.
- [18] A. D. Becke, *J. Chem. Phys.* **1993**, *98*, 1372.



## 4.2 Fluorescence of a Chiral Pentaphene Derivative Derived from the Hexabenzocoronene Motif

---

<b>Authors</b>	<b>Philipp Rietsch, Jan Soyka, Steffen Brülls, Jasmin Er, Katrin Hoffmann, Julia Beerhues, Biprajit Sarkar, Ute Resch-Genger, and Siegfried Eigler</b>
<b>Journal</b>	<i>Chem. Commun.</i> 2019, 55, 10515-10518
<b>DOI</b>	10.1039/C9CC05451K
<b>Links</b>	<a href="https://doi.org/10.1039/C9CC05451K">https://doi.org/10.1039/C9CC05451K</a>
<b>Detailed scientific contribution</b>	<p>The concept of this manuscript was elaborated by P. Rietsch and Prof. Dr. S. Eigler.</p> <p>S. Brülls synthesized reference compound 5. J. Er did the reference reaction to yield compound 7. J. Soyka synthesized compound 4. Compound 4 was crystallized by P. Rietsch. All photophysical measurements were done by P. Rietsch except of the confocal laser scanning microscopy, which were done by Dr. K. Hoffmann. J. Beerhues measured the single crystal XRD. Dr. U. Resch-Genger, Prof. Dr. B. Sarkar, and Prof. Dr. S. Eigler supervised the theoretical and experimental work.</p> <p>The manuscript was written by P. Rietsch and Prof. Dr. S. Eigler.</p>
<b>Estimated own contribution</b>	~35 %

---



## Fluorescence of a chiral pentaphene derivative derived from the hexabenzocoronene Motif†

Cite this: *Chem. Commun.*, 2019, 55, 10515

Received 16th July 2019,  
Accepted 8th August 2019

DOI: 10.1039/c9cc05451k

rsc.li/chemcomm

Philipp Rietsch,<sup>a</sup> Jan Soyka,<sup>a</sup> Steffen Brülls,<sup>b</sup> Jasmin Er,<sup>a</sup> Katrin Hoffmann,<sup>b,c</sup> Julia Beerhues,<sup>d</sup> Biprajit Sarkar,<sup>b</sup> Ute Resch-Genger<sup>b,\*c</sup> and Siegfried Eigler<sup>b,\*a</sup>

**A new fluorescent pentaphene derivative is presented that differs from hexabenzocoronene (HBC) by one carbon atom in the basal plane skeleton. A 500% increased fluorescence quantum yield is measured compared to the HBC derivative. The pentaphene compound, obtained by a modified Scholl oxidation, is also emissive in the solid-state, due to the packing motif in the crystal.**

Hexabenzocoronenes (HBCs), a subgroup of polyaromatic hydrocarbons (PAHs), have 42 sp<sup>2</sup>-carbon atoms assembled by linking seven benzene rings. The resulting properties make them interesting for optical and electronic applications,<sup>1–5</sup> self-assembly,<sup>2,6</sup> surface functionalisation<sup>7</sup> and the bottom-up synthesis of graphene.<sup>8–10</sup> The HBC scaffold has D<sub>6</sub> symmetry. Through the variation and arrangement of the substituents, a plethora of derivatives with a wide range of different chemical properties and of well-defined symmetry (C<sub>3</sub>, C<sub>2</sub> and C<sub>1</sub>) was synthesized.<sup>7,11,12</sup>

Pentaphenes, another interesting subgroup of PAHs, have been synthesized since the 1940s, mostly by cycloaddition reactions and subsequent oxidation.<sup>13–17</sup> The fluorescence properties of pentaphene derivatives, which emit light between 400 and 500 nm, were studied by Fetzer *et al.*<sup>18,19</sup> However, neither the fluorescence quantum yields (Φ<sub>Fl</sub>) nor an emission in the solid-state were reported.<sup>18,19</sup> The pentaphene motif can also be found in HBCs, which show a red-shifted fluorescence with a similar vibronic fine structure at about 500 nm.<sup>5,7</sup> Another dye class related to HBCs are hexapyrrolohexaazacoronenes or

hybrids with HBC as reported by Müllen *et al.* in 2013.<sup>20</sup> In 2017, Jux *et al.* prepared a racemic [5]helicene, structurally closely related to HBCs, that contains one pyrrole moiety.<sup>21</sup> Recently, high Φ<sub>Fl</sub> values exceeding 80% were found for oxa[7]superhelicenes, realized by ether-bridging two hexaphenylbenzene moieties, followed by oxidation. This yielded a chiral fluorescent oxa[7]superhelicene. Another strategy that can lead to a high fluorescence are push-pull systems. This was as *e.g.* reported for HBCs substituted by B-, N-containing moieties and diamino-dicyanoquinone-derivatives.<sup>22,23</sup>

Herein, we present the synthesis and optical-spectroscopic characterization of an enantiomeric pentaphene derivative **4**, with 41 sp<sup>2</sup>-carbon atoms. Compound **4** could be prepared by implementing an unprecedented Scholl oxidation step (Fig. 4).<sup>24</sup> First, a Diels-Alder reaction<sup>25,26</sup> between 1,4-bis(4-*tert*-butyl)phenyl)buta-1,3-diyne **2** and **1** was performed to yield hexaarylbenzene **3**. Under Scholl oxidation conditions compound **3** (conditions: CH<sub>3</sub>NO<sub>2</sub>, 12 eq. FeCl<sub>3</sub>, room temperature (RT), 15 h) was transformed into compound **4** in 80% yield, due to an unprecedented ring-closing reaction. The ring-closing reaction between the alkyne moiety and the benzene ring (Fig. 1A step iii) proceeds in analogy to the synthesis of, *e.g.* corannulenes, HBCs or naphthalenes.<sup>27–30</sup> The analytical characterization of **4** including single-crystal X-ray analysis, is given in the ESI.† We tested the reproducibility of this reaction by synthesizing the phenanthrene derivative, 9-(4-methoxyphenyl)phenanthrene, starting from 2-((4-methoxyphenyl)ethynyl)-1,1'-biphenyl (ESI†). This reaction was performed in dry dichloromethane with 0.9 eq. FeCl<sub>3</sub> with a yield of 69%. In addition, for our photophysical property studies, HBC **5** was synthesized as reference compound by a reported one pot reaction of hexaphenylbenzene and *tert*-BuCl with FeCl<sub>3</sub> acting as oxidant and Lewis acid catalyst.<sup>31</sup>

Compared to the HBC core with 42 sp<sup>2</sup>-carbon atoms, the missing carbon atom in compound **4** induces chirality as shown by the structural analysis. Moreover, **4** reveals a strong fluorescence, both in solution, as well as in the solid-state.

To gain first insights into the photophysics of these compounds, we analyzed the photophysical characteristics of

<sup>a</sup> Institute of Chemistry and Biochemistry, Freie Universität Berlin, Takustraße 3, Berlin, 14195, Germany. E-mail: siegfried.eigler@fu-berlin.de

<sup>b</sup> Chalmers University of Technology, Gothenburg, SE-412 96, Sweden

<sup>c</sup> Bundesanstalt für Materialforschung und -prüfung (BAM), Department 1, Division Biophotonics, Richard Willstätter Straße 11, Berlin, 12489, Germany. E-mail: ute.resch@bam.de

<sup>d</sup> Institute of Chemistry and Biochemistry, Freie Universität Berlin, Fabbeckstraße 34-36, Berlin, 14195, Germany

† Electronic supplementary information (ESI) available. CCDC 1923092. For ESI and crystallographic data in CIF or other electronic format see DOI: 10.1039/c9cc05451k

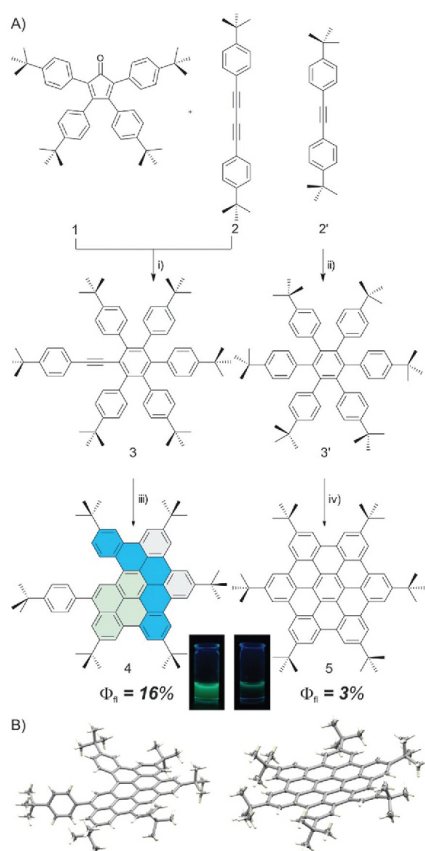


**Fig. 1** (A) Synthetic route to the pentaphene derivative **4** and hexabenzocoronene (HBC) **5**. A Diels–Alder reaction between **1** and dialkyne **2** leading to hexaphenylbenzene **3** was used. Trimerization of alkyne **2'** leads to hexaphenylbenzene **3'**. Cyan: pentaphene moiety; green: pyrene moiety. (i) 24 h, 250 °C in diphenylether; (ii)  $\text{Co}(\text{CO})_8$ , dioxane, 24 h, reflux; (iii) and (iv)  $\text{CH}_3\text{NO}_2$ , 12 eq.  $\text{FeCl}_3$ , 15 h, RT. The inset shows solutions of the respective compound in dichloromethane under irradiation at 366 nm. The respective  $\Phi_{\text{FI}}$  is given below each compound. (B) Single-crystal X-ray structures of **4** and **5**. Ellipsoids are drawn at 50% probability.

**4** in comparison to **5** in three solvents of varying polarity and proticity, here cyclohexane (CH; apolar and aprotic), dichloromethane (DCM; medium polarity, aprotic) and ethanol (EtOH; polar and protic). The absorption spectra and normalized fluorescence spectra of both compounds in CH are shown in Fig. 2. Whereas the molar absorption coefficients reach values of about  $60\,000\ \text{L mol}^{-1}\ \text{cm}^{-1}$  at 360 nm for both compounds, the  $\Phi_{\text{FI}}$  of **4** is about five times higher than that of compound **5** (Table 1 and Fig. 2).

In addition, we measured fluorescence maps (excitation emission matrices (EEM); see Fig. S11 and S12, ESI†). For both

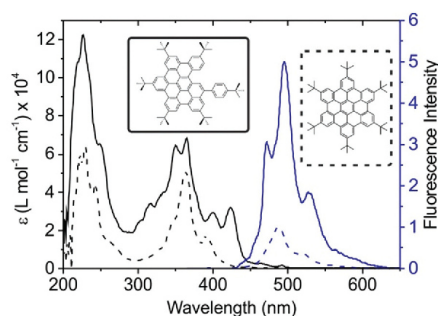


**Fig. 2** Absorption spectra (black) and fluorescence spectra (blue, normalized and multiplied by the correspondingly measured  $\Phi_{\text{FI}}$ ) of compound **4** ( $\Phi_{\text{FI}} = 11\%$ ) in cyclohexane is about five times higher than that of HBC **5** ( $\Phi_{\text{FI}} = 2\%$ ) in this solvent. Both compounds were measured at a concentration of  $4 \times 10^{-6}\ \text{mol L}^{-1}$  and excited at 375 nm.

**Table 1**  $\Phi_{\text{FI}}$  and amplitude-weighted mean fluorescence lifetimes  $\tau$  of **4** and **5** in solvents of different polarity. Values for the normalized Dimroth–Reichardt parameter  $E_{\text{T}}^{\text{N}}$  were taken from ref. 34

$E_{\text{T}}^{\text{N}}$	Solvent	<b>4</b>		<b>5</b>	
		$\Phi_{\text{FI}}$ [%]	$\tau$ [ns]	$\Phi_{\text{FI}}$ [%]	$\tau$ [ns]
0.207	CH	11	17.2	2	12.4
0.386	DCM	16	21.4	3	14.2
0.654	EtOH	11	17.8	2	11.0
	Solid	11	—	2	—

compounds, excitation at 370 nm leads to the highest fluorescence (Fig. S12, ESI†) with the fluorescence maxima being located between 470 and 500 nm. The emission spectrum of **4** reveals a more pronounced vibrational fine structure compared to **5** and resembles, with its two main peaks and shoulders, the emission spectra of the pentaphene derivatives investigated by Fetzter *et al.*<sup>18,19</sup>

An overview of the absorption and emission maxima together with the Stokes shift, which is between 100–130 nm for both compounds, is given in Table S2 (ESI†). The  $\Phi_{\text{FI}}$  and the mean fluorescence lifetimes  $\tau$  (derived from the multi-exponential decay kinetics) of **4** and **5** in the three solvents used are summarized in Table 1 (ESI†). Obviously,  $\Phi_{\text{FI}}$  of **4** always exceeds that of **5**, reaching a maximum of 16% in DCM compared to 3% obtained for **5**. The mean fluorescence lifetimes of **4** are also always longer than those of **5** with values of 17.2 ns (CH) and 21.4 ns (DCM) compared to 11.0 ns (CH) and 14.2 ns (DCM), respectively. Temperature-dependent studies of the decay kinetics of both compounds in the temperature range of  $-100\ ^\circ\text{C}$  to  $50\ ^\circ\text{C}$  (see ESI†, Fig. S14) reveal an increase in mean fluorescence lifetime by about a factor of 3.5 when comparing mean lifetimes recorded at  $50\ ^\circ\text{C}$  (**4**: 18.02 ns, **5**: 7.93 ns) and  $-100\ ^\circ\text{C}$  (**4**: 63.23 ns, **5**: 27.67 ns), respectively. An increase in fluorescence lifetime upon cooling has been observed for many dye classes including rhodamines<sup>32</sup> and

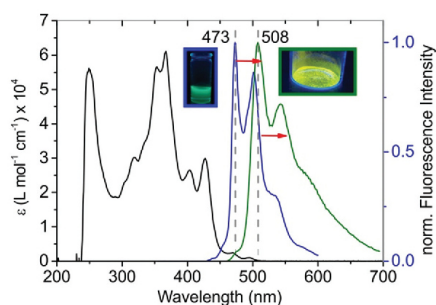


Fig. 3 Comparison of the solution (blue, in DCM) and solid-state fluorescence (green) of **4**. The absorption spectra in solution (DCM) is shown in black. The excitation wavelength was 355 nm, respectively. The solid-state fluorescence, recorded with a spectral scanning laser scanning microscope (CLSM), is bathochromically shifted by about 35 nm. The insets show the fluorescence in solution (left, blue frame) and in the solid-state (right, green frame).

the recently analyzed diaminodicyanoquinones.<sup>22</sup> It typically suggests that at least one non-radiative decay channel involves a rotation that is slowed down or even completely hindered at very low temperatures.<sup>33</sup>

Surprisingly, **4** shows an intense solid-state fluorescence with  $\Phi_{\text{el}} = 11\%$  (Fig. 3 and Fig. S15–S17 in the ESI†), while  $\Phi_{\text{el}}$  of **5** is only 2% (Table 1 and Fig. S15, ESI†). The solid-state fluorescence of **4** is bathochromically shifted by about 35 nm compared to the emission in DCM although the spectral shape and vibronic fine structure of the emission band is only slightly altered and broadened.

The latter is often observed for solid-state emission (inhomogeneous broadening). The Stokes shift is thus increased from 130 nm in solution to 165 nm in solid-state. Whether this shift originates from polarity and/or crystal packing effects or a combination of both remains to be shown. For **5**, this shift amounts only to 4 nm. In addition, the solid-state emission band of **5** is broadened by about 100 nm and thereby extended from 600 nm in solution to 700 nm (Fig. S15 and S17, ESI†).

To correlate the solid-state fluorescence of **4** (see Fig. 3) with the molecular structure and the crystalline packing motif,<sup>35</sup> we studied the crystal structure of **4** and **5**. The pentaphene **4** crystallizes in a triclinic lattice with the space group  $P\bar{1}$ , similar to the previously mentioned helicene-HBC hybrid.<sup>21</sup> As discussed by Müllen *et al.* the  $\pi$ -system of **5** is slightly bent due to the sterically demanding *tert*-butyl groups.<sup>36</sup> According to the four basic packing types of aromatic systems,<sup>37,38</sup> the structure of compound **5** is classified as a sandwich herringbone structure with an inter-planar distance of 3.44 Å.

The  $\pi$ - $\pi$  interactions as well as C-H- $\pi$  interactions determine this packing motif. This dense packing in the crystal might induce an aggregation induced quenching of the fluorescence. In contrast, the pentaphene **4** presents a  $\beta$ -system with graphitic planes (Fig. 4) separated by 9.24 Å. The space between the  $\pi$ -planes is filled by the bulky *tert*-butyl groups (Fig. 4).

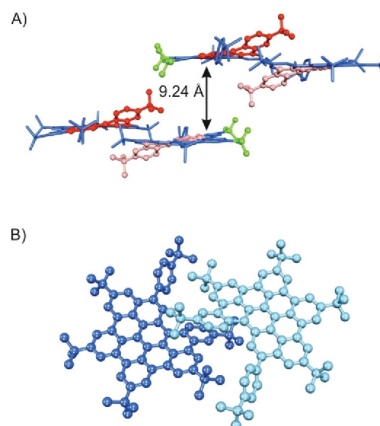


Fig. 4 Arrangement of the molecules of **4** in the crystal. (A) *tert*-Butyl groups in green and the helical moieties in red. The interplanar distance is 9.24 Å. (B) Enantiomeric pair of **4**. Blue M(-) and turquoise P(+).

The pentaphene derivatives published by Kakiuchi *et al.* have a distance of the  $\pi$ -planes of about 3.52 Å.<sup>17</sup> As the inter-planar distance in **4** is induced by the helicene motif (Fig. 5A), which is absent for **5**, we compared the angles between the planes A–D of **4** with those of [4]helicene (Fig. 5 and Table 2).<sup>39</sup> The A–D angle of 32.46° of **4** compared to 26.68° ([4]helicene) indicates a stronger curvature of **4**, which is mainly induced by ring D, with 20% (A–D) up to almost 100% (C–D) increased angles compared to [4]helicene.

The reasons for this is probably the sterically demanding phenyl ring, which is twisted around the dihedral angle  $D_{\alpha}$  by 67.58° (Fig. 5A), and the three hydrogen atoms (Fig. 5C). In addition, the helical chirality is visible in the crystal structure as enantiomeric pairs (Fig. 4B). The enantiomers of [4]helicenes cannot be separated at RT as the racemisation barrier is below 25 kcal mol<sup>-1</sup>.<sup>40,41</sup> Nevertheless, we used density functional theory (DFT) at the B3LYP/6-31G(d) level of theory to calculate

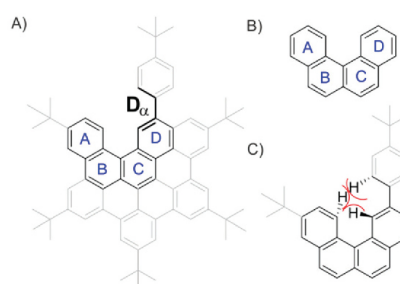


Fig. 5 (A) Schematic presentation of the [4]helicene moiety in compound **4** with the crucial benzene rings defined A–D. (B) [4]Helicene. (C) Steric hindrance between hydrogen atoms in an extract of compound **4**.

**Table 2** Angles between planes A–D (Fig. 5A) of **4** and [4]helicene<sup>39</sup> derived from crystallographic data

	A–B	A–C	A–D	B–C	B–D	C–D
<b>4</b>	5.24°	16.76°	32.46°	11.86°	27.23°	16.54°
[4]Helicene	10.26°	18.12°	26.68°	7.87°	16.55°	8.83°

the racemisation barrier of **4**,<sup>42,43</sup> which is about 10 kcal mol<sup>-1</sup> (Fig. S18, ESI†).

In conclusion, we reported a novel pentaphene derivative, which is closely related to HBCs, however, with only 41 sp<sup>2</sup>-carbon atoms, instead of 42. Consequently, the pentaphene **4** is chiral and crystallizes as enantiomeric pair with a distance of the  $\pi$ -planes of almost 1 nm. This substitution pattern results in an enhanced fluorescence in solution and the solid state compared to the HBC motif. The presented synthetic strategy to pentaphenes could lead to more advanced derivatives with improved photo-physical properties.

## Conflicts of interest

There are no conflicts to declare.

## References

- 1 I. Diez-Perez, Z. Li, J. Hihath, J. Li, C. Zhang, X. Yang, L. Zang, Y. Dai, X. Feng, K. Müllen and N. Tao, *Nat. Commun.*, 2010, **1**, 31.
- 2 L. Chen, K. S. Mali, S. R. Puniredd, M. Baumgarten, K. Parvez, W. Pisula, S. De Feyter and K. Müllen, *J. Am. Chem. Soc.*, 2013, **135**, 13531–13537.
- 3 H. Seyler, B. Purushothaman, D. J. Jones, A. B. Holmes and W. W. H. Wong, *Pure Appl. Chem.*, 2012, **84**, 1047–1067.
- 4 Y. Liu, T. Marszalek, K. Müllen, W. Pisula and X. Feng, *Chem. – Asian J.*, 2016, **11**, 2107–2112.
- 5 F. Hinkel, D. Cho, W. Pisula, M. Baumgarten and K. Müllen, *Chem. – Eur. J.*, 2015, **21**, 86–90.
- 6 X. Dou, W. Pisula, J. Wu, G. J. Bodwell and K. Müllen, *Chem. – Eur. J.*, 2008, **14**, 240–249.
- 7 X. Feng, W. Pisula, T. Kudernac, D. Wu, L. Zhi, S. De Feyter and K. Müllen, *J. Am. Chem. Soc.*, 2009, **131**, 4439–4448.
- 8 R. Liu, D. Wu, X. Feng and K. Müllen, *J. Am. Chem. Soc.*, 2011, **133**, 15221–15223.
- 9 Y. Byun and A. Coskun, *Chem. Mater.*, 2015, **27**, 2576–2583.
- 10 F. Cataldo, O. Ursini, G. Angelini and S. Iglesias-Groth, *Fullerenes, Nanotubes, Carbon Nanostruct.*, 2011, **19**, 713–725.
- 11 Y.-J. Huang, T.-C. Li, C.-W. Chang and H.-H. Chen, *Liq. Cryst.*, 2017, **44**, 1253–1258.
- 12 X. Feng, W. Pisula and K. Müllen, *Pure Appl. Chem.*, 2009, **81**, 2203–2224.
- 13 N. Saino, T. Kawaji, T. Ito, Y. Matsushita and S. Okamoto, *Tetrahedron Lett.*, 2010, **51**, 1313–1316.
- 14 M. Zander, *Chem. Ber.*, 1959, **92**, 2749–2751.
- 15 K. F. Lang and M. Zander, *Chem. Ber.*, 1965, **98**, 597–600.
- 16 E. Clar, *J. Chem. Soc.*, 1949, 2013–2016.
- 17 Y. Suzuki, K. Yamada, K. Watanabe, T. Kochi, Y. Ie, Y. Aso and F. Kakiuchi, *Org. Lett.*, 2017, **19**, 3791–3794.
- 18 W. E. Acree, A. I. Zvaigzne and J. C. Fetzer, *Appl. Spectrosc.*, 1990, **44**, 1193–1195.
- 19 S. A. Tucker, A. I. Zvaigzne, W. E. Acree, J. C. Fetzer and M. Zander, *Appl. Spectrosc.*, 1991, **45**, 424–428.
- 20 M. Takase, T. Narita, W. Fujita, M. S. Asano, T. Nishinaga, H. Benten, K. Yoza and K. Müllen, *J. Am. Chem. Soc.*, 2013, **135**, 8031–8040.
- 21 F. Ammon, S. T. Sauer, R. Lippert, D. Lungerich, D. Reger, F. Hampel and N. Jux, *Org. Chem. Front.*, 2017, **4**, 861–870.
- 22 P. Rietsch, F. Witte, S. Sobotka, G. Germer, A. Becker, A. Guttler, B. Sarkar, B. Paulus, U. Resch-Genger and S. Eigler, *Angew. Chem., Int. Ed.*, 2019, **58**, 8235–8239.
- 23 R. Kurata, K. Kaneda and A. Ito, *Org. Lett.*, 2017, **19**, 392–395.
- 24 A. Gourdon, S. K. Sadhukhan and C. Viala, *Synthesis*, 2003, 1521–1525.
- 25 D. Lungerich, J. F. Hitzberger, M. Marcia, F. Hampel, T. Drewello and N. Jux, *Angew. Chem., Int. Ed.*, 2014, **53**, 12231–12235.
- 26 W. Diltthey, W. Schommer and O. Trösken, *Ber. Dtsch. Chem. Ges.*, 1933, **66**, 1627–1628.
- 27 G. Zimmermann, U. Nuechter, S. Hagen and M. Nuechter, *Tetrahedron Lett.*, 1994, **35**, 4747–4750.
- 28 P. M. Donovan and L. T. Scott, *J. Am. Chem. Soc.*, 2004, **126**, 3108–3112.
- 29 H. C. Shen, J. M. Tang, H. K. Chang, C. W. Yang and R. S. Liu, *J. Org. Chem.*, 2005, **70**, 10113–10116.
- 30 C. A. Merlic and M. E. Pauly, *J. Am. Chem. Soc.*, 1996, **118**, 11319–11320.
- 31 R. Rathore and C. L. Burns, *J. Org. Chem.*, 2003, **68**, 4071–4074.
- 32 L. B. A. Johansson and A. Niemi, *J. Phys. Chem.*, 1987, **91**, 3020–3023.
- 33 B. Valeur, *Molecular Fluorescence: Principles and Applications*, Wiley VCH, Somerset, 2002.
- 34 C. Reichardt, *Chem. Rev.*, 1994, **94**, 2319–2358.
- 35 K. Hoffmann, B. Dietzel, B. Schulz, G. Reck, A. Hoffmann, I. Orgzall, U. Resch-Genger and F. Emmerling, *J. Mol. Struct.*, 2011, **988**, 35–46.
- 36 P. T. Herwig, V. V. Enkelmann, O. Schmelz and K. Müllen, *Chem. – Eur. J.*, 2000, **6**, 1834–1839.
- 37 G. R. Desiraju and A. Gavezzotti, *Acta Crystallogr., Sect. B: Struct. Sci.*, 1989, **45**, 473–482.
- 38 G. R. Desiraju and A. Gavezzotti, *J. Chem. Soc., Chem. Commun.*, 1989, 621–623.
- 39 P. F. Thomson, D. Parrish, P. Pradhan and M. K. Lakshman, *J. Org. Chem.*, 2015, **80**, 7435–7446.
- 40 S. Grimme and S. D. Peyerimhoff, *Chem. Phys.*, 1996, **204**, 411–417.
- 41 H. A. Staab, M. Diehm and C. Krieger, *Tetrahedron Lett.*, 1995, **36**, 2967–2970.
- 42 P. J. Stephens, F. J. Devlin, C. F. Chabalowski and M. J. Frisch, *J. Phys. Chem.*, 1994, **98**, 11623–11627.
- 43 A. D. Becke, *J. Phys. Chem.*, 1993, **98**, 5648–5652.



Journal Name

COMMUNICATION

## Fluorescence of a Chiral Pentaphene Derivative Derived from the Hexabenzocoronene Motif

Received 00th January 20xx,  
Accepted 00th January 20xx

Philipp Rietsch,<sup>[a]</sup> Jan Soyka,<sup>[a]</sup> Steffen Brülls,<sup>[d]</sup> Jasmin Er,<sup>[a]</sup> Katrin Hoffmann,<sup>[b]</sup> Julia Beerhues,<sup>[c]</sup>  
Biprajit Sarkar,<sup>[c]</sup> Ute Resch-Genger,<sup>[b]</sup>\* and Siegfried Eigler<sup>[a]</sup>\*

DOI: 10.1039/x0xx00000x

[www.rsc.org/](http://www.rsc.org/)

---

<sup>a</sup> M. Sc. Philipp Rietsch, Prof. Dr. Siegfried Eigler, Institute of Chemistry and Biochemistry  
Freie Universität Berlin Takustraße 3, 14195 Berlin, Germany.  
E-mail: [siegfried.eigler@fu-berlin.de](mailto:siegfried.eigler@fu-berlin.de)

<sup>b</sup> Dr. Ute Resch-Genger, Dr. Katrin Hoffmann, Bundesanstalt für Materialforschung und -prüfung (BAM), Department 1, Division Biophotonics, Richard Willstätter Straße 11, 12489 Berlin, Germany, E-Mail: [ute.resch@bam.de](mailto:ute.resch@bam.de)

<sup>c</sup> M. Sc. Julia Beerhues, Prof. Dr. Biprajit Sarkar  
Institute of Chemistry and Biochemistry, Freie Universität Berlin, Fabeckstraße 34-36, 14195 Berlin, Germany

<sup>d</sup> Chalmers University of Technology SE-412 96 Gothenburg, Sweden

---

\* Address here.

† Footnotes relating to the title and/or authors should appear here.

Electronic Supplementary Information (ESI) available: [details of any supplementary information available should be included here]. See DOI: 10.1039/x0xx00000x

## Table of contents

1. General Information .....	3
2. Synthetic procedure.....	4
Synthesis of 1-(1-( <i>tert</i> -Butyl)-4-ethynylbenzen)-2,3,4,5,6-(penta-(4- <i>tert</i> -phenyl)benzene ( <b>3</b> ) .....	4
Synthesis of 2,5,8,11,14-penta- <i>tert</i> -butyl-18-(4-( <i>tert</i> -butyl)phenyl)dibenzo[fg,ij]pyreno[5,4,3,2,1-pqrst]pentaphene ( <b>4</b> ).....	5
Hexa- <i>tert</i> -butylhexa- <i>peri</i> -hexabenzocoronene ( <b>5</b> ) .....	7
2-((4-methoxyphenyl)ethynyl)-1,1'-biphenyl ( <b>6</b> ) .....	7
9-(4-methoxyphenyl)phenanthrene ( <b>7</b> ) .....	8
3. Crystal structure .....	10
4. UV/Vis and fluorescence measurements.....	13
5. Fluorescence lifetimes measurements .....	17
6. Solid state fluorescence measurements.....	18
7. Computational Study of the racemization barrier.....	21

## 1. General Information

All reagents were purchased from commercial sources and used without further purification. Dry solvents were purchased from Acros Organics. ALUGRAM Xtra SIL G/UV<sub>254</sub> plates by Macherey-Nagel were used for thin-layer chromatography. Isolation of products by chromatography was performed with silica from Macherey-Nagel Silica 60 M (0.04-0.063 mm). NMR spectra were recorded on a JOEL ECX 400 (<sup>1</sup>H 400 MHz, <sup>13</sup>C 101 MHz), JEOL Eclipse+ 500 (<sup>1</sup>H 500 MHz, <sup>13</sup>C 126 MHz) and BRUKER AVANCE 700 (<sup>1</sup>H 700 MHz, <sup>13</sup>C 176 MHz) spectrometer at 25 °C. The chemical shifts  $\delta$  are calibrated on the respective solvent peak as internal standard. All shifts are reported in ppm and NMR multiplicities are abbreviated as s (singlet), d (duplet), t (triplet), m (multiplet). Coupling constants J are reported in Hz. UV/Vis spectra were recorded on a Cary 50 Bio photospectrometer (Varian). Fluorescence spectra were recorded on a LS 50 B luminescence spectrometer from PerkinElmer. UV/Vis and Fluorescence spectra were measured in quartz glass cuvettes with 1 cm path length. IR Spectra were recorded on a FT/IR 4100 spectrometer from JASCO. Elemental analysis was performed on an VARIO EL from Elementar.

Single crystals suitable for X-ray diffraction analysis were grown by slow evaporation from chloroform and methanol (9:1). X-ray data were collected on a Bruker D8 Venture system at 100(2) K using graphite-monochromated MoK $\alpha$  radiation ( $\lambda = 0.71073$  Å). The strategy for the data collection was evaluated using APEX3 software and the data were collected by the omega + phi scan techniques. The data were scaled and reduced using SAINT+ and SADABS software. The structure was solved by intrinsic phasing using SHELXT-2014/7. It was refined by full matrix least-squares using SHELXL-2014/7 and was refined on F<sup>2</sup>. Non-hydrogen atoms were refined anisotropically.<sup>[1-7]</sup> CCDC (1923092) contains the supplementary crystallographic data for this paper.

Photoluminescence quantum yields ( $\Phi$ ) were determined absolutely with an integrating sphere setup from Hamamatsu (Quantaurus-QY C11347-11). All  $\Phi$  measurements were performed at 25 °C using special 10 mm x 10 mm long neck quartz cuvettes from Hamamatsu. The fluorescence lifetime ( $\tau$ ), the average time in which the fluorophore is in an excited state before it relaxes to the ground state, was recorded on a fluorometer FLS 920 (Edinburgh Instruments) equipped with a Hamamatsu R3809U-50 (range 200–850 nm, response width <25 ps), Multi-Channel Plate (MCP) detector, Czerny-Turner double monochromators and either a supercontinuum laser (Fianium SC400-2-PP) or a Edinburgh Instrument EPLED-330 (picosecond pulsed light emitting diode) for excitation at 375 nm, or a Edinburgh Instrument EPL-375 (picosecond pulsed diode laser) for excitation at 330 nm. All the measurements were performed at T = 298 K using 10 mm x 10 mm quartz cuvettes from Hellma GmbH always filled with 2 mL of solvent or dye solution. Before each measurement, the instrument response function (IRF) was measured. The lifetime measurements were analysed with Edinburgh Instruments FAST Software and fitted with a deconvolution fit. All the lifetimes could be evaluated mono, bi- or tri-exponentially with a reduced X<sup>2</sup> between 0.8 and 3.0.

The fluorescence spectra of the crystals in the solid state and microscopic images were recorded with an Olympus FluoView FV1000 (Olympus GmbH, Hamburg, Germany). For UV excitation, a DPSS Cobolt Zouk® (355 nm; 10 mW), and for transmission imaging an additional multiline argon ion laser (30 mW, 488 nm) were used as excitation sources, which were reflected by a beamsplitter (BS 20/80) and focused onto the sample through an Olympus objective UPLSAPO 10X (numerical aperture N.A. 0.40). The emitted photons were recollectored with the same objective and focused onto a PMT. Emission signals were detected in a wavelength range between 460 nm and 700 nm with spectral resolution of 5 nm and a step width of 2 nm. The spatial resolved fluorescence spectra are raw spectra, not specifically corrected for the wavelength-dependent spectral responsivity of the detection system of the microscope.



## 2. Synthetic procedure

### Synthesis of 1-(1-(*tert*-Butyl)-4-ethynylbenzen)-2,3,4,5,6-(penta-(4-*tert*-phenyl)benzene) (3)

The synthesis of **3** was done as depicted in Figure S1. All procedures and analytic results of compounds **1**, **2** and **8-12** were in accordance with the literature.<sup>[8-9]</sup> The reaction description below is for the Diels-Alder reaction leading to compound **3**.

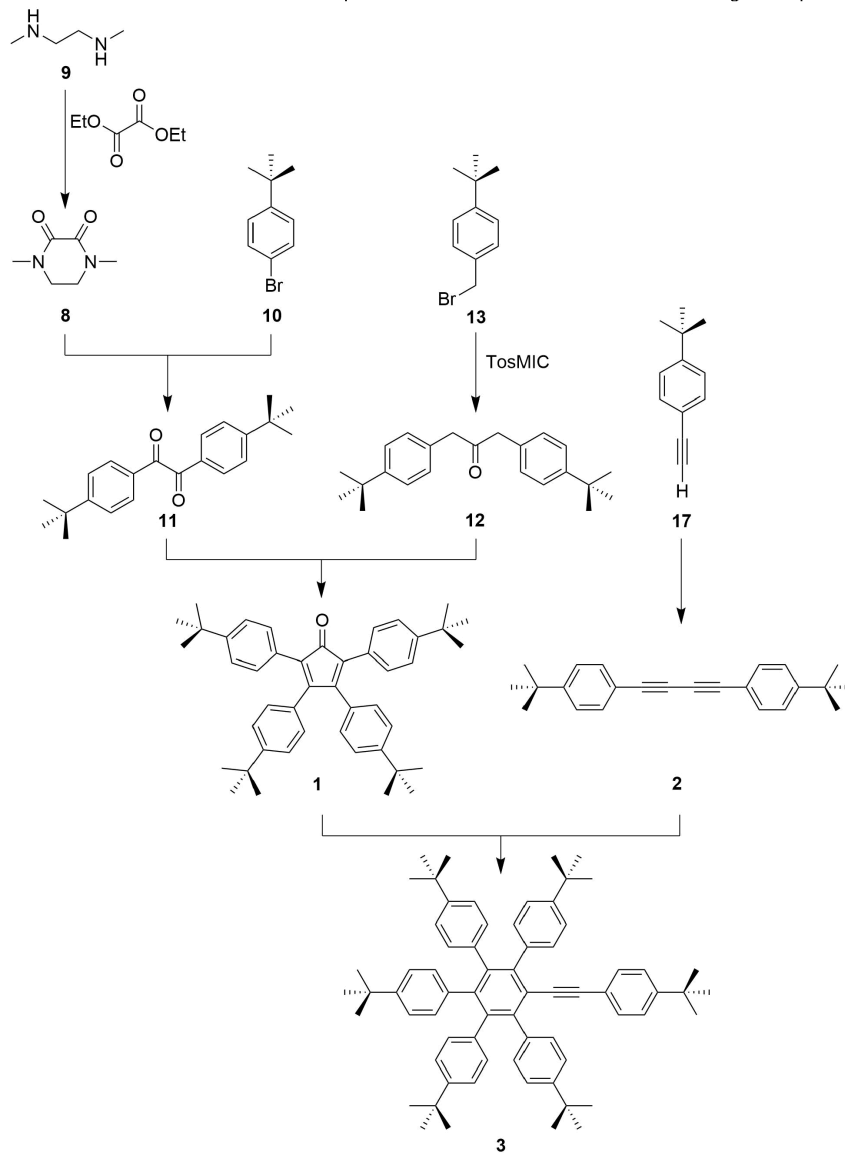


Figure S1: Synthetic route towards hexaarylbenzene derivative **3**.

2,3,4,5-Tetrakis(4-(*tert*-butyl)phenyl)cyclopenta-2,4-dien-1-one (0.249 g, 0.41 mmol, 0.95 eq.) **1** and 1,4-Bis(4-(*tert*-butyl)phenyl)buta-1,3-diyne (0.121 g, 0.38 mmol, 1.0 eq) **2** were dissolved in diphenyl ether (2 mL) under argon atmosphere. The solution was stirred at 250 °C for 24 hours. The red solution was cooled to RT, DCM (5 mL) and subsequently methanol (75 mL) were added. A colorless precipitate formed which was filtered and washed with cold methanol (3x 5 mL). The raw product was purified by column chromatography (SiO<sub>2</sub>, hexane/DCM, 7:1). After drying, 1-(1-(*tert*-butyl)-4-ethynylbenzen)-2,3,4,5,6-(penta-(4-*tert*-phenyl)benzene was yielded as a colorless solid (0.24 mmol, 0.216 g, 59%)

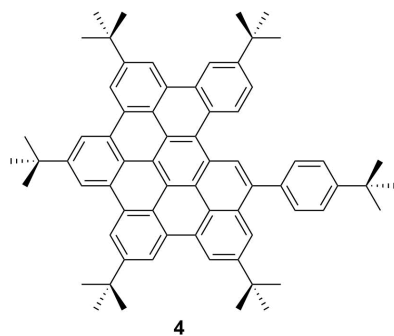
**<sup>1</sup>H-NMR** (700 MHz, CDCl<sub>3</sub>): δ [ppm] = 1.09 (s, 9H, *t*-Bu), 1.11 (s, 18H, *t*-Bu), 1.22 (s, 9H, *t*-Bu), 1.29 (s, 18H, *t*-Bu), 6.62 – 6.64 (d, *J*<sub>H,H</sub> = 8.4 Hz, 2H, Ar), 6.66 – 6.68 (d, *J*<sub>H,H</sub> = 8.4 Hz, 2H, Ar), 6.72 – 6.74 (d, *J*<sub>H,H</sub> = 8.0 Hz, 4H, Ar), 6.80 – 6.82 (d, *J*<sub>H,H</sub> = 8.4 Hz, 2H, Ar), 6.84 – 6.86 (d, *J*<sub>H,H</sub> = 8.0 Hz, 4H, Ar), 7.07 – 7.09 (d, *J*<sub>H,H</sub> = 8.4 Hz, 2H, Ar), 7.16 – 7.20 (m, 17H, Ar)

**<sup>13</sup>C-NMR** (175 MHz, CDCl<sub>3</sub>): δ [ppm] = 31.26 (*t*-Bu), 31.31 (*t*-Bu), 31.33 (*t*-Bu), 31.54 (*t*-Bu), 34.20 (Ar-C(Me)<sub>3</sub>), 34.23 (Ar-C(Me)<sub>3</sub>), 34.53 (Ar-C(Me)<sub>3</sub>), 34.74 (Ar-C(Me)<sub>3</sub>), 96.60 (Ar-C≡C-Ar), 89.79 (Ar-C≡C-Ar), 121.14 (Ar), 122.80 (Ar), 123.23 (Ar), 123.33 (Ar), 123.73 (Ar), 124.84 (Ar), 130.74 (Ar), 130.98 (Ar), 131.02 (Ar), 131.11 (Ar), 137.33 (Ar), 137.57 (Ar), 137.95 (Ar), 140.44 (Ar), 137.57 (C Ar), 137.95 (Ar), 140.44 (Ar), 141.48 (Ar), 143.14 (Ar), 147.77 (Ar), 147.88 (Ar), 148.72 (Ar), 150.76 (Ar).

**MS** (EI): *m/z* = 894.53 [M<sup>+</sup>] (calc. 894.61).

**EA** [%]: C: 89.99 (calc. 91.22), H: 8.86 (calc. 8.78).

Synthesis of 2,5,8,11,14-penta-*tert*-butyl-18-(4-(*tert*-butyl)phenyl)dibenzo[*fg,ij*]pyreno[5,4,3,2,1-*pqrst*]pentaphene (**4**)



Under argon atmosphere compound **3** (0.1004 g, 0.112 mmol, 1.0 eq.) was dissolved in DCM (50 mL) and cooled to 0 °C. A solution of pre-dried iron (III) chloride (0.218 g, 1.344 mmol, 12.0 eq.) in freshly distilled nitromethane (5 mL) was added dropwise. The solution was then stirred for 1 hour at 0 °C and subsequent stirring for 15 hours at RT. The red solution was then quenched with methanol (50 mL) which gave a yellow suspension. Water (50 mL) was added and extracted with DCM (3x 50 mL). The organic phases were combined, dried, evaporated, and dried. The resulting crude product was purified by column chromatography (SiO<sub>2</sub>, hexane/DCM, 8:1) to yield a yellow solid (0.079 g, 0.090 mmol, 80%).

**<sup>1</sup>H-NMR** (700 MHz, CDCl<sub>3</sub>): δ [ppm] = 1.51 (s, 9H, *t*-Bu), 1.64 (s, 9H, *t*-Bu), 1.66 (s, 9H, *t*-Bu), 1.78 (s, 9H, *t*-Bu), 1.81 (s, 9H, *t*-Bu), 1.82 (s, 9H, *t*-Bu), 7.68 – 7.69 (d, *J*<sub>H,H</sub> = 8.4 Hz, 2H, Ar), 7.81 – 7.85 (d, *J*<sub>H,H</sub> = 8.4 Hz, 2H, Ar), 7.86–7.87 (m, 1H, Ar), 8.51 (s, 1H, Ar), 8.93 (s, 1H, Ar), 9.08 (s, 1H, Ar), 9.16 – 9.20 (m, 3H, Ar), 9.26 – 9.29 (m, 4H, Ar), 9.37 (s, 1H, Ar).

**<sup>13</sup>C-NMR** (175 MHz, CDCl<sub>3</sub>): δ [ppm] = 150.49, 149.76, 149.33, 149.19, 149.11, 148.87, 138.87, 138.15, 131.37, 130.87, 130.75, 130.65, 130.58, 130.47, 130.29, 130.27, 130.16, 128.45, 128.40, 125.58, 124.60, 124.48, 124.34, 124.25, 123.98, 123.72, 123.58, 122.46, 122.10, 122.07, 121.00, 120.15, 119.96, 119.25, 119.06, 118.97, 118.90, 118.38, 118.09, 35.87, 35.79, 35.37, 34.93, 32.16, 32.14, 32.07, 31.76, 31.70

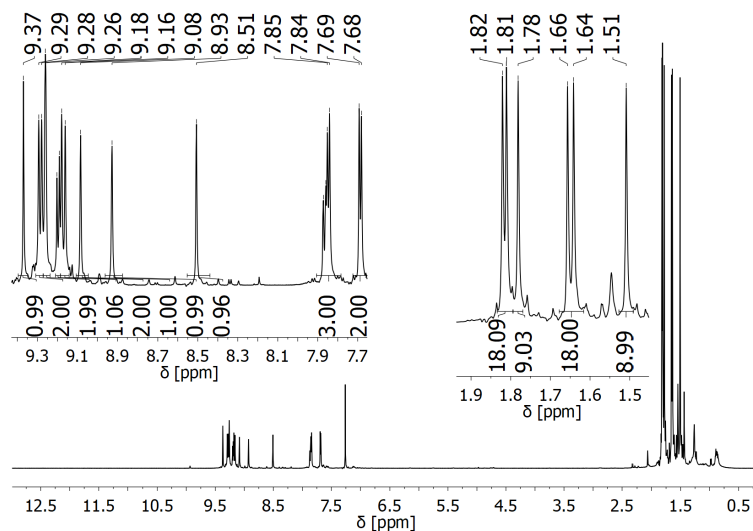
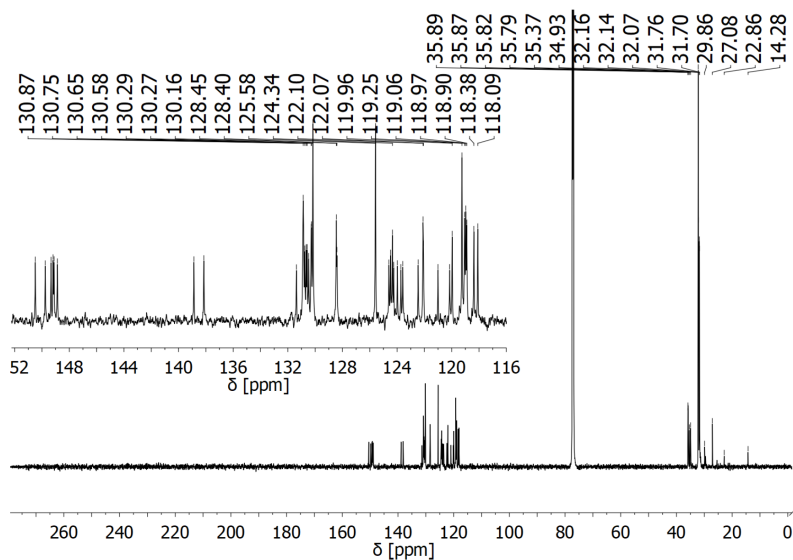
**MS** (EI): *m/z* = 886.52 [M<sup>+</sup>] (calc. 886.548).

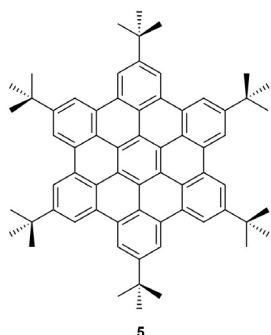
**EA** [%]: C: 92.04 (calc. 92.05), H: 7.98 (calc. 7.95).

**UV/Vis** (cyclohexane) λ<sub>max</sub> nm (ε [Lmol<sup>-1</sup> cm<sup>-1</sup>]): 226 (122706), 316 (34272), 350 (64773), 365 (67839), 400 (29242), 424 (32072)

**UV/Vis** (dichloromethane) λ<sub>max</sub> nm (ε [Lmol<sup>-1</sup> cm<sup>-1</sup>]): 250 (55670), 319 (30149), 353 (56649), 367 (61120), 404 (26447), 427 (28945)

**UV/Vis** (ethanol) λ<sub>max</sub> nm (ε [Lmol<sup>-1</sup> cm<sup>-1</sup>]): 229 (42468), 316 (22190), 349 (37410), 364 (38458), 400 (18163), 423

Figure S2:  $^1\text{H}$ -NMR spectrum of compound 4 recorded on BRUKER AVANCE 700 in  $\text{CDCl}_3$ .Figure S3:  $^{13}\text{C}$ -NMR spectrum of compound 4 recorded on BRUKER AVANCE 700 in  $\text{CDCl}_3$ .

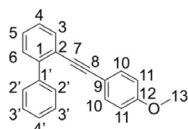
Hexa-*tert*-butylhexa-*peri*-hexabenzocoronene (**5**)

Compound **5** was synthesized by a one pot reaction of hexaphenylbenzene and *t*-BuCl with FeCl<sub>3</sub> acting as oxidant and Lewis acid catalyst. The reaction and analytical data were in accordance with the literature.<sup>[10]</sup>

**UV/Vis** (cyclohexane)  $\lambda_{\text{max}}$  nm ( $\epsilon$  [Lmol<sup>-1</sup> cm<sup>-1</sup>]): 229 (64097), 243 (42147), 364 (50680), 389 (17632)

**UV/Vis** (dichloromethane)  $\lambda_{\text{max}}$  nm ( $\epsilon$  [Lmol<sup>-1</sup> cm<sup>-1</sup>]): 231 (167666), 240 (128816), 343 (81265), 360 (181660), 390 (58991)

**UV/Vis** (ethanol)  $\lambda_{\text{max}}$  nm ( $\epsilon$  [Lmol<sup>-1</sup> cm<sup>-1</sup>]): 229 (48901), 242 (33511), 347 (20118), 363 (40746), 395 (11160)

2-((4-methoxyphenyl)ethynyl)-1,1'-biphenyl (**6**)

Under argon atmosphere, PdCl<sub>2</sub>(PPh<sub>3</sub>)<sub>2</sub> (0.11 g, 0.15 mmol, 0.21 eq.), 2-iodobiphenyl (0.13 ml, 0.71 mmol, 1.00 eq.) and CuI (0.04 g, 0.21 mmol, 0.30 eq.) were stirred in triethylamine (15 mL). 4-Methoxyphenylacetylene (0.10 mL, 0.73 mmol, 1.03 eq.) was added dropwise. The black suspension was stirred for 24 hours at RT and for 5 hours at 55 °C. After cooling to RT, the suspension was filtered and purified by column chromatography (SiO<sub>2</sub>; pentane / ethylacetate, 30:1) to yield 0.05 g (0.18 mmol, 25% yield) of a colourless liquid.

**<sup>1</sup>H-NMR** (500 MHz, CDCl<sub>3</sub>):  $\delta$  [ppm] = 7.70-7.63 (m, 3H, H-3, H-4, H-6), 7.49-7.31 (m, 6H, H-5, H-2', H-3', H-4'), 7.28 (d, <sup>3</sup>J = 8.7 Hz, 2H, H-10), 6.83 (d, <sup>3</sup>J = 8.7 Hz, 2H, H-11), 3.80 (s, 3H, H-13).

**<sup>13</sup>C-NMR** (125 MHz, CDCl<sub>3</sub>):  $\delta$  [ppm] = 159.66 (C-12), 143.77 (C-1), 140.83 (C-1'), 132.93 (C-10), 132.73 (C-3), 129.57 (C-3'), 128.29 (C-5), 127.98 (C-2'), 127.52 (C-4'), 127.16 (C-6), 122.07 (C-4), 120.04 (C-2), 115.76 (C-9), 114.06 (C-11), 92.41, (C-8), 88.23 (C-7), 55.41 (C-13).

**MS** (ESI):  $m/z$  = 323.08 (100) [M-K]<sup>+</sup>, 307.10 (60) [M-Na]<sup>+</sup>, 285.12 (35) [M-H]<sup>+</sup>.

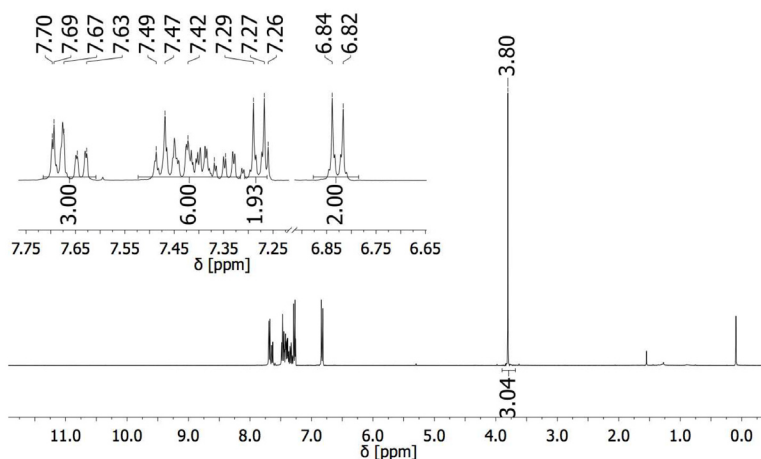
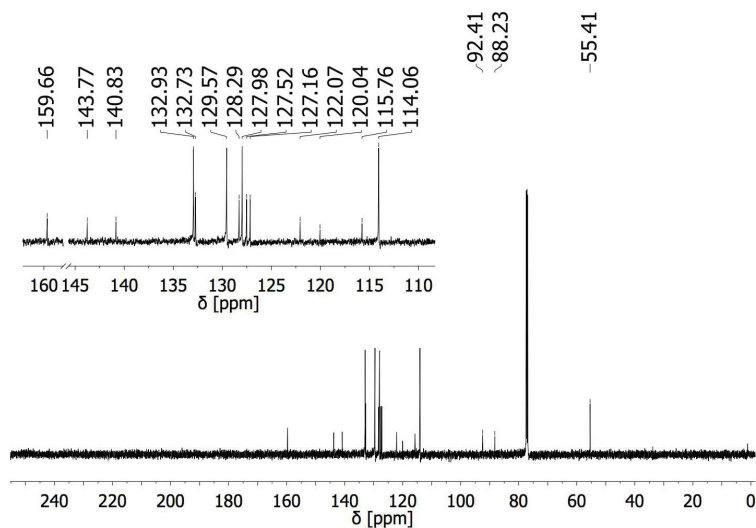
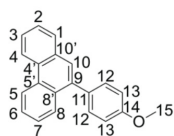


Figure S4: <sup>1</sup>H-NMR spectrum of compound **6** recorded on BRUKER AVANCE III 500 in CDCl<sub>3</sub>.

Figure S5:  $^{13}\text{C}$ -NMR spectrum of compound 6 recorded on BRUKER AVANCE III 500 in  $\text{CDCl}_3$ .

## 9-(4-methoxyphenyl)phenanthrene (7)

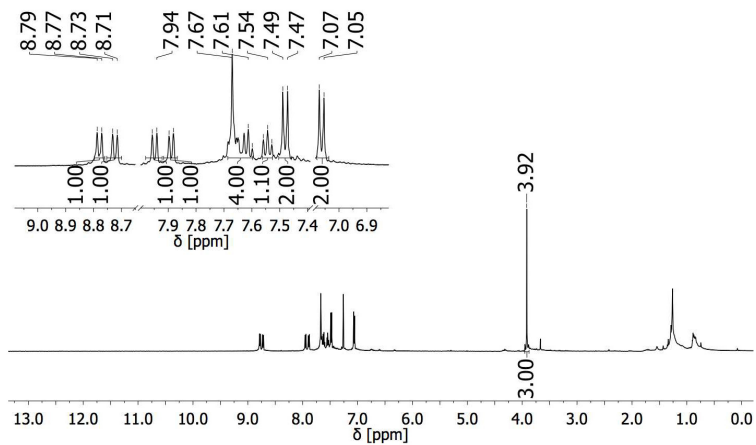
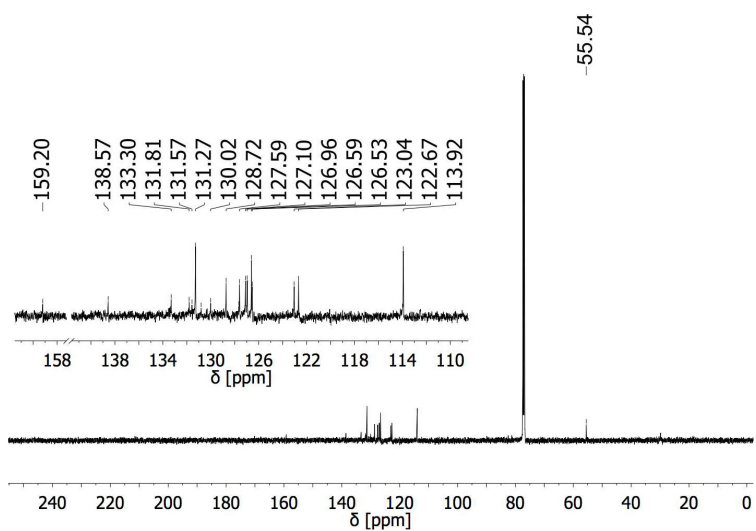


Under argon atmosphere,  $\text{FeCl}_3$  (0.02 g, 0.14 mmol, 0.88 eq.) was stirred in dry DCM (50 mL). 2-((4-methoxyphenyl)ethynyl)-1,1'-biphenyl (6) (0.045 g, 0.16 mmol, 1.00 eq.) was added dropwise to the black-green solution and stirred at RT. Controlling the reaction procedure by TLC, the reaction was quenched by the addition of methanol (5 mL). The suspension was filtered and the raw solution was purified by column chromatography ( $\text{SiO}_2$ ; pentane  $\rightarrow$  ethylacetate) to yield 9-(4-methoxyphenyl)phenanthrene as a brownish solid (0.032 g, 0.11 mmol, 69%).

$^1\text{H-NMR}$  (500 MHz,  $\text{CDCl}_3$ ):  $\delta$  [ppm] = 8.78 (d,  $^3J = 8.0$  Hz, 1H, H-5), 8.73 (d,  $^3J = 8.0$  Hz, 1H, H-4), 7.95 (d,  $^3J = 8.9$  Hz, 1H, H-8), 7.89 (d,  $^3J = 8.9$  Hz, 1H, H-1), 7.67-7.60 (m, 4H, H-3, H-6, H-7, H-10), 7.55 (t,  $^3J = 7.5$  Hz, 1H, H-2), 7.48 (d,  $^3J = 8.5$  Hz, 2H, H-12), 7.07 (d,  $^3J = 8.5$  Hz, 2H, H-13), 3.92 (s, 3H, H-15).

$^{13}\text{C-NMR}$  (125 MHz,  $\text{CDCl}_3$ ):  $\delta$  [ppm] = 159.20 (C-14), 138.57 (C-11), 133.30 (C-10'), 131.81 (C-9), 131.57 (C-5'), 131.27 (C-4'), 130.81 (C-12), 130.02 (C-8'), 128.72 (C-8), 127.65 (C-1), 127.59 (C-7), 127.10 (C-6), 126.96 (C-2), 126.59 (C-3), 126.53 (C-5), 123.04 (C-4), 122.67 (C-10), 113.92 (C-13), 55.54 (C-15).

$\text{MS}$  (EI):  $m/z = 284.12$  [ $\text{M}$ ] $^+$ , 285.12 [ $\text{M-H}$ ] $^+$ .

Figure S6:  $^1\text{H}$ -NMR spectrum of compound 7 recorded on BRUKER AVANCE III 500 in  $\text{CDCl}_3$ .Figure S7:  $^{13}\text{C}$ -NMR spectrum of compound 7 recorded on BRUKER AVANCE III 500 in  $\text{CDCl}_3$ .

### 3. Crystal structure

Single crystals of **4** were grown in a mixture of chloroform and methanol (9:1) by slow evaporation. For the comparison of the structures, the crystallographic data of **5** were taken from literature.<sup>[11]</sup>

Table S1: Crystallographic data and structure refinement details of compound 5.

Empirical formula	C <sub>34</sub> H <sub>35</sub>
Formula weight	443.62
Temperature/K	104(2)
Crystal system	triclinic
Space group	P-1
a/Å	11.0477(12)
b/Å	16.493(3)
c/Å	16.663(3)
$\alpha/^\circ$	109.226(4)
$\beta/^\circ$	102.182(4)
$\gamma/^\circ$	108.712(4)
Volume/Å <sup>3</sup>	2539.4(7)
Z	4
$\rho_{\text{calc}}/\text{cm}^{-3}$	1.160
$\mu/\text{mm}^{-1}$	0.065
F(000)	956.0
Crystal size/mm <sup>3</sup>	0.32 × 0.29 × 0.02
Radiation	MoK $\alpha$ ( $\lambda$ = 0.71073)
2 $\theta$ range for data collection/ $^\circ$	4.674 to 50.802
Index ranges	-13 ≤ h ≤ 12, -19 ≤ k ≤ 19, -20 ≤ l ≤ 20
Reflections collected	72902
Independent reflections	9328 [ $R_{\text{int}}$ = 0.1009, $R_{\text{sigma}}$ = 0.0490]
Data/restraints/parameters	9328/0/631
Goodness-of-fit on F <sup>2</sup>	1.024
Final R indexes [ $>2\sigma$ (I)]	$R_1$ = 0.0516, $wR_2$ = 0.1131
Final R indexes [all data]	$R_1$ = 0.0895, $wR_2$ = 0.1302
Largest diff. peak/hole / e Å <sup>-3</sup>	0.27/-0.26

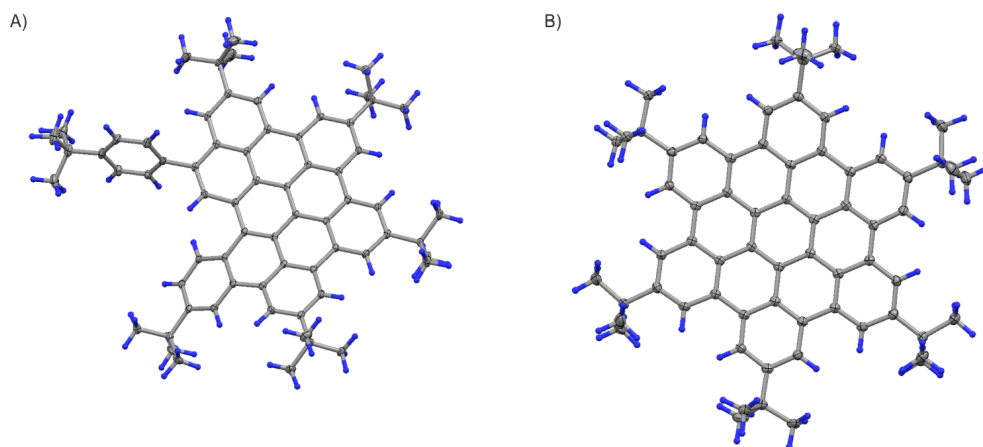


Figure S8: Crystal structures of 4 (A) and 5 (B). The thermal ellipsoids are shown in 50% probability.



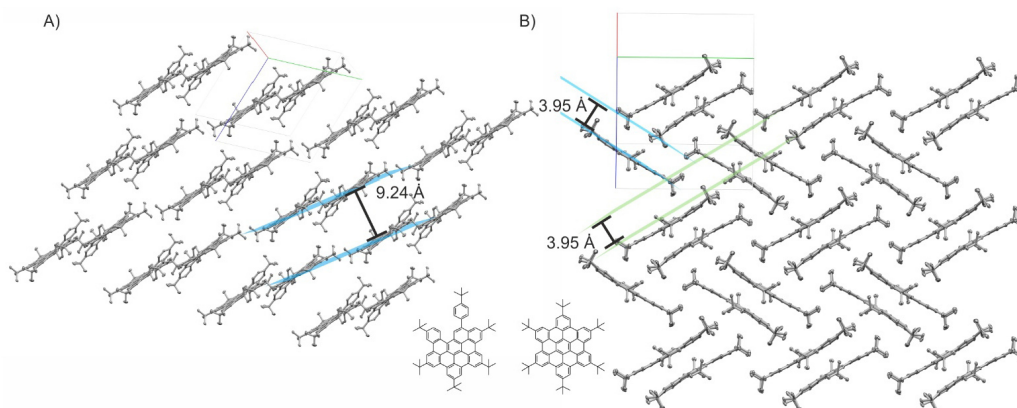


Figure S9: Molecular planes in compound **4** (A) and compound **5** (B). For **5**, the herringbone structure is clearly visible and the interplanar distance is below 4 Å. The interplanar distance of **4** is 9.24 Å. The crystallographic data of **5** was taken from reference<sup>[11]</sup>. The unit cell is depicted through the red (direction a), green (direction b) and blue (direction c) lines forming a cube. The depiction of **5** was 1 unit cell in a direction, 4 unit cells in b direction and 3 unit cells in c direction.

## 4. UV/Vis and fluorescence measurements

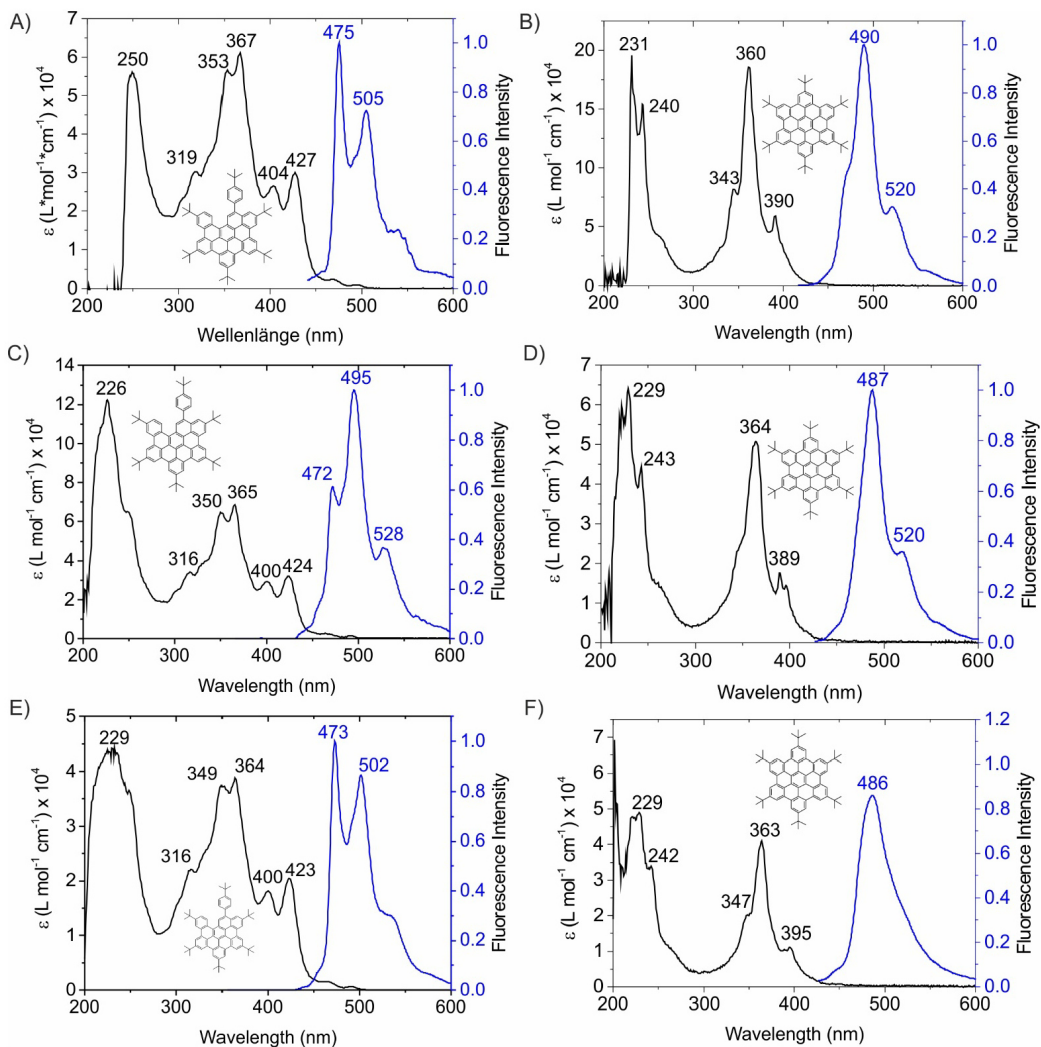


Figure S10: Absorption spectra (black) and fluorescence spectra (blue) of compound 4 (left side) and compound 4 (right side) respectively in dichloromethane (A and B), cyclohexane (C and D) and ethanol (E and F). The excitation wavelength was always chosen near the absorbance maximum about 350 nm. The numbers in the panels without unit refer to the respective absorption (black) and emission maxima (blue) on a wavelength scale. For a more detailed information on the excitation wavelength-s dependent fluorescence see Figure S11 and Figure S12.

Table S2: Absorption Maxima and emission maxima of **4** and **5** with the Stokes shift calculated from the respective absorption maxima about 350 nm and emission maxima, both marked with \* and written in italic.

	Absorption Maxima		Emission Maxima		Stokes Shift*	
	<b>4</b>	<b>5</b>	<b>4</b>	<b>5</b>	<b>4</b>	<b>5</b>
DCM	250 319 353 <i>367*</i> 404 427	231 240 343 <i>360*</i> 390	<i>475*</i> 505	<i>490*</i> 520	108	130
CH	226 316 350 <i>365*</i> 400 424	229 243 <i>364*</i> 389	472 <i>495*</i> 528	<i>487*</i> 520	130	123
EtOH	229 316 349 <i>364*</i> 400 423	229 242 347 <i>363*</i> 395	<i>473*</i> 502	<i>486*</i>	109	123

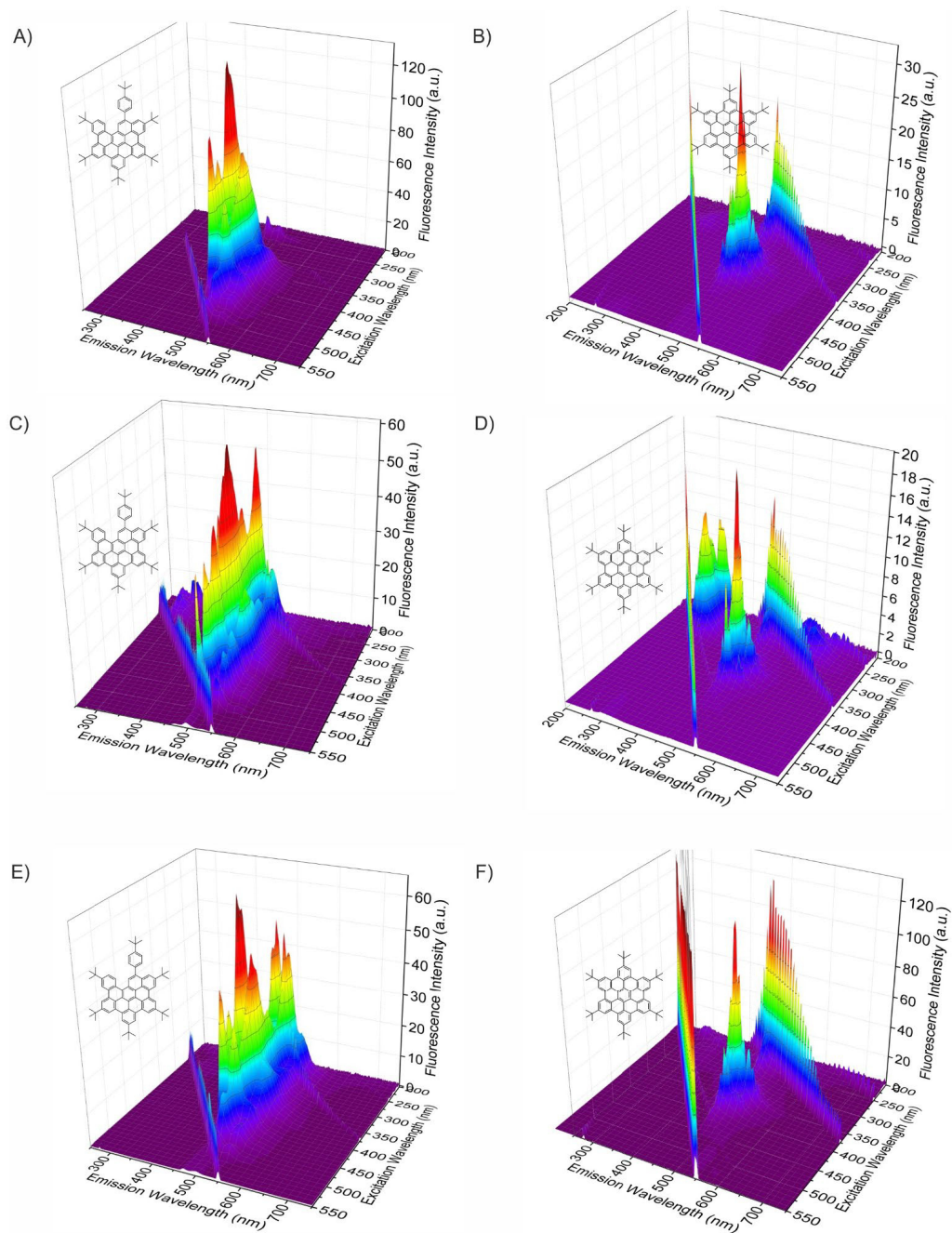


Figure S11: 3D fluorescence maps of **4** (left side) and **5** (right side) respectively. Solvents were dichloromethane in A and B, cyclohexane in C and D and ethanol in E and F. Red areas represent the highest fluorescence (normalized to 1), blue areas no fluorescence. The measurement conditions (slit widths, sensitivity, concentration) were kept constant. The intensity ratio of excitation lamp peak (diagonal lines) to the molecule peaks thus indicates the difference in fluorescence of **4** and **5**.

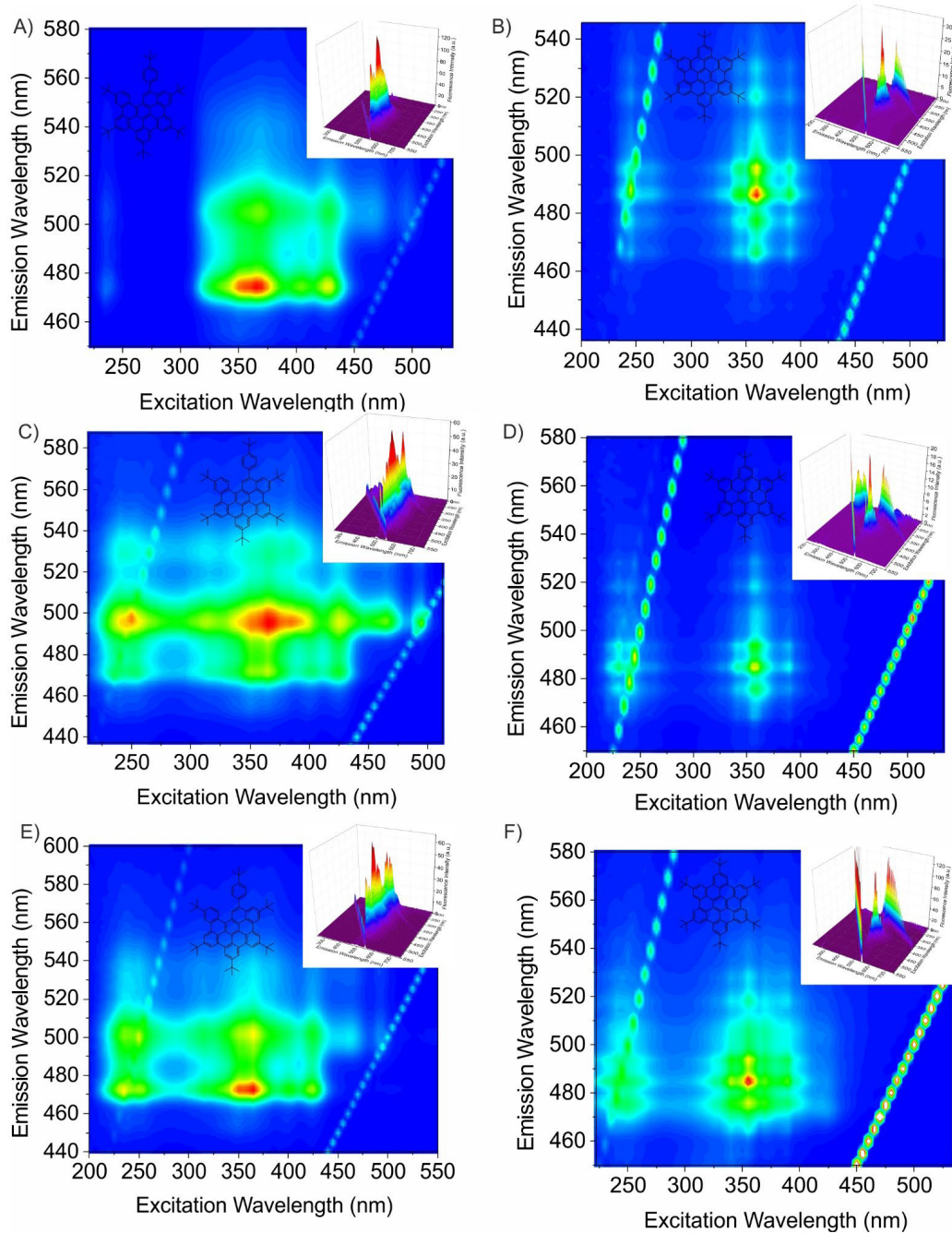


Figure S12: 2D fluorescence maps and 3D fluorescence maps (Insets) of **4** (left side) and **5** (right side) respectively. Solvents were dichloromethane in A and B, cyclohexane in C and D and ethanol in E and F. Red areas represent the highest fluorescence (normalized to 1), blue areas no fluorescence. The intensity ratio of excitation lamp peak (diagonal lines) to the molecule peaks thus indicates the difference in fluorescence of **4** and **5**.

## 5. Fluorescence lifetimes measurements

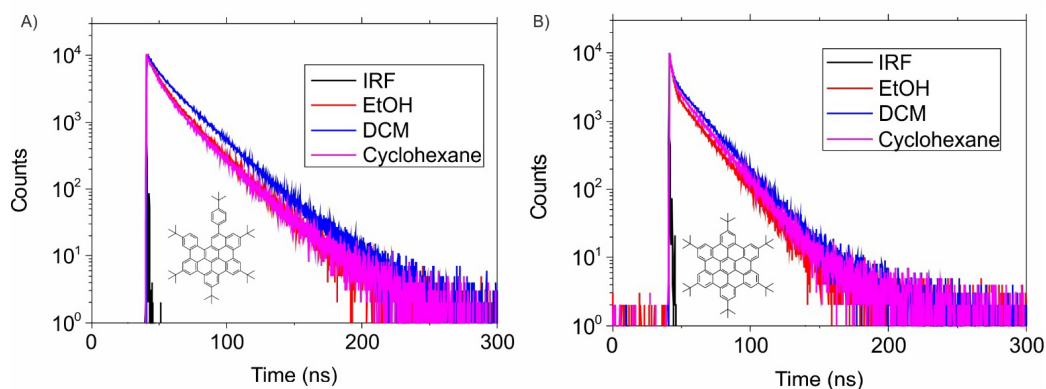


Figure S13: Fluorescence lifetimes of **4** (left side) and **5** (right side) in EtOH (red), DCM (blue) and cyclohexane (pink). Compound **4** was excited at 375 nm and the emission was measured at 490 nm. Compound **5** was excited at 375 nm and the emission was measured at 480 nm.

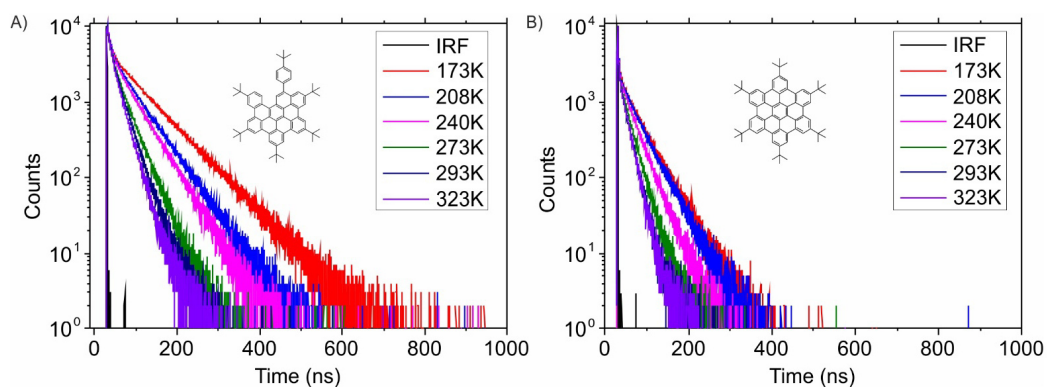


Figure S14: Fluorescence lifetimes of **4** (left side) and **5** (right side) in EtOH at different temperatures from -100 °C to 50 °C. The fluorescence lifetime of **5** decreases from 173K = 27.7 ns to 293K = 11.2 ns. The lifetime of **4** decreases from 63.2 ns at 173K to 20.39 ns at 293K (18.0 ns at 323K). Compound **4** was excited at 375 nm and the emission was measured at 490 nm. Compound **5** was excited at 375 nm and the emission was measured at 480 nm.

Table S3: Mean fluorescence lifetimes of **4** and **5** in EtOH measured at different temperatures from 50 °C to -100 °C.

	Compound 4	Compound 5
Temperature	$\tau$ [ns]	$\tau$ [ns]
173K	63.23	27.67
208K	44.09	23.62
240K	36.20	18.07
273K	24.00	11.83
293K	20.39	11.15
323K	18.02	7.93

## 6. Solid state fluorescence measurements

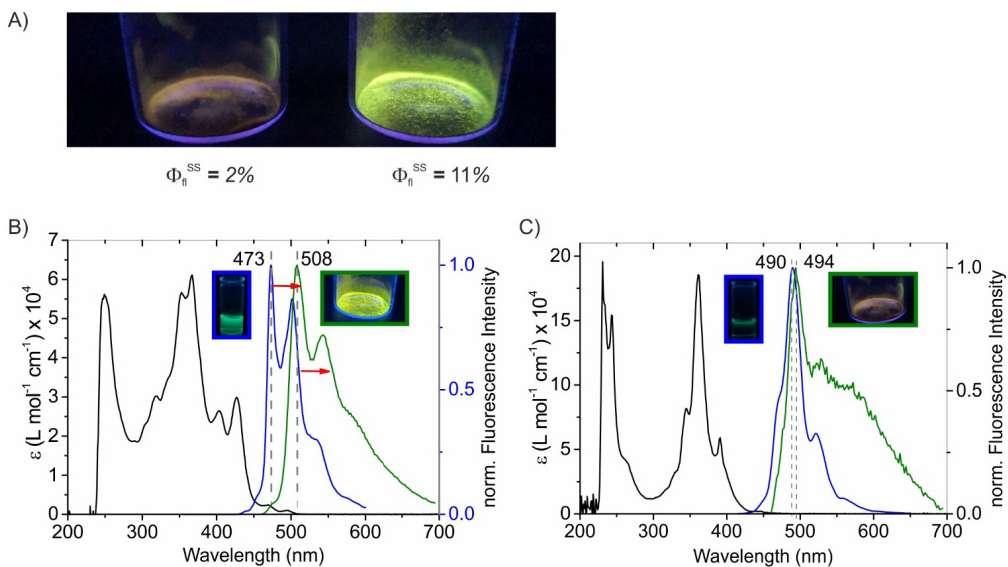


Figure S15: A) Comparison of the qualitative solid-state fluorescence of **4** (left side) and **5** (right side) under radiation of the UV lamp at 366 nm. The measured solid-state fluorescence quantum yields are given below, respectively. B and C) Comparison of the solution (blue, in DCM) and solid-state fluorescence (green) of **4** (B) and **5** (C). The absorption spectra in solution (DCM) is shown in black. The excitation wavelength was 355 nm, respectively. The solid-state fluorescence of **4** is bathochromically shifted 35 nm. The solid-state fluorescence of **5** bathochromically is shifted 4 nm. The insets show the fluorescence in solution (left, blue frame) and in solid-state (right, green frame).

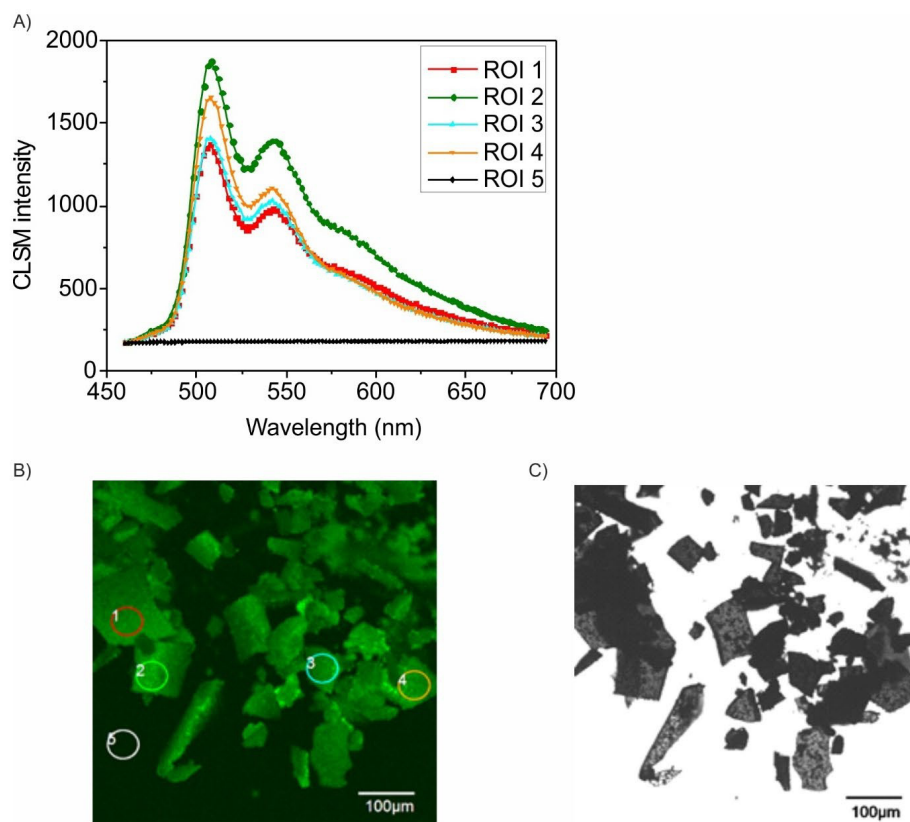


Figure S16: Spatial resolved solid state emission of **4** excited at 355 nm and at the respective region of interest (ROI) shown in B. B) Solid state emission of **4** (Exc. 355 nm; Excitation DM BS20/80; UPLSAPO 10X NA:0.40). C) Transmission image (Exc. 488 nm; 10x).



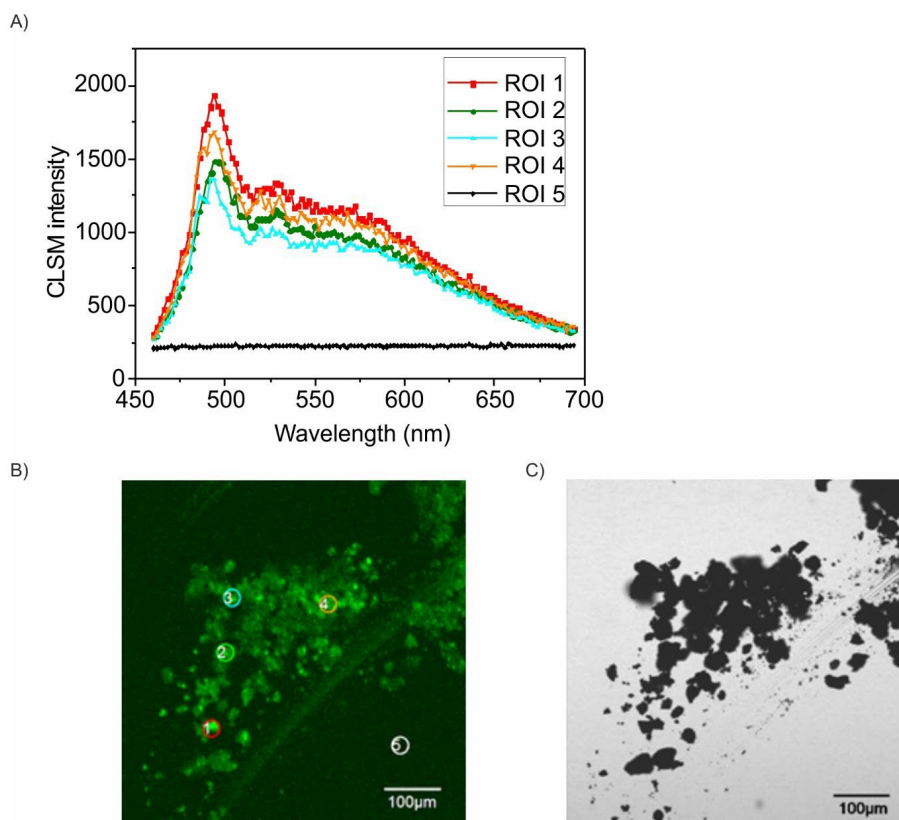


Figure S17: Spatially resolved solid state emission of **4** excited at 355 nm and at the respective ROI shown in B. B) Solid state emission of **4** (Exc. 355 nm; Excitation DM BS20/80; UPLSAPO 10X NA:0.40). C) Transmission image (Exc. 488 nm; 10x).

### 7. Computational Study of the racemization barrier

All calculations were performed using density functional theory (DFT) at the B3LYP/6-31G(d) level of theory in gaussian 09.<sup>[12-13]</sup> To elucidate the racemization barrier of compound **4** we took the initial dihedral angle of 34.45° between carbon atoms C1, C7, C22 and C38 (Figure ) from the crystal structure. The dihedral angle was then changed in steps of about 1° and the relaxed geometry was calculated at each dihedral angle using the Coordinate Scan within Gaussian with the keyword "Addredundant". The relative energies were calculated with respect to the energy of the crystal structure and are shown in Figure S13.

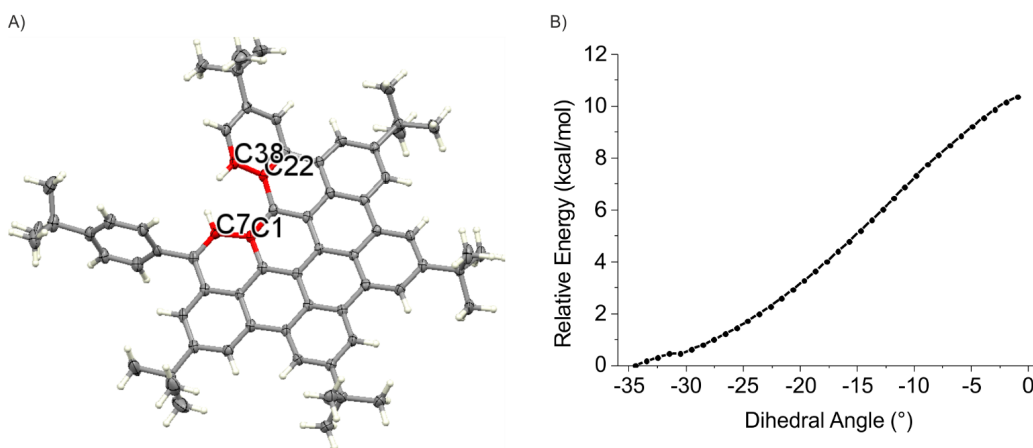


Figure S18: A) Crystal structure of **4** with the carbon atoms used for the evaluation of the racemization barrier marked in red. The dihedral angle is 34.45°. B) Calculation of the rotational barrier around the marked dihedral angle (A). The Calculation was done 1° steps from -35° to 0° using density functional theory (DFT) at the B3LYP/6-31G(d) level of theory.

To judge the accuracy of our calculations we calculated the rotational barrier of [4]helicene using our procedure. As visible in Figure S14 the rotational barrier is slightly above 4 kcal/mol and thus in accordance with the literature values.<sup>[14-15]</sup>

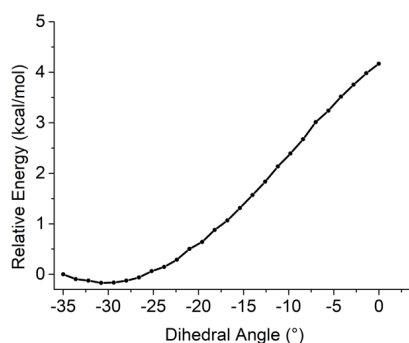


Figure S19: Calculations of the rotational barrier of [4]helicene density functional theory (DFT) at the B3LYP/6-31G(d) level of theory. The barrier is slightly above 4 kcal/mol and thus in accordance with literature values.<sup>[14]</sup>

## Notes and references

- [1] G. M. Sheldrick, *Acta Crystallogr., Sect. C: Cryst. Struct. Commun.* 2015, **71**, 3-8.
- [2] G. M. Sheldrick, *Acta Crystallogr., Sect. A: Found. Crystallogr.* 2008, **64**, 112-122.
- [3] C. B. Hubschle, G. M. Sheldrick, B. Dittrich, *J. Appl. Crystallogr.* 2011, **44**, 1281-1284.
- [4] in *APEX3*, Bruker AXS Inc., Madison, Wisconsin, USA, 2015.
- [5] G. M. Sheldrick, *Vol. Ver. 2008/1*, University of Göttingen, Germany, 2008.
- [6] SAINT+, Version 8.27b © ed., Bruker AXS Inc., Madison, Wisconsin, USA, 1997-2012.
- [7] G. M. Sheldrick, Version 2014/7 ed., University of Göttingen, Germany, 2014.
- [8] A. Gourdon, S. K. Sadhukhan, C. Viala, *Synthesis* 2003, 1521-1525.
- [9] M. H. Vilhelmsen, J. Jensen, C. G. Tortzen, M. B. Nielsen, *Eur. J. Org. Chem.* 2013, 701-711.
- [10] R. Rathore, C. L. Burns, *J. Org. Chem.* 2003, **68**, 4071-4074.
- [11] L. Zhai, R. Shukla, R. Rathore, *Org. Lett.* 2009, **11**, 3474-3477.
- [12] A. D. Becke, *J. Phys. Chem.* 1993, **98**, 5648-5652.
- [13] P. J. Stephens, F. J. Devlin, C. F. Chabalowski, M. J. Frisch, *J. Phys. Chem.* 1994, **98**, 11623-11627.
- [14] S. Grimme, S. D. Peyerimhoff, *Chem. Phys.* 1996, **204**, 411-417.
- [15] H. A. Staab, M. Diehm, C. Krieger, *Tetrahedron Lett.* 1995, **36**, 2967-2970.

### 4.3 Identification of the Irreversible Redox Behaviour of Highly Fluorescent Benzothiadiazoles

---

<b>Authors</b>	<b>Philipp Rietsch, Sebastian Sobottka, Katrin Hoffmann, Pascal Hildebrandt, Biprajit Sarkar, Ute Resch-Genger, and Siegfried Eigler</b>
<b>Journal</b>	ChemPhotoChem. 2020, 4, 1-7
<b>DOI</b>	10.1002/cptc.202000050
<b>Links</b>	<a href="https://doi.org/10.1002/cptc.202000050">https://doi.org/10.1002/cptc.202000050</a>
<b>Detailed scientific contribution</b>	<p>The concept of this manuscript was elaborated by P. Rietsch, S. Sobottka and Prof. Dr. S. Eigler.</p> <p>P. Hildebrandt synthesized compounds 1,2 and 4. P. Rietsch synthesized compound 3 and did all the photophysical measurements. S. Sobottka measured cyclic voltammetry and all spectroelectrochemical measurements. Dr. K. Hoffmann did the confocal laser scanning microscopy measurements. Dr. U. Resch-Genger, Dr. Katrin Hoffmann, Prof. Dr. B. Sarkar, and Prof. Dr. S. Eigler supervised the theoretical and experimental work.</p> <p>The manuscript was written by P. Rietsch, S. Sobottka and Prof. Dr. S. Eigler.</p>
<b>Estimated own contribution</b>	~50 %

---

## Identification of the Irreversible Redox Behavior of Highly Fluorescent Benzothiadiazoles

Philipp Rietsch,<sup>[a]</sup> Sebastian Sobottka,<sup>[b]</sup> Katrin Hoffmann,<sup>[c]</sup> Pascal Hildebrandt,<sup>[a]</sup>  
Biprajit Sarkar,<sup>[b, d]</sup> Ute Resch-Genger,<sup>\*[c]</sup> and Siegfried Eigler<sup>\*[a]</sup>

Redox switches are applied in various fields of research, including molecular lifts, electronic devices and sensors. Switching the absorbance between UV and Vis/NIR by redox processes is of interest for applications in light harvesting or biomedicine. Here, we present a series of push-pull benzothiadiazole derivatives with high fluorescence quantum yields in solution and in the crystalline solid state. Spectroelectrochemical analysis reveals the switching of UV-absorption in the neutral state to Vis/NIR absorption in the reduced state. We identify the partial irreversibility of the switching process, which appears to be reversible on the cyclic voltammetry timescale.

The class of benzothiadiazoles (BTD) bears tunable absorption and emission features. Hence, their bandgap and orbital energies can be adjusted making those fluorophores attractive for fundamental photophysical research. BTDs are synthetically accessible from *o*-phenylenediamine derivatives as starting materials. Subsequent coupling reactions like Sonogashira, Suzuki, and Buchwald-Hartwig coupling give access to a plethora of symmetrical and unsymmetrical derivatives.<sup>[1–4]</sup> BTDs can be applied in organic light-emitting diode (OLED) materials,<sup>[5–7]</sup> polymers with defined electronic and optical properties,<sup>[8–10]</sup> in sensory metal-organic frameworks,<sup>[11]</sup> solar cells<sup>[12]</sup> or in field-effect transistors (FET).<sup>[13]</sup> Furthermore, BTDs

can act as *ortho*-diamine protecting groups and can thus be used as precursors for other molecular compounds, e.g. diaminodicyanoquinones and quinoxalines.<sup>[14,15]</sup> Although, those applications involve redox processes, there are few publications where the BTD unit was considered as a redox switch.<sup>[16]</sup> In this regard, most currently used redox switches are based on, e.g. organometallic motives or complex organic structures such as peryleneimide-dithienylethene dyads.<sup>[17–20]</sup>

Up to now, spectroelectrochemical properties of BTDs have been investigated in studies on *p*- and *n*-doping effects in deposited thin films.<sup>[21,22]</sup> However, there are no examples reported which focus on establishing potentially electrochromic switches using the BTD molecular unit. In this regard, cyclic voltammetry (CV)-experiments give evidence for the electrochemical reversibility of redox processes. However, here we show that spectroelectrochemical investigations give a more reliable proof of the chemical (ir)reversibility of redox processes. Accordingly, herein we present a series of push-pull BTD derivatives with an identical electron-donating alkyne-methoxy group on one side and a variation of (electron-withdrawing) groups on the other side (Figure 1). We furthermore analyzed the fluorosolvatochromism of these compounds and measured fluorescence decay kinetics/fluorescence lifetimes ( $\tau$ ) and fluorescence quantum yields in solution ( $\Phi_f$ ) and solid state ( $\Phi_f^{SS}$ ). We investigated the non-radiative relaxation through measurements in primary alcohols of different chain length and in mixtures of ethanol and polyethylene glycol 400 (EtOH/PEG), thereby separating the effect of viscosity and polarity on BTD emission.

We started the synthesis of the presented BTD derivatives from *o*-diaminobenzene and followed the published procedure (Figure 1).<sup>[1]</sup> Compounds 1–4 were synthesized according to procedures of Park *et al.*<sup>[23]</sup> Compounds 2 and 4 were isolated from the same reaction mixture in respective yields of 12% and 54%.

The photophysical characterization was subsequently done in four solvents of varying polarity and proticity, namely *n*-hexane (apolar and aprotic), dichloromethane (DCM; medium polarity, aprotic), dimethylsulfoxide (DMSO; polar and aprotic), and ethanol (EtOH; polar and protic). The absorption and fluorescence spectra of 1–4 in DCM are shown in Figure 1B. The molar extinction coefficients ( $\epsilon$ ) of 1–4 reach a maximum at about 300 nm with values up to  $35,000 \text{ M}^{-1} \text{ cm}^{-1}$  and show a second absorption maximum around 400 nm with smaller  $\epsilon$  values of about  $10,000 \text{ M}^{-1} \text{ cm}^{-1}$ . The smaller  $\epsilon$  values in *n*-hexane and EtOH might arise either from solubility/aggregation issues, possibly in conjunction with the hydrogen bonding to

[a] P. Rietsch,\* P. Hildebrandt, Prof. Dr. S. Eigler  
Institute of Chemistry and Biochemistry  
Freie Universität Berlin  
Takustraße 3, 14195 Berlin (Germany)  
E-mail: siegfried.eigler@fu-berlin.de

[b] Dr. S. Sobottka,\* Prof. Dr. B. Sarkar  
Institute of Chemistry and Biochemistry  
Freie Universität Berlin

[c] Dr. K. Hoffmann, Dr. U. Resch-Genger  
Department 1, Division Biophotonics  
Bundesanstalt für Materialforschung und -prüfung (BAM)  
Richard Willstätter Straße 11, 12489 Berlin (Germany)  
E-mail: ute.resch@bam.de

[d] Prof. Dr. B. Sarkar  
Chair of Inorganic Coordination Chemistry  
Institute of Inorganic Chemistry  
University of Stuttgart  
Pfaffenwaldring 55, 70569 Stuttgart (Germany)

[\*] These authors contributed equally to this manuscript.

Supporting information for this article is available on the WWW under <https://doi.org/10.1002/cptc.202000050>

© 2020 The Authors. Published by Wiley-VCH Verlag GmbH & Co. KGaA. This is an open access article under the terms of the Creative Commons Attribution License, which permits use, distribution and reproduction in any medium, provided the original work is properly cited.

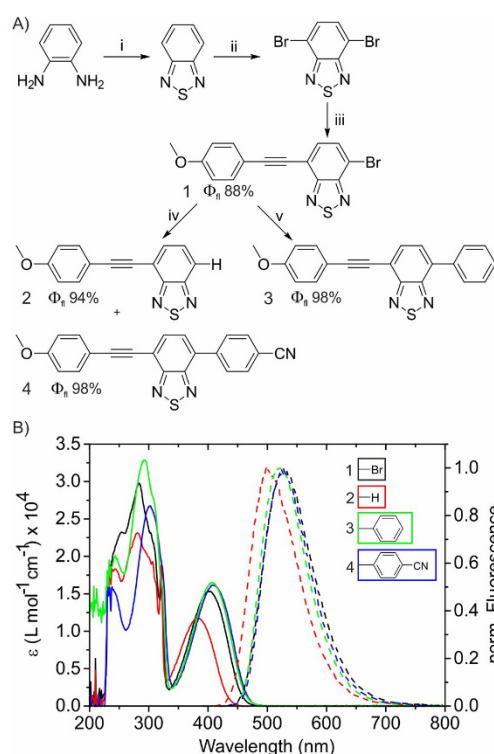


**Figure 1.** A) Synthetic route to benzothiadiazole derivatives 1–4. i)  $\text{SOCl}_2$ , dichloromethane (DCM), 5 h, reflux; ii)  $\text{HBr}$ ,  $\text{Br}_2$ ; iii) THF, TEA, 1-ethynyl-4-methoxybenzene,  $\text{Pd}(\text{PPh}_3)_2\text{Cl}_2$ , CuI; iv) THF/ $\text{H}_2\text{O}$ , 1.2 eq. of the respective boronic acid,  $\text{K}_2\text{CO}_3$ ,  $\text{Pd}(\text{PPh}_3)_4$ . Compounds 2 and 4 were isolated from the same reaction mixture in yields of 12% and 54%. v) THF/ $\text{H}_2\text{O}$ , 1.2 eq. phenyl boronic acid,  $\text{K}_2\text{CO}_3$ ,  $\text{Pd}(\text{PPh}_3)_4$ , yield: 96%. The fluorescence quantum yields ( $\Phi_f$ ) of 1–4 in DCM are given in %. B) Absorption spectra and normalized fluorescence spectra of 1–4 in DCM. The dye concentration was  $10^{-6}$ – $5 \times 10^{-5}$  M.

the nitrogen atom in the BT core unit in case of EtOH. The high energy absorption band around 300 nm was attributed to  $\pi$ - $\pi^*$  transitions and the low energy absorption band to the HOMO-LUMO transition involving an intramolecular charge transfer (ICT) state.<sup>[25,26]</sup> To elucidate the role of the two absorption bands on dye emission, we measured an excitation emission matrix (EEM) of 3 in hexane (Figure S2), thereby demonstrating that excitation at both absorption maxima induce the same emission located at 473 nm.

Subsequently, we assessed the influence of solvent polarity and proticity on the emission properties of 1–4. The red shift of the fluorescence maximum (Figure 2A) from 473 nm in hexane to 522 nm in DCM and 550 nm in DMSO of 4 is visible by the naked eye (Figure 2B).

The emission spectra in the polar aprotic and protic solvents DMSO and EtOH closely match. An increase in solvent polarity results also in a broadening of the emission band of 4,

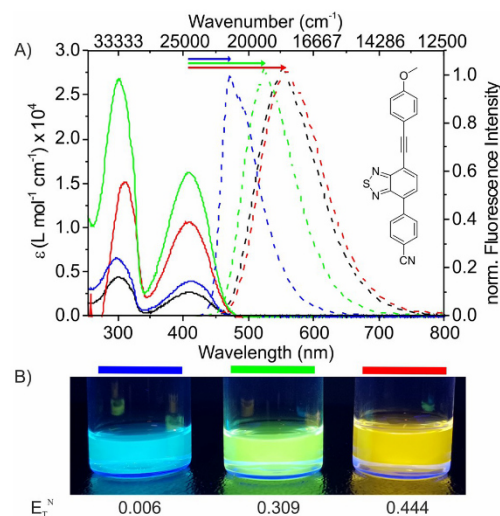


**Figure 2.** A) Absorption spectra (solid) and normalized fluorescence emission spectra (dashed, excitation at 410 nm) of 4 in solvents of different polarity. Hexane = blue, DCM = green, DMSO = red, EtOH = black. Arrows indicate the respective Stokes shift. B) Solutions of 4 in solvents of the same proticity (aprotic) but different polarity (left to right: hexane, DCM, DMSO) under illumination with 366 nm. Values for the normalized Dimroth-Reichardt Parameter  $E_T^N$  were taken from Ref. [24]. The dye concentrations used for these measurements were  $10^{-6}$ – $5 \times 10^{-5}$  M.

the full width at half maximum (FWHM) of the gaussian fits of the fluorescence spectra decrease from  $15 \times 10^4 \text{ cm}^{-1}$  in hexane to  $0.9 \times 10^4 \text{ cm}^{-1}$  in ethanol (Table S2). Exemplary spectroscopic results of fluorosolvatochromism are shown in Figure 3, where 4 was analyzed in primary alcohols of different chain length, from EtOH ( $E_T^N = 0.654$ ) to 1-decanol ( $E_T^N = 0.525$ ). As the polarity of these alcohols changes only slightly compared to the other solvents (hexane, DCM, DMSO, EtOH), the solvatochromic shifts are smaller. The absorption band is red shifted with increasing polarity whereas the fluorescence maxima are blue shifted. The  $S_1$ - $S_0$  energy gap is thus decreasing. This effect is furthermore enhanced by the increasing refractive index of the alcohols with increasing chain length.<sup>[27]</sup> Solvent dependency of absorption and emission was investigated by Lippert and Mataga separately in the 1950s and later merged in the Lippert-Mataga equation [Eq. (S1)].

Although this model is built on simplified solvent-chromophore interactions and the assumption of a spherical chromophore (Onsager radius), it is widely used to describe solvatochromism and was used for BTs before.<sup>[27–30]</sup> In Figure S7 the Lippert-Mataga plot of 1–4 is shown. The dipole change upon excitation is lowest for 1 (12.26 Debye) and highest for 4 (18 Debye). In addition, 4 also bears the highest ground state dipole moment as revealed by DFT calculations (Table S3). Both effects are ascribed to the cyano-group substituent. An increasing dipole moment upon excitation was found for BTs before and is a well-known phenomenon.<sup>[24,30]</sup> To explain the

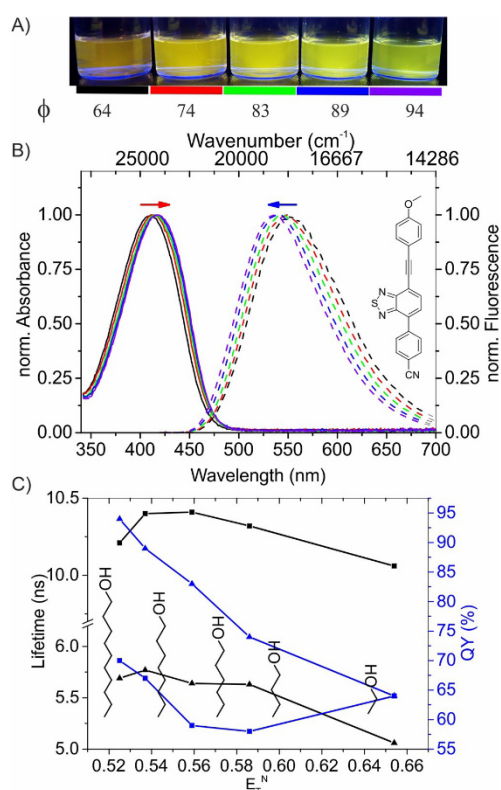


**Figure 3.** A) Photograph of solutions ( $10^{-5}$  M) of **4** in the alcohols ethanol (black), 1-butanol (red), 1-hexanol (green), 1-octanol (blue) and 1-decanol (purple) under illumination with 366 nm light. The respective quantum yields are indicated below in %. B) Normalized absorption spectra (solid lines) and emission spectra (dashed lines) of **4** (color code as in A). The Stokes shift decreases with increasing length of the alcohol chain and hence decreasing polarity. The red shift of the absorption and emission are marked by red and blue arrows, respectively. C) Fluorescence lifetime (black; right axis) and fluorescence quantum yield (blue; left axis) values in primary alcohols of decreasing chain length, revealing the polarity-induced changes of both features and their correlation. The concentrations of the measurements were  $10^{-6}$ – $10^{-7}$  M.

small difference in the change of the dipole moment for **4** in the two plots (aprotic solvents vs. series of primary alcohols in Figure S7), we measured **4** in EtOH-PEG mixtures containing increasing percentages of PEG400. There is almost no difference of the Dimroth-Reichardt polarity parameter  $E_T^N$  between PEG400 (0.66) and EtOH (0.65).<sup>[24,31]</sup> Thus, addition of PEG increases the viscosity drastically but changes the polarity only slightly (Figure S11).<sup>[32]</sup> We observe no shift in the absorption maximum and a small bathochromic shift of approx. 4 nm for the fluorescence maximum with increasing viscosity of the dye microenvironment. Thus, the polarity and the proticity of the alcohols seem to be responsible for the observed difference in the Lippert-Mataga plot.

We measured the  $\Phi_{fl}$  and the fluorescence decay kinetics and therefore  $\tau$  of the BDT dyes **1–4** in a series of solvents of increasing polarity and viscosity as well as in the solid state. The  $\Phi_{fl}$  are consistently maximal in DCM, with values of 98% for **3** and **4**, thus reaching almost unity (Table 1). All compounds show the lowest  $\Phi_{fl}$  in EtOH, the solvent with the highest polarity and highest hydrogen bonding strength.<sup>[33]</sup> Compounds **1** and **2** show a remarkably strong reduction of  $\Phi_{fl}$  in EtOH (15% and 16%) and reduced  $\tau$  of 4.12 ns (**1**) and 2.42 ns (**2**). This effect is ascribed to hydrogen bonding to the nitrogen atom of the BTD core, which is rather unprotected in **1** and **2** but sterically shielded by the phenyl substituents in **3** and **4**.

Furthermore, the formation of an ICT state in solvents of high polarity and emission from a locally excited (LE) state in solvents of low polarity, which was found to be dependent on the distance of the donor and acceptor moieties in push-pull systems, could explain the trend of the generally lower  $\Phi_{fl}$  and  $\tau$  in polar ethanol.<sup>[25,27,30,34]</sup> The highest  $\tau$  values (Table S5) are found for **2** in DCM (10.02 ns) and DMSO (9.05 ns).

With increasing chain length of the solvent alcohol, and thus decreasing polarity, decreasing hydrogen bonding strength and increasing viscosity,  $\tau$  and the  $\Phi_{fl}$  of **4** increase (Figure 3C and Table S6). Accordingly, from ethanol to 1-decanol  $\tau$  increases by 12.5% and  $\Phi_{fl}$  by 47%. Since  $\Phi_{fl}$  and  $\tau$  increase with increasing viscosity are well known phenomena,<sup>[15,35,36]</sup> we compared our results with solutions of **4** in mixtures of EtOH-PEG with increasing viscosity but only slightly changing polarity (Figure S11). Here, both values increase as well, 1.2% for  $\tau$  and 7.8% for  $\Phi_{fl}$  (Table S7). As the viscosity in the EtOH/PEG mixtures and the series of alcohols is increasing, we conclude that the drastic reduction of solvent polarity from ethanol to 1-decanol is the reason for the 47% change of  $\Phi_{fl}$ . This is in accordance with results published in 2014 by VanVeller *et al.*<sup>[3]</sup> and for other fluorophores with ICT character.<sup>[27]</sup>

Next, we measured the solid-state emission spectra (Figure 4 and Figure S14/S15) and  $\Phi_{fl}$ <sup>55</sup> (Table 1, last row). As the mechanochromic nature of BTDs was shown before, all samples were ground before the spectroscopic measurements.<sup>[37]</sup> The solid state fluorescence spectra of our BDT dyes (Figure 4 and Figure S14/S15) closely match with the respective fluorescence spectra in DCM. The  $\Phi_{fl}$ <sup>55</sup> are between 33% (**1**) and 72% (**3**) and are thus lower compared to the values determined in-

**Table 1.** Fluorescence quantum yields of compounds **1–4** in solvents of different polarity. The values for the normalized Dimroth-Reichardt Parameter  $E_T^N$  were taken from Ref. [38]. The values for the orientation polarization  $\Delta f$  were calculated as described in detail in the Supporting Information.

$E_T^N$	$\Delta f$	Solvent	<b>1</b> $\Phi$ [%]	<b>2</b> $\Phi$ [%]	<b>3</b> $\Phi$ [%]	<b>4</b> $\Phi$ [%]
0.006	0.00	n-hexane	77	55	78	79
0.309	0.22	DCM	88	94	98	98
0.444	0.30	DMSO	58	83	78	87
0.654	0.29	EtOH	15	16	58	64
		Solid state	33	41	72	58

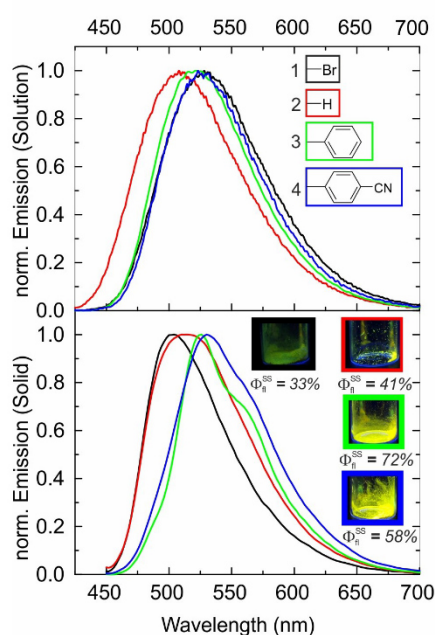


**Figure 4.** Normalized emission spectra of 1–4 in DCM (top,  $10^{-6}$ – $10^{-5}$  M) and in the solid-state (bottom). The insets show the molecular structure (top) with a color code used for the spectra and photographs of the crystal powders (bottom) under illumination with 366 nm light as well as the fluorescence quantum yields measured in the solid state ( $\Phi_f^{ss}$ ).

hexane, DCM or DMSO, but higher compared to EtOH (exception: 4 with 64% vs. 58%) in the solid state.

Overall, 1 is the least emissive compound and 3 and 4 are the more fluorescent ones of this series in solution, particularly in polar solvents, as well as in the solid-state. Moreover, the  $\Phi_f^{ss}$  values observed in this study for solid 1–4 (Table 1) considerably exceed the  $\Phi_f^{ss}$  values published for BTDs so far, that are below 25%, even though these values were measured in spin-coated thin films.<sup>[2]</sup>

To gain more insights into the redox behavior of our BTD dyes we performed cyclic voltammetry (CV) as well as spectroelectrochemical (UV/Vis/NIR) measurements for 1–4 in a 0.1 M  $\text{Bu}_4\text{NPF}_6$  solution of DCM (Figure 5 and S16–S18). The values of the electrochemical potentials are given relative to the ferrocene/ferrocenium couple ( $\text{Fc}/\text{Fc}^+$ ). All compounds show at least one reduction process, which is electrochemically reversible for 2–4 with potentials around  $-1.75$  V (Table S8).

The reduction of compound 1 is only partially reversible. Compounds 2 and 4 show another irreversible reductive process at  $-2.11$  V and  $-2.23$  V, respectively (Table S8). This is rather surprising, since BTDs are well known to expel the sulfur atom upon reduction.<sup>[14,39]</sup> However, the reduction of compound 1 most likely results in partial dehalogenation. All compounds show irreversible oxidation processes around

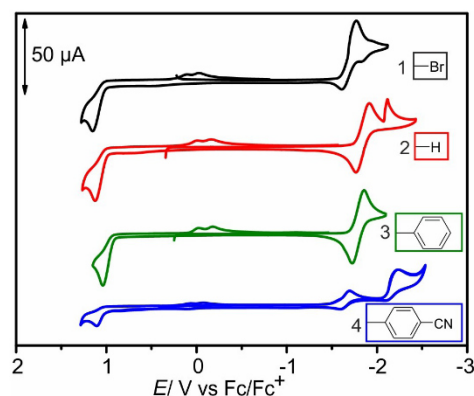


**Figure 5.** Cyclic voltammogram of 1–4 measured at 100 mV/s in 0.1 M  $\text{Bu}_4\text{NPF}_6$  solution of DCM.

$+1$  V, which most likely induce a chemical reaction involving the alkyne moiety. This chemical reaction might be a ring-closure with the nitrogen atoms, as this seems to be a common feature in electrochemical reactions of similar compounds.<sup>[40]</sup> The resulting species show re-reduction processes at around 0 V for 1–4. Scan direction-dependent measurements of 4 (starting with either oxidation or reduction first) indicate that these peaks are linked to the oxidation (Figure S18). The same observation holds true for 1–3, if an appropriate starting potential is chosen. For compound 4, the inset in Figure 6 confirms that the oxidation is crucial for the redox process at 0 V.

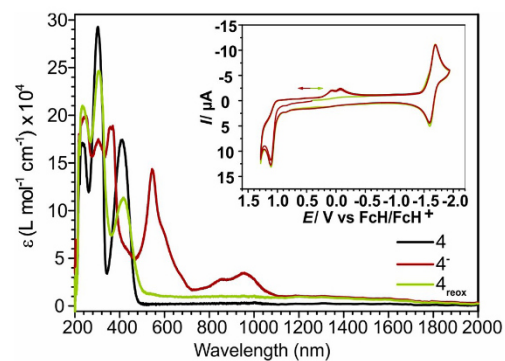


**Figure 6.** Absorption spectra of 4 (black), resulting species upon reduction (red) and after re-oxidation (green) of a  $10^{-6}$ – $10^{-5}$  M solution of DCM. The initial spectrum is not completely regained, indicating the irreversibility of the process. Inset: Cyclic voltammogram of 4 measured from 1.4 V to  $-2.0$  V in both directions, oxidative direction (red) and reductive direction first (green). The follow up process observed at 0 V is visible after running through the oxidation at 1.11 V indicating that the reacting species is generated on the oxidative side.



The double peak at around 0 V only appears after the first oxidation (Figure 6, inset, red line) and it does not appear starting from 0.3 V to the reductive side (Figure 6, inset, green line). The peaks also appear, if one cycles first through reduction and then oxidation, so these peaks are clearly caused by a product that forms after oxidation (Figure S18B and C).

In order to probe the chemical reversibility of the redox processes and the follow-up reactions, UV/Vis/NIR-spectroelectrochemistry was employed for **3** and **4** (Figure 7 and Figure S19–S20). This was done using optically transparent thin layer electrochemical cells (OTTLE) with defined starting concentrations of about  $1 \times 10^{-4}$  M of the respective compound.<sup>[41]</sup> The absorption bands of the radical anions  $3^-$  and  $4^-$  formed upon reduction of **3** and **4** cover the whole visible spectrum and extend to the NIR. The respective maxima are located at 503 nm and 544 nm for  $3^-$  and  $4^-$  and have molar extinction coefficients of 12,000 and 14,000  $M^{-1} cm^{-1}$ , respectively (Figure 7 and Table S9). Species  $3^-$  features two absorption bands at about 800 nm with a molar extinction coefficient of about 3,000  $M^{-1} cm^{-1}$  (Figure 7A).

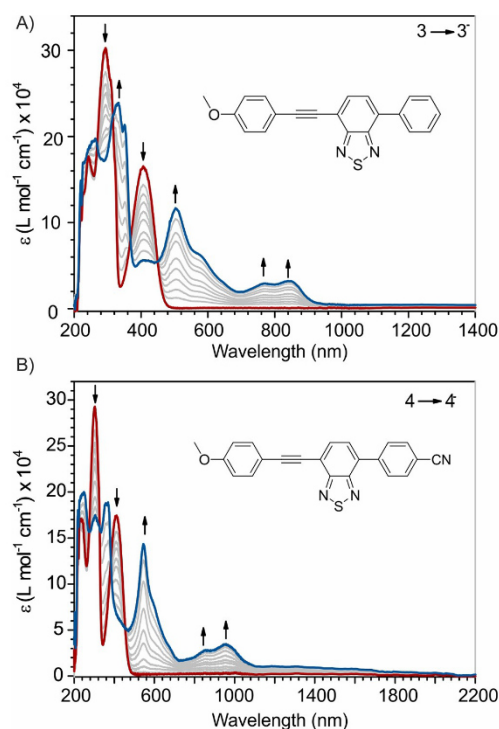


**Figure 7.** Absorption spectra of **3** (A) and **4** (B) before (red) and after first reduction (blue). Both show one pronounced maximum around 500 nm and a broad band absorption around 800–900 nm. The concentration was  $10^{-4}$  M in DCM.

These absorption maxima are red-shifted to around 900 nm for species  $4^-$  and have comparable molar extinction coefficients. The absorption spectra of the re-oxidized compounds reveal that the reduction process is not completely reversible (Figure 6 and Figure S19/S20), since the absorption spectra of the respective neutral species after reduction are reduced relative to the initial spectra by about 25% and 35% for **3** and **4**, respectively. For **4**, the absorption spectrum may provide a hint for a possible polymerization (Figure 6). The oxidation of **3** leads to a decreased and slightly shifted absorption in the UV region at 307 nm with a molar extinction coefficient of about 18,000  $M^{-1} cm^{-1}$ . Species  $3^+$  shows a broad absorption covering the complete Vis region extending up to 1,000 nm with molar extinction coefficients around 4,000  $M^{-1} cm^{-1}$  and a weak maximum at 566 nm. The irreversibility of this oxidation process is shown by the purple line and further proven by the absorption behavior after re-reduction highlighting a follow-up chemical reaction or decomposition of the compound (Figure S19). Since the oxidation processes of compounds **1–4** are very similar, only compound **3** was investigated exemplarily. As our spectroelectrochemical analysis of **3** and **4** showed irreversibility of the, seemingly reversible CV experiments, the characterization of **1** and **2** was omitted, owing to the higher reactivity already apparent in the cyclic voltammograms.

We presented a series of push-pull benzothiadiazole derivatives with photophysical properties governed by LE and ICT states that reveal fluorescence quantum yields ( $\Phi_f$ ) of up to 98% in aprotic organic solvents of medium polarity and up to 60% in the polar protic ethanol. We succeeded in separating the effect of microenvironment polarity and viscosity on the optical properties of these dyes, thereby demonstrating a polarity-induced reduction in  $\Phi_f$  and fluorescence lifetime. The fact that the viscosity barely affects  $\Phi_f$  and the fluorescence decay kinetics suggests that a molecular motion like a rotation in the excited state is not involved in radiation-less deactivation of the excited states of the BTD dyes. Fluorescence studies of BTD crystals revealed still relatively high  $\Phi_f$  of 30%–70%. Spectroelectrochemical investigations showed broad absorption bands in the Vis/NIR for the reduced species. As demonstrated by CV experiments the first reduction step is at least partly reversible, in contrast to the second reduction step and the oxidation process. Although highly fluorescent BTDs with reversible electrochemical behavior are an attractive class of molecules for use as electrochemical switches, further research and more complex architectures will be necessary to stabilize charged BTD species.

### Acknowledgements

We would like to acknowledge the assistance of the Core Facility BioSupraMol supported by the DFG.

### Conflict of Interest

The authors declare no conflict of interest.

**Keywords:** absorption switching · benzothiadiazoles · fluorescence · redox switches · spectroelectrochemistry

- [1] B. A. Da Silveira Neto, A. S. A. Lopes, G. Ebeling, R. S. Gonçalves, V. E. U. Costa, F. H. Quina, J. Dupont, *Tetrahedron* **2005**, *61*, 10975–10982.
- [2] Z. Wang, Z. Peng, K. Huang, P. Lu, Y. Wang, *J. Mater. Chem. C* **2019**, *7*, 6706–6713.
- [3] A. M. Thooft, K. Cassaidy, B. VanVeller, *J. Org. Chem.* **2017**, *82*, 8842–8847.
- [4] Z. Peng, Z. Wang, Z. Huang, S. Liu, P. Lu, Y. Wang, *J. Mater. Chem. C* **2018**, *6*, 7864–7873.
- [5] M. E. Mohanty, C. Madhu, V. L. Reddy, M. Paramasivam, P. R. Bangal, V. J. Rao, *Phys. Chem. Chem. Phys.* **2017**, *19*, 9118–9127.
- [6] M. D'Alessandro, A. Amadei, I. Daidone, R. Po', A. Alessi, M. Aschi, *J. Phys. Chem. C* **2013**, *117*, 13785–13797.
- [7] L. E. Polander, L. Pandey, S. Barlow, S. P. Tiwari, C. Risko, B. Kippelen, J.-L. Brédas, S. R. Marder, *J. Phys. Chem. C* **2011**, *115*, 23149–23163.
- [8] C.-Y. Mei, L. Liang, F.-G. Zhao, J.-T. Wang, L.-F. Yu, Y.-X. Li, W.-S. Li, *Macromolecules* **2013**, *46*, 7920–7931.
- [9] P. Ledwon, N. Thomson, E. Angioni, N. J. Findlay, P. J. Skabara, W. Domagala, *RSC Adv.* **2015**, *5*, 77303–77315.
- [10] M. J. McAllister, J.-L. Li, D. H. Adamson, H. C. Schniepp, A. A. Abdala, J. Liu, M. Herrera-Alonso, D. L. Milius, R. Car, R. K. Prud'homme, I. A. Aksay, *Chem. Mater.* **2007**, *19*, 4396–4404.
- [11] K. Shen, Z. Ju, L. Qin, T. Wang, H. Zheng, *Dyes Pigm.* **2017**, *136*, 515–521.
- [12] S. S. M. Fernandes, A. Pereira, D. Ivanou, A. Mendes, M. M. M. Raposo, *Dyes Pigm.* **2018**, *151*, 89–94.
- [13] M. Akhtaruzzaman, N. Kamata, J. Nishida, S. Ando, H. Tada, M. Tomura, Y. Yamashita, *Chem. Commun.* **2005**, 3183–3185.
- [14] F. S. Mancilha, B. A. DaSilveira Neto, A. S. Lopes, P. F. Moreira, F. H. Quina, R. S. Gonçalves, J. Dupont, *Eur. J. Org. Chem.* **2006**, 2006, 4924–4933.
- [15] P. Rietsch, F. Witte, S. Sobottka, G. Germer, A. Becker, A. Guttler, B. Sarkar, B. Paulus, U. Resch-Genger, S. Eigler, *Angew. Chem. Int. Ed.* **2019**, *58*, 8235–8239.
- [16] M. Shen, J. Rodriguez-Lopez, J. Huang, Q. Liu, X. H. Zhu, A. J. Bard, *J. Am. Chem. Soc.* **2010**, *132*, 13453–13461.
- [17] R. S. Sánchez, R. Gras-Charles, J. L. Bourdelande, G. Guirado, J. Hernando, *J. Phys. Chem. C* **2012**, *116*, 7164–7172.
- [18] H. V. Schroder, H. Hupatz, A. J. Achazi, S. Sobottka, B. Sarkar, B. Paulus, C. A. Schalley, *Chem. Eur. J.* **2017**, *23*, 2960–2967.
- [19] Q. Chen, J. Sun, P. Li, I. Hod, P. Z. Moghadam, Z. S. Kean, R. Q. Snurr, J. T. Hupp, O. K. Farha, J. F. Stoddart, *J. Am. Chem. Soc.* **2016**, *138*, 14242–14245.
- [20] C. M. Dickie, A. L. Laughlin, J. D. Wofford, N. S. Bhuvanesh, M. Nippe, *Chem. Sci.* **2017**, *8*, 8039–8049.
- [21] M. Waleśa-Chorab, M.-H. Tremblay, M. Ettaoussi, W. G. Skene, *Pure Appl. Chem.* **2015**, *87*, 649–661.
- [22] P. Ledwon, P. Zassowski, T. Jarosz, M. Lapkowski, P. Wagner, V. Cherpak, P. Stakhira, *J. Mater. Chem. C* **2016**, *4*, 2219–2227.
- [23] K.-W. Park, L. A. Serrano, S. Ahn, M. H. Baek, A. A. Wiles, G. Cooke, J. Hong, *Tetrahedron* **2017**, *73*, 1098–1104.
- [24] C. Reichardt, *Chem. Rev.* **1994**, *94*, 2319–2358.
- [25] D. Gudeika, A. Miasojedovas, O. Bezvikonnyi, D. Volyniuk, A. Gruodis, S. Jursenas, J. V. Grazulevicius, *Dyes Pigm.* **2019**, *166*, 217–225.
- [26] P. C. Rodrigues, L. S. Berlim, D. Azevedo, N. C. Saavedra, P. N. Prasad, W. H. Schreiner, T. D. Atvars, L. Akcelrud, *J. Phys. Chem. A* **2012**, *116*, 3681–3690.
- [27] J. R. Lakowicz, *Principles of Fluorescence Spectroscopy*, **2006**.
- [28] N. Mataga, Y. Kaiju, M. Koizumi, *Bull. Chem. Soc. Jpn.* **1955**, *28*, 690–691.
- [29] E. Lippert, *Z. Elektrochem.* **1957**, *61*, 962–975.
- [30] J. Pina, J. S. de Melo, D. Breusov, U. Scherf, *Phys. Chem. Chem. Phys.* **2013**, *15*, 15204–15213.
- [31] A. R. Harif-Mood, M. Abbasi, *J. Solution Chem.* **2018**, *47*, 1503–1513.
- [32] B. Y. Zaslavsky, L. M. Miheeva, E. A. Masimov, S. F. Djafarov, C. Reichardt, *J. Chem. Soc. Faraday Trans.* **1990**, *86*, 519–524.
- [33] C. Hadad, S. Achelle, J. C. Garcia-Martinez, J. Rodriguez-Lopez, *J. Org. Chem.* **2011**, *76*, 3837–3845.
- [34] M. N. Paddon-Row, A. M. Oliver, J. M. Warman, K. J. Smit, M. P. De Haas, H. Oevering, J. W. Verhoeven, *J. Phys. Chem.* **1988**, *92*, 6958–6962.
- [35] N. Scholz, A. Jadhav, M. Shreykar, T. Behnke, N. Nirmalanathan, U. Resch-Genger, N. Sekar, *J. Fluoresc.* **2017**, *27*, 1949–1956.
- [36] R. M. Yusop, A. Unciti-Broceta, M. Bradley, *Bioorg. Med. Chem. Lett.* **2012**, *22*, 5780–5783.
- [37] C.-Y. Yu, C.-C. Hsu, H.-C. Weng, *RSC Adv.* **2018**, *8*, 12619–12627.
- [38] C. Reichardt, *Chem. Rev.* **1994**, *94*, 2319–2358.
- [39] M. Prasad, Y. Liu, O. Repič, *Tetrahedron Lett.* **2001**, *42*, 2277–2279.
- [40] G. M. Martins, B. Shirinfar, T. Hardwick, A. Murtaza, N. Ahmed, *Catal. Sci. Technol.* **2019**, *9*, 5868–5881.
- [41] S. R. Domingos, H. Luyten, F. van Anrooij, H. J. Sanders, B. H. Bakker, W. J. Buma, F. Hartl, S. Woutersen, *Rev. Sci. Instrum.* **2013**, *84*, 033103.

Manuscript received: June 4, 2020  
Revised manuscript received: April 27, 2020  
Accepted manuscript online: April 29, 2020  
Version of record online: ■■■■■

# ChemPhotoChem

Supporting Information

## Identification of the Irreversible Redox Behavior of Highly Fluorescent Benzothiadiazoles

Philipp Rietsch<sup>†</sup>, Sebastian Sobottka<sup>†</sup>, Katrin Hoffmann, Pascal Hildebrandt, Biprajit Sarkar, Ute Resch-Genger,<sup>\*</sup> and Siegfried Eigler<sup>\*</sup>

## Table of contents

1. General Information .....	3
2. Synthetic procedure .....	4
4-(7-(4-methoxyphenyl)ethynyl)benzo[c][1,2,5]thiadiazol-4-yl)benzonitrile (1) .....	4
4-((4-methoxyphenyl)ethynyl)benzo[c][1,2,5]thiadiazole (2) .....	5
4-((4-methoxyphenyl)ethynyl)-7-phenylbenzo[c][1,2,5]thiadiazole (3).....	5
4-(7-(4-methoxyphenyl)ethynyl)benzo[c][1,2,5]thiadiazol-4-yl)benzonitrile (4).....	6
3. Excitation Emission matrix (EEM) of Compound 3 .....	7
4. UV/Vis and fluorescence measurements in solvents of different polarity – Lippert-Mataga Plot .....	8
5. Calculation of Dipole Moments .....	13
6. UV/Vis and Fluorescence measurements in primary alcohols of different chain length.....	14
7. Measurements in mixtures of ethanol and polyethyleneglycol (PEG).....	16
8. Fluorescence Lifetimes measurements .....	16
9. Solid-state Fluorescence Measurements .....	19
10. Cyclic voltammetry measurements.....	21
11. UV/Vis/NIR-spectroelectrochemistry .....	24
12. NMR spectra of 1-4.....	26

## 1. General Information

All reagents were purchased from commercial sources and used without further purification. Dry solvents were purchased from Acros Organics. ALUGRAM Xtra SIL G/UV<sub>254</sub> plates by Macherey-Nagel were used for thin-layer chromatography. Isolation of products by chromatography was performed with silica from Macherey-Nagel Silica 60 M (0.04-0.063 mm). NMR spectra were recorded on a JOEL ECX 400 (<sup>1</sup>H 400 MHz, <sup>13</sup>C 101 MHz), JEOL Eclipse+ 500 (<sup>1</sup>H 500 MHz, <sup>13</sup>C 126 MHz) and BRUKER AVANCE 700 (<sup>1</sup>H 700 MHz, <sup>13</sup>C 176 MHz) spectrometer at 25 °C. The chemical shifts  $\delta$  are calibrated on the respective solvent peak as internal standard. All shifts are reported in ppm and NMR multiplicities are abbreviated as s (singlet), d (duplet), t (triplet), m (multiplet). Coupling constants J are reported in Hz. UV/Vis spectra were recorded on a Cary 50 Bio photospectrometer (Varian). Fluorescence spectra were recorded on a LS 50 B luminescence spectrometer from PerkinElmer. UV/Vis and Fluorescence spectra were measured in quartz glass cuvettes with 1 cm path length. IR Spectra were recorded on a FT/IR 4100 spectrometer from JASCO. Elemental analysis was performed on an VARIO EL from Elementar.

Photoluminescence quantum yields ( $\Phi_{\text{PL}}$ ) were determined absolutely with an integrating sphere setup from Hamamatsu (Quantaurus-QY C11347-11). All  $\Phi_{\text{PL}}$  measurements were performed at 25°C using special 10 mm x 10 mm long neck quartz cuvettes from Hamamatsu. Values below 1% quantum yield are not reliable in the measurement setup and are therefore given as < 1%.

The fluorescence lifetime ( $\tau$ ), the average time in which the fluorophore is in an excited state before it relaxes to the ground state, was recorded on a fluorometer FLS 920 (Edinburgh Instruments) equipped with a Hamamatsu R3809U-50 (range 200–850 nm, response width <25 ps), Multi-Channel Plate (MCP) detector, Czerny-Turner double monochromators and either a supercontinuum laser (Fianium SC400-2-PP) or a Edinburgh Instrument EPLED-330 (picosecond pulsed light emitting diode) for excitation at 375 nm, or a Edinburgh Instrument EPL-375 (picosecond pulsed diode laser) for excitation at 330 nm. All the measurements were performed at T = 298 K using 10 mm x 10 mm quartz cuvettes from Hellma GmbH always filled with 2 mL of solvent or dye solution. Before each measurement, the instrument response function (IRF) was measured. The lifetime measurements were analysed with Edinburgh Instruments FAST Software and fitted with a reconvolution fit. All the lifetimes could be evaluated mono, bi- or tri-exponentially with a reduced  $\chi^2$  between 0.8 and 3.0.

The fluorescence spectra of the crystals in the solid-state and microscopic images were recorded with an Olympus FluoView FV1000 (Olympus GmbH, Hamburg, Germany). For UV excitation, a DPSS Cobolt Zouk® (355 nm; 10 mW), and for transmission imaging an additional multiline argon ion laser (30 mW, 488 nm) were used as excitation sources, which were reflected by a beamsplitter (BS 20/80) and focused onto the sample through an Olympus objective UPLSAPO 10X (numerical aperture N.A. 0.40). The emitted photons were recollecting with the same objective and focused onto a PMT. Emission signals were detected in a wavelength range between 460 nm and 700 nm with spectral resolution of 5 nm and a step width of 2 nm. The spatial resolved fluorescence spectra are raw spectra, not specifically corrected for the wavelength-dependent spectral responsivity of the detection system of the microscope.

### Electrochemistry

Cyclic voltammograms were recorded with a PAR VersaStat 4 potentiostat (Ametek) or a VersaStat 4 by working in anhydrous and degassed dichloromethane (99.8 % extra dry) distilled from CaH<sub>2</sub> with 0.1 M NBu<sub>4</sub>PF<sub>6</sub> (dried, > 99.0 %, electrochemical grade) as electrolyte. A three-electrode setup was used with a glassy carbon, gold or platinum working electrode, a coiled platinum wire as counter electrode, and a coiled silver wire as a pseudoreference electrode. The ferrocene/ferrocenium couple was used as internal reference.

### UV/Vis/NIR spectroscopy and spectroelectrochemistry

UV/Vis/NIR spectra were recorded with an Avantes spectrometer consisting of a light source (AvaLight-DH-S-Bal), a UV/Vis detector (AvaSpec-ULS2048), and an NIR detector (AvaSpec-NIR256-TEC). Spectroelectrochemical measurements were carried out in an optically transparent thin-layer electrochemical (OTTLE) cell (CaF<sub>2</sub> windows) with a platinum-mesh or a gold-mesh working electrode, a platinum-mesh counter electrode, and a silver-foil pseudoreference electrode. The OTTLE cell with the gold working electrode was build analogous to the one with the platinum working electrode (100 mesh woven from 0.064 mm diameter wire; 99.99% (metals basis)). The molar extinction coefficients of the electrochemically produced oxidized (radical cations) and reduced (radical anions) intermediates were derived for samples containing a known concentration of the BDTs 1-4 which was about 1x10<sup>-4</sup> M.

## 2. Synthetic procedure

The synthesis of **1-4** was done as depicted in Figure S 1. The synthesis of compounds **6** and **7** was done according to literature and the spectroscopic results were in accordance with literature.<sup>[1]</sup> Taking compound **7** the reaction conditions of Park *et al.* were used to synthesize compounds **1-4**.<sup>[2]</sup> Compound **2** and **4** were isolated from the same reaction. The numbers of the compounds were chosen for an easier understanding in the paper. The NMR spectra of **1-4** are given at the end of this document.

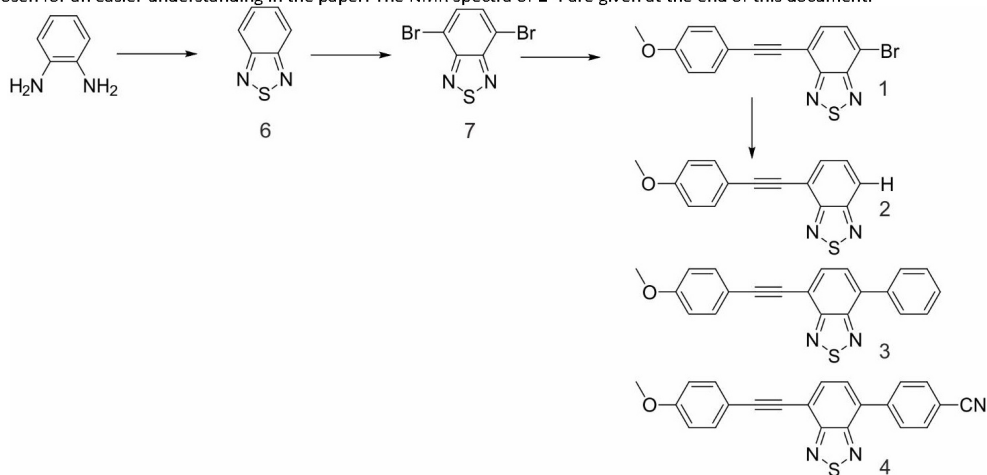
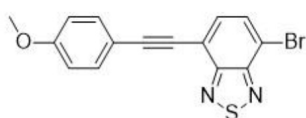


Figure S 1: Synthetic route towards benzothiadiazole derivatives **1-4**.

### 4-(7-(4-methoxyphenyl)ethynyl)benzo[c][1,2,5]thiadiazol-4-yl)benzonitrile (**1**)



Under argon atmosphere, 4,7-Dibromobenzo[c][1,2,5]thiadiazole (1.92 g, 6.52 mmol, 1.5 eq.), 1-Ethynyl-4-methoxybenzene (574.40 mg, 4.35 mmol, 1.0 eq.), Pd(PPh<sub>3</sub>)<sub>4</sub> (93.70 mg, 0.08 mmol, 0.1 eq.) and CuI (22.00 mg, 0.12 mmol, 0.15 eq.) were stirred at 70°C in a degassed

mixture of tetrahydrofuran (17.5 mL) and triethylamine (17.5 mL) for 24 hours. The mixture was cooled to room temperature, diluted with water (30 mL). The suspension was extracted with dichloromethane (3x 30 mL). The united organic phases were dried over MgSO<sub>4</sub>, filtered and the solvent was removed under reduced pressure. The crude product was purified by column chromatography with dichloromethane/hexane (1/1) to afford 4-bromo-7-((4-methoxyphenyl)ethynyl)benzo[c][1,2,5]thiadiazole (768.90 mg, 2.23 mmol, 51%) as an orange-yellow solid.

<sup>1</sup>H NMR (500 MHz, CDCl<sub>3</sub>, RT): δ (ppm) = 7.85 – 7.80 (m, 1H), 7.66 – 7.57 (m, 3H), 6.94 – 6.88 (m, 2H), 3.85 (s, 3H).

<sup>13</sup>C NMR (126 MHz, CDCl<sub>3</sub>, RT): δ (ppm) = 160.41, 154.29, 153.20, 133.62, 132.46, 132.10, 117.20, 114.52, 114.21, 114.16, 97.31, 83.61, 55.43.

**FT-IR** (ATR)  $\tilde{\nu}$  (cm<sup>-1</sup>): 3076 (w), 3048 (w), 3002 (w), 2957 (w), 2930 (w), 2830 (w), 2204 (m), 1601 (m), 1574 (m), 1525 (m), 1507 (s), 1480 (m), 1435 (m), 1297 (m), 1248 (s), 1167 (s), 1024 (s), 886 (s), 845 (s), 828 (vs)

**UV/Vis** (DCM)  $\lambda_{\text{max}}$  nm ( $\epsilon$  [Lmol<sup>-1</sup> cm<sup>-1</sup>]): 284 (30000), 402 (15000)

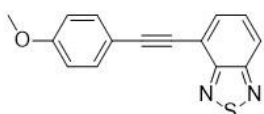
**Fluorescence** (DCM)  $\lambda_{\text{max}}$  nm ( $\Phi_{\text{Fl}}$ ): 529 (93)

**MS** (EI):  $m/z$  = 343.969 [M]<sup>+</sup> (100), 344.972 (16), 345.960 (100), 346.967 (16)

**EA**<sup>\*</sup>: C<sub>15</sub>H<sub>9</sub>BrN<sub>2</sub>OS, calc.: C, 52.19; N, 8.11; H, 2.63; S, 9.29 meas.: C, 50.90; N, 7.98; H, 2.75; S, 10.09

\*small amounts of dichloromethane and water may be responsible for the deviations of calculated and measured values

#### 4-((4-methoxyphenyl)ethynyl)benzo[c][1,2,5]thiadiazole (**2**)



Under argon atmosphere, 4-bromo-7-((4-methoxyphenyl)ethynyl)benzo[c][1,2,5]thiadiazole (350.00 mg, 1.01 mmol, 1 eq.), (4-cyanophenyl)boronic acid (178.80 mg, 1.22 mmol, 1.2 eq.), K<sub>2</sub>CO<sub>3</sub> (1.40 g, 10.14 mmol, 10 eq.) and Pd(PPh<sub>3</sub>)<sub>4</sub> (93.70 mg, 0.08 mmol, 0.1 eq.) were stirred at 70°C in a degassed mixture of tetrahydrofuran (15 mL) and water (5 mL) for 24 hours. The mixture was cooled to room temperature, diluted with water (10 mL). The suspension was extracted with dichloromethane (3x 15 mL). The united organic phases were dried over MgSO<sub>4</sub>, filtered and the solvent was removed under reduced pressure. The crude product was purified by column chromatography with dichloromethane/hexane (1/1) to afford 4-((4-methoxyphenyl)ethynyl)benzo[c][1,2,5]thiadiazole (33.10 mg, 0.012 mmol, 12%) as a bright yellow solid.

**<sup>1</sup>H NMR** (500 MHz, CDCl<sub>3</sub>, RT):  $\delta$  (ppm) = 7.97 (dd,  $J$  = 8.9, 1.0 Hz, 1H), 7.77 (dd,  $J$  = 7.0, 1.0 Hz, 1H), 7.62 – 7.55 (m, 3H), 6.93 – 6.89 (m, 2H), 3.84 (s, 3H).

**<sup>13</sup>C NMR** (126 MHz, CDCl<sub>3</sub>, RT):  $\delta$  (ppm) = 160.24, 154.74, 133.60, 132.33, 129.36, 121.44, 117.65, 114.79, 114.15, 96.13, 84.03, 55.41.

**FT-IR** (ATR)  $\tilde{\nu}$  (cm<sup>-1</sup>): 3058 (vw), 3036 (vw), 2953 (m), 2922 (m), 2837 (m), 2212 (s), 1605 (m), 1582 (w), 1538 (m), 1502 (s), 1439 (w), 1303 (m), 1288 (m), 1244 (s), 1169 (s), 1105 (w), 1025 (s), 910 (m), 843 (s), 811 (s), 755 (s)

**UV/Vis** (DCM)  $\lambda_{\text{max}}$  nm ( $\epsilon$  [Lmol<sup>-1</sup> cm<sup>-1</sup>]): 280 (25000), 382 (12000)

**Fluorescence** (DCM)  $\lambda_{\text{max}}$  nm ( $\Phi_{\text{Fl}}$ ): 500 (94)

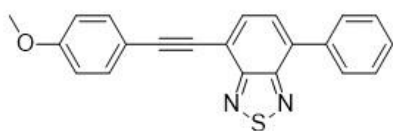
**MS** (EI):  $m/z$  = 267.052 (22), 266.052 [M]<sup>+</sup> (100), 251.052 (50), 223.030 (18)

**EA**<sup>\*</sup>: C<sub>22</sub>H<sub>13</sub>N<sub>3</sub>OS, calc.: C, 67.65; N, 10.52; H, 3.78; S, 12.05 meas.: C, 64.00; N, 9.86; H, 3.97; S, 10.85

\*small amounts of dichloromethane and water may be responsible for the deviations of calculated and measured values

#### 4-((4-

#### methoxyphenyl)ethynyl)-7-phenylbenzo[c][1,2,5]thiadiazole (3)



Under argon atmosphere, 4-bromo-7-((4-methoxyphenyl)ethynyl)benzo[c][1,2,5]thiadiazole (100.00 mg, 0.29 mmol, 1 eq.), Phenylboronic acid (42.38 mg, 0.35 mmol, 1.2 eq.),  $K_2CO_3$  (400.34 mg, 2.90 mmol, 10 eq.) and  $Pd(PPh_3)_4$

(33.47 mg, 0.029 mmol, 0.1 eq.) were refluxed in a degassed mixture of tetrahydrofuran (5 mL) and water (3 mL) for 24 hours. The mixture was cooled to room temperature, diluted with water (10 mL). The suspension was extracted with dichloromethane (3x 15 mL). The united organic phases were dried over  $MgSO_4$ , filtered and the solvent was removed under reduced pressure. The crude product was purified by column chromatography with dichloromethane/hexane (1/1.5) to afford 4-((4-methoxyphenyl)ethynyl)-7-phenylbenzo[c][1,2,5]thiadiazole (95.00 mg, 0.28 mmol, 96%) as a bright yellow solid.

**$^1H$  NMR** (500 MHz,  $CDCl_3$ , RT):  $\delta$  (ppm) = 7.99 – 7.93 (m, 2H), 7.86 (d,  $^3J = 7.3$  Hz, 1H), 7.70 (d,  $^3J = 7.3$  Hz, 1H), 7.65 – 7.61 (m, 2H), 7.57 – 7.52 (m, 2H), 7.49 – 7.44 (m, 1H), 6.95 – 6.90 (m, 2H), 3.86 (s, 3H).

**$^{13}C$  NMR** (125 MHz,  $CDCl_3$ , RT):  $\delta$  (ppm) = 160.23, 155.39, 137.13, 134.33, 133.61, 132.63, 129.31, 128.73, 127.79, 114.92, 114.16, 96.34, 84.38, 55.42.

**FT-IR** (ATR)  $\tilde{\nu}$  ( $cm^{-1}$ ): 3059 (w), 3028 (w), 3013 (w), 2960 (w), 2923 (m), 2853 (w), 2205 (w), 1606 (m), 1564 (w), 1546 (w), 1511 (m), 1447 (w), 1290 (m), 1250 (s), 1177 (m), 1157 (m), 1104 (m), 1033 (m), 1019 (s), 884 (m), 833 (s), 761 (s), 695 (s)

**UV/Vis** (DCM)  $\lambda_{max}$  nm ( $\epsilon$  [ $Lmol^{-1} cm^{-1}$ ]): 293 (32000), 406 (16000)

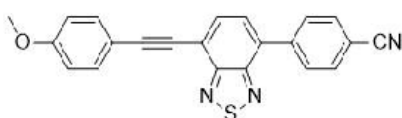
**Fluorescence** (DCM)  $\lambda_{max}$  nm ( $\Phi_f$ ): 520 (98)

**MS** (EI):  $m/z$  = 343.084 (40), 342.081 [ $M$ ] $^+$  (100), 327.053 (35)

**EA\***:  $C_{21}H_{14}N_2OS$ , calc.: C, 73.66; N, 8.18; H, 4.12; S, 9.36 meas.: C, 71.96; N, 7.50; H, 3.92; S, 8.38

\*small amounts of dichloromethane and water may be responsible for the deviations of calculated and measured values

#### 4-(7-(4-methoxyphenyl)ethynyl)benzo[c][1,2,5]thiadiazol-4-yl)benzonitrile (4)



Under argon atmosphere, 4-bromo-7-((4-methoxyphenyl)ethynyl)benzo[c][1,2,5]thiadiazole (350.00 mg, 1.01 mmol, 1 eq.), (4-cyanophenyl)boronic acid (178.80 mg, 1.22 mmol, 1.2 eq.),  $K_2CO_3$  (1.40 g, 10.14 mmol, 10 eq.) and

$Pd(PPh_3)_4$  (93.70 mg, 0.08 mmol, 0.1 eq.) were stirred at 70°C in a degassed mixture of tetrahydrofuran (15 mL) and water (5 mL) for 24 hours. The mixture was cooled to room temperature, diluted with water (10 mL). The suspension was extracted with dichloromethane (3x 15 mL). The united organic phases were dried over  $MgSO_4$ , filtered and the solvent was removed under reduced pressure. The crude product was purified by column chromatography with dichloromethane/hexane (1/1) to afford 4-(7-(4-



methoxyphenyl)ethynyl)benzo[*c*][1,2,5]thiadiazol-4-yl)benzonitrile (201.20 mg, 0.55 mmol, 54%) as a bright yellow solid.

**<sup>1</sup>H NMR** (500 MHz, CDCl<sub>3</sub>, RT): δ (ppm) = 8.12 – 8.09 (m, 2H), 7.87 (d, <sup>3</sup>J = 7.4 Hz, 1H), 7.84 – 7.81 (m, 2H), 7.74 (d, <sup>3</sup>J = 7.4 Hz, 1H), 7.65 – 7.60 (m, 2H), 6.96 – 6.91 (m, 2H), 3.86 (s, 3H).

**<sup>13</sup>C NMR** (126 MHz, CDCl<sub>3</sub>, RT): δ (ppm) = 160.44, 141.45, 133.70, 132.46, 132.24, 131.81, 129.87, 128.51, 120.66, 114.23, 112.12, 84.18, 55.44.

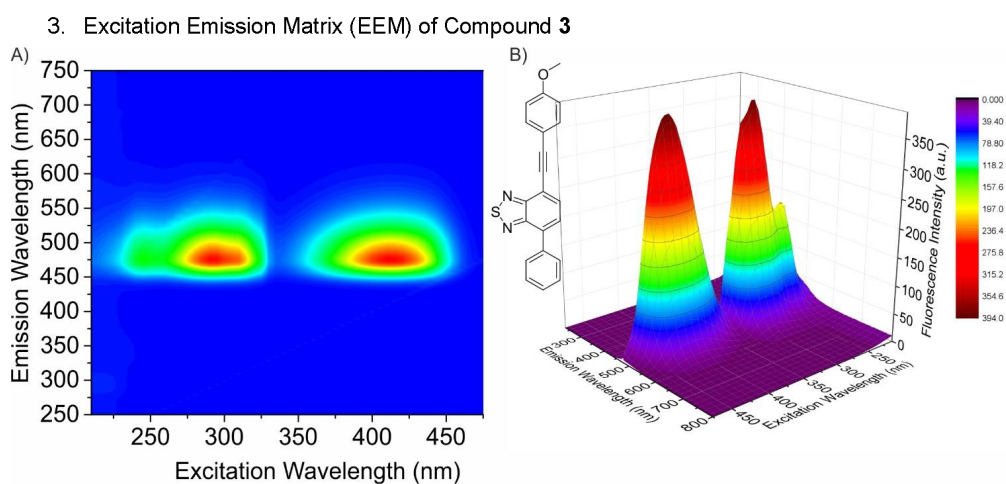
**FT-IR** (ATR)  $\tilde{\nu}$  (cm<sup>-1</sup>): 3091 (w), 3052 (w), 2965 (m), 2939 (w), 2844 (m), 2364 (w), 2226 (m), 2200 (m), 1607 (s), 1547 (s), 1506 (s), 1446 (m), 1408 (m), 1295 (m), 1250 (s), 1159 (m), 1106 (w), 1026 (m), 888 (m); 835 (s), 821 (s)

**UV/Vis** (DCM)  $\lambda_{\text{max}}$  nm ( $\epsilon$  [Lmol<sup>-1</sup> cm<sup>-1</sup>]): 301 (28000), 409 (17000)

**Fluorescence** (DCM)  $\lambda_{\text{max}}$  nm ( $\Phi_{\text{F}}$ ): 524 (98)

**MS** (EI): *m/z* = 368.076 (24), 367.075 [M]<sup>+</sup> (100), 352.051 (20)

**EA**: C<sub>22</sub>H<sub>13</sub>N<sub>3</sub>OS, calc.: C, 71.92; N, 11.44; H, 3.57; S, 8.73 meas.: C, 71.99; N, 11.50; H, 3.60; S, 8.75



#### 4. UV/Vis and fluorescence measurements in solvents of different polarity – Lippert-Mataga Plot

$$\Delta\tilde{\nu}_{AE} = \frac{2}{hc} \times \left( \frac{\epsilon_r - 1}{2\epsilon_r + 1} - \frac{n^2 - 1}{2n^2 + 1} \right) \times \frac{(\mu_E - \mu_G)^2}{\alpha^3} + constant$$

Equation S 1: Lippert-Mataga Equation, details and the meaning of each variable are described below.

As the energy difference between ground (G) and excited state (E) is directly linked to the interplay of the fluorophore with the solvent, it can be correlated with the refractive index and the polarity of the solvent. Shown above is the Lippert-Mataga equation which describes the solvent-dependent spectral shift of absorption and emission.<sup>[3-5]</sup> The shift between the absorption and the emission maxima  $\Delta\tilde{\nu}_A - \Delta\tilde{\nu}_E$  is directly linked to the change of dipole moment ( $\mu_E - \mu_G$ ).  $\alpha$  is the cavity of the fluorophore (most of the times the Onsager Radius is used),  $h$  is Planck's constant,  $c$  is the speed of light,  $\epsilon_r$  is the dielectric constant of the solvent and  $n$  is the refractive index of the solvent. As the assumption of spherical molecules is a harsh simplification of the model, we assumed Onsager Radii of our molecule between 5-7 Å, which are in line with values taken in other publications and our DFT calculations.<sup>[6]</sup>

$$\Delta f = \frac{\epsilon_r - 1}{2\epsilon_r + 1} - \frac{n^2 - 1}{2n^2 + 1}$$

Equation S 2: Formula used to calculate the orientation polarization (polarizability) of the solvent  $\Delta f$  from the dielectric constant  $\epsilon_r$  and the refractive index  $n$ .<sup>[8]</sup>

Orientation polarization  $\Delta f$  derived from the dielectric constant  $\epsilon_r$  and the refractive index  $n$ . "The first term accounts for the spectral shift due to both the reorientation of the solvent dipoles and to redistribution of the electrons in the solvent molecules. The second term only accounts for the redistribution of the electrons."<sup>[3]</sup>

Table S 1: Values of the dielectric constant  $\epsilon_r$ , the refractive index  $n$  and the resulting orientation polarizability taken from reference<sup>[8]</sup>.

	$\epsilon_r$	$n$	$\Delta f$
Hexane	1.874	1.372	-0.001111783
DCM	8.93	1.42	0.218511422
DMSO	46.68	1.36	0.303306702
EtOH	24.3	1.35	0.292685944

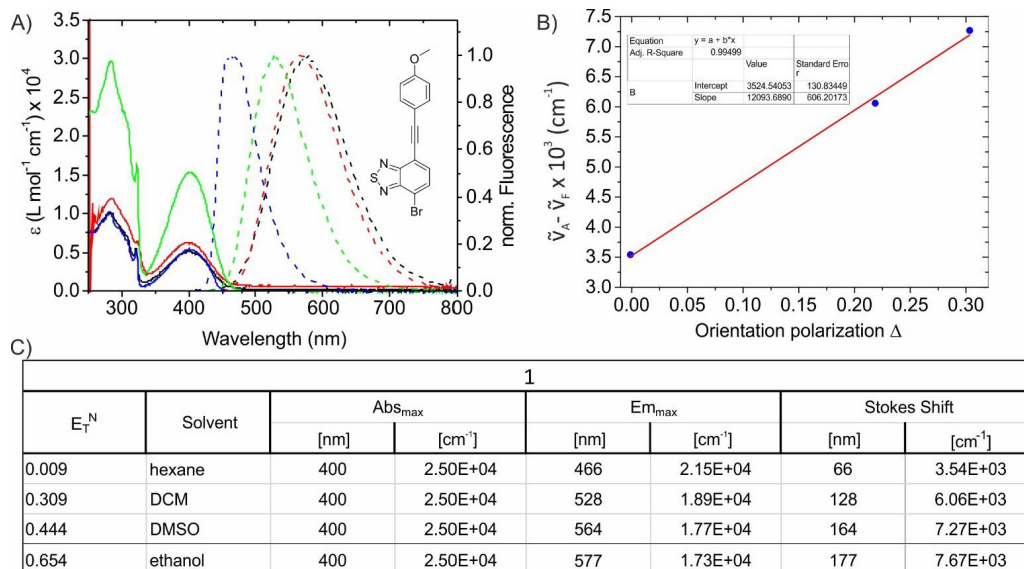


Figure S 3: A) Absorption spectra (solid) and normalized fluorescence spectra (dashed) of **1** in solvents of different polarity. Hexane = blue, DCM = green, DMSO = red, EtOH = black with the molecular structure in the inset. B) Lippert-Mataga plot of **1** with the solvent ethanol left out due to its proticity. The fit data is given in the inset table. C) Absorption maxima, fluorescence maxima and Stokes shift in wavelength and energy units for all four solvents ordered according to the normalized Dimroth-Reichardt Parameter E<sub>T</sub><sup>N</sup> taken from Ref.<sup>[7]</sup>

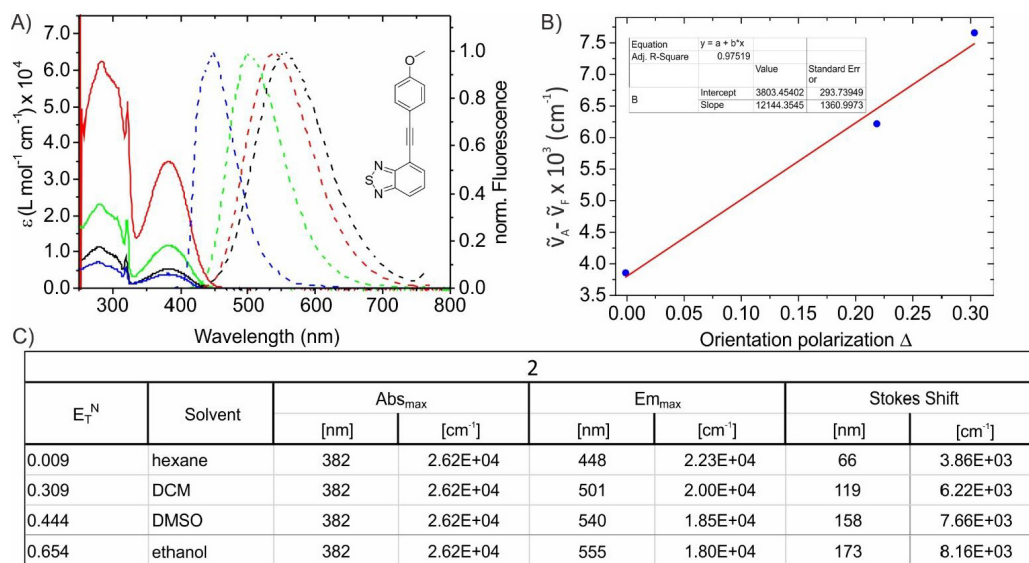


Figure S 4: A) Absorption spectra (solid) and normalized fluorescence spectra (dashed) of **2** in solvents of different polarity. Hexane = blue, DCM = green, DMSO = red, EtOH = black with the molecular structure in the inset. B) Lippert-Mataga plot of **2** with the solvent ethanol left out due to its proticity. The fit data is given in the inset table. C) Absorption maxima, fluorescence maxima and Stokes shift in wavelength and energy units for all four solvents ordered according to the normalized Dimroth-Reichardt Parameter  $E_T^N$  taken from Ref.<sup>[7]</sup>

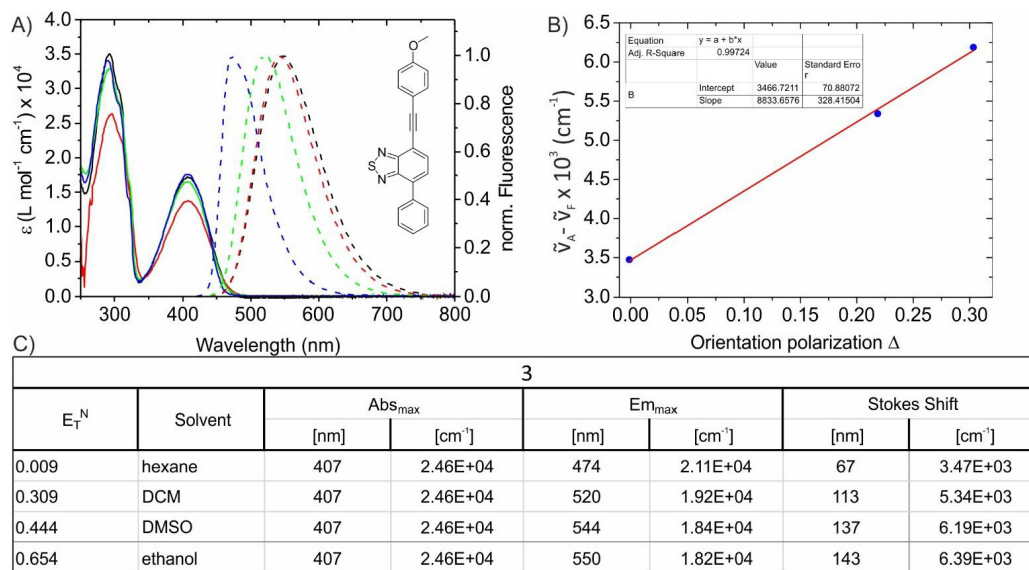


Figure S 5: A) Absorption spectra (solid) and normalized fluorescence spectra (dashed) of **3** in solvents of different polarity. Hexane = blue, DCM = green, DMSO = red, EtOH = black with the molecular structure in the inset. B) Lippert-Mataga plot of **3** with the solvent ethanol left out due to its proticity. The fit data is given in the inset table. C) Absorption maxima, fluorescence maxima and Stokes shift in wavelength and energy units for all four solvents ordered according to the normalized Dimroth-Reichardt Parameter  $E_T^N$  taken from Ref.<sup>[7]</sup>

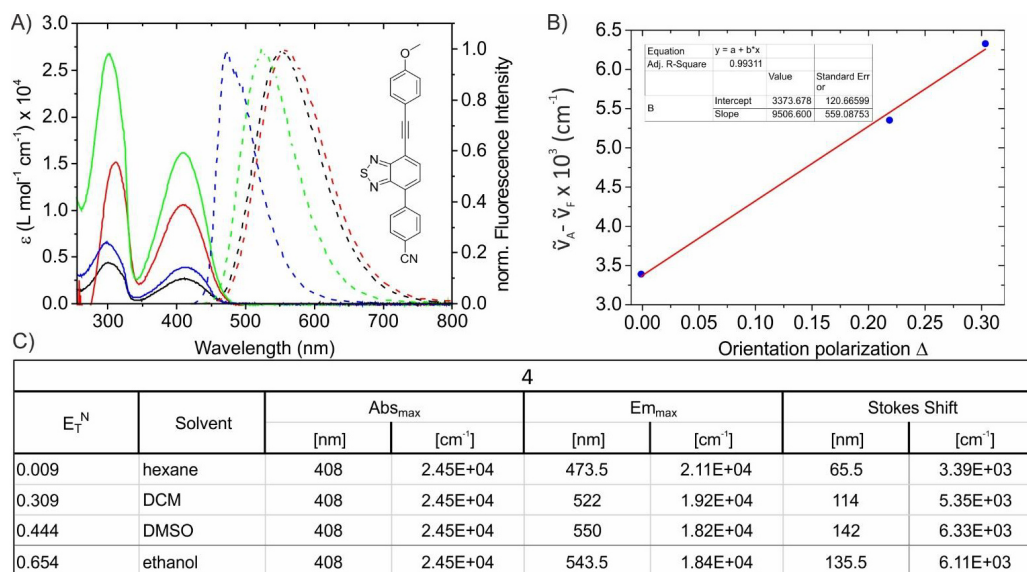


Figure S 6: A) Absorption spectra (solid) and normalized fluorescence spectra (dashed) of **4** in solvents of different polarity. Hexane = blue, DCM = green, DMSO = red, EtOH = black with the molecular structure in the inset. B) Lippert-Mataga plot of **4** with the solvent ethanol left out due to its proticity. The fit data is given in the inset table. C) Absorption maxima, fluorescence maxima and Stokes shift in wavelength and energy units for all four solvents ordered according to the normalized Dimroth-Reichardt Parameter  $E_T^N$  taken from Ref.<sup>[7]</sup>

Table S 2: Full width at half maximum (FWHM) in nanometers (nm) and energy scale (cm<sup>-1</sup>) and area of the gaussian fits of the fluorescence spectra of **4** in solvents of different polarity. The FWHM increases with increasing polarity of the solvent.

	FWHM [nm]	FWHM [cm <sup>-1</sup> ]	Area [a.u.]
Hexane	66.40	150609.21	68.49
DCM	88.14	113457.15	92.12
DMSO	99.07	100941.79	102.19
EtOH	103.64	96484.12	106.47

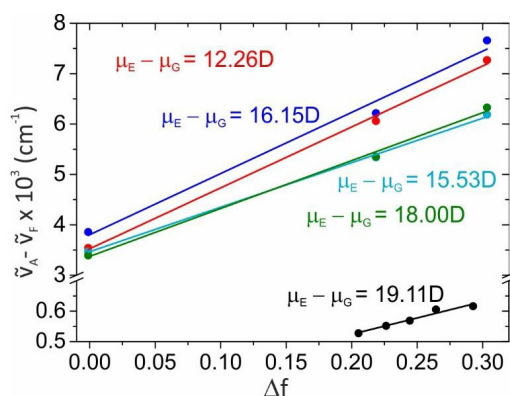


Figure S 7: Lippert-Mataga plot with linear fit of **1-4** with data points hexane ( $\Delta f = 0.00$ ), DCM ( $\Delta f = 0.22$ ) and DMSO ( $\Delta f = 0.30$ ). We omitted the solvent ethanol in the plots of **1-4** in the different organic solvents due to its proticity. In black, the plot for **4** in primary alcohols is shown. **1** = red, **2** = blue, **3** = petrole, **4** = olive and **4** in different primary alcohols = black. The  $\Delta f$  values of the alcohols are in between 0.21 (1-dec.) to 0.29 (EtOH). The fit data (slopes, intercepts) are summarized in **Table S3** and are in line (slope values around 10000) with so far published investigations of BTDs.<sup>[6]</sup> We calculated the ground state dipole moments by DFT-B3LYP; 6-311++G(d,p) and calculated the excited state dipole moment with the values of the change of dipole moment (insets) derived from the Lippert-Mataga Equation.<sup>[9, 10]</sup>

Table S 3: Values of the plots built on the Lippert-Mataga equation for **1-4** and for **4** in primary alcohols of different chain length. The ground-state dipole moments (GS-DM) of **1-4** in Debye were calculated at DFT-B3LYP; 6-311++G(d,p) level of theory. The difference of dipole moment ( $\Delta D$ ) upon excitation was calculated from the Lippert-Mataga equation as described above. The excited state dipole moments (ES DM) are sum of the calculated GS DM and  $\Delta D$ . All dipole moments are given in Debye.

Compound	Slope from fit	Intercept from fit	Onsager Rad. [Ang]	$\Delta D$ [Debye]	GS DM [Debye]	ES DM [Debye]
1	12093.689	3524.541	5	12.26	3.95	16.21
2	12144.355	3803.454	6	16.15	2.32	18.47
3	8833.658	3466.72	6.5	15.53	1.76	17.29
4	9506.6	3373.678	7	18.00	8.1	26.10
4 <sub>prim.Alcohols</sub>	10711	3098.82	7	19.11	8.1	27.21

## 5. Calculation of Dipole Moments

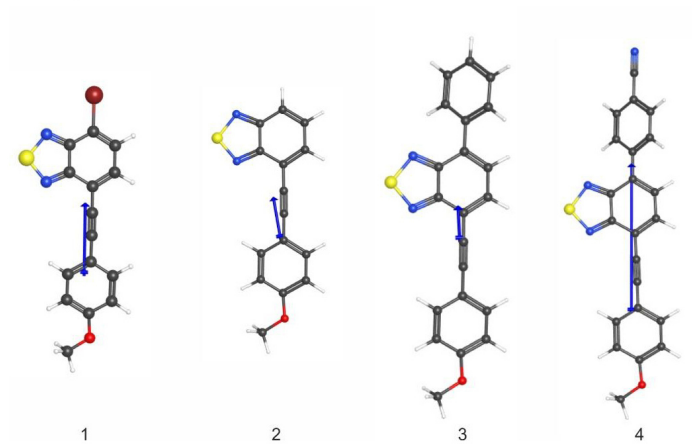


Figure S 8: Depiction of the DFT calculated structure of **1-4** from left to right. The blue arrows indicate the relative height and the direction of the dipole moment given in Table S2. Level of theory: DFT-B3LYP; 6-311++G(d,p)<sup>[9, 10]</sup>

## 6. UVVis and Fluorescence Measurements in Primary Alcohols of different Chain Length

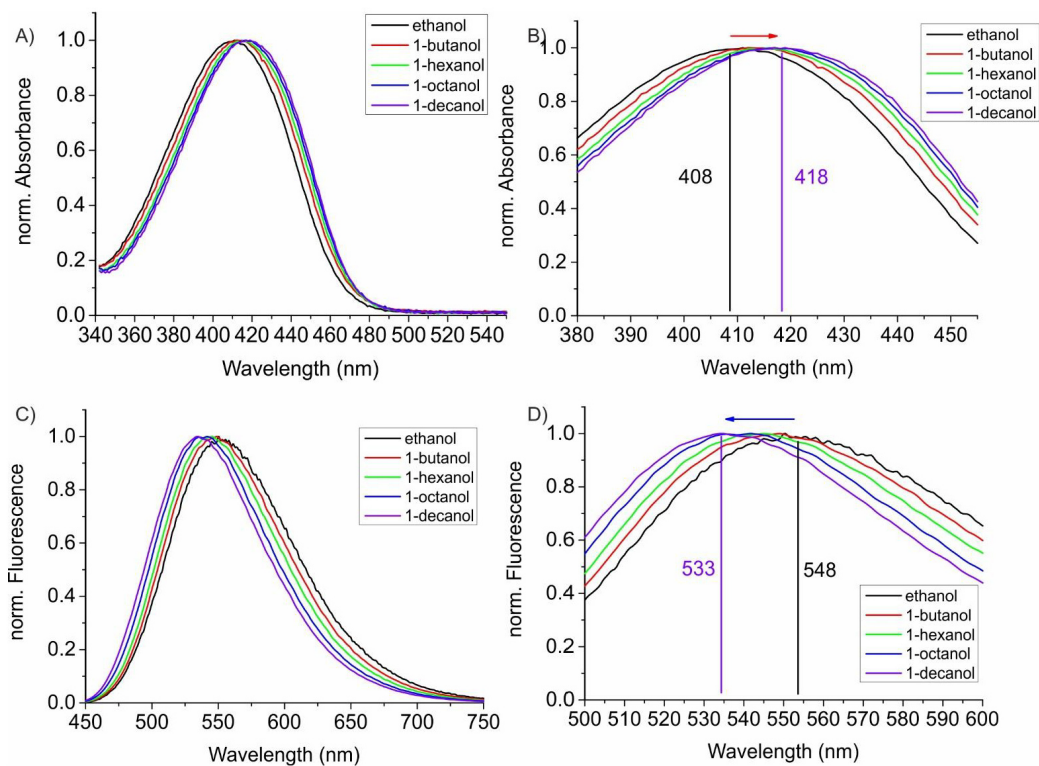


Figure S 9: Absorption spectra (A), zoomed Absorption spectra (B), Fluorescence spectra (C) and zoomed fluorescence spectra (D) of **4** in ethanol (black), 1-butanol (red), 1-hexanol (green) and 1-octanol (blue) and 1-decanol (purple). As the polarity of the alcohol increases from 1-decanol to 1-butanol the Stokes shift decreases. The red shift of absorption and the blue shift of the fluorescence is marked by the respectively coloured horizontal arrows.

Table S 4: Values of the viscosity, dielectric constant  $\epsilon_r$ , the refractive index  $n$  and the resulting orientation polarizability of the five used primary alcohols taken from reference<sup>B.11, 12</sup>.

	Viscosity [mPa s]	$\epsilon_r$	$n$	$\Delta f$
1-Decanol	11.9	8.1	1.437	0.205191892
1-Octanol	7.5	10.3	1.427	0.226258518
1-Hexanol	4.5	13.3	1.418	0.244370791
1-Butanol	3.0	17.85	1.399	0.264353401
Ethanol	1.1	24.3	1.35	0.292685944



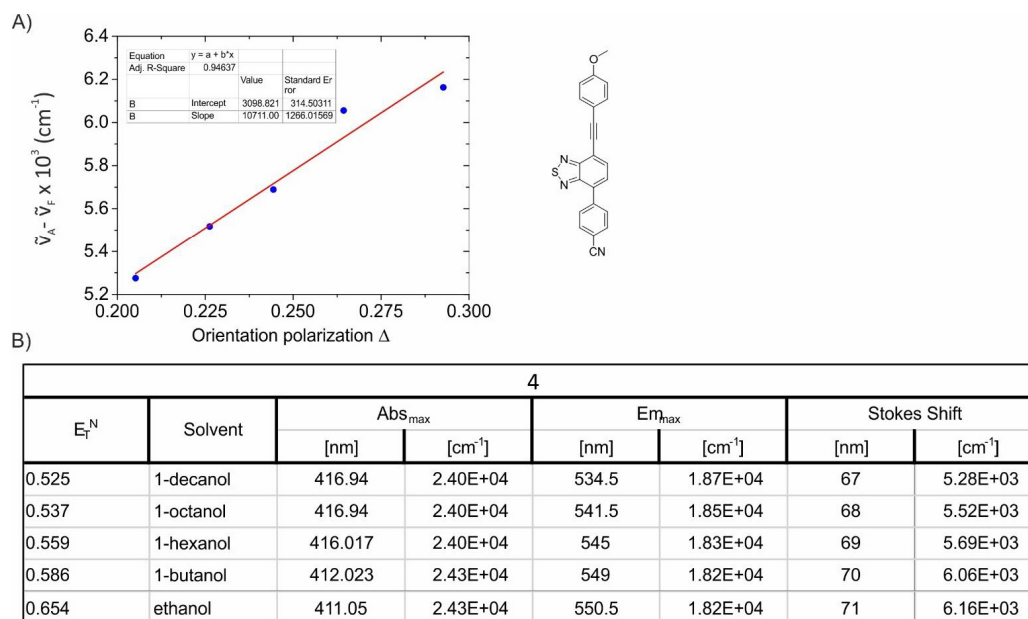


Figure S 10: A) Lippert-Mataga plot of **4** in primary alcohols of different chain length with fit values given in the inset. B) Absorption and Emission maxima and resulting Stokes shift of **4** in primary alcohols of different chain length in wavelength and energy units. Values for the normalized Dimroth-Reichardt Parameter  $E_T^N$  were taken from Ref.<sup>[7]</sup>

COMMUNICATION

7. Measurements in Mixtures of Ethanol and Polyethylene Glycol (PEG)

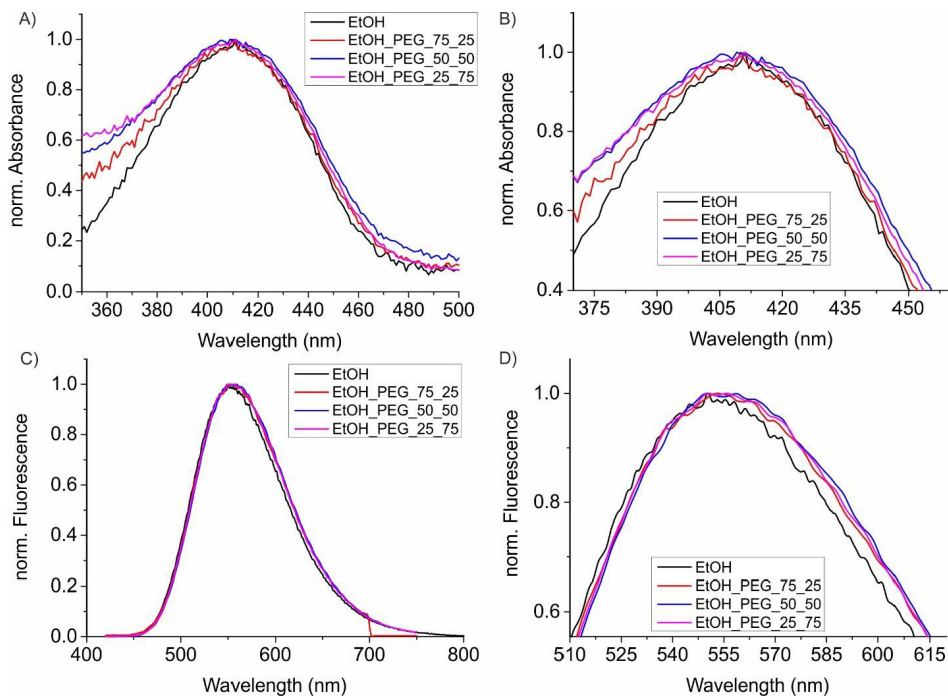


Figure S 11: Absorption spectra (A and B – B is zoomed in) and fluorescence spectra (C and D – D is zoomed in) of **4** in mixtures of ethanol / polyethylene glycol (PEG): 100/0 (black), 75/25 (red), 50/50 (blue), 25/75 (pink).

8. Fluorescence Lifetime Measurements

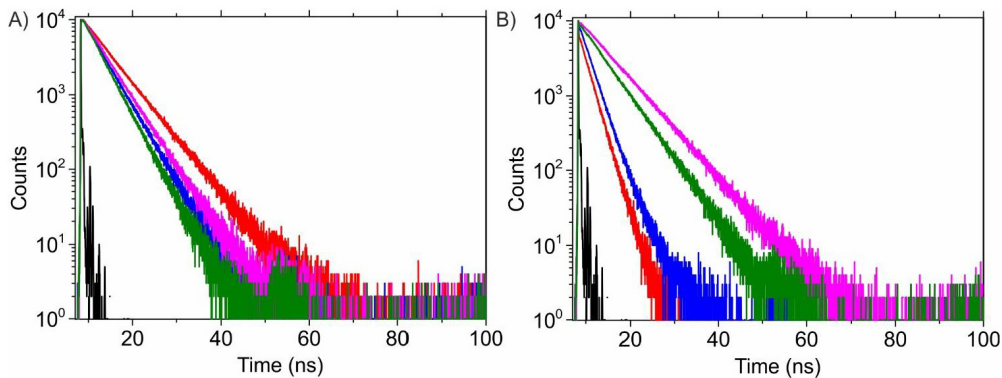


Figure S 12: Fluorescence lifetime of **1-4** in hexane (left side) and ethanol (right side). Instrument response function = black, 1 = red, 2 = blue, 3 = pink, 4 = olive.

Table S 5: Mean fluorescence lifetimes of **1-4** in solvents of different polarity. Values for the normalized Dimroth-Reichardt Parameter  $E_T^N$  were taken from Ref.<sup>[2]</sup>

$E_T^N$	Solvent	1	2	3	4
0.006	n-hexane	$\tau$ [ns] 5.77	$\tau$ [ns] 4.20	$\tau$ [ns] 4.64	$\tau$ [ns] 3.79
0.309	DCM	8.73	10.02	7.70	5.71
0.444	DMSO	6.14	9.05	7.46	5.42
0.654	EtOH	4.12	2.42	6.41	5.06

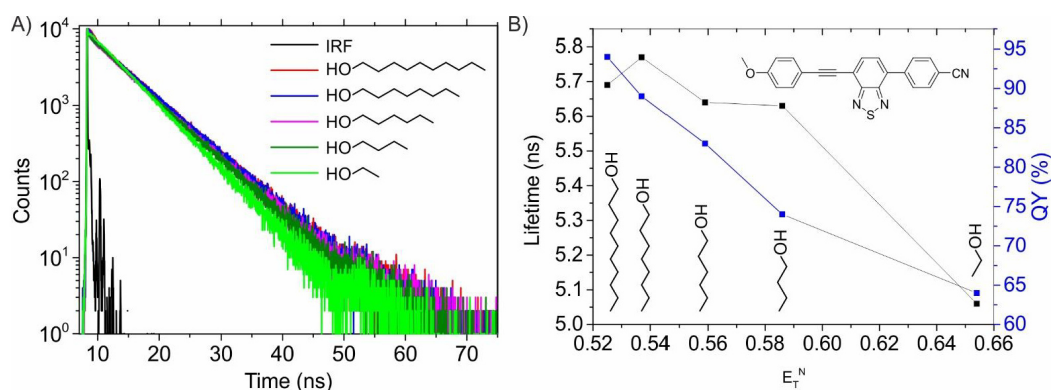


Figure S 13: A) Fluorescence lifetime of **4** in primary alcohols of different chain length. Colour code as given in the inset. B) mean fluorescence lifetime values and fluorescence quantum yield vs. the normalized Dimroth-Reichardt Parameter  $E_T^N$  taken from Ref.<sup>[2]</sup> With increasing chain length of the alcohol, and thus decreasing polarity and increasing viscosity, the mean fluorescence lifetime and the fluorescence quantum yield increase (values see Table S5).

Table S 6: Mean fluorescence lifetimes and fluorescence quantum yields of **4** in primary alcohols of different chain length. The % change was calculated with reference to ethanol. Values for the normalized Dimroth-Reichardt Parameter  $E_T^N$  were taken from Ref.<sup>[2]</sup>

$E_T^N$	Solvent	<b>4</b>			
		$\tau$ [ns]	% change	$\Phi$ [%]	% change
0.654	ethanol	5.06	0%	64	0%
0.586	1-butanol	5.63	11.3%	74	16.0%
0.559	1-hexanol	5.64	11.5%	83	30.0%
0.537	1-octanol	5.77	14.0%	89	39.1%
0.525	1-decanol	5.69	12.5%	94	47.0%

Table S 7: Mean fluorescence lifetimes and fluorescence quantum yields of **4** different EtOH/PEG ratios. The % change was calculated with reference to ethanol.

<b>4</b>			

$E_{1N}$	Solvent EtOH/PEG	$\tau$ [ns]	% change	$\Phi$ [%]	% change
	100/0	5.06	0%	64	0%
	75/25	5.10	0.8%	60	0%
	50/50	5.20	2.8%	65	1.6%
	25/75	5.12	1.2%	69	7.8%

#### 4.4 Substitution-Pattern Controlled Tuning of the Fluorescence Lifetime of Fluoranthene Dyes

---

Authors	Philipp Rietsch, Mohammad Zeyat, Katrin Hoffmann, Maximilian Kutter, Alice Paskin, Julian Uhlig, Dieter Lentz, Ute Resch-Genger, and Siegfried Eigler
Journal	submitted
DOI	---
Links	---
Detailed scientific contribution	<p>The concept of this manuscript was elaborated by P.Rietsch, Dr. U. Resch-Genger, and Prof. Dr. S. Eigler.</p> <p>M. Zeyat with the help of M. Kutter synthesized all compounds, except of the dienon derivative "DPC", which was synthesized by Alice Paskin.</p> <p>P. Rietsch did the embedding in particles and the photophysical measurements where he was supported by J. Uhlig. K. Hoffmann helped with the lifetime multiplexing measurements and did the confocal laser scanning microscopy measurements.</p> <p>Dr. U. Resch-Genger, Prof. Dr. D. Lentz and Prof. Dr. S. Eigler supervised the theoretical and experimental work.</p> <p>The manuscript was written by P. Rietsch, M. Zeyat and Prof. Dr. S. Eigler.</p>
Estimated own contribution	~45 %

---

## 5 Publications - Minor Contributions

### 5.1 Unravelling Diaminodicyanoquinone Aggregation Behavior in Solution: Complex Photophysical Properties Induced by Metastable Dimers

---

Authors	F. Witte, P. Rietsch, S. Sinha, A. Krappe, J. O. Joswig, J. P. Götze, N. Nirmalananthan-Budau, U. Resch-Genger, S. Eigler and B. Paulus
Journal	submitted
DOI	---
Links	---
Detailed scientific contribution	<p>The concept of this manuscript was elaborated by F. Witte, P. Rietsch, Prof. Dr. S. Eigler and Prof. Dr. B. Paulus.</p> <p>The theoretical work was done by F. Witte, J. O. Joswig and J. P. Götze. P. Rietsch synthesized compound 1 and 2, A. Krappe synthesized the rest of the compounds. The photophysical characterization was done by P. Rietsch, A. Krappe and S. Sinha. N. Nirmalananthan-Budau, Dr. U. Resch-Genger, Prof. Dr. S. Eigler and Prof. Dr. B. Paulus supervised the theoretical and experimental work.</p> <p>The manuscript was mainly written by F. Witte and P. Rietsch.</p>
Estimated own contribution	~20 %

---

## 5.2 Between Aromatic and Quinoid Structure: A Symmetric UV to Vis/NIR Benzothiadiazole Redox-Switch

---

Authors	Philipp Rietsch, Sebastian Sobottka, Katrin Hoffmann, Alexey Popov; Pascal Hildebrandt, Biprajit Sarkar, Ute Resch-Genger, and Siegfried Eigler
Journal	submitted to <i>Chem. Eur. J.</i> , under minor Revision
DOI	---
Links	---
Detailed scientific contribution	<p>The concept of this manuscript was elaborated by P. Rietsch, S. Sobottka and Prof. Dr. S. Eigler.</p> <p>P. Hildebrandt synthesized compounds 1. P. Rietsch did all the photophysical measurements. S. Sobottka measured cyclic voltammetry and all spectroelectrochemical measurements. Dr. K. Hoffmann did the confocal laser scanning microscopy measurements. Dr. U. Resch-Genger, Dr. Katrin Hoffmann, Prof. Dr. B. Sarkar, and Prof. Dr. S. Eigler supervised the theoretical and experimental work.</p> <p>The manuscript was written by P. Rietsch, S. Sobottka and Prof. Dr. S. Eigler.</p>
Estimated own contribution	~35 %

---

## List of Abbreviations

1-dec	1-Decanol
Abs	Absorption
ACN	Acetonitrile
AIE	Aggregation induced Emission
BTD	Benzothiadiazole
CH	Cyclohexane
CLSM	Confocal laser scanning microscope
CV	Cyclic voltammetry
DADQ	Diaminodicyanoquinone
DCM	Dichloromethane
DFT	Density functional theory
DMABN	4- <i>N,N</i> -dimethylaminobenzonitrile
DMSO	Dimethyl sulfoxide
DMF	<i>N,N</i> -Dimethylformamide
D	Debye
EA	Elemental analysis
EEM	Excitation-Emission matrix
Em	Emission
EOA	Electro-optical absorption
EPR	Electron paramagnetic resonance
EtOH	Ethanol
$\epsilon$	Molar absorption coefficient



HBC	Hexabenzocoronene
HOMO	Highest occupied molecular orbital
HPB	Hexaphenylbenzene
ICT state	Inter charge transfer state
IR	Infrared spectroscopy
ISC	Intersystem crossing
LE state	Locally excited state
LUMO	Lowest unoccupied molecular orbital
MeOH	Methanol
MRCI	Multi-reference configuration interaction
MS	Mass spectrometry
M	Monomer
NIR	Near infrared region (780-3000 nm)
NMR	Nuclear magnetic resonance
OLED	Organic Light-Emitting Diode
OTTLE	Optically transparent thin layer electrochemical cells
PAH/PAK	Polycyclic aromatic hydrocarbons
PEG	Poly ethylene glycol
PES	Potential Energy Surface
PSP	Polystyrene particles
PTCNQ	7-pyrrolidino-7,8,8-tricyanoquinomethane

S	Singlet (state)
TCSPC	Time-correlated single photon counting
TD-DFT	Time dependent-density functional theory
TICT	Twisted intramolecular charge transfer
THF	Tetrahydrofuran
T	Triplet (state)
UV	Ultraviolet
Vis	Wavelength region of visible light (380-780 nm)
XRD	X-ray diffraction
$\Phi$	Fluorescence quantum yield
$\Phi_{Sol}$	Fluorescence quantum yield in solution
$\Phi_{SS}$	Fluorescence quantum yield in the solid state
$\Phi_{PSP}$	Fluorescence quantum yield in polystyrene particle
$\tau$	Fluorescence lifetime

## List of Publications

1.	<p><u>P. Rietsch</u>, F. Witte, S. Sobottka, G. Germer, A. Becker, A. Guttler, B. Sarkar, B. Paulus, U. Resch-Genger, and S. Eigler; Diaminodicyanoquinones: Fluorescent Dyes with High Dipole Moments and Electron-Acceptor Properties. <i>Angew. Chem. Int. Ed.</i> <b>2019</b>, <i>58</i>, 8235-8239.</p>
2.	<p><u>P. Rietsch</u>, J. Soyka, S. Brülls, J. Er, K. Hoffmann, J. Beerhues, B. Sarkar, U. Resch-Genger, and S. Eigler; Fluorescence of a Chiral Pentaphene Derivative Derived from the Hexabenzocoronene Motif. <i>Chem. Commun.</i> <b>2019</b>, <i>55</i>, 10515-10518.</p>
3.	<p><u>P. Rietsch</u>, S. Sobottka, K. Hoffmann, P. Hildebrandt, B. Sarkar, U. Resch-Genger, and S. Eigler; Identification of the Irreversible Redox Behaviour of Highly Fluorescent Benzothiadiazoles <i>ChemPhotoChem.</i> <b>2020</b>, <i>4</i>, 1-7.</p>
4.	<p><u>P. Rietsch</u>, M. Zeyat, K. Hoffmann, M. Kutter, A. Paskin, J. Uhlig, D. Lentz, U. Resch-Genger, and S. Eigler; Substitution-pattern Controlled Tuning of the Fluorescence Lifetime of Fluoranthene Dyes submitted</p>
5.	<p>F. Witte, <u>P. Rietsch</u>, S. Sinha, A. Krappe, J. O. Joswig, J. P. Götze, N. Nirmalanathan-Budau, U. Resch-Genger, S. Eigler and B. Paulus; Unraveling diaminodicyanoquinone aggregation behavior in solution: Complex photophysical properties induced by metastable dimers. submitted</p>
6.	<p><u>P. Rietsch</u>, S. Sobottka, K. Hoffmann, A. Popov, P. Hildebrandt, B. Sarkar, U. Resch-Genger, and S. Eigler; Between Aromatic and Quinoid Structure: A symmetric UV to Vis/NIR Benzothiadiazole Redox-Switch Submitted to <i>Chem. Eur. J.</i>, under minor Revision</p>

## References

- [1] a) D. S. Acker, W. R. Hertler, *J. Am. Chem. Soc.* **1962**, *84*, 3370; b) L. R. Melby, R. J. Harder, W. R. Hertler, W. Mahler, R. E. Benson, W. E. Mochel, *J. Am. Chem. Soc.* **1962**, *84*, 3374; c) D. S. Acker, R. J. Harder, W. R. Hertler, W. Mahler, L. R. Melby, R. E. Benson, W. E. Mochel, *J. Am. Chem. Soc.* **1960**, *82*, 6408.
- [2] a) G. J. Ashwell, E. J. C. Dawnay, A. P. Kuczynski, M. Szablewski, I. M. Sandy, M. R. Bryce, A. M. Grainger, M. Hasan, *J. Chem. Soc., Faraday Trans.* **1990**, *86*, 1117; b) M. Szablewski, M. A. Fox, F. B. Dias, H. Namih, E. W. Snedden, S. M. King, D. Dai, L. O. Palsson, *J. Phys. Chem. B* **2014**, *118*, 6815; c) P. Srujana, T. Gera, T. P. Radhakrishnan, *J. Mater. Chem. C* **2016**, *4*, 6510.
- [3] a) R. J. Mortimer, *Annu. Rev. Mater. Res.* **2011**, *41*, 241; b) P. R. Somani, S. Radhakrishnan, *Mater. Chem. Phys.* **2003**, *77*, 117.
- [4] a) H. V. Schroder, H. Hupatz, A. J. Achazi, S. Sobottka, B. Sarkar, B. Paulus, C. A. Schalley, *Chem. Eur. J.* **2017**, *23*, 2960; b) E. H. van Dijk, D. J. Myles, M. H. van der Veen, J. C. Hummelen, *Org. Lett.* **2006**, *8*, 2333; c) J. Liao, J. S. Agustsson, S. Wu, C. Schonenberger, M. Calame, Y. Leroux, M. Mayor, O. Jeannin, Y. F. Ran, S. X. Liu, S. Decurtins, *Nano Lett.* **2010**, *10*, 759; d) T. Ye, A. S. Kumar, S. Saha, T. Takami, T. J. Huang, J. F. Stoddart, P. S. Weiss, *ACS Nano* **2010**, *4*, 3697.
- [5] a) W. E. Acree, A. I. Zvaigzne, J. C. Fetzer, *Appl. Spectrosc.* **1990**, *44*, 1193; b) S. A. Tucker, A. I. Zvaigzne, W. E. Acree, J. C. Fetzer, M. Zander, *Appl. Spectrosc.* **1991**, *45*, 424.
- [6] A. U. Acuna, F. Amat-Guerri, P. Morcillo, M. Liras, B. Rodriguez, *Org. Lett.* **2009**, *11*, 3020.
- [7] Splarka, [https://commons.wikimedia.org/wiki/File:Tonic\\_water\\_uv.jpg](https://commons.wikimedia.org/wiki/File:Tonic_water_uv.jpg) **2005**, accessed: 01.09.2020.
- [8] a) D. Brewster, *Trans. R. Soc. Edinburgh* **2013**, *12*, 538; b) *Philos. Trans. R. Soc. London* **1997**, *135*, 143.
- [9] D. Descouens, <https://commons.wikimedia.org/wiki/File:FluoriteUV.jpg> **2009**, accessed: 21.08.2020, CC-BY-SA-4.0.
- [10] G. G. Stokes, *Philos. Trans. R. Soc. London* **1997**, *142*, 463.
- [11] a) H. Hötzl, *Environ. Geol.* **1996**, *27*, 87; b) A. Knop, in *Neues Jahrbuch für Mineralogie, Geologie und Palaeontologie*, Schweizerbart, E., Stuttgart, **1878**.
- [12] a) A. Salehi-Reyhani, *Sci. Rep.* **2017**, *7*, 17957; b) S. Shashkova, M. C. Leake, *Biosci. Rep.* **2017**, *37*.
- [13] A. J. Kuehne, M. C. Gather, *Chem. Rev.* **2016**, *116*, 12823.
- [14] a) R. C. Chiechi, R. J. Tseng, F. Marchioni, Y. Yang, F. Wudl, *Adv. Mater.* **2006**, *18*, 325; b) S. Kumar, D. Kumar, Y. Patil, S. Patil, *J. Mater. Chem. C* **2016**, *4*, 193; c) C. W. Tang, S. A. VanSlyke, *Appl. Phys. Lett.* **1987**, *51*, 913; d) A. Salehi, X. Fu, D. H. Shin, F. So, *Adv. Funct. Mater.* **2019**, *29*.
- [15] a) K. Hoffmann, T. Behnke, D. Drescher, J. Kneipp, U. Resch-Genger, *ACS Nano* **2013**, *7*, 6674; b) S. Birtwell, H. Morgan, *Integr. Biol.* **2009**, *1*, 345; c) J. P. Nolan, F. Mandy, *Cytometry A* **2006**, *69*, 318.
- [16] P. Zijlstra, J. W. Chon, M. Gu, *Nature* **2009**, *459*, 410.
- [17] J. M. Meruga, W. M. Cross, P. Stanley May, Q. Luu, G. A. Crawford, J. J. Kellar, *Nanotechnology* **2012**, *23*, 395201.
- [18] L. M. Smith, J. Z. Sanders, R. J. Kaiser, P. Hughes, C. Dodd, C. R. Connell, C. Heiner, S. B. Kent, L. E. Hood, *Nature* **1986**, *321*, 674.
- [19] a) R. A. Kyle, M. A. Shampo, *JAMA* **1979**, *242*, 744; b) Valeur, *Molecular Fluorescence: Principles and Applications*, Wiley VCH, Somerset, **2002**.
- [20] a) J. R. Lakowicz, *Principles of Fluorescence Spectroscopy*, **2006**; b) M. Kasha, *Discuss. Faraday Soc.* **1950**, *9*.
- [21] B. S. Basel, J. Zirzmeier, C. Hetzer, S. R. Reddy, B. T. Phelan, M. D. Krzyaniak, M. K. Volland, P. B. Coto, R. M. Young, T. Clark, M. Thoss, R. R. Tykwinski, M. R. Wasielewski, D. M. Guldi, *Chem* **2018**, *4*, 1092.

- [22] J. Bartelmess, B. Ballesteros, G. de la Torre, D. Kiessling, S. Campidelli, M. Prato, T. Torres, D. M. Guldi, *J. Am. Chem. Soc.* **2010**, *132*, 16202.
- [23] a) L. Oberleitner, J. Grandke, F. Mallwitz, U. Resch-Genger, L. A. Garbe, R. J. Schneider, *J. Agric. Food. Chem.* **2014**, *62*, 2337; b) R. S. Bilan, V. A. Krivenkov, M. A. Berestovoy, A. E. Efimov, Agapov, II, P. S. Samokhvalov, I. Nabiev, A. Sukhanova, *ChemPhysChem* **2017**, *18*, 970.
- [24] R. Kotzick, R. Niessner, *Fresenius J. Anal. Chem.* **1996**, *354*, 72.
- [25] U. Lieberwirth, J. Arden-Jacob, K. H. Drexhage, D. P. Herten, R. Müller, M. Neumann, A. Schulz, S. Siebert, G. Sagner, S. Klingel, M. Sauer, J. Wolfrum, *Anal. Chem.* **1998**, *70*, 4771.
- [26] S. H. Mihindukulasuriya, T. K. Morcone, L. B. McGown, *Electrophoresis* **2003**, *24*, 20.
- [27] S. A. Soper, B. L. Legendre, Jr., D. C. Williams, *Anal. Chem.* **1995**, *67*, 4358.
- [28] a) M. Y. Berezin, W. J. Akers, K. Guo, G. M. Fischer, E. Daltrozzi, A. Zumbusch, S. Achilefu, *Biophys J.* **2009**, *97*, L22; b) A. T. N. Kumar, S. S. Hou, W. L. Rice, *Optica* **2018**, *5*, 624.
- [29] C. Reichardt, *Chem. Rev.* **1994**, *94*, 2319.
- [30] a) A. Mishra, R. K. Behera, P. K. Behera, B. K. Mishra, G. B. Behera, *Chem. Rev.* **2000**, *100*, 1973; b) M. J. Minch, S. S. Shah, *J. Chem. Educ.* **1977**, *54*; c) U. Rosch, S. Yao, R. Wortmann, F. Würthner, *Angew. Chem. Int. Ed.* **2006**, *45*, 7026.
- [31] a) J. Pina, J. S. de Melo, D. Breusov, U. Scherf, *Phys. Chem. Chem. Phys.* **2013**, *15*, 15204; b) U. Warde, N. Sekar, *Opt. Mater.* **2017**, *72*, 346; c) B. Maity, A. Chatterjee, D. Seth, *Photochem. Photobiol.* **2014**, *90*, 734.
- [32] P. Bhyrappa, M. Sankar, *Spectrochim. Acta, Part A* **2018**, *189*, 80.
- [33] a) N. Mataga, Y. Kaifu, M. Koizumi, *Bull. Chem. Soc. Jpn.* **1955**, *28*, 690; b) E. Lippert, *Z. Elektrochem.* **1957**, *61*, 962.
- [34] H. Liu, S. Yan, R. Huang, Z. Gao, G. Wang, L. Ding, Y. Fang, *Chem. Eur. J.* **2019**, *25*, 16732.
- [35] K. Dimroth, C. Reichardt, T. Siepmann, F. Bohlmann, *Liebigs Ann. Chem.* **1963**, *661*, 1.
- [36] a) R. Van Wachem, F. H. De Leeuw, A. Dymanus, *J. Phys. Chem.* **1967**, *47*, 2256; b) D. Menard, M. Chabanel, *J. Phys. Chem.* **1975**, *79*, 1081.
- [37] a) V. Parthasarathy, R. Pandey, M. Stolte, S. Ghosh, F. Castet, F. Würthner, P. K. Das, M. Blanchard-Desce, *Chem. Eur. J.* **2015**, *21*, 14211; b) J. Wudarczyk, G. Papamokos, V. Margaritis, D. Schollmeyer, F. Hinkel, M. Baumgarten, G. Floudas, K. Müllen, *Angew. Chem. Int. Ed.* **2016**, *55*, 3220; c) Z. R. Grabowski, K. Rotkiewicz, W. Rettig, *Chem. Rev.* **2003**, *103*, 3899.
- [38] T. Förster, *Ann. Phys.* **2006**, *437*, 55.
- [39] S. Beckmann, K.-H. Etzbach, P. Krämer, K. Lukaszuk, R. Matschiner, A. J. Schmidt, P. Schuhmacher, R. Sens, G. Seybold, R. Wortmann, F. Würthner, *Adv. Mater.* **1999**, *11*, 536.
- [40] A. M. Thooft, K. Cassaidy, B. VanVeller, *J. Org. Chem.* **2017**, *82*, 8842.
- [41] a) E. R. Draper, L. Wilbraham, D. J. Adams, M. Wallace, R. Schweins, M. A. Zwijnenburg, *Nanoscale* **2019**, *11*, 15917; b) F. Würthner, *Acc. Chem. Res.* **2016**, *49*, 868.
- [42] a) E. E. Jelley, *Nature* **1936**, *138*, 1009; b) E. E. Jelley, *Nature* **1937**, *139*, 631; c) G. Scheibe, L. Kandler, H. Ecker, *Die Naturwissenschaften* **1937**, *25*, 75; d) G. Scheibe, *Angew. Chem.* **1937**, *50*, 212.
- [43] M. Kasha, H. R. Rawls, M. Ashraf El-Bayoumi, *Pure Appl. Chem.* **1965**, *11*, 371.
- [44] a) F. Würthner, T. E. Kaiser, C. R. Saha-Moller, *Angew. Chem. Int. Ed.* **2011**, *50*, 3376; b) A. Liess, A. Lv, A. Arjona-Esteban, D. Bialas, A. M. Krause, V. Stepanenko, M. Stolte, F. Würthner, *Nano Lett.* **2017**, *17*, 1719; c) H. von Berlepsch, C. Böttcher, L. Dähne, *J. Phys. Chem. B* **2000**, *104*, 8792.
- [45] N. J. Hestand, F. C. Spano, *Chem. Rev.* **2018**, *118*, 7069.
- [46] a) M. Bayda, F. Dumoulin, G. L. Hug, J. Koput, R. Gorniak, A. Wojcik, *Dalton Trans.* **2017**, *46*, 1914; b) E. A. Margulies, L. E. Shoer, S. W. Eaton, M. R. Wasielewski, *Phys. Chem. Chem. Phys.* **2014**, *16*, 23735; c) C. Zheng, C. Zhong, C. J. Collison, F. C. Spano, *J. Phys. Chem. C* **2019**, *123*, 3203.
- [47] a) A. Liess, A. Arjona-Esteban, A. Kudzus, J. Albert, A. M. Krause, A. Lv, M. Stolte, K. Meerholz, F. Würthner, *Adv. Funct. Mater.* **2019**, *29*; b) T. Eder, J. Vogelsang, S. Bange, K. Remmersen,

- D. Schmitz, S. S. Jester, T. J. Keller, S. Hoger, J. M. Lupton, *Angew. Chem. Int. Ed.* **2019**, *58*, 18898.
- [48] R. S. Becker, J. Seixas de Melo, A. L. Maçanita, F. Elisei, *J. Phys. Chem.* **1996**, *100*, 18683.
- [49] W. R. Dawson, M. W. Windsor, *J. Phys. Chem.* **1968**, *72*, 3251.
- [50] O. Ostroverkhova, A. D. Platt, W. E. B. Shepherd, J. Day, J. E. Anthony, *Proc. SPIE, Linear and Nonlinear Optics of Organic Materials IX* **2009**, 7413.
- [51] J. O. Escobedo, O. Rusin, S. Lim, R. M. Strongin, *Curr. Opin. Chem. Biol.* **2010**, *14*, 64.
- [52] B. Purushothaman, S. R. Parkin, J. E. Anthony, *Org. Lett.* **2010**, *12*, 2060.
- [53] M. J. Lin, A. Jimenez, C. Burschka, F. Würthner, *Chem. Commun.* **2012**, *48*, 12050.
- [54] a) E. Yamaguchi, C. Wang, A. Fukazawa, M. Taki, Y. Sato, T. Sasaki, M. Ueda, N. Sasaki, T. Higashiyama, S. Yamaguchi, *Angew. Chem. Int. Ed.* **2015**, *54*, 4539; b) T. Beppu, K. Tomiguchi, A. Masuhara, Y. J. Pu, H. Katagiri, *Angew. Chem. Int. Ed.* **2015**, *54*, 7332.
- [55] A. Kellmann, *J. Phys. Chem.* **1977**, *81*, 1195.
- [56] a) K. P. Wall, R. Dillon, M. K. Knowles, *Biochem. Mol. Biol. Educ.* **2015**, *43*, 52; b) R. F. Kubin, A. N. Fletcher, *J. Lumin.* **1982**, *27*, 455.
- [57] E. Lippert, W. Lüder, F. Moll, W. Nägele, H. Boos, H. Prigge, I. Seibold-Blankenstein, *Angew. Chem.* **1961**, *73*, 695.
- [58] K.-M. Bark, R. K. Forcé, *Spectrochim. Acta, Part A* **1993**, *49*, 1605.
- [59] C. H. Huang, P. J. Wu, K. Y. Chung, Y. A. Chen, E. Y. Li, P. T. Chou, *Phys. Chem. Chem. Phys.* **2017**, *19*, 8896.
- [60] M. A. El-Sayed, *J. Phys. Chem.* **1963**, *38*, 2834.
- [61] M. Baroncini, G. Bergamini, P. Ceroni, *Chem. Commun.* **2017**, *53*, 2081.
- [62] G. N. Lewis, D. Lipkin, T. T. Magel, *J. Am. Chem. Soc.* **1941**, *63*, 3005.
- [63] C. Li, X. Tang, L. Zhang, C. Li, Z. Liu, Z. Bo, Y. Q. Dong, Y.-H. Tian, Y. Dong, B. Z. Tang, *Adv. Opt. Mater.* **2015**, *3*, 1184.
- [64] J. Z. Liao, L. Meng, J. H. Jia, D. Liang, X. L. Chen, R. M. Yu, X. F. Kuang, C. Z. Lu, *Chem. Eur. J.* **2018**, *24*, 10498.
- [65] Z. An, C. Zheng, Y. Tao, R. Chen, H. Shi, T. Chen, Z. Wang, H. Li, R. Deng, X. Liu, W. Huang, *Nat. Mater.* **2015**, *14*, 685.
- [66] K. T. Yeung, W. P. To, C. Sun, G. Cheng, C. Ma, G. S. Tong, C. Yang, C. M. Che, *Angew. Chem. Int. Ed.* **2017**, *56*, 133.
- [67] T. Forster, K. Kasper, *Z. Elektrochem.* **1955**, *59*, 976.
- [68] a) W. Wang, J. J. Han, L.-Q. Wang, L.-S. Li, W. J. Shaw, A. D. Q. Li, *Nano Lett.* **2003**, *3*, 455; b) K. Yamana, T. Iwai, Y. Ohtani, S. Sato, M. Nakamura, H. Nakano, *Bioconjugate Chem.* **2002**, *13*, 1266; c) S. S. Atik, M. Nam, L. A. Singer, *Chem. Phys. Lett.* **1979**, *67*, 75.
- [69] a) M. A. Fox, P. F. Britt, *Macromolecules* **1990**, *23*, 4533; b) J. Cornil, D. A. dos Santos, X. Crispin, R. Silbey, J. L. Brédas, *J. Am. Chem. Soc.* **1998**, *120*, 1289; c) S. A. Jenekhe, J. A. Osaheni, *Science* **1994**, *265*, 765; d) J. A. Osaheni, S. A. Jenekhe, *Chem. Mater.* **1992**, *4*, 1282.
- [70] E. A. Chandross, C. J. Dempster, *J. Am. Chem. Soc.* **1970**, *92*, 3586.
- [71] S. Grimme, *Angew. Chem. Int. Ed.* **2008**, *47*, 3430.
- [72] a) Y. Shen, H. Liu, S. Zhang, Y. Gao, B. Li, Y. Yan, Y. Hu, L. Zhao, B. Yang, *J. Mater. Chem. C* **2017**, *5*, 10061; b) T. M. Figueira-Duarte, P. G. Del Rosso, R. Trattnig, S. Sax, E. J. List, K. Müllen, *Adv. Mater.* **2010**, *22*, 990; c) Z. Zhao, P. Lu, J. W. Y. Lam, Z. Wang, C. Y. K. Chan, H. H. Y. Sung, I. D. Williams, Y. Ma, B. Z. Tang, *Chem. Sci.* **2011**, *2*, 672.
- [73] a) A. Vogel, *Ann. Phys. (Berlin)* **1820**, *64*, 161; b) W. H. Perkin, *J. Chem. Soc.* **1868**, *21*, 53.
- [74] A. J. Kuehne, M. C. Gather, *Chem. Rev.* **2016**, *116*, 12823.
- [75] D. W. Fink, W. R. Koehler, *Anal. Chem.* **2002**, *42*, 990.
- [76] M. El-Kemary, W. Rettig, *Phys. Chem. Chem. Phys.* **2003**, *5*.
- [77] A. Baeyer, *Ber. Dtsch. Chem. Ges.* **1871**, *4*, 555.
- [78] M. M. Martin, L. Lindqvist, *J. Lumin.* **1975**, *10*, 381.
- [79] K. Ravindra, R. Sokhi, R. Vangrieken, *Atmos. Environ.* **2008**, *42*, 2895.

- [80] C.-E. Boström, P. Gerde, A. Hanberg, B. Jernström, C. Johansson, T. Kyrklund, A. Rannug, M. Törnqvist, K. Victorin, R. Westerholm, *Environ. Health Perspect.* **2002**, *110*, 451.
- [81] a) I. Diez-Perez, Z. Li, J. Hihath, J. Li, C. Zhang, X. Yang, L. Zang, Y. Dai, X. Feng, K. Müllen, N. Tao, *Nat. Commun.* **2010**, *1*, 31; b) L. Chen, K. S. Mali, S. R. Puniredd, M. Baumgarten, K. Parvez, W. Pisula, S. De Feyter, K. Müllen, *J. Am. Chem. Soc.* **2013**, *135*, 13531; c) H. Seyler, B. Purushothaman, D. J. Jones, A. B. Holmes, W. W. H. Wong, *Pure Appl. Chem.* **2012**, *84*, 1047; d) Y. Liu, T. Marszalek, K. Müllen, W. Pisula, X. Feng, *Chem. Asian J.* **2016**, *11*, 2107; e) F. Hinkel, D. Cho, W. Pisula, M. Baumgarten, K. Müllen, *Chem. Eur. J.* **2015**, *21*, 86.
- [82] X. Dou, W. Pisula, J. Wu, G. J. Bodwell, K. Müllen, *Chem. Eur. J.* **2008**, *14*, 240.
- [83] X. Feng, W. Pisula, T. Kudernac, D. Wu, L. Zhi, S. De Feyter, K. Müllen, *J. Am. Chem. Soc.* **2009**, *131*, 4439.
- [84] a) R. Liu, D. Wu, X. Feng, K. Müllen, *J. Am. Chem. Soc.* **2011**, *133*, 15221; b) Y. Byun, A. Coskun, *Chem. Mater.* **2015**, *27*, 2576; c) F. Cataldo, O. Ursini, G. Angelini, S. Iglesias-Groth, *Fuller. Nanotub. Car. N.* **2011**, *19*, 713.
- [85] Ö. Delikaya, M. Zeyat, D. Lentz, C. Roth, *ChemElectroChem* **2019**, *6*, 3892.
- [86] M. Matussek, M. Filapek, P. Gancarz, S. Krompiec, J. Grzegorz Małecki, S. Kotowicz, M. Siwy, S. Maćkowski, A. Chrobok, E. Schab-Balcerzak, A. Słodek, *Dyes Pigm.* **2018**, *159*, 590.
- [87] a) N. Venkatramaiah, S. Kumar, S. Patil, *Chem. Commun.* **2012**, *48*, 5007; b) J. Gershberg, M. Radic Stojkovic, M. Skugor, S. Tomic, T. H. Rehm, S. Rehm, C. R. Saha-Moller, I. Piantanida, F. Würthner, *Chem. Eur. J.* **2015**, *21*, 7886; c) M. Tounsi, M. Ben Braiek, A. Baraket, M. Lee, N. Zine, M. Zabala, J. Bausells, F. Aloui, B. Ben Hassine, A. Maaref, A. Errachid, *Electroanalysis* **2016**, *28*, 2892.
- [88] P. T. Herwig, V. V. Enkelmann, O. Schmelz, K. Müllen, *Chem. Eur. J.* **2000**, *6*, 1834.
- [89] A. Gourdon, S. K. Sadhukhan, C. Viala, *Synthesis* **2003**, 1521.
- [90] X. Feng, W. Pisula, K. Müllen, *Pure Appl. Chem.* **2009**, *81*, 2203.
- [91] a) D. Lungerich, D. Reger, H. Holzel, R. Riedel, M. M. Martin, F. Hampel, N. Jux, *Angew. Chem. Int. Ed.* **2016**, *55*, 5602; b) S. Suzuki, Y. Segawa, K. Itami, J. Yamaguchi, *Nat. Chem.* **2015**, *7*, 227.
- [92] H. Güsten, G. Heinrich, *J. Photochem.* **1982**, *18*, 9.
- [93] a) D. Reger, P. Haines, F. W. Heinemann, D. M. Guldi, N. Jux, *Angew. Chem. Int. Ed.* **2018**, *57*, 5938; b) K. Katayama, I. Kawajiri, Y. Okano, J. i. Nishida, T. Kawase, *ChemPlusChem* **2019**, *84*, 722; c) F. Würthner, S. Ahmed, C. Thalacker, T. Debaerdemaeker, *Chem. Eur. J.* **2002**, *8*, 4742; d) R. Berger, M. Wagner, X. Feng, K. Müllen, *Chem. Sci.* **2015**, *6*, 436; e) A. Kratzer, J. M. Englert, D. Lungerich, F. W. Heinemann, N. Jux, A. Hirsch, *Faraday Discuss.* **2014**, *173*, 297; f) Z. H. Zhao, M. Y. Zhang, D. H. Liu, C. H. Zhao, *Org. Lett.* **2018**, *20*, 7590.
- [94] a) T. Kaehler, M. Bolte, H. W. Lerner, M. Wagner, *Angew. Chem. Int. Ed.* **2019**, *58*, 11379; b) M. Stolte, T. Schembri, J. Süß, D. Schmidt, A.-M. Krause, M. O. Vysotsky, F. Würthner, *Chem. Mater.* **2020**, *32*, 6222; c) V. M. Hertz, J. G. Massoth, M. Bolte, H. W. Lerner, M. Wagner, *Chem. Eur. J.* **2016**, *22*, 13181; d) K. Schickedanz, J. Radtke, M. Bolte, H. W. Lerner, M. Wagner, *J. Am. Chem. Soc.* **2017**, *139*, 2842.
- [95] N. I. Nijegorodov, W. S. Downey, *J. Phys. Chem.* **1994**, *98*, 5639.
- [96] a) M. Albota, *Science* **1998**, *281*, 1653; b) M. Szablewski, P. R. Thomas, A. Thornton, D. Bloor, G. H. Cross, J. M. Cole, J. A. K. Howard, M. Malagoli, F. Meyers, J.-L. Brédas, W. Wenseleers, E. Goovaerts, *J. Am. Chem. Soc.* **1997**, *119*, 3144; c) J. M. Hales, J. Matichak, S. Barlow, S. Ohira, K. Yesudas, J. L. Bredas, J. W. Perry, S. R. Marder, *Science* **2010**, *327*, 1485.
- [97] a) S. Y. Leblebici, T. L. Chen, P. Olalde-Velasco, W. Yang, B. Ma, *ACS Appl. Mater. Interfaces* **2013**, *5*, 10105; b) P. Gratia, A. Magomedov, T. Malinauskas, M. Daskeviciene, A. Abate, S. Ahmad, M. Gratzel, V. Getautis, M. K. Nazeeruddin, *Angew. Chem. Int. Ed.* **2015**, *54*, 11409; c) R. Grisorio, B. Roose, S. Colella, A. Listorti, G. P. Suranna, A. Abate, *ACS Energy Lett.* **2017**, *2*, 1029; d) A. Hagfeldt, G. Boschloo, L. Sun, L. Kloo, H. Pettersson, *Chem. Rev.* **2010**, *110*, 6595; e) N. Camaioni, R. Po, *J. Phys. Chem. Lett.* **2013**, *4*, 1821.

- [98] K. Klaue, W. Han, P. Liesfeld, F. Berger, Y. Garmshausen, S. Hecht, *J. Am. Chem. Soc.* **2020**, *142*, 11857.
- [99] N. Karton-Lifshin, L. Albertazzi, M. Bendikov, P. S. Baran, D. Shabat, *J. Am. Chem. Soc.* **2012**, *134*, 20412.
- [100] D. Gudeika, A. Miasojedovas, O. Bezikonny, D. Volyniuk, A. Gruodis, S. Jursenas, J. V. Grazulevicius, *Dyes Pigm.* **2019**, *166*, 217.
- [101] B. Tang, C. Wang, Y. Wang, H. Zhang, *Angew. Chem. Int. Ed.* **2017**, *56*, 12543.
- [102] M. Ravi, D. N. Rao, S. Cohen, I. Agranat, T. P. Radhakrishnan, *J. Mater. Chem.* **1996**, *6*, 1853.
- [103] a) P. Gangopadhyay, S. Sharma, A. J. Rao, D. N. Rao, S. Cohen, I. Agranat, T. P. Radhakrishnan, *Chem. Mater.* **1999**, *11*, 466; b) M. R. Bryce, E. Chinarro, A. Green, N. Martín, A. J. Moore, L. Sánchez, C. Seoane, *Synth. Met.* **1997**, *86*, 1857; c) S. Jayanty, T. P. Radhakrishnan, *Chem. Eur. J.* **2004**, *10*, 791; d) C. G. Chandaluri, T. P. Radhakrishnan, *Opt. Mater.* **2011**, *34*, 119.
- [104] a) T. Yanai, D. P. Tew, N. C. Handy, *Chem. Phys. Lett.* **2004**, *393*, 51; b) V. Barone, M. Cossi, *J. Phys. Chem. A* **1998**, *102*, 1995.
- [105] a) S. Grimme, M. Waletzke, *J. Phys. Chem.* **1999**, *111*, 5645; b) I. Lyskov, M. Kleinschmidt, C. M. Marian, *J. Chem. Phys.* **2016**, *144*, 034104; c) A. D. Becke, *J. Phys. Chem.* **1993**, *98*, 1372; d) F. Weigend, R. Ahlrichs, *Phys. Chem. Chem. Phys.* **2005**, *7*, 3297.
- [106] a) Z. Wang, Z. Peng, K. Huang, P. Lu, Y. Wang, *J. Mater. Chem. C* **2019**, *7*, 6706; b) B. A. DaSilveira Neto, A. S. A. Lopes, G. Ebeling, R. S. Gonçalves, V. E. U. Costa, F. H. Quina, J. Dupont, *Tetrahedron* **2005**, *61*, 10975.
- [107] a) M. E. Mohanty, C. Madhu, V. L. Reddy, M. Paramasivam, P. R. Bangal, V. J. Rao, *Phys. Chem. Chem. Phys.* **2017**, *19*, 9118; b) M. D'Alessandro, A. Amadei, I. Daidone, R. Po', A. Alessi, M. Aschi, *J. Phys. Chem. C* **2013**, *117*, 13785; c) L. E. Polander, L. Pandey, S. Barlow, S. P. Tiwari, C. Risko, B. Kippelen, J.-L. Brédas, S. R. Marder, *J. Phys. Chem. C* **2011**, *115*, 23149.
- [108] a) C.-Y. Mei, L. Liang, F.-G. Zhao, J.-T. Wang, L.-F. Yu, Y.-X. Li, W.-S. Li, *Macromolecules* **2013**, *46*, 7920; b) P. Ledwon, N. Thomson, E. Angioni, N. J. Findlay, P. J. Skabara, W. Domagala, *RSC Adv.* **2015**, *5*, 77303; c) M. J. McAllister, J.-L. Li, D. H. Adamson, H. C. Schniepp, A. A. Abdala, J. Liu, M. Herrera-Alonso, D. L. Milius, R. Car, R. K. Prud'homme, I. A. Aksay, *Chem. Mater.* **2007**, *19*, 4396.
- [109] K. Shen, Z. Ju, L. Qin, T. Wang, H. Zheng, *Dyes Pigm.* **2017**, *136*, 515.
- [110] S. S. M. Fernandes, A. Pereira, D. Ivanou, A. Mendes, M. M. M. Raposo, *Dyes Pigm.* **2018**, *151*, 89.
- [111] M. Akhtaruzzaman, N. Kamata, J. Nishida, S. Ando, H. Tada, M. Tomura, Y. Yamashita, *Chem. Commun.* **2005**, 3183.
- [112] a) M. Shen, J. Rodriguez-Lopez, J. Huang, Q. Liu, X. H. Zhu, A. J. Bard, *J. Am. Chem. Soc.* **2010**, *132*, 13453; b) M. Shen, X. H. Zhu, A. J. Bard, *J. Am. Chem. Soc.* **2013**, *135*, 8868; c) Z. Li, W. Qin, G. Liang, *Nanoscale* **2020**, *12*, 8828.
- [113] P. C. Rodrigues, L. S. Berlim, D. Azevedo, N. C. Saavedra, P. N. Prasad, W. H. Schreiner, T. D. Atvars, L. Akcelrud, *J. Phys. Chem. A* **2012**, *116*, 3681.
- [114] a) A. R. Harifi-Mood, M. Abbasi, *J. Solution Chem.* **2018**, *47*, 1503; b) B. Y. Zaslavsky, L. M. Miheeva, E. A. Masimov, S. F. Djafarov, C. Reichardt, *J. Chem. Soc., Faraday Trans.* **1990**, *86*, 519.
- [115] a) P. Rietsch, F. Witte, S. Sobottka, G. Germer, A. Becker, A. Guttler, B. Sarkar, B. Paulus, U. Resch-Genger, S. Eigler, *Angew. Chem. Int. Ed.* **2019**, *58*, 8235; b) R. M. Yusop, A. Unciti-Broceta, M. Bradley, *Bioorg. Med. Chem. Lett.* **2012**, *22*, 5780; c) N. Scholz, A. Jadhav, M. Shreykar, T. Behnke, N. Nirmalanathan, U. Resch-Genger, N. Sekar, *J. Fluoresc.* **2017**, *27*, 1949.
- [116] G. M. Martins, B. Shirinfar, T. Hardwick, A. Murtaza, N. Ahmed, *Catal. Sci. Technol.* **2019**, *9*, 5868.
- [117] S. R. Domingos, H. Luyten, F. van Anrooij, H. J. Sanders, B. H. Bakker, W. J. Buma, F. Hartl, S. Woutersen, *Rev. Sci. Instrum.* **2013**, *84*, 033103.



- [118] S. F. Nelsen, M. N. Weaver, J. P. Telo, *J. Phys. Chem. A* **2007**, *111*, 10993.
- [119] F. Ammon, S. T. Sauer, R. Lippert, D. Lungerich, D. Reger, F. Hampel, N. Jux, *Org. Chem. Front.* **2017**, *4*, 861.
- [120] a) G. Zimmermann, U. Nuechter, S. Hagen, M. Nuechter, *Tetrahedron Lett.* **1994**, *35*, 4747; b) P. M. Donovan, L. T. Scott, *J. Am. Chem. Soc.* **2004**, *126*, 3108; c) H. C. Shen, J. M. Tang, H. K. Chang, C. W. Yang, R. S. Liu, *J. Org. Chem.* **2005**, *70*, 10113; d) C. A. Merlic, M. E. Pauly, *J. Am. Chem. Soc.* **1996**, *118*, 11319.
- [121] a) P. J. Stephens, F. J. Devlin, C. F. Chabalowski, M. J. Frisch, *J. Phys. Chem.* **1994**, *98*, 11623; b) A. D. Becke, *J. Phys. Chem.* **1993**, *98*, 5648.
- [122] L. B. A. Johansson, A. Niemi, *J. Phys. Chem.* **1987**, *91*, 3020.
- [123] a) M. Sauer, K. T. Han, R. Müller, S. Nord, A. Schulz, S. Seeger, J. Wolfrum, J. Arden-Jacob, G. Deltau, N. J. Marx, C. Zander, K. H. Drexhage, *J. Fluoresc.* **1995**, *5*, 247; b) M. Sauer, K. T. Han, V. Ebert, R. Müller, A. Schulz, S. Seeger, J. Wolfrum, J. Arden-Jacob, G. Deltau, N. J. Marx, K. H. Drexhage, *Proc. SPIE* **1994**, *2137*, 762.
- [124] a) Y. Ma, Y. Dong, P. She, S. Liu, M. Xie, Y. Yu, Y. Li, Q. Zhao, W. Huang, *Adv. Opt. Mater.* **2018**, *6*, 1; b) U. Kaiser, N. Sabir, C. Carrillo-Carrion, P. del Pino, M. Bossi, W. Heimbrodtt, W. J. Parak, *Nanotechnology* **2016**, *27*, 055101.
- [125] a) D. Kage, K. Hoffmann, M. Wittkamp, J. Ameskamp, W. Gohde, U. Resch-Genger, *Sci. Rep.* **2018**, *8*, 16715; b) J. Napp, T. Behnke, L. Fischer, C. Wurth, M. Wottawa, D. M. Katschinski, F. Alves, U. Resch-Genger, M. Schaferling, *Anal. Chem.* **2011**, *83*, 9039; c) P. D. Quevedo, T. Behnke, U. Resch-Genger, *Anal. Bioanal. Chem.* **2016**, *408*, 4133.
- [126] T. Behnke, C. Würth, E.-M. Laux, K. Hoffmann, U. Resch-Genger, *Dyes Pigm.* **2012**, *94*, 247.

## Acknowledgments

An dieser Stelle möchte ich vor allem meinem Doktorvater Prof. Dr. Siegfried Eigler für die Möglichkeit danken, das spannende Thema der Fluoreszenz verschiedener organischer Verbindungen erforschen zu dürfen. Darüber hinaus möchte ich Ihm für sein Interesse am Fortschritt meiner Arbeit, seine fachliche Unterstützung, der Schaffung einer kollegialen Arbeitsatmosphäre, als auch für den kreativen Freiraum, in dem ich mich bewegen durfte, danken.

Ich bedanke mich zudem bei allen ehemaligen Kommilitonen und Kollegen die mich auf meinem Weg durch Studium und Promotion begleitet haben, die mich unterstützt haben und die die Zeit zu einem freudigen, spannenden Erlebnis gemacht haben. Außerdem danke ich allen Studenten mit denen ich gemeinsam an Projekten gearbeitet habe, die ich betreut habe und durch deren Anleitung ich selber viel gelernt habe. Hervorheben möchte ich Jan Philipp Soyka und Alexander Krappe, die in Ihren Bachelorarbeiten entscheidende Beiträge zu später erfolgten Publikationen geleistet haben.

Mein Dank gilt darüber hinaus sämtlichen Kooperationspartnern. Mein besonderer Dank Felix Witte aus der AG Paulus, für sämtliche Rechnungen und daraus abgeleiteten Erkenntnisse, und Sebastian Sobottka aus der AG Sarkar für die tollen elektrochemischen und elektrochemisch-spektroskopischen Messungen! Außerdem möchte ich Dr. Ute Resch-Genger sowie Ihrer Gruppe, insbesondere Katrin Hoffmann, Arne Güttler und Jutta Pauli, für Ihre Einweisung und Hilfe mit verschiedensten Geräten und speziellen Messungen danken.

Kirill Greben danke ich für sämtliche fachliche Gespräche und die Zusammenarbeit, sowie noch viel mehr für unsere Gespräche über Gott und die Welt, aus denen ich stets wichtige Erkenntnisse gewonnen habe.

Zudem möchte ich meiner Familie danken. Meiner Tante Petra sowie Ihren Töchtern Lena und Luisa möchte ich für das nette willkommen heißen in Berlin danken, für die gemeinsamen Treffen und Feste und die guten Gespräche. Mein größter Dank gilt meinen Eltern Evi und Norbert, sowie meinem Bruder Stefan. Eure Unterstützung, sowie euer bedingungsloser Glaube an mich haben es mir ermöglicht so weit zu kommen und die Grundlage geschaffen um mich stets weiter zu entwickeln und zu verbessern. Josie, ich danke dir für die wundervolle Zeit die wir bis jetzt miteinander verbracht haben und die wir miteinander verbringen werden. Ich bin überglücklich, dass wir uns gefunden haben und liebe dich.

## Statement of the Author

I declare on the affidavit that I have written the dissertation independently and have used no sources other than those I have indicated and that there are no facts which make me unworthy of the conduct of a doctoral degree under the provisions of the law governing academic degrees. Further I declare my consent that the electronic version of my dissertation, while maintaining my copyrights and data protection, may be subjected to a separate review regarding the independent preparation of the dissertation. I have not submitted the dissertation anywhere else to obtain an academic degree and have not already passed this or a similar doctoral exam without success.

Berlin, 23.9.2020